# HYDROLOGY OF THE UPPER HUNTER CATCHMENT

by

Falguni Biswas

A thesis submitted for the degree of Doctor of Philosophy

in

The Fenner School of Environment and Society

of the Australian National University

October 2010


THE AUSTRALIAN NATIONAL UNIVERSITY

# CANDIDATE'S DECLARATION

This thesis contains no material which has been accepted for the award of any other degree or diploma in any university. To the best of the author's knowledge, it contains no material previously published or written by another person, except where due reference is made in the text.

Falguni Biswas Date:20/10/2010

# ACKNOWLEDGEMENTS

I would like to express my heartiest gratitude to my supervisor Professor Ian White and co-supervisors Dr Ben Macdonald and Dr Sara Beavis at the Fenner School of Environment and Society (FESS, formerly Centre for Resource and Environmental Studies, CRES), Australian National University. Thanks Ian for all of your kind efforts, support, continual guidance and encouragement throughout my PhD. Big thanks to Dr Ben Macdonald (CSIRO and formerly the Fenner School) for his guidance, discussion, advice from beginning to end of my PhD.

I would like to acknowledge Australian Research Council (ARC) for the linkage Grant LP0560743 and NSW Department of Environment and Climate Change, Department of Environment & Water and Energy and the Hunter Central River Catchment Management Authority for further fund and valuable data.

I would also like to thank to the other academic staffs of FESS specially Professor Michael Hutchinson, Lachlan Newham, John Stein, Janet Stein, Sue Holzknecht, Jenny Kesteven for their valuable advices and support. Thanks also go to Barry Croke and Ross Brodie of Bureau of Rural Science for the support of IHACRES model and hydrographic separation technique respectively. Big thanks to Damian Jellett for his coding of water balance model.

Thanks to David Hoey, John Paul Williams and Anthony Belcher of Department of Natural Resources at Newcastle who provided valuable support and supplied groundwater level data.

Thanks go to my friends and my fellow PhD students at FESS for their invaluable support.

I am indebted to my parents for their moral support, my husband for vital ongoing support and my sons for making me pleasant at all time.

# ABSTRACT

One of the ten objectives of the 2004 Australian National Water Initiative is to manage surface and groundwater as a single resource. In order to do that it is necessary to understand the interactions between surface and groundwater, as well as the impacts of water abstraction, land use change and climate variability. In Australia, not just the quantity of water, but also its quality and particularly its salinity are critically important. Some of the difficulties facing agencies in managing surface and groundwater as a single resource are the extreme variability of climate in Australia, the lack of long-term streamflow and groundwater level data sets and the very limited temporal records on water quality.

This thesis presents a study of surface and groundwater interaction and salinity in a selected catchment in the Hunter Valley in mid New South Wales, eastern Australia, where data records are limited and incomplete. The hypotheses tested in this work are that (1) salinity discharge in the Hunter is largely determined by mineral weathering and deep groundwater inflows and (2) a simple parameter-efficient coupled surface and groundwater model can accurately predict groundwater and streamflow behaviour over monthly time scale and is useful in determining surface –groundwater interactions.

In the Hunter, water is a fundamentally important for power generation, coal mining, horticulture, irrigation, stock production and community water supplies. The Hunter however has significant salinity issues, particularly in groundwater. Because of this it is the location of the world's first salinity trading scheme. The site chosen here for detailed study is Wybong Creek, a left bank tributary on the Goulburn River which is a right bank tributary of the Hunter River. As a component of the water reform process in Australia, NSW has been developing water sharing plans designed to return a better share of water to the environment. These plans in general have been based on limited information about surface and groundwater interaction and have largely ignored water quality altogether.

To facilitate better management, this thesis aims to fill in the data sets, investigate impacts of land use change and climate variability, determine water and salt balance, solute sources and identify the interactions between surface and groundwater within the catchments using an improved, parameter efficient monthly, conceptual model. The long-term changes in rainfall and runoff are analysed for identifying whether the long-

term declines in yield are due to 50 year drought-dominated cycles or to changes in land use. Stream discharge and electrical conductivity data are analysed for identifying salinity distribution and discharge. The annual salt load is estimated and the salt balance is also investigated by using an Output/Input (O/I) ratio. The specific salt yield of the catchment for the period 1993 to 2008 was estimated to be 17 tonnes $km^{-2}$ $year^{-1}$ and the annual salt O/I ratio was 5.5 showing that the catchment is not in equilibrium.

Hydrogeochemistry and water isotopes data are employed to identify the solute sources in the catchment. It was found that mineral weathering originated from basalt and sandstone in the upper catchment, with weathering fractions relative to cyclic salt being as high as 80%. Cyclic salt is not an end member of the mixing curve in the catchment but marine origin water is. In the lower catchment, marine-origin groundwater and possibly halite dissolution from the Permian coal seams dominates the stream and groundwater salinity.

The Q-lag method was used to examine stream and groundwater interaction. Comparisons between streamflow percentiles (Q90 percentile flow) and relevant rainfall percentile (7dayR10 rainfall percentile) curve gave reasonable correlations ($r_m$>0.7) between the shifted flow percentile curves and the reference rainfall percentile curve. These demonstrate that Wybong streamflow is predominantly a stream interacting with the deep groundwater system with a 206 days lag between rainfall and flow. Baseflow separation analysis was used to examine the base flow system in the catchment. Baseflow indices ranged from 0.22 in 2007 to 0.83 in 1982 with the average baseflow index from 1972 to 2000 of 0.53.

The conceptual Xiong and Guo (XG) model was examined for its ability to predict streamflow and groundwater levels. The model performed well, under calibration. R-squared values of calibration are more than 80% for spatially interpolated monthly rainfall and pan evaporation data which is a good fit between observed and predicted values. From 1990 to 2000, up to 42% of the discharge flowing from the catchments each month is groundwater flow. However, the model parameter values needed to fit the data were physically unrealistic and it was concluded that the model has limited applicability in situations with very low stream flows. Modification of the model to include a physically more realistic evaporation component did not improve the model fit or the parameter values. Ungauged water extraction from the catchment during the 2000 to 2008 could have contributed to the poor performance of the model.

As with most catchments, there are significant problems in attempting to test the hypotheses of this thesis due to the limited and incomplete data on stream flow and stream salinity. In the case of stream salinity, despite the fact that salinity was recognised as a major issue in the Hunter more than six decades ago, there is an extremely short continuous salinity record. This limitation was compounded by the severe drought years that extended for much of the salinity record. It has been shown here that catchments in eastern Australia are subject to approximately 50 year cycles of flood- and drought-dominated regimes. The relevance of a less than two decade salinity record to such long cycles is problematic. In the upper catchment, the hydro and geochemistry results here unequivocally show that weathering products make up the major portion of the stream salt load. So the results here have verified the first hypothesis above but the difficulties with fitting the simple conceptual modelled to the rejection of the second hypothesis.

# TABLE OF CONTENTS

# FIGURES

# TABLE

# CHAPTER 1: INTRODUCTION

## 1.1 Background

There are increasing concerns throughout the world over the impacts of land use change and water abstraction as well as climate change and variability on the quantity and quality of surface and groundwater, particularly on stream salinity, and on the interactions between ground and surface waters (Ghassemi *et al.,* 1995). In Australia, these concerns are heightened by to the generally dry and highly variable climate, ancient continent and large-scale land use changes following European settlement (Olley and Wasson, 2003). Australia shares with South Africa the highest stream flow variability in the world (Chiew *et al*., 1998; Finlayson and McMahon, 1991 and McMahon *et al*., 1992) and has marked variability of rainfall from season-to-season and year-to-year with an annual average rainfall across the content of less than 300mm.

The correlation between rainfall over all of Australia and the SOI is 0.58 for positive SOI years and 0.25 for negative SOI years (Chiew and McMahon, 2002; Stone and Auliciems, 1992) which reflects the Australian rainfall variability. Rainfall variability has significant impacts on catchment yield and regional salinity. The full impacts of climate variability on salinity are uncertain. However, it is probably the areas with lower rainfall will be the most vulnerable (AGO, 2002).

There is a strong climatic influence on the shallow fractured-rock groundwater systems in Murray-Darling Basin (Rancic *et al*., 2009). Annual rainfall in the Basin increased after 1947, but over the last decade it has been decreasing in most areas. These increases in rainfall increased recharge in many groundwater systems and changed catchment salinity dynamics. The continued discharge of saline groundwater into surface streams, particularly in Western Australia and the Murray-Darling Basin is a major threat to domestic and irrigation water supplies and aquatic ecosystems. For improved management of water resources, it is crucial to understand the mechanisms and quantify the exchange processes and pathways between groundwater and surface water.

The release of salinity into streams has been attributed to groundwater discharge containing salt sourced from marine-origin cyclic salts deposited in rainfall and concentrated by evapotranspiration (Peck, 1978; Allison and Hughes, 1983; Williamson

*et al.,* 1987; Allison and Schonfeldt, 1989; Schofield and Ruprecht, 1989; Simpson and Herczeg, 1994; Jolly *et al.*, 2001, Peck and Hatton, 2003). Land use change and particularly the clearing of deep-rooted native vegetation and its replacement with shallow-rooted pastures or annual crops have been blamed for increasing groundwater recharge, raising groundwater levels and augmenting salt discharges and the salinity of streams (Ghassemi *et al.*, 1995). Australia's recently completed $1.4B National Action Plan (NAP) for Salinity and Water Quality aimed to reverse salinity increases and to move towards sustainable landscape management. Through the NAP and the regional component of the Natural Heritage Trust, over 340,000 hectares of agricultural land have been improved through activities such as perennial pasture establishment and the application of lime to address acid soils. Sustainable irrigation systems have been established on over 19,000 hectares of land. Regions have developed nearly 3,500 sub-catchment plans and nearly 6,500 property management plans. Revegetation and rehabilitation activities have been conducted across 300,000 hectares of land. As well 1.4 million hectares of land has been protected for native species, and almost 16 million hectares have been managed for pest plants and animals (NAP 2005).

Some authors suggest that meteoric input of salt may not be the only source of salinity (Gunn, 1985; Kellett *et al.,* 1989; Dalhaus *et al.*, 2000; Acworkth and Jankowski*,* 2001). Other processes such as groundwater discharge and mineral weathering can also be of salinity sources in the catchment (Conyers *et al.,* 2008; White *et al*., 2009). Beavis (2000) proposed that the role of geological structural controls on water chemistry is also an important source of salinity. Australian soils and geological strata contain very large salt stores as the result of the continent's geological history particularly over the past 30 million years. An understanding of the sources of salts in Australian rivers is not merely of academic interest; it has major implication for the selection of management strategies to mitigate impacts (Conyers *et al*., 2008).

Most Australian studies of stream salinisation and surface-ground water interactions have concentrated on lower rainfall areas such as the Murray-Darling Basin (e.g. Herczeg *et al.*, 1993; 2001; Simpson and Herczeg 1991; 1994) or south-western Australia (Peck and Hurle, 1973; Ghassemi *et al.,* 1995). Higher rainfall areas such as coastal catchments in eastern Australia have been assumed generally free from salinity export problems and have been less well studied although there are exceptions, particularly where there are sulfidic soils underlying floodplains. A notable exception is

the Hunter River Catchment in mid-coastal New South Wales (NSW), where salinity problems coupled with mining and agricultural conflicts have seen the introduction of the Hunter River Salinity Trading Scheme, a world- pioneering scheme using economic instruments and regulation to control saline discharge (Department of Environment and Conservation 2003).

Rainfall variability and water use by industries and agriculture in the Hunter impact on the region's surface and groundwater. Quantification of the impacts of water abstraction and climate variability on the stream and groundwater resources is fundamental to the sustainable management of catchments.

In the past in Australia, surface and groundwater have been managed as separate systems. The Council of Australian Government's 2004 National Water Initiative (NWI) recognised that separate management of interconnected surface and groundwater systems. One of the NWI's ten goals was to manage surface and groundwater as a single system. This poses significant challenges for water management agencies. Coupled surface-groundwater models appear useful tools for assisting in meeting this challenge. One of the major challenges, however, is that surface and particularly groundwater data are limited and monitoring records have significant gaps in data (Chapman, 1990). These make parameter identification difficult in the construction of coupled surface-groundwater models. One way of supplementing missing data on the processes occurring in catchments is to examine the hydro- and geochemistry of surface and groundwater. Chemical properties tend to integrate over time and sometimes space.

In this thesis, Wybong and Wollombi catchments in the Hunter River have been chosen for study because of their strategic importance in both agriculture and mining. These catchments have incomplete hydrological records and techniques are used here to examine filling-in data sets. Hydrochemistry and geochemistry are also used to provide details on the processes occurring in the catchments and to estimate salt export. Using the in-filled data, a simple, parameter efficient-coupled surface (Xiong and Guo, 1999) and groundwater model (Jellett, 2005) is examined to explore its ability to predict both groundwater level and streamflow.

## 1.2 Hypothesis:

The main hypotheses examined in this thesis is that (1) salinity discharge in the Hunter is largely determined by mineral weathering and deep groundwater inflows and

(2) a simple parameter-efficient coupled surface and groundwater model can accurately predict groundwater and streamflow behaviour over monthly time scale and is useful in determining surface –groundwater interactions.

## 1.3 Aim and Objectives:

The aim of this study is to determine the water and salt balance and interactions between ground and surface water systems in sub-catchments in the Hunter with limited data sets, using techniques to in-fill data, hydro- and geochemical information to identify processes and an improved, a parameter efficient model to predict groundwater levels and streamflow at the monthly time scale.

This study has the following objectives:

1. Characterise the climate variability and water yield of the Wybong catchment (chapter 3)

2. Determine salinity discharge and the water and salt balances at a subcatchment scale (chapter 4)

3. Assess of sources and trends in salinity in the study catchment (chapter 5)

4. Identify surface and groundwater connectivity and rate of groundwater discharge (chapter 6)

5. Examine the performance of a parameter efficient model for predicting stream flow and groundwater levels (chapter 7 and chapter 8)

## 1.4 Thesis Structure

**Chapter 1: Introduction**

An overview of importance for stream and groundwater interactions, climate impact on water, salinity and sources of salinity are discussed. The importance of groundwater modeling for water resources management is outlined in this chapter. Finally the introductory chapter gives the hypothesis, aims and objectives of this thesis and also outlines the subsequent chapters.

**Chapter 2: Study Site**

Chapter 2 describes the study sites chosen in this work. It firstly discusses the importance of Hunter Valley and salinity problem in Hunter. It also briefly discusses the Hunter salinity trading scheme. Then the Wybong Creek study site is described together with the catchment's location, geology, soil, land use, vegetation, hydrogeology and surface and groundwater systems. Finally the water sharing plan for the Wybong Catchment is outlined and the Wollombi Brook and the Goulburn River study sites are described.

**Chapter 3: Climate Characteristics and Water Yield**

Chapter 3 describes the available climate data including monthly rainfall and pan evaporation and streamflow. It describes spatial interpolation of point values to produce a rainfall and pan evaporation surface. It also explains data processing such as filling missing streamflow data. Water abstraction, long term changes in rainfall and correlation between the Southern Oscillation Index (SOI) and Wybong rainfall are discussed. This chapter identifies the impact of drought on catchment yield and investigates whether land use change has altered the rainfall-runoff process.

**Chapter 4: Salinity Discharge and Water Salt Balance in Wybong Catchment**

Chapter 4 discuss data treatment, filling data gaps in streamflow and stream electrical conductivity, EC data, and calculation of rain input salt load and stream salinity output. Different sources of stream salinity are identified and the long term salt load and an import-export budget of salt for the catchment are also estimated in this chapter.

**Chapter 5: Sources of Salinity in the Catchment**

Chapter 5, details the sampling procedure showing surface water and groundwater sampling sites. It also investigates the solute transport via groundwater discharge and the impact of mineral weathering for salt load in the catchment.

**Chapter 6: Surface and Groundwater Interaction**

Chapter 6 provides an assessment of surface and groundwater interactions using different techniques included Lyne and Hollick baseflow separation, frequency analysis and comparing groundwater level with stream height. Streamflow hydrograph analysis in carried out in which a frequency analysis approach is used to compare streamflow percentiles with relevant rainfall percentile curves. Impact of water extraction and contribution of the deeper aquifers with longer flowpaths are also discussed.

**Chapter 7: Model for Groundwater Dynamics**

Chapter 7 gives an overview of the monthly water balance model, the available data and data processing required for the modeling. Available data used are discussed and include monthly spatially interpolated rainfall and pan evaporation in Hunter, groundwater level data for 12 bores in the Wybong and Wollombi Brook catchments, streamflow data for three streams located in the Wybong and Wollombi Brook. This chapter also introduces the Xiong and Guo water balance model for predicted a monthly streamflow together with modified groundwater.

**Chapter 8: Model testing for Streamflow and Groundwater Level**

Chapter 8 details the model testing process and performances on groundwater level prediction in the Wybong and Wollombi Brook. Hv-block cross-validation method is explained which is used for model testing procedures. It also presents some applications of the model including different temporal and spatial scales, prediction of streamflow after calibration on groundwater level data and prediction of groundwater levels after calibration on streamflow data.

**Chapter 9: Conclusions**

Chapter 9 summarizes the main findings of this study, provides conclusions drawn from the study and suggests future research.

# CHAPTER 2: STUDY SITE DESCRIPTION

This Chapter provides an introduction to three subcatchments in the Hunter River studied in this thesis, which are Wybong Creek, Wollombi Brook and Goulburn River. The importance of the Hunter Valley is outlined and the salinity problems in the Hunter discussed together with the Hunter salinity trading scheme. The site selected for detail study Wybong Creek is discussed and the catchment's location, geology, soil and land use, climate, vegetations, hydrogeology, surface and groundwater systems and water sharing plan are also discussed. This chapter also describes of the Wollombi Brook and Goulburn River which are also studied in less detail in this thesis.

## 2.1 Hunter Valley

The Hunter Valley in New South Wales (see **Figure 2.1**) is one of the most economically significant regions in Australia. Major agricultural industries in the region include dairy farming, broad acre cropping which is mainly large-scale, capital-intensive cropping and mostly monoculture. Beef cattle, sheep production, horse studs and irrigated market gardening also are important along its extensive riverine floodplains. The Hunter Valley is famous for wine-production. It produces 23,818 tons of wine per year using 4534 hectares of land. Coal mining is a major industrial activity in the Hunter catchment, extracting over 60 Mt of coal each year (Hancock *et al*., 2005) and total export was more than 90 million tonnes in 2008. Australia earns $1442 million dollars from the coal industry. Coal-fired power stations in the Hunter produce 91% of NSW's power supply.

Coal mining in the area however has major impacts on groundwater due to loss of coal measure aquifer pressure and leakage of groundwater from shallow alluvial aquifers. In the upper Hunter catchment, groundwater salinities typically exceed the maximum ANZECC (2000) limits for drinking, irrigation and stream ecosystems (NSW Department of Planning, 2005). Salinity leakage from deeper aquifers into alluvial aquifers and streams, via changes in the hydrologic regimes in catchments, constitutes a significant threat to the fresh water resources of the Upper Hunter catchment (NSW Department of Planning 2005).

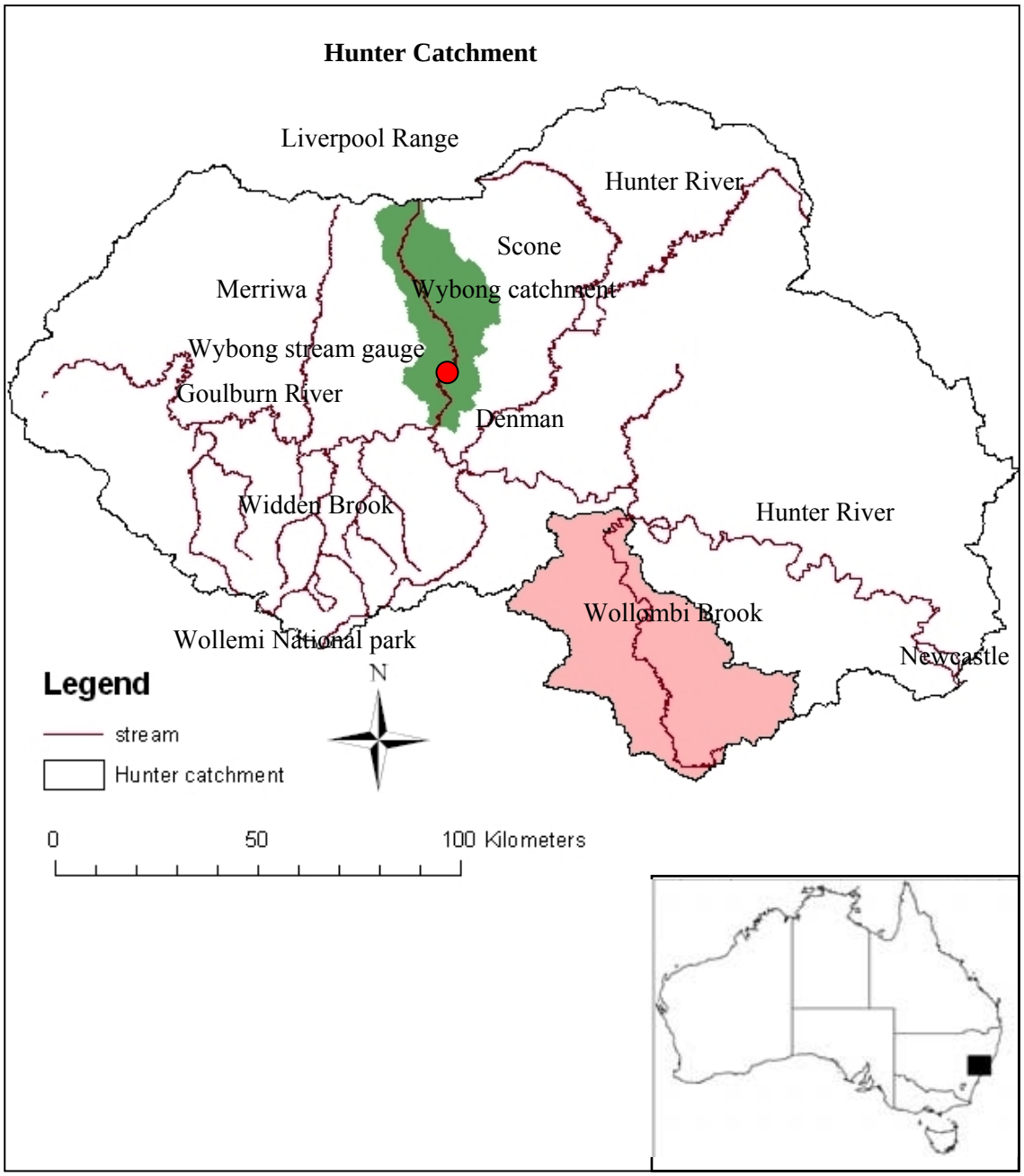


**Figure 2.1** Location of the Wybong Creek and Wollombi Brook catchments in Hunter Valley

## 2.2 Salinity Problems in Hunter Region

The Hunter Valley, New South Wales has a long history of primary and secondary salinity which is an increasing concern for managing resources in this region (DLWC, 2000). It has been estimated that each year salinity cost NSW in the order of $180 - $200 million. Costs associated with increasing salinity include loss of productive land,

lack of suitable water for irrigation, and increased costs for industry. It has been estimated, for example, that the costs to Macquarie Generation, which provides 40% of New South Wales, electricity generation capacity, of an increase in of stream electrical conductivity, EC, 10µS/cm in the Hunter River at Liddell is of the order of $180,000 per annum (NSW Department of Land and Water Conservation, 2003). Many pastures and crops grown commonly in the Hunter have a low tolerance to saline irrigation water. Grapes, leafy vegetables and many clover varieties and perennial pastures suffer from yield decline when root zone salinity exceeds 1500µS/cm. The Hunter Salinity Audit (NSW Department of Land and Water Conservation, 2003) predicted that the Goulburn River at Sandy Hollow will exceed on EC of 1500µS/cm for 20% of the time by 2050 unless works are put in place to address rising salinity levels in the Hunter.


**Figure 2.2** Satellite image of the Hunter Valley with Wybong catchment and Wollombi. Source: (Google Earth, 2009).

Poor water quality is an issue in the Wybong catchment of the Hunter valley. Salinity of lower Wybong Creek is considerably high with an EC of 5460µS/cm. The salinity during low flows has the potential to cause environmental damage when water is used for irrigation, causing soil degradation, salinisation of the alluvial aquifer and a decline in crop yields. The reason advanced for these high levels of salinity is ground water accession from a fault line which adjoins the creek (Mackie Environmental Research 2006).

## 2.3 Hunter Salinity Trading Scheme

The Hunter River Salinity Trading Scheme has been operating since 1995 (NSW Department of Land and Water Conservation, 2003). The aim of the scheme is to reduce the impact of saline discharges on the water users and the ecosystem of the Hunter River. Under the scheme, coal mines and power generators are conditionally allowed to discharge specified amounts of saline water, when its effect on the electrical conductivity level in the river will be minimized through dilution by a high volume of freshwater flowing in the river. When the river is in low flow, no discharges are allowed. When the river is in high flow, limited discharge is allowed and is controlled by a system of salt credits which allocates a total of 1000 credits to be shared among the participating coal mines. Each credit allows the credit holder to discharge 0.1% of the total allowable discharge. The amount of discharge allowed depends on the ambient salinity in the river, so it can change daily. The total allowable discharge is calculated so that the river electrical conductivity does not exceed 900µS/cm at the junction of the Hunter River and Glennies Creek and in the Hunter River at Singleton (**Figure 2.2**) or and is limited to 600µS/cm at Denman (**Figure 2.1**). When the river is in flood, unlimited discharges are allowed as long as EC does not go above 900µS/cm (NSW Department of Land and Water Conservation, 2003).

## 2.4 Location of the Major Study Area

In this thesis Wybong Creek has been chosen as a study site because of the salinity problems occurring in the catchment and because of the importance of surface-groundwater interactions. The study area Wybong Creek Catchment is located in Hunter valley in Australia (**Figure 2.1**). Satellite Image of the Wybong Catchment also shown

in **Figure 2.3**. Wybong Creek is the most eastern of the 6 major tributaries of the Goulburn River and collects water from the northern part of the Goulburn River catchment.

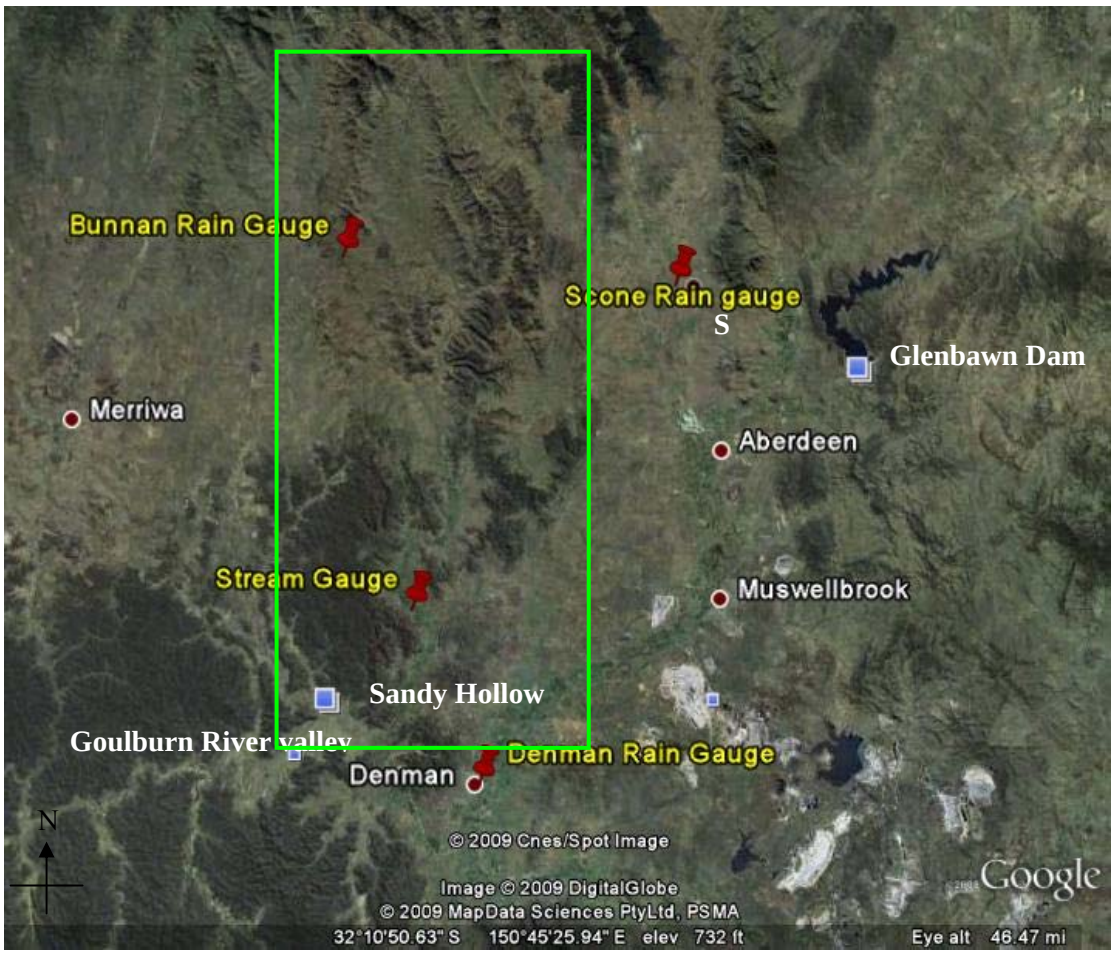


**Figure 2.3** Satellite Image of the Wybong Catchment. Source: (Google Earth 2009)

The Goulburn River is a major tributary of the Hunter River which drains almost half of the Hunter catchment but contributes only 23% of the mean Hunter river flow (NSW Department of Infrastructure, Planning and Natural Resources, 2002). Wybong creek drains south, west of the Dart Brook catchment and drains from Towarri National Park at an elevation of 1100 m (NSW Department of Planning, 2005). Wybong Creek runs southeast for distance of 90 km to join the Goulburn River downstream of Denman, at an elevation of around 130 m. The major tributaries of Wybong Creek include Terell Creek, Beales Creek, Little Creek, Gathabawn Creek, White Rock Gully, Cuan Creek, Happy Valley Creek, Gulf Creek, Scotts Creek, Big Flat Creek and Reedy

Creek. The area of Wybong Creek catchment is approximately 793 $km^2$, of which 10% is contained within the Towarri National Park and the Manobalai Nature Reserve. The remainder lies within private holdings used for grazing beef cattle, production of irrigated pasture, as well as hobby farms and vineyards.

## 2.5 Geology of the Catchment

The Wybong catchment is located within the northern margin of the Sydney Basin. The Sydney Basin forms the southern section of the Sydney-Gunnedah-Bowen Basin, a composite structural basin extending for 1700 kilometers from southern New South Wales to central Queensland. The coal bearing formations of the Sydney Basin are Permian in age and are typically associated with low lying or undulating topography. Overlying rocks of Triassic age, which form prominent escarpments, cover large parts of the basin, particularly in the central, southern and western areas. Three coal bearing sequences occur in the Hunter Coalfield; the Early to mid- Permian Greta Coal Measures, the Late Permian Wittingham Coal Measures and the overlying Late Permian Wollombi Coal Measures. The coal measure sequences are separated by marine strata of the Maitland Group and Denman Formation respectively (NSW Geological Survey, 2004).

**Figure 2.4** shows a geological map of the Wybong catchment. The geology of the catchment consists of Quaternary Alluvium, Tertiary basalt, Triassic sandstone and conglomerate, Permian coal, shale deposits along the flood plain of Wybong creek, and the Narrabeen Group outcropping along the slops and ridges of the catchment. The majority of Wybong Creek is situated within the Merriwa Plateau where its elevation ranges from about 100 m near the Goulburn River to over 600 m in the Liverpool Range in the north (NSW Department of Infrastructure, Planning and Natural Resources, 2002). The plateau has formed on Tertiary basalt flows but some Jurrasic rocks have been exposed by stream incision. In the southern portion of the catchment, near the confluence with the Goulburn River the stream has incised down into the Permian sandstone and conglomerate (NSW Department of Infrastructure, Planning and Natural Resources, 2002). **Table 2.1** has shown the Stratigraphic units in the Catchment.

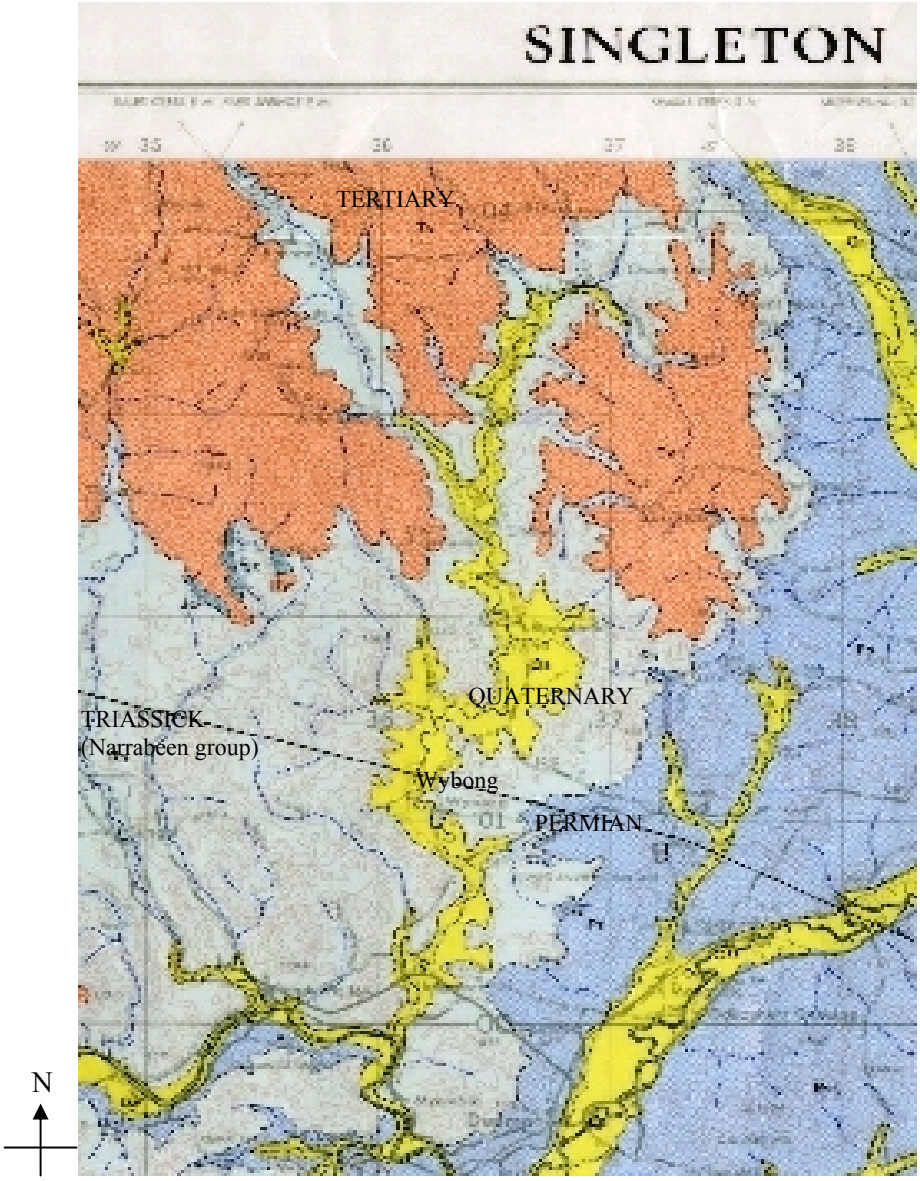


**Figure 2.4** Geological map in the Wybong catchment (1:250,000 map sheet). Source: DNR 2006.

**Key for Figure 2.3**

- TRIASSIC (Narrabeen group)
- PERMIAN
- QUATERNARY
- TERTIARY (Liverpool Basalts)

**Table 2.1** Stratigraphic units in the Wybong Catchment (Kellet *et al*. 1989)

| Age | Geological unit and median thickness (m) | | | Lithology |
|---|---|---|---|---|
| Quaternary | Alluvium 10~12 | | | Heterogeneous clays, silts, sands and gravels |
| Tertiary | Intrusive and Liverpool basalts 100 | | | Olivine basalts Dolerite silts, laccoliths, necks |
| Early Triassic | Narrabeen Group 200 | | | Interbedded shales and sandstones on basal conglomerate |
| Late Permian | Singleton Supergroup | Wollombi Coal Measures 230 | | Coal measure sequence with numerous tuff, conglomerate, arenite and claystone interseam beds |
| | | Wittingham Coal Measure | Jerrys Plains Subgroup 410 | Coal measure sequence with 12 major named seams and numerous splits. Fluvial conglomerate, sandstone and claystone interseam beds of irregular thickness terminating in marine laminites (Denman Formation) |
| | | | Vane Subgroup 80 | Coal measure sequence with 7 major named seams. Fluvial sandstone and siltstone interbeds terminating in marine laminated siltstone (Bulga Formation) |
| | | | Saltwater Creek formation 20 | Massive sandstone with basal silty phases |

## 2.6 Soils of the Catchment

The soil landscapes mapping undertaken by the Soil Conservation Service of NSW (Kovac and Lawrie, 1991) shows a large number of soil landscapes are present within Wybong creek catchment. Soil landscapes areas are shown in **Figure 2.5** and in **Table 2.2**, together with the associated soil units.

The Merriwa soil landscape is the dominant landscape within the catchment. It covers the terraces and floodplains on the Merriwa Plateau in the Wybong area and is dominated by basaltic Quaternary alluvium. This soil landscape is found on the edge of the Merriwa Plateau and is dominated by basaltic colluvium from the surrounding hills. Soil downstream of the catchment confluence with the Goulburn River, includes the loams and the clayey sands of the Sandy Hollow soil landscape on mid-slopes, the shallow siliceous sands and shallow loams of the Lees Pinch soil landscape on ridge tops and the alluvial soils of the Wollombi soil landscape in the channel and the floodplain area of Wybong creek. Soil landscape data indicates that moderate stream bank erosion is likely along water courses within the Wollombi soil landscape (Kovac and Lawrie, 1991).

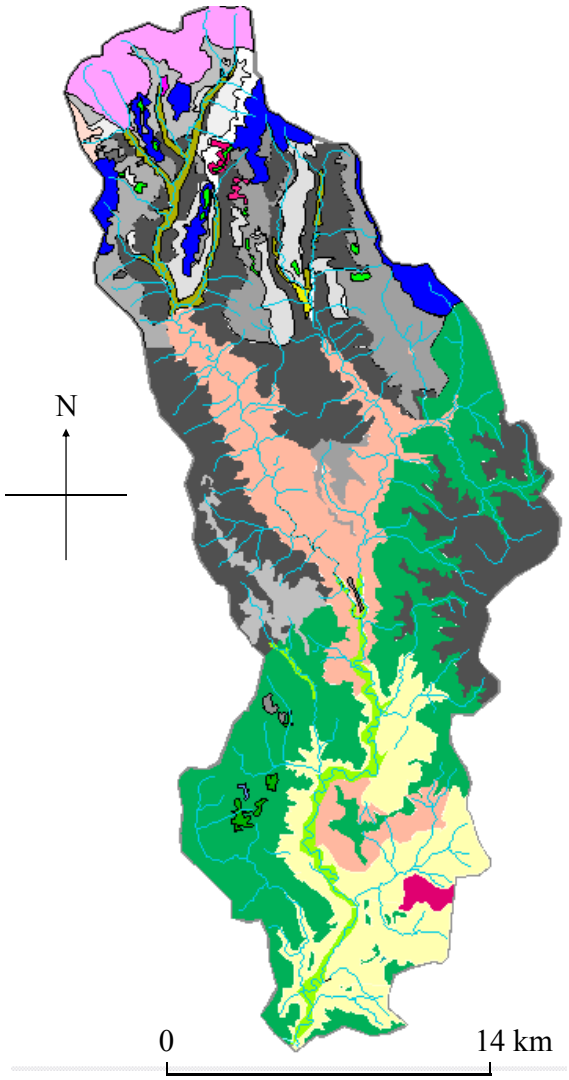


**Figure 2.5** Soil map in the Wybong catchment (Jasonsmith, 2010) (key on next page)

## Key for Figure 2.5

| | |
|---|---|
| RG – Rossgole | Tertiary olivine basalt. Local relief 60 – 120 m; slopes 2 – 7 %. Black earths on steeper slopes; euchrozems on less steep slopes. |
| AH – Ant Hill | Tertiary olivine basalt. Local relief 100 –180 m, slopes 5 – 15 %. Black earths on mid-lower slopes; red clays on upper slopes; brown clays on mid-slopes; grey clays in poorly drained watercourses; euchrozems on well drained slopes. |
| Aha – Ant Hill: outcrops | Similar to Ant Hill, but with minor cropping occurring on gently sloping benched areas. |
| CB – Coober Bulga | Tertiary olivine basalt. Local relief < 600 m; slopes > 33%. Red euchrozems and black earths on steeper slopes; black earths and prairie soils on less steep slopes. |
| CE – Cranbourne | Tertiary olivine basalt. Local relief to 30 m; slopes 0 – 7 %. Black earths on steeper slopes; euchrozems on the plateau. |
| ER – Erin | Tertiary olivine basalt. Local relief 0 – 70 m; slopes 1 – 8 %. Black earths on upper and lower slopes. |
| YM – Yarramoor | High energy narrow floodplains and low terraces of the Liverpool Ranges. |
| WP – Wappinguy | Permian and Jurassic quartz and lithic sandstone, shale, conglomerate and siltstone; local relief 40 – 80 m, slopes 15 %. Red solodic regoliths with yellow, brown and grey solodic regoliths on mid-lower slopes; siliceous and earthy sands, gleyed soloths, red earth euchrozem intergrades, and occasional prairie regoliths on lower slopes. Red and yellow euhcrozhems have moderate-high salinity. |
| SY – Sandy Hollow | Quaternary colluvium derived from sandstone, conglomerate and shale. Relief 20 – 40 m, slopes to 10 %. Yellow and red solodic regoliths on mid-upper slopes; Siliceous and earthy sands on lower slopes. High salinity in sodic regoliths. |
| CR – Castle Rock | Permian sandstone and conglomerate. Local relief 40–80 m; slopes 1 – 5 %. Stony solodic soils on flat slopes and alluvial soils in drainage lines. |
| GG – Galla Gilla | Tertiary olivine basalt. Local relief 50 – 200 m; slopes > 33 %. Lithosols on steeper slopes; black earths/euchrozems on side slopes. |
| LP – Lees Pinch | Triassic sandstone. Relief 100 – 300 m, slopes 10 – 30 %. Shallow siliceous sands, shallow loams. Some yellow and brown earths, yellow and grey soloths on the breaks of slope. Yellow podzolic regoliths and earthy sands on upper slopes. Low-high salinity. |
| MP – Munghorn Plataeu | Triassic sandstone and shale. Relief 20 – 60 m, slopes 2 –10 %. Siliceous sands on crests; sandy yellow earths on lower slopes; yellow soloths on drainage lines. |
| MW – Merriwa | Alluvial and gently undulating rises up to 12 m above the stream bead. Alluvial soils, chernozems, prairie soils, grey clays, and black earths on second terraces. |

**Table 2.2** Soil landscape and associated soil units (Kovac and Lawrie, 1991)

| Soil Landscape | Location | Associated soil units |
|---|---|---|
| Merriwa | Dominant soil landscape and covers the terraces and floodplains with basaltic alluvium on the Merriwa Plateau and in the Wybong area | Alluvial Soils (sands, loams), Chernozems, Grey Clays, Brown Clays, Black Earths on second terraces and Prairie Soils. |
| Sandy Hollow | Dominant soil landscape associated with drainage lines and gentle slopes throughout the Wybong area | Yellow Solodic, Brown Solodic, red solodic Deep Sands, Alluvial Soils, Siliceous and earthy sands. |
| Lees Pinch | Minor soil landscape associated with steep outcropping sandstone hills | Shallow (Siliceous) Sands, shallow loams. Yellow Soloths, Grey Soloths, Brown and Yellow earths, Yellow Podzolic Soils and earthy sands. |
| Dartbrook | Minor soil landscape associated with the undulating slopes and low hills | Brown Clays, Black Earths |
| Castle Rock | Minor soil landscape associated with undulating low hills | Permian sandstone, conglomerate Stony solodic soils, alluvial soils and other sediments. |
| Hunter | Minor soil landscape associated with flat alluvial plains of the Hunter River | Black Alluvial Clay, Brown Clays |
| Wollombi soil landscape | Minor soil landscape channel and the floodplain area of Wybong creek | Alluvial soils (Sands, Earthy Sands) |

## 2.7 Climate

Climate of the study area will discuss briefly in Chapter 3 of Section 3.3.1. Climate within the region is subhumid with significant variation in the annual rainfall and evaporation during the year, and a high variability of rainfall throughout the catchment. The average rainfall within the Wybong catchment for the period 1903 to 2008 is 638 mm $year^{-1}$ (Bunnan Station # 61007). On average, rainfall is slightly summer dominated. A number of periods during the last decade have witnessed below-average rainfalls with moderately dry years occurring from 1994 to 1997 and exceptionally dry conditions occurring from 2002 to 2006.

The average annual pan evaporation at Scone (Station #61089 is 1633 mm for the available record of 1972-2008. Analysis of the historical record shows an expected seasonal variation in evapotranspiration increasing during the summer months and decreasing during the winter months. Summers in the region are relatively hot with average maximum January temperatures of approximately 29–32°C. The average minimum temperature ranges from $16.9^0$C in summer to $4.7^0$C in winter.

## 2.8 Vegetation

Vegetation cover along the length of Wybong Creek is fairly inconsistent in density with pasture and Willows (*Salix sp*) being the most dominant vegetation within the riparian zone. In the upper reaches on the Liverpool Range native vegetation still dominates but this quickly gives way to pasture and more exotic species moving downstream along Wybong Creek. The Manobalai Nature Reserve is dominated by native vegetation but this area only makes up 3.3% of the catchment and therefore has limited affect on vegetation communities along the lower reaches of Wybong Creek. Much of the riparian vegetation that would have originally occurred along Wybong Creek has been cleared and/or lost through bank erosion and in some areas no riparian vegetation exists at all. Weeds compete with other plants and can eventually replace native species through competition for moisture, light and nutrients. As a result of saline discharges from the catchment salt tolerant species such as Swamp Oaks (Allocasuarina) have increased in numbers along the lower reaches of Wybong Creek (NSW Department of Infrastructure, Planning and Natural Resources, 2002).

There are over 784 known native species in this area. Originally Eucalypt woodland dominated the Wybong catchment consisting of Ironbarks, snow gum (Eucalyptus pauciflora), mountain gum (E. dalrymplena), grey gum (E. punctata), *Casuarina cunninghamiana* (river oak). Other common tree species include *Angophora floribunda* (roughbarked apple), *Eucalyptus melliodora* (yellow box), *E. tereticornis* (forest red gum), *E. moluccana* (grey box), apple box (E.bridgesina) and occasional *E. albens* (white box), rusty fig (Ficus rubiginosa), Dywers red gum (E.dwyeri), Callistris sp and silver-top stringybark (E. laevopinea). Ground cover species include wallaby grasses *(Danthonia* spp.), corkscrew grass (*Stipa setacea*), Queensland blue grass *(Dichanthium sericeum*), kidney weed (Dichondra repens) and three awn spear grass (*Aristida ramosa*) (NSW Department of Planning 2005).

## 2.9 Land Use

Various agricultural and residential activities are reliant on Wybong Creek and related surface water run-off and groundwater aquifers. Lower areas are mainly used for irrigated agriculture for beef cattle and pastoral grazing. Some crops, including wheat, oats, barley and grain sorghum, are grown on the Wybong Creek alluvial floodplain. A thoroughbred racehorse spelling facility has been established at the confluence of Wybong and Dry Creeks.

Wybong Creek valley has the potential for the development of more intensive agricultural industries such as vineyards or olive groves although these may be limited by the availability of water and its quality. The rugged, elevated land flanking the Wybong Creek valley is heavily vegetated and is mainly Crown Land (Mackie Environmental Research 2006). This area has also been partly subdivided for rural residence and used for tourism. Many areas are cleared and coal mines have been established in the Wybong area, 20 kilometres west of Muswellbrook and approximately 10 kilometres north of the township of Denman. Land clearing may have increased the portion of water mobilized to the fresh water system via throughflow or groundwater discharge, and thus increases the solute concentration entering the stream from the landscape through decreased evapotranspiration of replacement pastures and crops.

## 2.10 Surface Water System

Wybong Creek runs north-south with long sloping flanks from the catchment boundaries. Wybong Creek is the most westerly catchment of the Goulburn/Hunter River System, flowing as a left bank tributary into the Goulburn River (see **Figure 2.1**). The Goulburn River joins the Hunter River approximately 4.8 kilometers downstream from Denman. The headwaters of the catchment are in the Liverpool ranges to the north. Wybong creek in upstream to Goulburn river ranges in width between 80 to 100 meters with bank heights ranging from 2.5 meters to in excess of 20 meters in some locations (NSW Department of Infrastructure, Planning and Natural Resources, 2002) but bank heights are typically 10 to 12 meters. Slopes within the catchment vary from approximately $1^0$ to $3^0$ in low lying floodplain areas in the south of the catchment, to up to $45^0$ in the upper slopes in the north of the catchment, including those surrounding

Pendle Mountain and Black Mountain in the Liverpool ranges (Mackie Environmental Research 2006).

Wybong creek exhibits a wide diversity of instream habitats. Pool and riffle habitats are common, with pool/riffle sequences evident in the low flow channel. The Creek flows from confined headwaters through a partly confined valley and then into a wider valley (DLWC, 2000). A narrow strip of alluvial fill composed of sand or boulders with minor clay lenses is associated with the water source. The channel of the stream in the lower section traverses sand and gravel bed reaches with some bed rock outcrops. The rocky sandstone and conglomerate outcrops within an extensive system of surface and groundwater catchments, channelling rainfall run-off into the various creek lines and recharging groundwater aquifers that feed the stream. **Figure 2.6** shows an elevation profile along Wybong Creek with the different geomorphic categories in relation to the elevation.

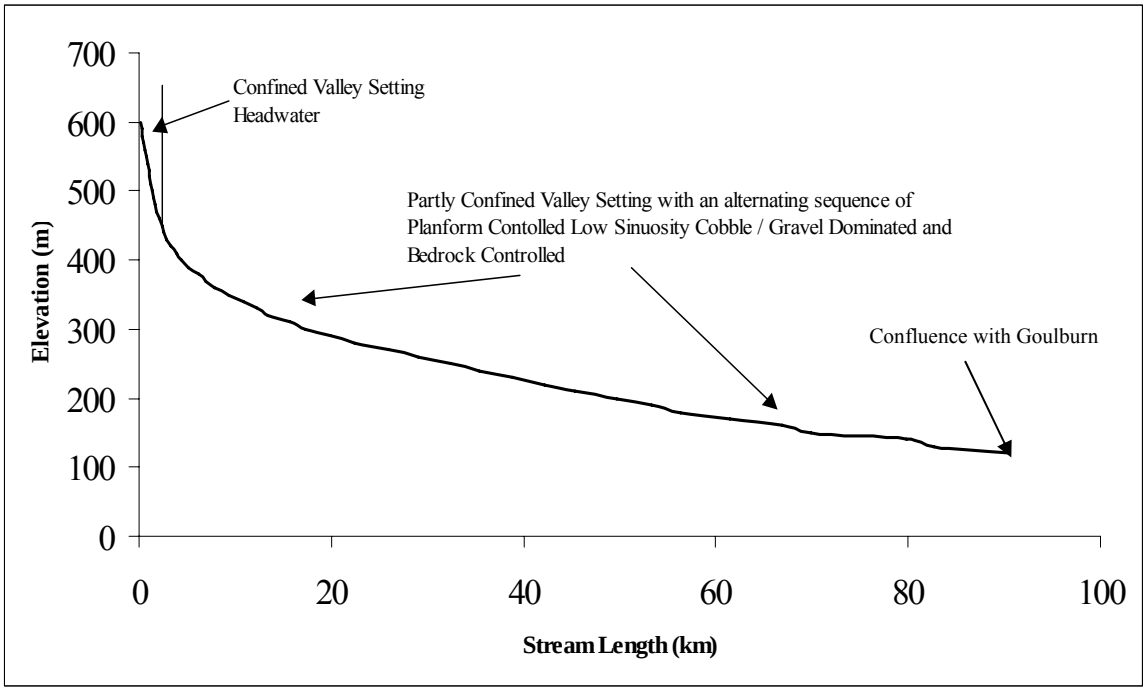


**Figure 2.6** Elevation Profile along Wybong Creek showing the different geomorphic categories in relation to the elevation.

### 2.10.1 Flow Characteristics

Wybong Creek has large variation in both annual and daily flows. The river flow recorded at the downstream gauging site is probably not representative of the flow in the

upper catchment as the lower catchment has a much larger alluvial storage. In dry periods, the water-bearing aquifers continue to contribute flow to the Creek for a considerable period. However, the upstream flow has to fill the alluvial storage that is depleted by evapo-transpiration during prolonged dry periods before a flow at the gauge is recorded. The Creek experiences zero daily flow approximately 15% of the time. Flows in excess of 100 ML/day occur less than 10% of the time, and flows in excess of 1,000 ML/day are measured less than 1.5% of the time (NSW Department of Planning, 2005). During periods of zero flow, water remaining in Wybong Creek forms refuge pools which provide critical habitat for aquatic species and protect the organisms which recolonise the stream when flow recommences.

The Creek is highly connected to an alluvial aquifer system (NSW Department of Planning, 2005). The cross-sectional area of catchment alluvial aquifer is 5265 $m^2$ where alluvium aquifer is recharged at the rate of about 6000 ML/year. About 3000 ML of this (10% of the annual stream flow of 30000 ML/year) is believed to be direct recharge from stream. The stream has been assessed as highly stressed due to high levels of extraction, unstable stream banks, streambed degradation and high environmental stress i.e., sedimentation, high levels of salinity and high levels of nutrients (NSW Department of Planning 2005). Surface water flow in this system has been fully allocated.The Water Sharing Plan negotiated by the Wybong Water Users group identified a Cease to Pump level on the Wybong Creek when flow fells to 0.5 ML/day.

### 2.10.2 Stream Water Quality

Wybong Creek is characterised by high salinity, high nutrient and sediment levels, and poor macro invertebrate (NSW Department of Planning, 2005). The creek is a highly saline stream with an average EC of 1560 μS/cm and a maximum recorded value of 3517 μS/cm (NSW Department of Planning, 2005). Water quality data for the lower section suggests that the creek is a source of relatively poor quality water as salinity levels exceed the ANZECC water quality Guidelines for Fresh and Marine Waters (1992) for aquatic ecosystems. Stream water is only suitable for irrigation of salt tolerant crops and watering most stock. Recent investigations show that the condition is worsening with the latest maximum obtained EC of 5460 μS/cm (Mackie Environmental Research 2006). Upstream pH ranges (7.44- 8.32) and downstream

ranges (7.19-8.9) indicate that the water is neutral to alkaline. Turbidity is extremely variable but it has been classified as relatively good to for low flows (NSW Department of Planning, 2005). The unstable stream banks and degraded streambeds evident in Wybong Creek deliver high levels of silt and sediments during rainfall, and the ensuing high flow events. During low and no flow periods, sediment is deposited in the stream channel where it is remobilized during elevated flow events.

## 2.11 Groundwater System

The upper Hunter Region hosts three recognised types of aquifer systems, alluvial aquifers, hard rock aquifers and aquifers in the shallow weathered zone or regolith (Mackie Environmental Research 2006).

### 2.11.1 Alluvial Aquifers

The alluvial aquifer of the catchment consists of the unconsolidated sediments (sands, pebbles, gravels, silts and clays) of the floodplains of the Wybong Creek (Kellet *et al*. 1989). The alluvial aquifer has a significantly higher water storage capacity than the underlying rock. The differences in aquifer storage capacity and a wide variation in saturated thickness results in wide range of potential for groundwater flow. Unconsolidated materials in the alluvial lands are mostly silty and clayey and with low hydraulic conductivities and are semi-confined at depth. These shallow aquifers generally exhibits high salinity, with EC values ranging from 5,000 to more than 20,000 µS/cm. Bore yield in alluvial the aquifer about 0.21 L/s (NSW Department of Planning, 2005).

### 2.11.2 Hard Rock Aquifers

**(a) Tertiary basalt:** Tertiary basalt flows cover much of the north portion of the Wybong Creek catchment. The basalt terrain can be quite productive in terms of groundwater. The highest yields occur where a combination of gas cavities are interconnected with joints, fractures and faults (NSW Department of Planning, 2005). Other aquifers associated with the basalt can form due to weathering and erosion on the surface of the lava sheet prior to subsequent lava flows. The water quality associated with basaltic terrain generally good with low salinity. However, in some locations the

water may exhibit hardness due to calcium and magnesium carbonates or may be slightly acidic and contain iron. Bore yield in the Tertiary aquifer typically 5 L/sec (NSW Department of Planning, 2005).

**(b) Permo-Triassic sedimentary rocks:** Underlying the basalts are shallow marine and continental Permo-Triassic sedimentary rocks. Permeable zones of the Triassic Narrabeen Group of sedimentary rocks are occasionally associated with coarser grained materials containing relatively higher pore space. However, secondary porosity features, such as bedding plane partings and the network of joints, are the predominant pathways for permeability. Bores yields are generally in the ranges 0.2 to 2.5 L/sec (NSW Department of Planning, 2005). Groundwater quality is good with total dissolved solids usually less than 1,000 mg/L and pH (around 6) which may reflect high levels of iron (Mackie Environmental Research 2006).

**(c) The Permian rocks/ Coal seam aquifers:** The Permian rocks can be subdivided into the Upper and Lower Coal Measures and the intervening Marine Sequence. The saline water associated with this geological unit is thought to have a controlling influence on the overall water quality of the Hunter River (Kellet *et al*. 1989). The fine grained, consolidated nature of these rocks is reflected in a low primary porosity, with most groundwater flow associated with secondary faults, fractures and joints. The coal seams exhibit many joints and cleats and are the main aquifers within these rocks. Groundwater quality is generally brackish to saline (Mackie Environmental Research 2006). Salinity within the hard rock aquifers associated with the Hunter coal seams is typically around an EC of 4,000-12,000 μS/cm, but has been recorded at over 26,000 μS/cm. The pH values range from 5.78 to 9.18 with an average around 7.1 (NSW Department of Planning 2005).

Water tables and pressures in the coal measures appear to be sustained by rainfall percolation into out-cropping strata at a generally low rate. Estimates of rainfall recharge varying from zero to no more than 2% of annual rainfall based upon previous studies in the Upper Hunter region (Mackie Environmental Research 2006).

### 2.11.3 Weathered Zone or Regolith

Parts of the overlying weathered zone or regolith act as an intergranular aquifer storage. These zones may source springs following periods of high rainfall but most are depleted during extended dry and drought periods. Water quality is variable from fresh

to saline (Mackie Environmental Research 2006). Water tables in the regolith can be isolated from deeper coal measures through the presence of the massive and relatively impermeable conglomerates that overly the coal seams. This isolation is however likely to be interrupted at locations where vertical faulting provides a connecting pathway to deeper strata. These same pathways could also facilitate charge to deeper strata or vertical mixing of groundwaters (Mackie Environmental Research 2006).

## 2.12 Water Sharing Plan for Wybong Catchment

Wybong Creek is associated with a narrow strip of alluvial fill composed of sand or boulders with minor clay lenses. Anecdotal and scientific observations of the water source suggest that surface and ground water are highly connected (NSW Department of Sustainable Natural Resources 2003). The alluvium is essentially continuous and has a significant store of water. Extraction from it is expected to impact on the stream flow. Equally, extraction from the creek itself will access groundwater. A water sharing plan for Wybong Creek Water Source is based on the notion that the surface and groundwater sources should be managed as a single resource. The water sharing plan for Wybong catchments was implemented on 1$^{st}$ of July 2003 under the Water Management Act 2000 (WMA). The plan was initially proposed for the 10 year period until 30$^{th}$ June 2013. Under the Water Management Act 2000 (WMA), water sharing plans define the water sharing arrangements between the environment and water users, including towns, domestic, stock watering, irrigation, Aboriginal cultural and spiritual needs, and recreational activities. The plans are designed to provide for healthier rivers and aquifers and dependent ecosystems. The objectives of the plan are to

(a) Protect natural water levels in pools during periods of no flows.
(b) Protect natural low flows and restore a proportion of moderate flows (freshes) and high flows.
(c) Protect, maintain or restore the natural inundation patterns and distribution of floodwaters supporting natural wetland and floodplain ecosystems.
(d) Maintain groundwater within natural levels and variability critical to surface flows and ecosystems.
(e) Minimise the impacts of in-river structures.
(f) Ensure river flow management provides for contingencies.

(g) Maintain or improve the ecological condition of the water source and its riparian areas over the longer term.

(h) Recognise and protect the contribution of this water source to downstream water sources' environmental and basic right requirements

(i) Maintain water supply priority for basic landholder rights which is estimated at 1.8 ML/day.

(j) Provide an agreed level of water sharing for irrigation and other industry.

(k) Recognise and protect traditional values of water to aboriginal people, and

(l) Contribute to the achievement of water quality to support the environmental values of this water source (NSW Department of Sustainable Natural Resources, 2003).

At the start of the Plan, the requirements identified for unregulated, domestic and stock access licences from the stream water source total approximately 7,942 ML/year. In addition, aquifer access licences total approximately 267 ML/year (NSW Department of Sustainable Natural Resources 2003).

Total daily extraction limits (hereafter *TDEL*) specify the volume available for extraction from low, medium and high flows on a daily basis. The limits set by the plan for each flow class as follows:

- For surface water licences

(a) When the flow at the end of the river is between <0.5 and <1 ML/day for the very low flow class, this limit is 0 ML/day.

(b) When the flow at the end of the river is between 0.5 and 7 ML/day for B class (or medium flows) flows, this limit is 7 ML/day.

***Note.*** *7 ML/day represents 28% of the top of B class flows for the critical month (December) and 50% of the estimated recharge of groundwater (expressed on a daily basis).*

(c) Between 7 and 16 ML/day for C class (or high flows) flows, the limit is 13.5 ML/day.

***Note.*** *13.5 ML/day represents 40% of the top of C class flows for the critical month (December) and 70% of the recharge (expressed on a daily basis).*

(d) Between 16 and 100 ML/day for D class or very high flows, the limit is 21 ML/day.

***Note.*** *21 Ml/day represents 13% of the 15th percentile flows for the critical month (December) and 70% of the recharge (expressed on a daily basis).*

(e) At flows above 100 ML/day for E class (or extremely high flows) flows, the limit is 37 ML/day.

***Note.*** *37 ML/day represents 30% of the 15th percentile in the critical month (December) and 70% of the recharge (expressed on a daily basis).*

For aquifer licences, when the flow at the end of the river is at or below 0.5 ML/day on a falling river or 1 ML/day on a rising river, this limit is 0 ML/day. Between 0.5 ML/day (on a falling river) or 1 ML/ day (on a rising river) and 7 ML/day, this limit is 5 ML/day. At all other times, the limit is 7 ML/day.

Water level management

(1) In order to protect groundwater levels within the aquifer in this water source, local access rules are to apply in a defined area known as a local impact area.

(2) If water levels in any part of the aquifer in this water source have declined to such an extent that adverse impact is occurring, or is likely to occur, extraction from all water supply works (bores) within a local impact area declared under subclause (1) from which access is authorised by an aquifer access licence will be restricted to such an extent and for such time as is required to reinstate water levels to such a degree as to mitigate or avoid that impact.

**Note:** This provision recognises that in some locations, at certain periods of high groundwater demand, critical water level declines may occur, and that additional extraction limitations may be required.

## 2.13 Wollombi Brook Catchment Overview

The Wollombi Brook Catchment is a right bank sub-catchment of the Hunter River and is located approximately 150 km north of Sydney in Australia. A map and satellite image of the Wollombi Brook Catchment is shown in **Figure 2.7 and Figure 2.8.** The Wollombi Brook Catchment has steep topography, bounded to the south-east, where the highest peak is 640 m AHD. Its lowest point is 60 m AHD at its northern boundary where the Wollombi Brook meets the Hunter River. The catchment area is 1682 $km^2$ and 80% of this area is forested (DLWC, 2000). The primary fresh water resource users in the catchment are agricultural enterprises, predominantly viticulture and beef.

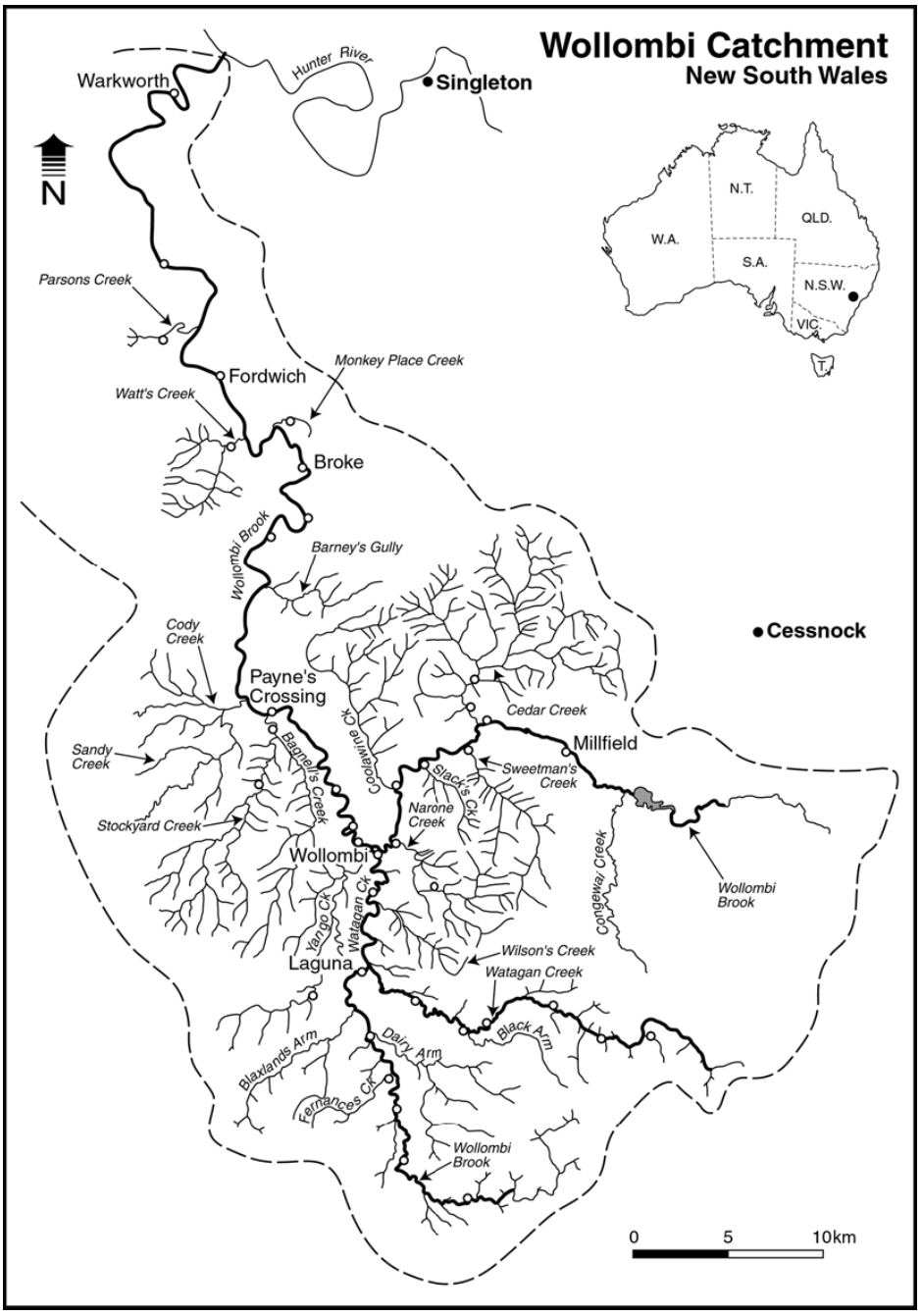


**Figure 2.7** Map of the Wollombi Brook Catchment (Source: Pritchard, 2005)


**Figure 2.8** Satellite image of the Wollombi Brook Catchment. Source: Google Earth

### 2.13.1 Climate

The Wollombi Catchment has a temperature sub-tropical climate, characterised by hot summers and mild winters. Daily maximum temperatures average around 29ºC during summer and 18ºC during winter at Broke (1957 to 2002). Average minimum temperatures range between 17ºC during summer and 6ºC in winter. Mean annual rainfalls (over a period of 111 years) in the lower Wollombi Catchment at Broke are 651 mm (1889 to 2002) and 856mm (1973-2004 as shown in **Figure 2.9a**), however precipitation increases with elevation. Rainfall is summer-dominated, with more than

30% of annual rainfall occurring between December and February at Broke. Less than 20% of annual rainfall typically occurs during winter. The mean annual rainfall at Brooke is exceeded by the mean pan evaporation (1510 mm), however, average monthly rainfall exceeds pan evaporation between April and July as shown in **Figure 2.9b (**Pritchard, 2005).

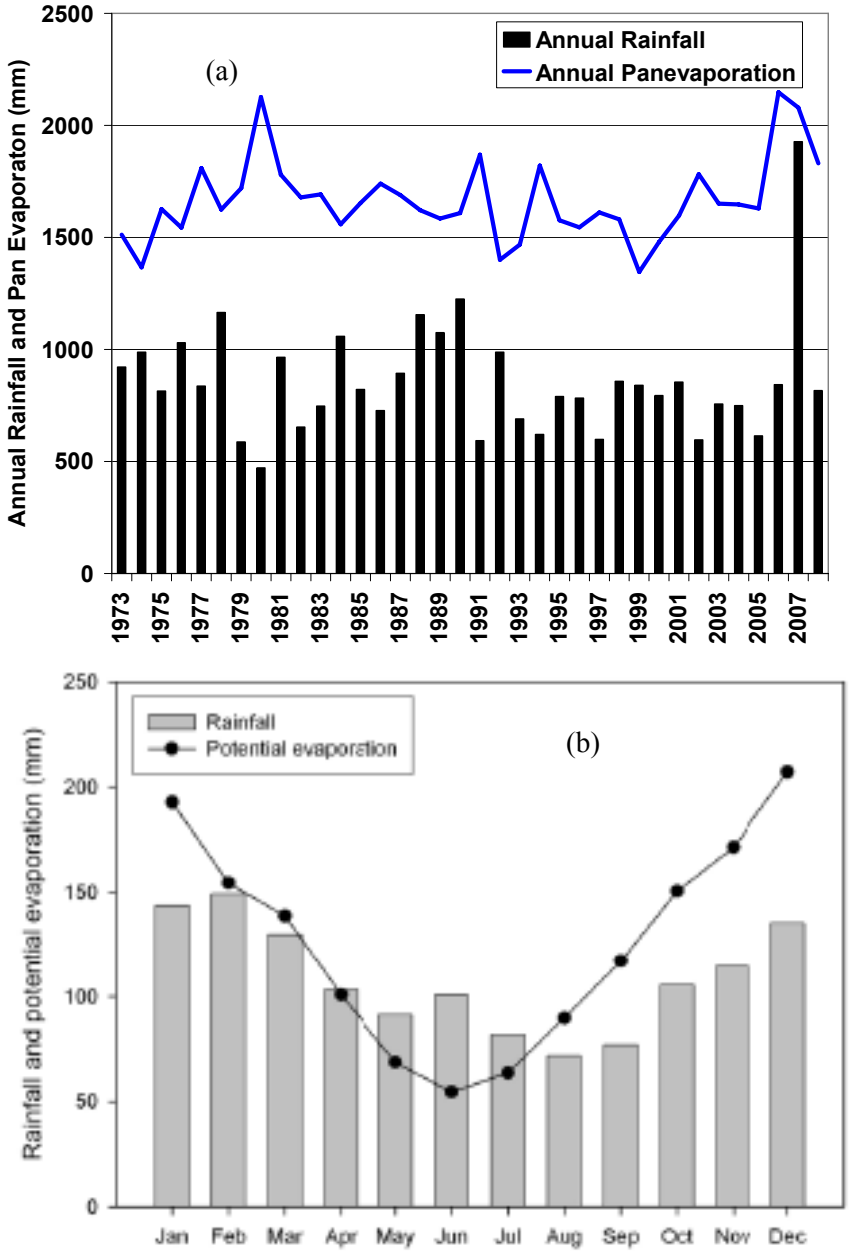


**Figure 2.9** Relationship between **(a)** mean monthly rainfalls (1973 to 2004) and evaporation (1972 to 2002) **(b)** mean monthly rainfalls (1889 to 2002) and potential evaporation (1972 to 2002) at Wollombi Brook taken from Pritchard (2005)

### 2.13.2 Stream Characteristics

Stream flow in the lower Wollombi Brook is perennial, with peak stream flows typically occurring during summer and early autumn (January to March) and gradually decreasing flows throughout the rest of the year (Warkworth). Annual flow of the Wollombi Brook is typically greater than 2% and less than 7% of total flow. Wollombi Brook is a sand bed stream with high transmission losses of water. It can be thought of as intermittent in that dislocation of the main channel occurs most years. Pools become isolated from the main channel and stream discharge is highly responsive to rainfall events. It is likely that these pools and the water in the channel itself remain connected via groundwater in a shallow alluvial aquifer during these periods (Pritchard, 2005).

### 2.13.3 Groundwater System

Two main aquifer systems exist in the Wollombi Brook Catchment, these are the shallow alluvial aquifers associated with Wollombi Brook and its tributaries, and the regional hard rock aquifer (Mackie Environmental Research 2006). The shallow alluvial aquifer is comprised of unconsolidated Quaternary alluvium (interlayered silty to coarse sands and silty to coarse gravels) generated by flood erosion and deposition (Erskine 1994). The alluvial aquifer overlies the regional aquifer system that predominantly consists of Triassic sandstone with some shale. This is the main surficial aquifer in the south-western catchment area, Permian sediments (sandstone, shale, mudstone, conglomerate and coal) derived from ancient marine sediments, which outcrops upstream of Millfield and downstream of Broke occur in the north-eastern catchment area. The regional aquifer also contains Tertiary basalts that outcrop east of Fordwich, and Permian tuff, lava sandstone, siltstone and conglomerate, and Carboniferous sediments with some volcanics that outcrop north of Millfield (Erskine 1994).

## 2.14 Goulburn River Catchment

The Goulburn River is a right bank tributary to the Hunter River in New South Wales, Australia (**Figure 2.1** and **Figure 2.10**). The catchment area of the Goulburn River is 6540 $km^2$ and average stream flow from the Goulburn represents approximately 23% of total average flow in the Hunter Valley system (Monika, 2006). The Catchment extends from $31^0$46`S to $32^0$51`S and $149^0$40`E to $150^0$36`E, with elevations ranging

from around 100 m in the floodplains to around 1300 m in the northern and southern mountain ranges.

The catchment includes floodplains, undulating hills, and mountainous terrain, basalt-derived soils in the north and sandstone-derived soils in the south. The geology of the Goulburn River catchment can be distinguished into two types: the north, which is predominantly Tertiary basalt (Atkinson, 1966; Story *et al*., 1963), a product of Cainozoic volcanism that took place throughout much of eastern Australia (Branagan and Packham, 2000); and the south, which is dominated by rocks of the Triassic age laid down as sediments in lagoons and consisting of sandstone, conglomerate, and shale (Story *et al*., 1963). The Goulburn River runs generally from west to east, with tributaries from the north and south, so that the catchment is dominated by easterly and westerly aspects.

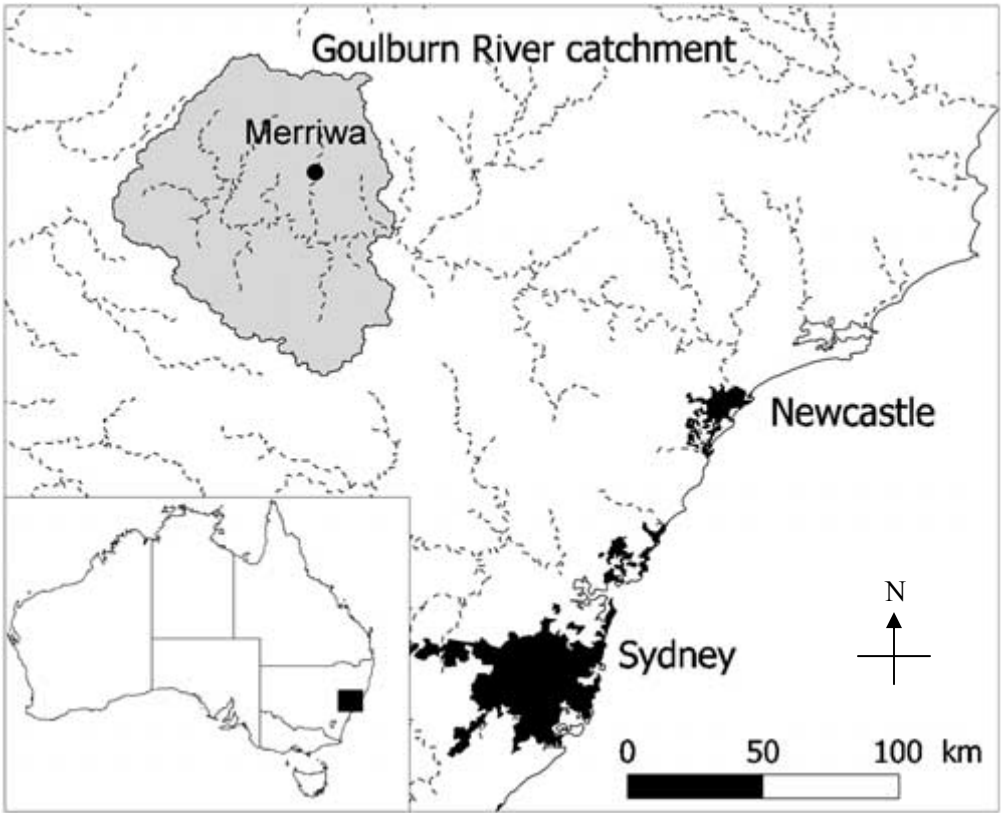


**Figure 2.10** Regional map showing the location of the Goulburn River

### 2.14.1 Climate

The general climate within the region is subhumid or temperate (Stern *et al*., 2000), with significant variation in the annual rainfall and evaporation during the year, and a

high variability of rainfall throughout the catchment (Bridgman, 1984). While the average annual rainfall in the Goulburn River catchment is approximately 650 mm, it varies from 500 to 1100 mm depending on altitude. Major rainfall events generally occur from November to March with an average monthly precipitation of 68 mm, while the monthly average precipitation in June is 32 mm. The average annual pan areal evaporation for the study region is about 1300 mm, with a maximum of 1360 mm and a minimum of 1240 mm. The minimum monthly pan evaporation is in July with an average of 50 mm, and a maximum in January reaching 180 mm. Monthly mean maximum temperatures reach approximately $30^0$C in summer and $14^0$C in winter, with mean minimum values of $16^0$C and $2^0$C, respectively (Australian Bureau of Meteorology, 1988). Except for elevated areas, frost is unlikely to occur during daytime in winter, but night time minimum temperatures in winter are frequently less than $0^0$C.

## 2.15 Concluding Remarks

Based on the study site description, the saline water associated with the geological units (Quaternary Alluvium, Tertiary basalt, Triassic sandstone and conglomerate, Permian coal, shale deposits) are considered to have a controlling influence on the overall water quality of the Hunter River. Salinity problems occur in the Wybong catchment as the Creek is highly connected to an alluvial aquifer system. Shallow aquifers generally exhibit high salinity, with EC values ranging from 5,000 to more than 20,000 μS/cm. Water quality of the Wybong catchment is poor and considerably high salinity of lower catchment with an EC of 5460 μS/cm. The reason for these high levels of salinity is ground water accession from a fault line and also salinity leakage from deeper aquifers into alluvial aquifers and streams, via changes in the hydrologic regimes in catchments.

Land clearing may have increased the portion of water mobilized to the fresh water system via throughflow or groundwater discharge, and thus increases the solute concentration entering the stream from the landscape. Coal mining in the area also has major impacts on groundwater due to loss of coal measure aquifer pressure and leakage of groundwater from shallow alluvial aquifers.

Climate of the region is highly variable with significant variation in the annual rainfall and evaporation during the year, and a high variability of rainfall throughout the catchments. Rainfall variability and extraction from the creek itself will access

groundwater and expected to impact on the stream flow. Wybong Creek has large variation in both annual and daily flows and experienced zero daily flow during the dry years.

Average annual rainfall in the Goulburn River catchment is approximately 650 mm. The Goulburn Rivers flows through Triassic sandstones, Tertiary basalt rocks in the west and Carboniferous rocks in the north. Streams are classified as having highly-connected surface and groundwater systems.

Wollombi Brook catchment is characterised by hot summers and mild winters. The mean annual rainfall (651 mm) at Wollombi Brooke is much less than the mean annual pan evaporation (1510 mm). The annual flow of the Wollombi Brook is typically greater than 2% and less than 7% of total flow of the Hunter River. Wollombi Brook is a sand bed stream with high transmission losses of water and its stream discharge is highly responsive to rainfall events.

In the next chapters, long-term changes in rainfall and its impact on stream flow, stream salinity sources, process and interaction between surface-groundwater in the Wybong Creek catchment will be discussed.

# CHAPTER 3: CLIMATE CHARACTERISTICS AND WATER YIELD

This chapter examines the long-term changes in rainfall and its impact on stream flow in the Wybong Creek catchment, Hunter River. The impact of climate variability on runoff is analysed using a nonparametric percentile ranking method. Percentile ranking rainfall method is used to identify the severity of drought and floods. Stream discharge and climatic data are employed to analyse the impact of climate variability on catchment yield. Long-term changes in rainfall, drought, and their correlation with the Southern Oscillation Index (SOI) are analysed. Rainfall statistics and seasonality of rainfall are investigated and a relationship between runoff and rainfall using a regression model is developed for investigating runoff changes due to rainfall change. This chapter also analyses drought impact on catchment yield and finally, compares the percentile rankings of runoff and rainfall in order to investigate the influence of rainfall-runoff process.

## 3.1 Introduction

Rainfall variability in Australia occurs over a range of temporal scales from seasonal patterns, to year-to-year differences in annual totals, to decadal and longer term trends (e.g. Bureau of Meteorology, 1989; Cocks, 1992; Chiew *et al*., 1998; Chiew and McMahon, 2002 and Beeton *et al*., 2006). Nicholls and Wong (1990) demonstrated that variability is higher in regions of the world affected by the El Ninõ Southern Oscillation (ENSO), such as Australia.

Australian average temperatures have risen by between 0.5 and 1.0 $^{o}$C over the last century (IPCC, 2001). Global warming is predicted (Chiew, 2006) to change precipitation and evaporation patterns in Australia, which impact on catchment runoff. Changes in precipitation are amplified in runoff, while higher temperatures increase potential evapotranspiration, which may lead to a reduction in runoff and soil moisture levels. Climatological research (Speer, 2008) has associated changes in the variability in rainfall in eastern Australia with global warming. It is difficult however, to separate normal variability from changes due to global warming. Collins and Della-Marta (2002) and Gallant *et al*. (2007) found a statistically significant decrease in east coast rainfall in

Australia during the last century. The rainfall decline in the Southwest of Australia has been attributed to human-induced climate change with both large-scale atmospheric emissions (Timbal *et al*., 2006) and local land clearance (Timbal and Arblaster, 2006). Temporal climatic variability can significantly alter the hydrological cycle. In Western and South-Eastern Australia, catchment yields have unexpectedly declined since the late 1960's (Timbal and Jones, 2008). Longer term drying trends and wetting trends over 50 years cycles have been recorded in eastern Australia (Erskine, 1988). These trends are examined here in the Wybong Creek catchment.

## 3.2 Methods

### 3.2.1 Spatial Data:

A Digital Elevation Model (DEM) provided by Department of Natural Resources, DNR, with 25m resolution based on contour and streamline data mapped at 1:25,000 scale was used for generating the Wybong catchment boundary. Details of the procedures for generating the catchment boundary are given in appendix A.

### 3.2.2. Climate Data

#### 3.2.2.1 Rainfall

Monthly total rainfalls from 1903 to December 2008 were obtained from the Bureau of Meteorology (BOM) for all of Australia's rainfall gauges for generating monthly rainfall surface for Australia. Daily rainfall data for the Wybong catchment were also sourced from the BOM for 1903 to 2008 and were summed to monthly values. **Figure 3.1** shows the location of rainfall gauge station #61007 at Bunnan.

#### 3.2.2.2 Pan Evaporation

Monthly totals of pan evaporation data from 1972 to December 2005 were obtained from the BOM for all of Australia's pan evaporation gauges for generating monthly evaporation surface for Australia. Daily pan evaporation data from 1972 to 2008 were also obtained from the nearest pan evaporation to the Wybong station at Scone (#61089) and 30 km to the north-east of the catchment (**Figure 3.1**). The daily pan evaporation data for the Wybong were summed to monthly values. To approximate potential

evaporation, monthly evaporation was calculated by multiplying pan evaporation with a pan factor 0.67. In case of forests, the value of the pan factor was found close to 0.84, while for short grass and crops the value was close to 0.5 (Zhang, 1999). Since the Wybong catchment has about 55% forest cover, the pan factor was taken as the mean of these two extremes, 0.67. **Figure 3.1** shows the location of Scone pan evaporation gauge station #61089.


**Figure 3.1** Location of Bunnan, Denman and Scone rain gauge in Hunter region

### 3.2.2.3 Spatial Thin-Plate Smoothing Spline Interpolation of Data

Monthly rainfall and pan evaporation data are suitable for spatial interpolation because rainfall and evaporation processes are spatially consistent at the monthly time scale (Hutchinson, 1998a). In order to estimate the representative rainfall and pan evaporation over the catchment, each month of rainfall and pan evaporation data were

spatially interpolated. The monthly Rainfall and Evaporation surface for Australia used in this study was generated by using ANUSPLINE (Hutchinson and Kesteven, 1998).

Thin-plate smoothing splines (Wahba, 1990) were used for the spatial interpolation. Splines provide a global interpolation procedure using all of the data given to calculate the value at each interpolated point. A thin-plate smoothing spline is a surface (thin-plate) that does not pass exactly but smoothes through the data points to which it is fitted. Spatial correlation results from points that are spatially close being dependent. This violates the statistical assumption of independence of observations. Tri-variate splines were used with longitude, latitude and elevation as predictors. Elevation was in units of kilometres and the longitude and latitude in degrees. One degree is approximately 100 kilometres. Tri-variate splines were necessary because changes in elevation produce a change in rainfall of approximately 100 times the change that the same displacement in the horizontal direction would cause (Hutchison, 1995b). The software used to perform the spline fitting procedure was ANUSPLIN version 4.3 (Hutchinson, 2002). This software provided detection of possibly erroneous data by flagging values that were more than 3.6 standard deviations from the spline. This procedure used the requirement that the spline residuals be normally distributed (Sharples *et al*., 2005). Monthly Rainfall and Evaporation surfaces in the Hunter in January and July 2000 are shown in **Figure 3.2(a), 3.2(b)** and **3.2(c)** and **Figure 3.3(a), 3.3(b)** and **3.3(c).**

### 3.2.2.4 Extracted Climate Data within the Catchment Boundary

The catchment-wide rainfall was estimated by spatial interpolation of available monthly rainfall data across Australia from 16642 rainfall stations (source of data: BOM). Australia-wide monthly rainfall and evaporation surfaces from 1973 to 2005 were generated using the ANU spline program (Hutchinson, 2002) and then the Hunter region was extracted as shown in **Figure 3.2(b) and 3.3(b)**. The surfaces were 0.01 degrees (approximately 5km) grid resolution for rainfall in units of 0.1 mm. The monthly rainfall surface grids were projected and then clipped to the required Wybong catchment boundary. An ARC/INFO Macro Language (AML, geoprocessing script tool) routine was then used to calculate the area-weighted monthly rainfall for the catchment for each month of the record. Area-weighted monthly evaporation data were also calculated using the same procedure.

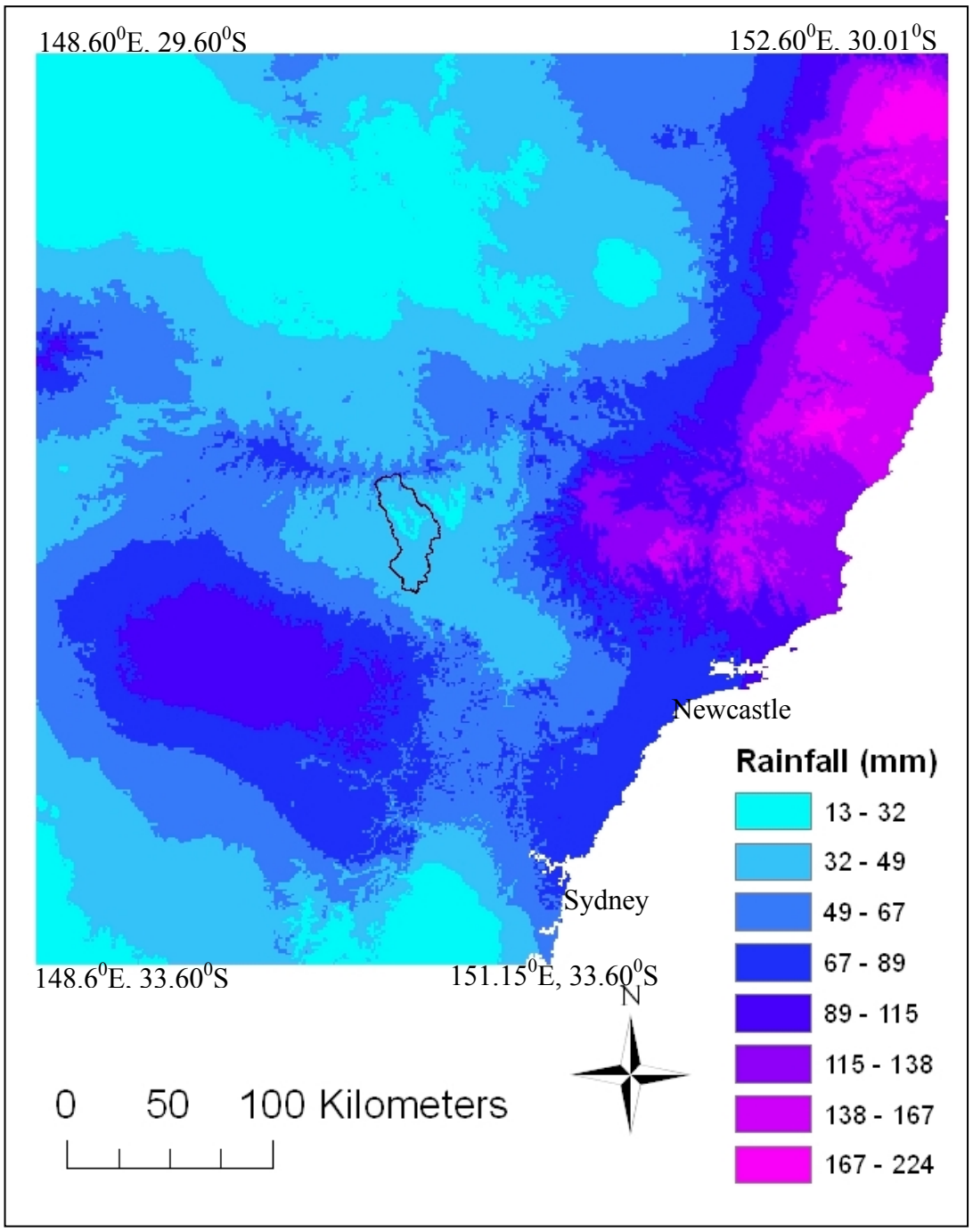


**Figure 3.2 (a)** Monthly rainfall surface for Eastern NSW for January 2000

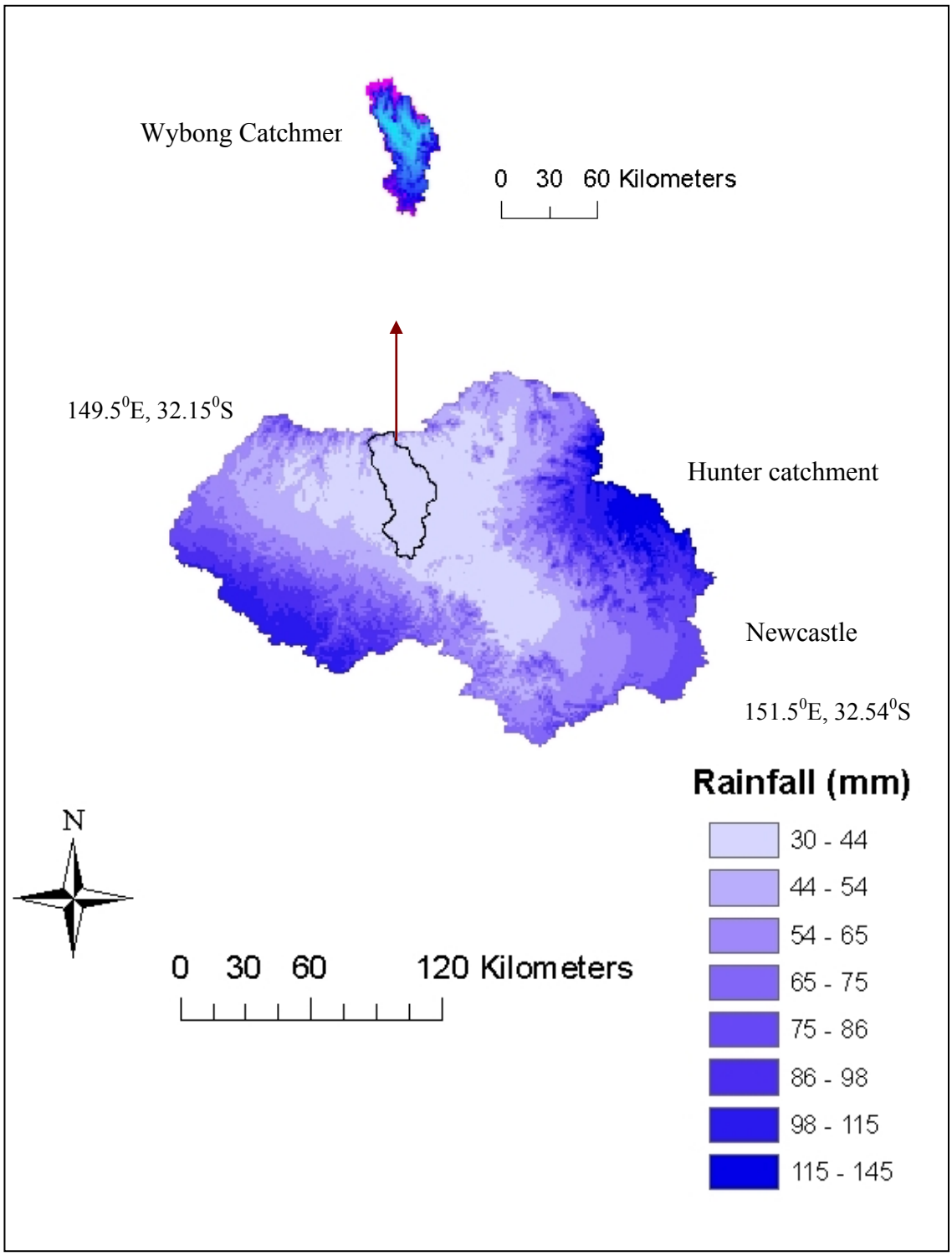


**Figure 3.2 (b)** Monthly rainfall surface for January 2000 for the Hunter region

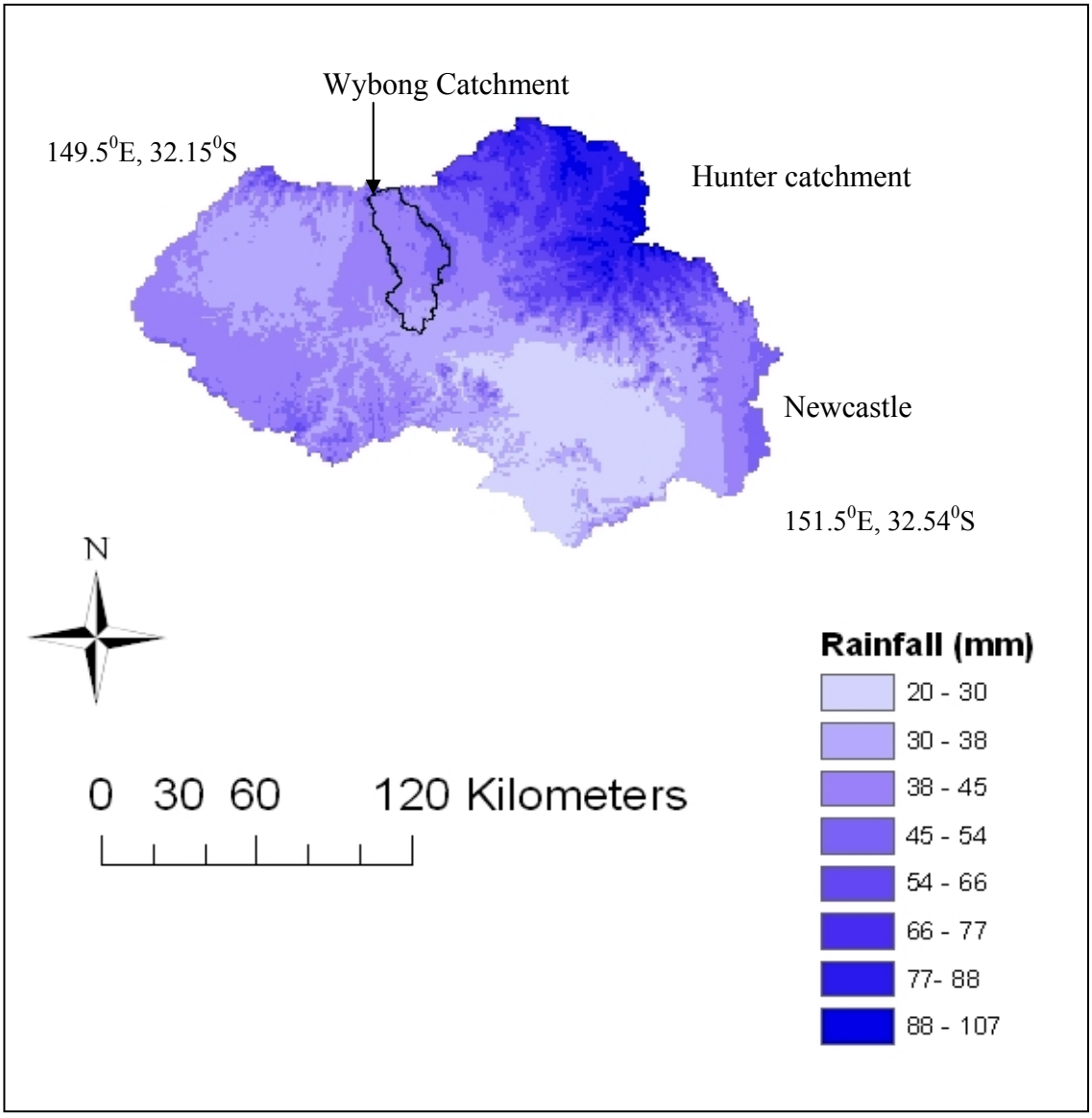


**Figure 3.2 (c)** Monthly rainfall surface for July 2000 for the Hunter region

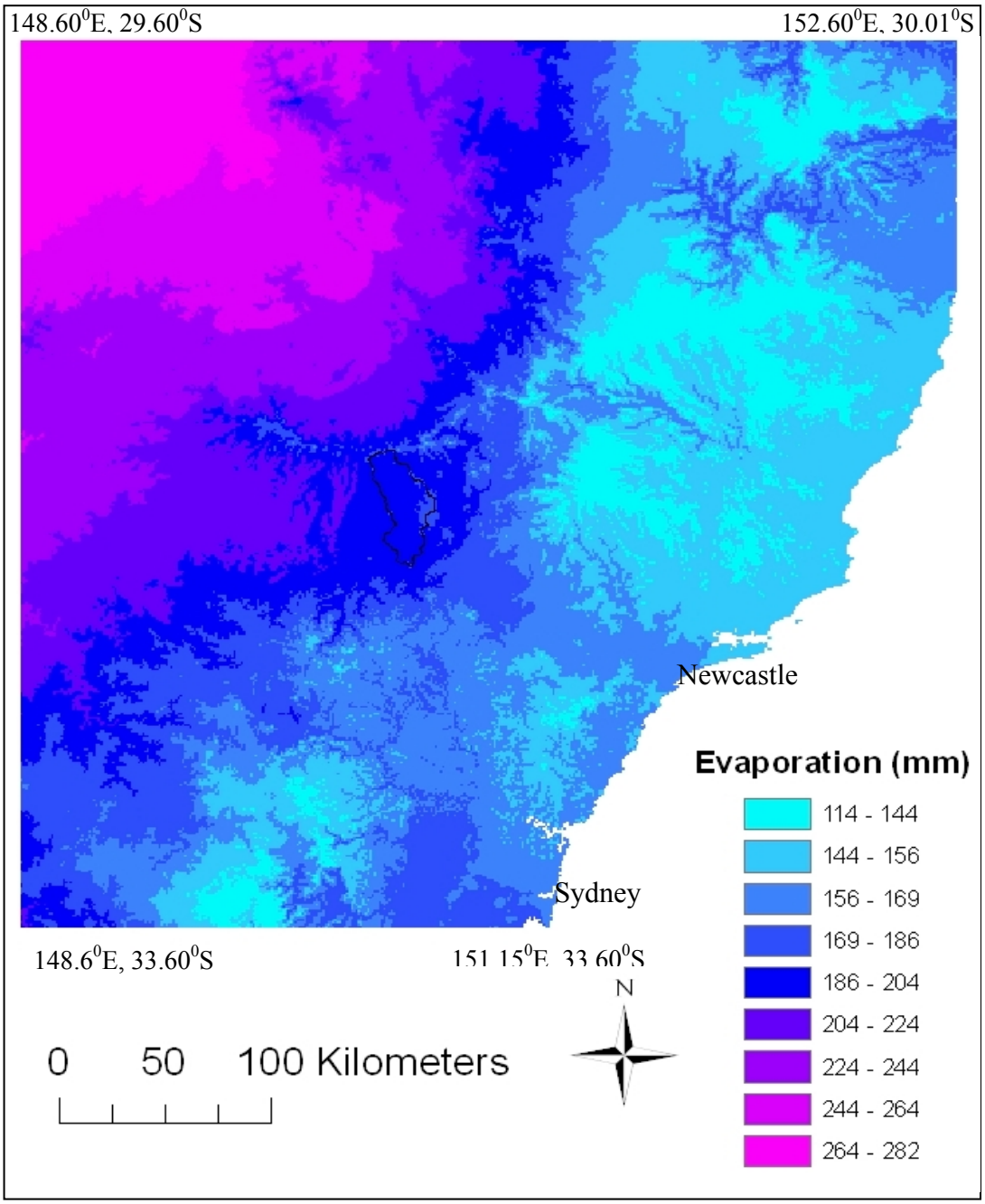


**Figure 3.3 (a)** Monthly pan evaporation surface for Eastern NSW for January

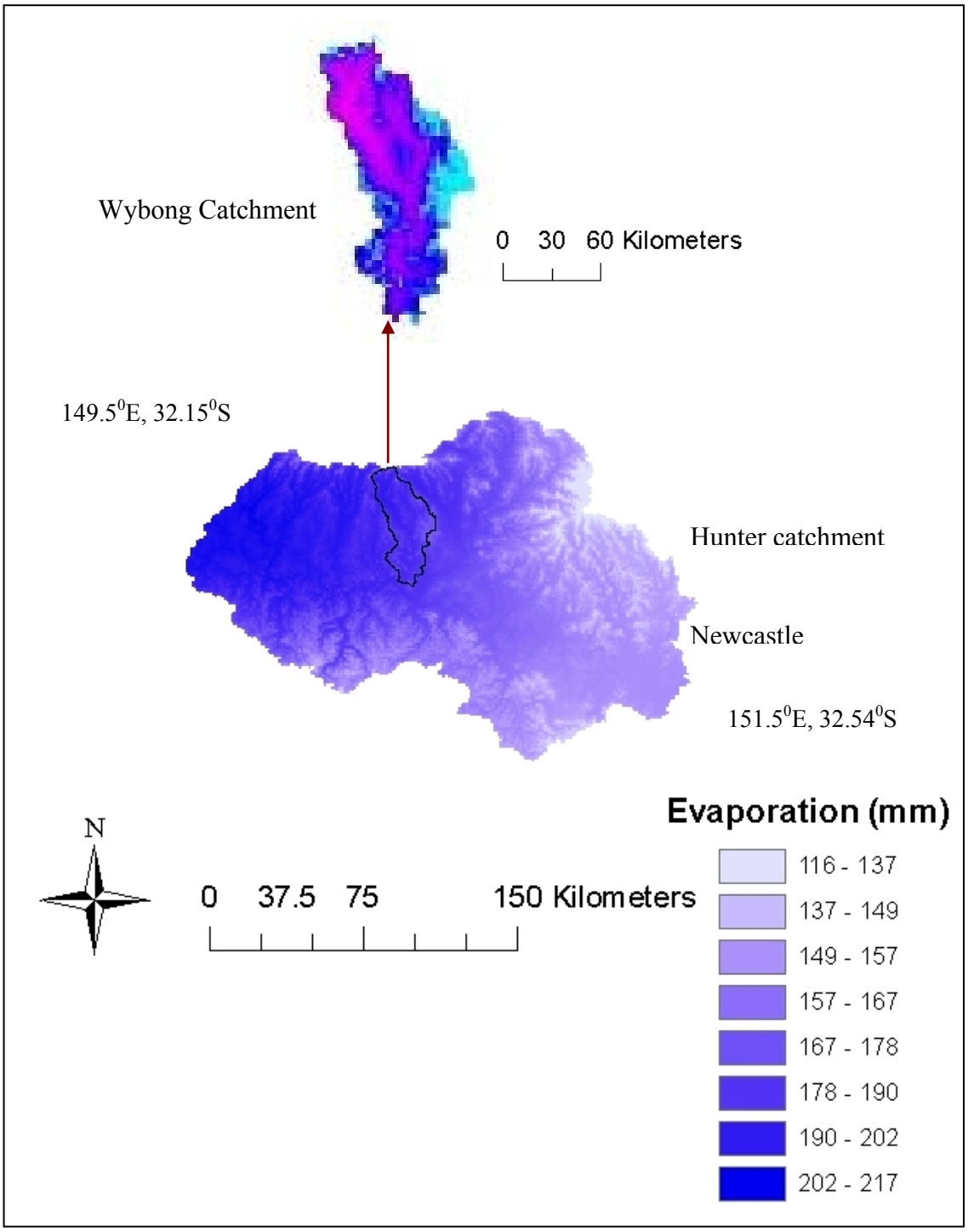


**Figure 3.3 (b)** Monthly pan evaporation surface for January 2000 for Hunter region

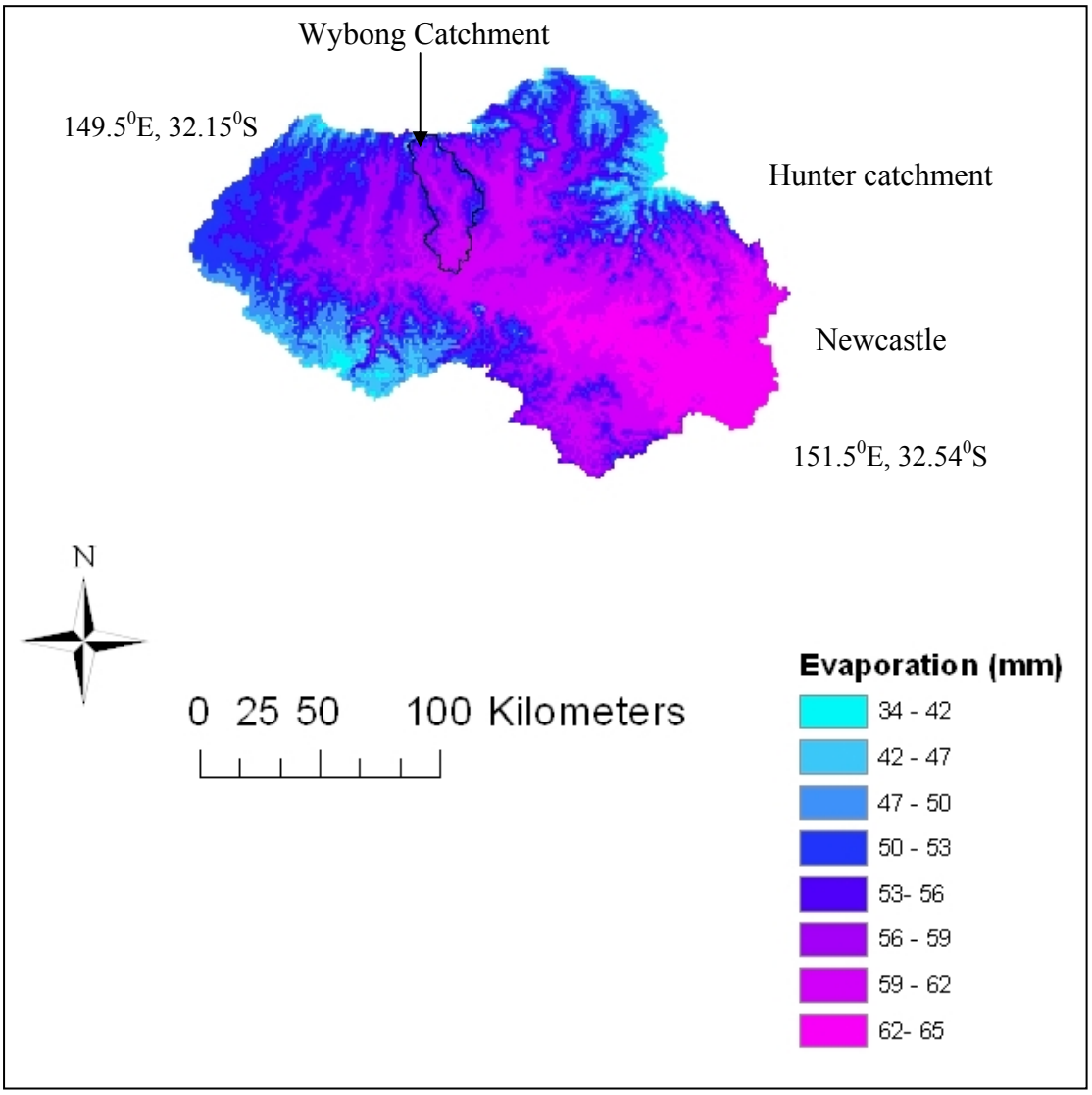


**Figure 3.3 (c)** Monthly pan evaporation surface for July 2000 for Hunter region

### 3.2.3 Interpolated Rainfall and Evaporation

Monthly rainfall surface were available only from 1973 to 2005. In order to extend the record of spatially weighted rainfall over the full historic local rainfall record, the relationship between the areal average rainfall (mm) of the catchment and the Bunnan gauge rainfall was found (**Figure 3.4**).

$$P_A = 0.992 \times P_B \tag{3.1}$$

$$R^2 = 0.979 \tag{3.2}$$

where $P_A$ and $P_B$ are the spatially average rainfall and Bunnan point monthly rainfall data respectively. Equation (3.1) was then used to interpolate and extrapolate the aerially averaged rainfall from 1900 to 1972 and from 2006 to 2008.

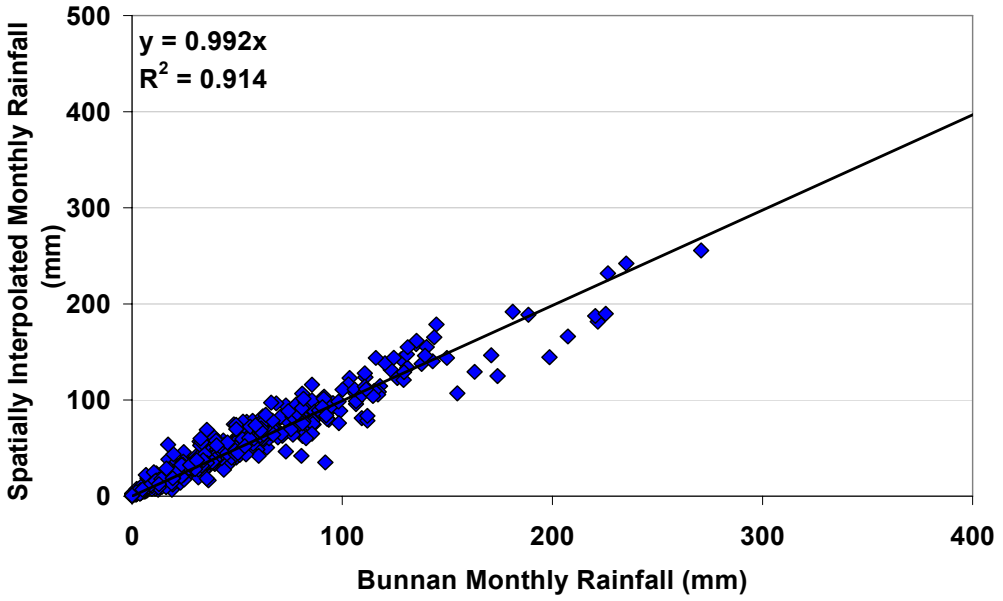


**Figure 3.4** Relationship between monthly catchment-weighted rainfall and monthly Bunnan (station #61089) rainfall

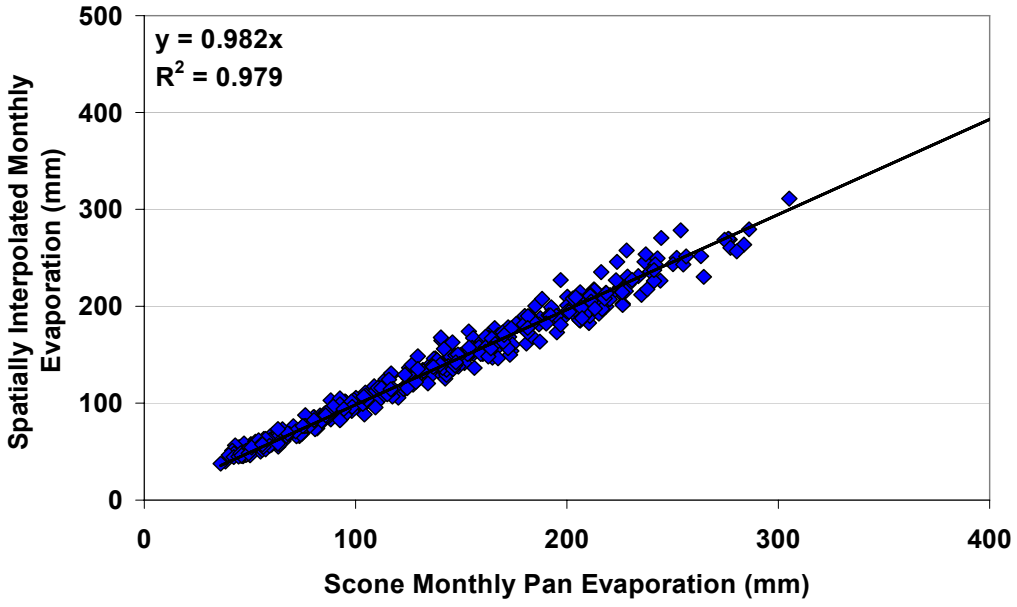


**Figure 3.5** Relationship between monthly aerial averaged catchment pan evaporation and Scone (station #61089) pan evaporation

Similarly, areal average monthly evaporation data was found to be related to the Scone data (as of **Figure 3.5**)

$$E_A = 0.992 \times E_S \tag{3.3}$$

$$R^2 = 0.914 \tag{3.4}$$

where $E_A$ and $E_S$ are aerial average monthly pan evaporation and the Scone station's evaporation.

The constants in relation between spatial rainfall and spatial evaporation with point data from Equation 3.1 and 3.3 are similar. This is because the monthly point rainfall and evaporation data have relatively small spatial variability over such a relatively small catchment. The constant is only slightly less that 1.0 probably because Bunnan is at an approximate mid point of the catchment.

The spatially interpolated monthly rainfalls from 1900 to 2008 were used for analysing long term change in rainfall, seasonality of rainfall and drought. Spatially interpolated rainfalls from 1955 to 2008 data were used for drought and rainfall runoff analysis. Runoff-rainfall analysis was only carried out for this time period, since stream flow data was only available from 1955 to 2008.

### 3.2.4. Drought Analysis

A number of existing techniques are used to measure of the effect of prolonged dry periods on water storage. Techniques are the Palmer Drought Index, the Standardised Precipitation Index, the Decile Method, and the Rainfall Depreciation Method (White *et al.,* 1999).

The Palmer drought severity index, developed for agricultural drought, purports to be based on the soil water balance of the soil root zone. It has been claimed, however, that the method of normalisation of the index, essentially removes evapotranspiration, making the index predominantly a rainfall index for agricultural drought (Smith *et al*., 1992). Moreover, the index is arbitrary and also requires data on temperature and soil water content.

The standardised precipitation index (McKee *et al*., 1993*)*, a parametric method, recognises that different water storages require rainfalls to be summed over different

periods. For shorter summation periods (less than 12 months), this technique requires rainfall data to be transformed into a variable with a normal distribution. In addition, different transformation may be required for different seasons of the year. The rainfall depreciation method (Falkland, 1999b) is a surrogate water balance method which recognises demand and losses need to be subtracted. Its assumption of constant proportional losses, however, is unrealistic and, in its present form, it is not an index.

Percentile ranking is a non-parametric decile method (Gibbs and Maher, 1967), is more attractive in that it makes no assumption of the form of rainfall distribution and is easier to calculate since it does not require any data transformation. In addition, the decile method provides a direct, easily understood ranking of the actual rainfall, providing immediate information on whether the rainfall for the period in question is above normal, above or below normal, or extremely wet or dry. It can also be used for comparison between different sites and times. Moreover, rainfall deciles have a much higher spatial coherence than actual monthly rainfall totals. This is because deciles are essentially normalised departures from average conditions and are related to broad scale synoptic patterns (Smith *et al*., 1992). These suggest that it has advantages over other mentioned methods.

To identify significant drought in the Wybong catchment, percentile rankings of monthly rainfall were calculated. Percentile rankings have been adopted by the BOM as the standard for identifying drought in Australia (White and O'Meagher, 1995). Rainfall deciles rank the rainfall over the period of interest in terms of the relative quantity of rain that fall in that period compared with the total distribution of all recorded rainfalls over the same period.

Percentile rankings of monthly rainfall were determined for the period of 1955 to 2008. The total quantity of rain, $TP_n$, for an $n$ month accumulation period is just:

$$TP_n = P_0 + \sum_{i=1}^{n-1} P_{-i} \tag{3.5}$$

Here $P_0$ is the rainfall for the current month $P_{-i}$ is the rainfall for the previous $i$th month (-1 is the previous month and so on). The rainfall against the total record were then ranked and expressed as a percentile of the total distribution. The data are distributed into 10 equal parts. Each of this distribution signifies a specified fraction of the total number of ranked values. Thus, the $10^{th}$ percentile is the lowest 10 per cent of the observations. The percentile rankings below 10% were considered to be significant

meteorological droughts as it is relative to the climatologically appropriate moisture supplied for the catchment.

The accumulation period over which rainfall is summed is an important consideration and relates to the size of the water store under consideration. The BOM reports rainfall percentiles summed over 3 month periods. This is appropriate for agriculture drought as this approximate the residence time of soil water. For groundwater-fed streams, a residence time of about 12 months appears appropriate and 12 month rainfall accumulation period will be used here. An advantage of this period is that the seasonality of rainfall doesn't need to be preserved.

### 3.2.5 Stream Flow

Daily stream flow data ($Q_d$, MLday$^{-1}$) for the Yarraman gauging station (#210040) in the lower Wybong catchment (see **Figure 3.6**) and Coggan (#210006), which is located on the main Goulburn channel, were sourced from the Pinneena Database CD (DNR 2008). The areas of the catchments up to the Yarraman and Coggan gauging stations are 675 km$^2$ and 3340 km$^2$, respectively.

#### 3.2.5.1 Filling Missing Stream Flow

Daily stream flow data begun in 1955 and data from 1955 to April 2008 were used in this study. Over this time period 615 daily data points were missing. Missing data were due to logging and power supply problems, and equipment failures. Missing stream flow data were filled in using the specific yield, Q/A (mm/day) relationship between Yarraman stream gauge and Coggan stream gauge as is explained below. Daily stream flow ($Q_d$) was summed over each month to calculate monthly flow ($Q_m$; ML month$^{-1}$).

When the number of daily records was less than 15 days, the monthly flow was assigned a missing value. However, if the number of records was greater than 15 but less than the monthly total, the average daily flow for the month was calculated and used to estimate the monthly flow ($Q_m$) by

$$Q_m = \frac{\sum \mathrm{Q_d}}{\mathrm{n}} \times \sum \text{Days in the month}$$

$$\text{If Day} < 15, \text{NA}$$

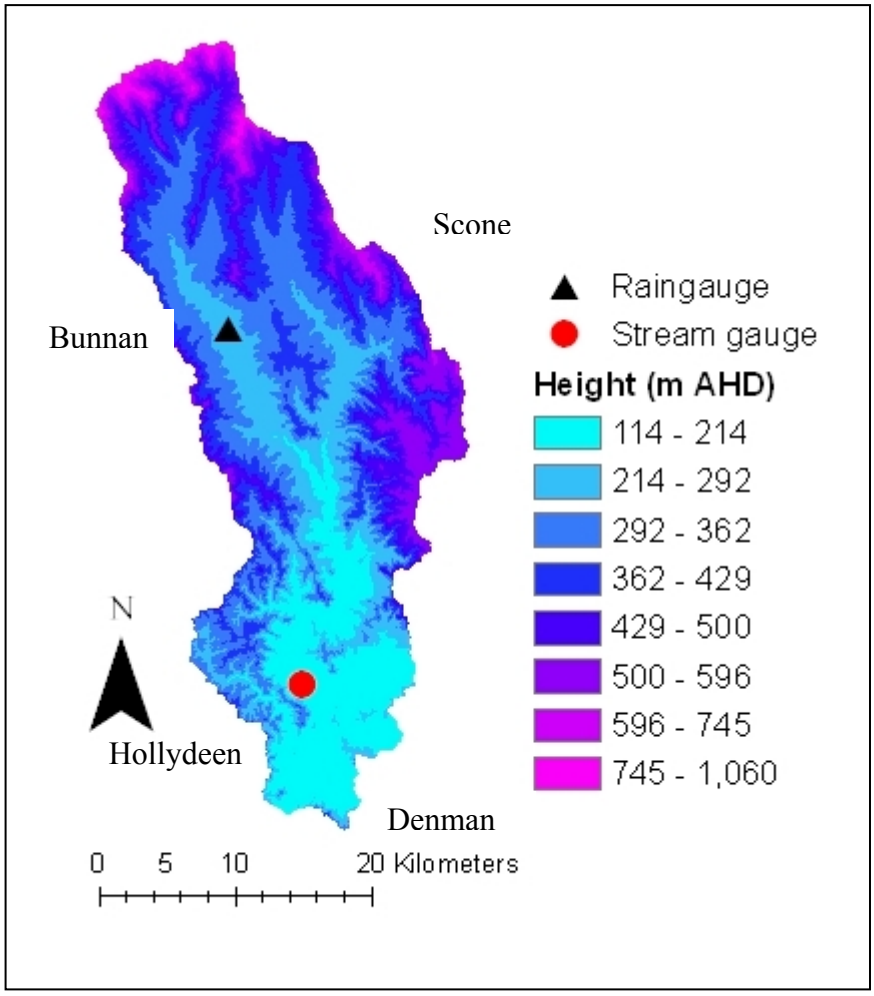


**Figure 3.6** DEM location of Wybong stream gauge (station #210040) Bunnan rain gauge (station #61007)

The mean monthly specific discharge of the catchments were calculated by the division of stream flow ($Q_m$, ML month$^{-1}$) to catchment area (A, km$^2$) up to the gauging station.

Specific discharge was calculated from

$$q = \sum_{1m} \frac{Q_m}{A} \tag{3.6}$$

where, $Q_m$ = monthly stream flow, A=catchment area upstream of the gauge

Linear regression between Wybong and Coggan monthly specific yield data was used as a first approximation for infilling the missing values in each of the data sets for

individual months. This method assumed that there was no autocorrelation or partial autocorrelation in the monthly time series data. This assumption seems reasonable since the gauges are in different catchments. Missing values were in-filled based on the monthly runoff relationship for each month. **Figure 3.7** shows the relationship between Wybong runoff and Coggan runoff for the month of July which has the highest value of $R^2$. Values of $R^2$ and the linear regression coefficients are listed in **Table 3.1**. Since there were no missing data in December, the coefficient was not used for filling data.

The missing $Q_m$ data were then filled-in using

$$q_m(Wybong) = a.q_m(Coggan) \tag{3.7}$$

The in-filled dataset is referred to as $Q_i$.

**3.1 Table** Coefficients and $R^2$ for filling missing streamflow data (Y=AX)

| Month | Coefficient, (a) | $R^2$ |
|---|---|---|
| January | 2.035 | 0.80 |
| February | 2.608 | 0.88 |
| March | 1.054 | 0.83 |
| April | 1.550 | 0.74 |
| May | 1.154 | 0.68 |
| June | 1.218 | 0.83 |
| July | 1.672 | 0.94 |
| August | 1.604 | 0.91 |
| September | 1.472 | 0.79 |
| October | 1.687 | 0.77 |
| November | 0.716 | 0.55 |
| December | 0.719 | 0.21 |

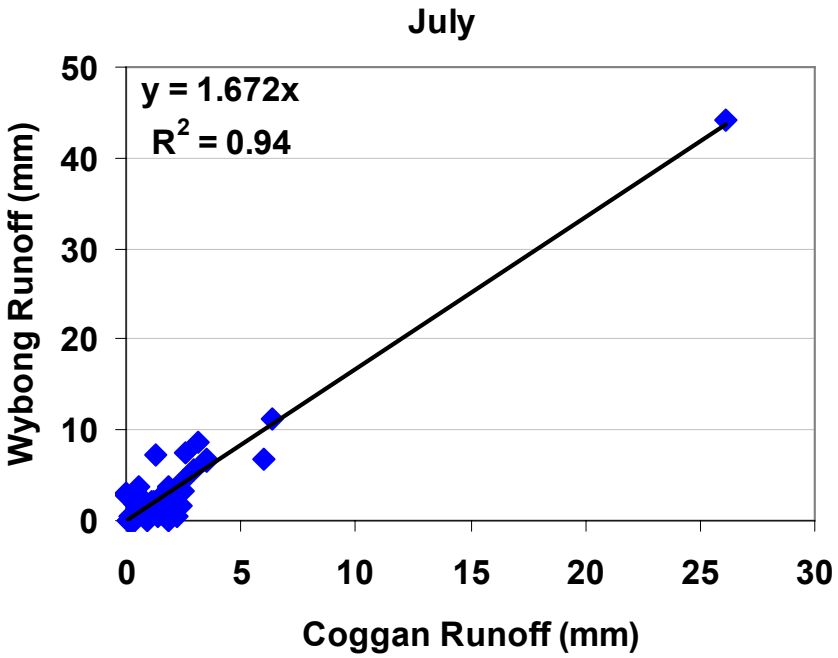


**Figure 3.7** Relationship between Wybong (#210040) runoff and Coggan (#210006) runoff for the July

### 3.2.5.2 Annual Catchment Runoff and Runoff Coefficient

The annual catchment runoff coefficient (C) was calculated from the ratio of the annual specific discharge from the catchment to annual interpolated rainfall

$$C = \left( \sum_{1y} [q] \Big/ \sum_{1y} P \right) \tag{3.8}$$

### 3.2.5.3 Cumulative Specific yield and Rainfall

Cumulative specific yield $q_{cum}/A$ was calculated by

$$q_{cum} = \sum_{i=1}^{n} q_i \tag{3.9}$$

And, cumulative rainfall $P_{cum}$ was calculated from

$$P_{cum} = \sum_{i=1}^{n} P_i \tag{3.10}$$

for n monthly records.

### 3.2.5.4 Percentile Ranking of Runoff

The previous 12 months monthly runoff were summed and then ranked into percentiles using the procedure described in **Section 3.2.4**.

### 3.2.5.5 Catchment Yield

Average annual yield of the catchment was calculated by

$$q_a = \frac{1}{12n} \sum_{i=1}^{n} q_i \tag{3.11}$$

Where, n = number of months

### 3.2.5.6 Water Abstraction from the Catchment

The Wybong creek has been assessed as a highly stressed stream due to environmental degradation and the high level of water extraction, as most of the water is extracted during summer low flow periods (NSW Department of Planning 2005).

Under the water management policy for extracting water in this catchment, 124 allocated licensees can extract about 8,300 ML/year. Of this annual volume, about 8,200 ML are able to be extracted for irrigation and remaining 100 ML is for domestic, stock and farming purposes. The water sharing plan sets a limit, or a cap, on overall extractions on an annual basis, the long-term average extraction limit, and also limits daily extractions (total daily extraction limit, TDEL). Daily extractions are set on the volume of water that can be taken over a series of flow classes in the Wybong Creek on a daily basis. The total TDEL for all water access licences (both river and aquifer) in each flow class is shown in **Table 3.2**.

**Table 3.2** Total daily extraction limits (ML/day)

| Flow Class (At the Wybong stream gauge) | Domestic and stock access licence TDEL* | Unregulated river and aquifer access licences TDEL | All water access licences TDEL* |
|---|---|---|---|
| Very low flows or A Class<br><1 ML/day (rising)<br>< 0.5 ML/day (falling) | 0 | 0 | 0 |
| Medium flows or B Class<br>1 – 7 ML/day (rising)<br>0.5 – 7 ML/day (falling) | 0.2 | 6.8 | 7 |
| High flows or C Class<br>7 – 16 ML/day | 0.2 | 13.3 | 13.5 |
| Very high flows or D Class<br>16 - 100 ML/day | 0.2 | 19.8 | 20 |
| Extremely high flows or E Class<br>> 100 ML/day | 0.2 | 36.8 | 37 |

* Water for basic landholder rights has been estimated at 1.8 ML/day. This is in addition to the licensed TDELs.

### 3.2.5.7 Southern Oscillation Index (SOI)

The Southern Oscillation Index (SOI) is a simple measure of the status of the Walker Circulation, a major atmospheric circulation, in the equatorial Asia/Pacific region whose variability affects rainfall in eastern and North Australia (Chew *et al*, 1998; Gibbs, 1975; Nicholls 1988). The strength of the Southern Oscillation is measured by a simple index, the SOI. Sustained negative values of the SOI often indicate El Niño (or warm phase) episodes and positive values of the SOI indicate La Niña (cool phase) episodes. During El Niño events cooling of seas around Australia occurs, as well as a slackening of the Pacific trade winds, which in turn feeds less moisture into Australia. There is then an increased probability that eastern and northern Australia will be drier than normal.

The link between SOI and rainfall across southern and eastern Australia is strongest during the winter and spring periods (June-November) (McBride and Nicholls, 1983). SOI values between April and September are used to produce rainfall outlooks for winter-spring rains, with low values of SOI often linked with below average rainfall

in eastern Australia (Evans, 2008). These conditions are reversed in the opposite phase to El Niño as La Niña. Positive values of the SOI are associated with stronger Pacific trade winds and warmer sea temperatures to the north of Australia. Together these give an increased probability that eastern and northern Australia will be wetter than normal.

SOI data from 1900 to 2007 were obtained from National Climate Centre (NCC) of the Australian BOM for investigating its relationship with rainfall variability in the Wybong catchment.

The National Climate Centre (NCC) has revised the SOI calculation although still based on the Troup formula (Troup, 1965). The formula for calculating the SOI relative to the 1933-92 base period is

$$SOI = \frac{PA(Tahiti) - PA(Darwin)}{Std.Dev.Dif} \times 10$$

where: PA(Tahiti, Darwin) = the Pressure Anomaly at the particular location = monthly mean minus long-term mean for the 1933-1992 base period

St.Dev.Diff. = Standard deviation of the difference for the 1933-1992 base period.

## 3.3. Results and Discussion

### 3.3.1 Climate of the Study Area

#### 3.3.1.1 Rainfall

The climate of the Upper Hunter is characterised by warm dry summers and cool, dry winters. It is influenced to some extent by coastal weather patterns. The average annual rainfall within the Wybong catchment for the period 1903 to 2008 is 638 mm year$^{-1}$ (Bunnan Station # 61007). On average, rainfall is slightly summer dominated, but significant falls may occur at any time of the year. A number of periods during the last decade have witnessed below-average rainfalls as shown in **Figure 3.8(a)** with moderately dry years occurring from 1994 to 1997 and exceptionally dry conditions occurring from 2002 to 2006. Analysis of rainfall data for Bunnan (Station # 61007), Denman (Station #61016) and Scone (Station #61089) for the periods from 1950 to 2008 shows that the average annual rainfall at these stations is 670, 639 mm and 646 mm, respectively. Bunnan, Denman and Scone, for the period from 1950 to 2008, have similar average annual rainfall (in **Figure 3.8(b) and 3.8(c**). The Scone (Station

#61089) rainfall data was only available from 1950 to 2008 for this comparison. The correlation coefficient between Bunnan and Denman is 0.85 from 1903 to 2008.

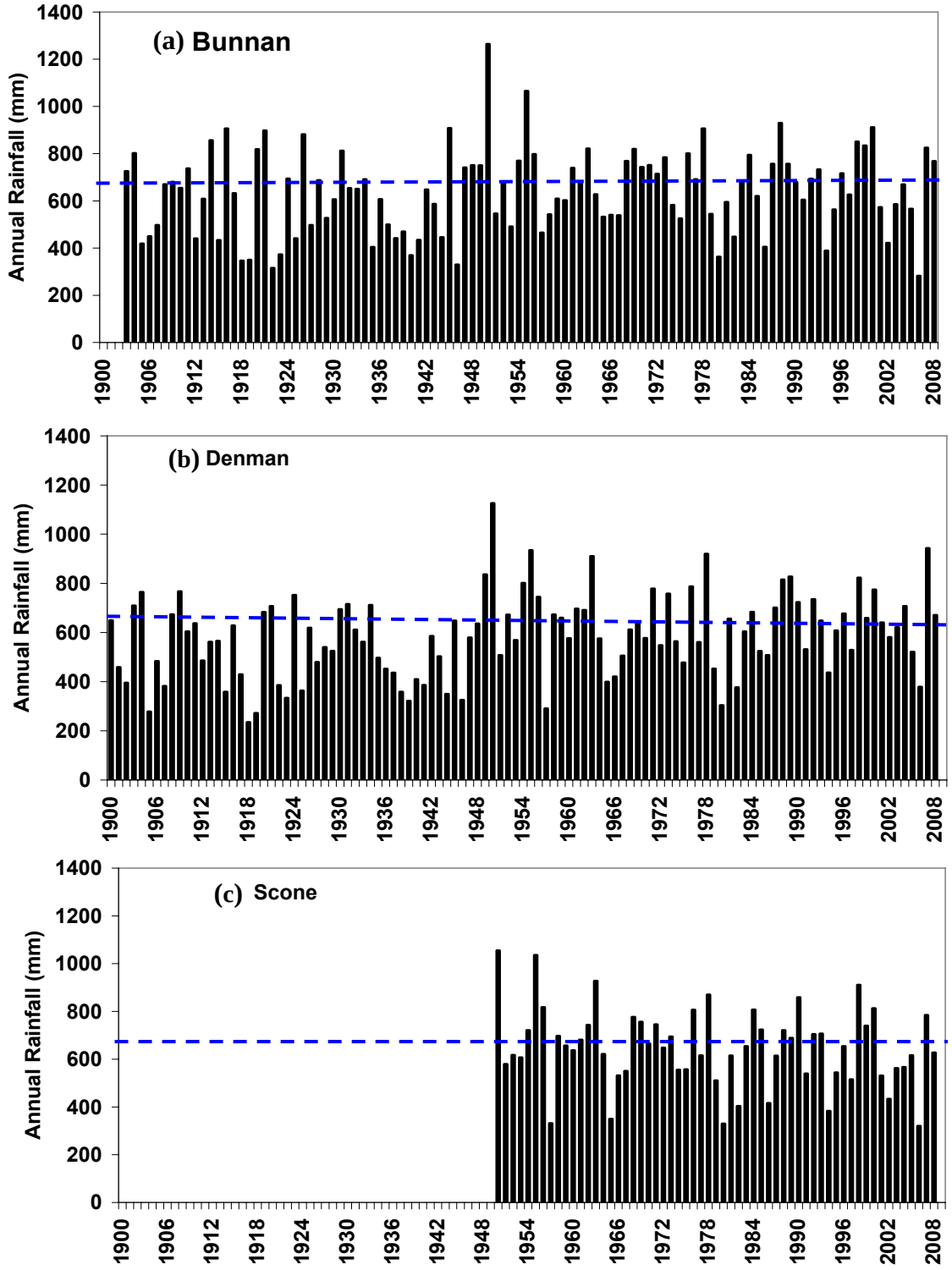


**Figure 3.8** Annual rainfall at **(a)** Bunnan (Station # 61007), **(b)** Denman (Station # 61016) and **(c)** Scone (Station # 61089) from 1900 to 2008. The dotted lines are annual average rainfalls

From the double mass curve (**Figure 3.9**) for Bunnan and Denman station's data follow a straight line that represents both stations with the same trends and extent. **Table 3.3 (a) and Table 3.3(b)** summarise the statistics of the annual rainfall and evaporation data and lists the lowest and highest rainfalls, mean rainfall over the entire rainfall record, standard deviation, coefficient of variation and value of rainfall at the 10 percentile.

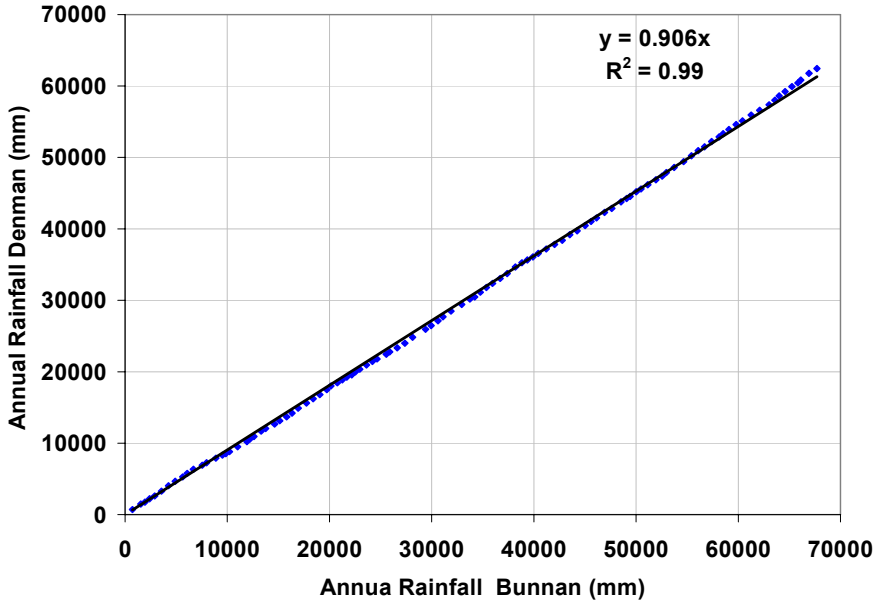


**Figure 3.9** Double mass curve for Bunnan and Denman rainfall data from 1903 to 2008

### 3.3.1.2 Evaporation

The average annual pan evaporation at Scone is 1634 mm (**Table 3.3a**) for the available record for 1972-2008. Analysis of the historical record shows an expected seasonal variation in evapotranspiration, estimated as 0.67 times pan evaporation, increasing during the summer months and decreasing during the winter months. Historical data from Scone and Bunnan indicate that evapotranspiration exceeds rainfall for most of the months in the year, except of May and June (**Figure 3.10**).

**Table 3.3(a)** Annual rainfall and pan evaporation statistics goes near the Wybong

| Parameters | Bunnan | Denman | Scone |
|---|---|---|---|
| Periods of Rainfall data | 1903 - 2008 | 1900 - 2008 | 1950 - 2008 |
| Lowest rain (mm) | 282 | 234 | 319 |
| Highest rain (mm) | 1264 | 1126 | 1055 |
| Mean annual rainfall (mm) | 638.6 | 586 | 646 |
| Standard Deviation | 176 | 167 | 163 |
| CV | 0.28 | 0.29 | 0.25 |
| 10 percentile rain (mm) | 412 | 362 | 413 |
| Median | 649 | 586 | 647 |
| Period of evaporation data | | | 1972 - 2008 |
| Lowest evaporation (mm) | | | 1336 |
| Highest evaporation (mm) | | | 2167 |
| Mean annual evaporation (mm) | | | 1634 |
| Standard Deviation (mm) | | | 202 |
| CV | | | 0.12 |

**Table 3.3 (b)** Rainfall statistics for monthly data, for January 1903 to December 2008

| | Bunnan | | | Denman | | |
|---|---|---|---|---|---|---|
| Month | Mean monthly rainfall | Standard Deviation | CV | Mean monthly rainfall | Standard Deviation | CV |
| January | 80.1 | 61.8 | 0.8 | 72.6 | 55.2 | 0.7 |
| February | 70.8 | 69.6 | 1.0 | 67.5 | 65.5 | 1.0 |
| March | 54.4 | 54.7 | 1.0 | 51.4 | 44.1 | 0.9 |
| April | 41.2 | 37.4 | 0.9 | 39.3 | 34.9 | 0.9 |
| May | 39.6 | 39.2 | 1.0 | 35.3 | 36.4 | 1.0 |
| June | 44.6 | 40.9 | 0.9 | 41.4 | 45.8 | 1.1 |
| July | 39.8 | 35.3 | 0.9 | 38.7 | 33.9 | 0.9 |
| August | 37.0 | 26.4 | 0.7 | 34.1 | 28.5 | 0.8 |
| September | 40.5 | 31.6 | 0.8 | 38.2 | 30.0 | 0.8 |
| October | 51.5 | 36.9 | 0.7 | 49.6 | 37.8 | 0.8 |
| November | 61.0 | 43.1 | 0.7 | 53.7 | 40.8 | 0.8 |
| December | 73.1 | 51.8 | 0.7 | 65.0 | 43.4 | 0.7 |

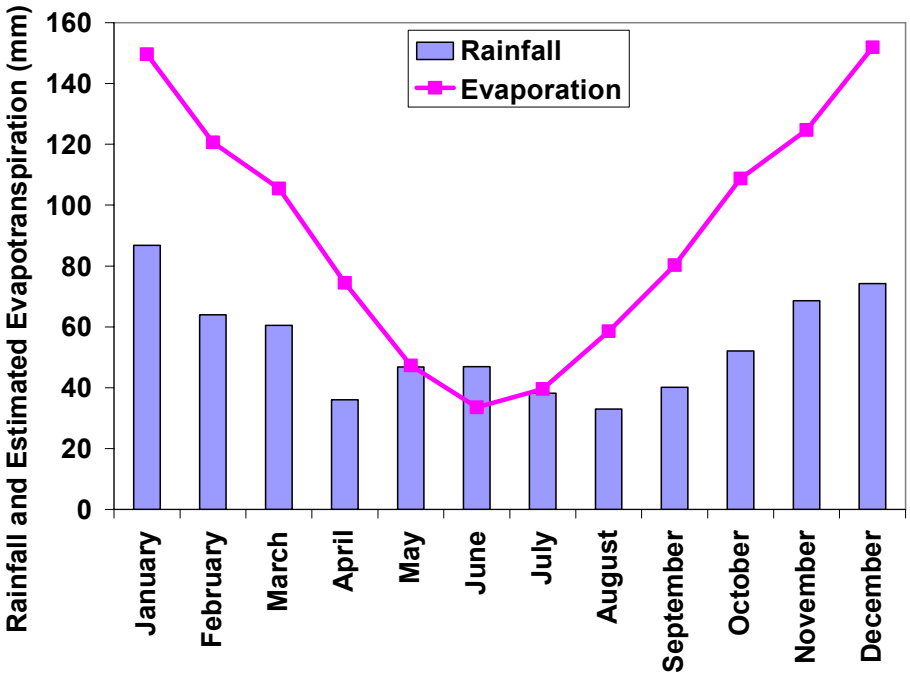


**Figure 3.10** Relationship between mean monthly rainfalls at Bunnan (Station # 61007) and mean monthly estimated evapotranspiration, at Scone (Station # 61089) from 1972 to 2008

### 3.3.1.3 Temperature

Summers in the Hunter-Central Rivers region are relatively hot with average maximum January temperatures of approximately 29–32°C. On average, Scone experiences 17 days above 35ºC and 1 day above 40°C each year. Winters are mild, with average maximum July temperatures of 17–18°C. Scone experiences approximately five frost days per year. The average minimum temperature ranges from 16.9$^0$C in summer to 4.7$^0$C in winter and the yearly average is 17.7$^0$C. **Figure 3.11** shows mean monthly max and min temperature at Scone (Station # 61089) from 1955 to 2008.

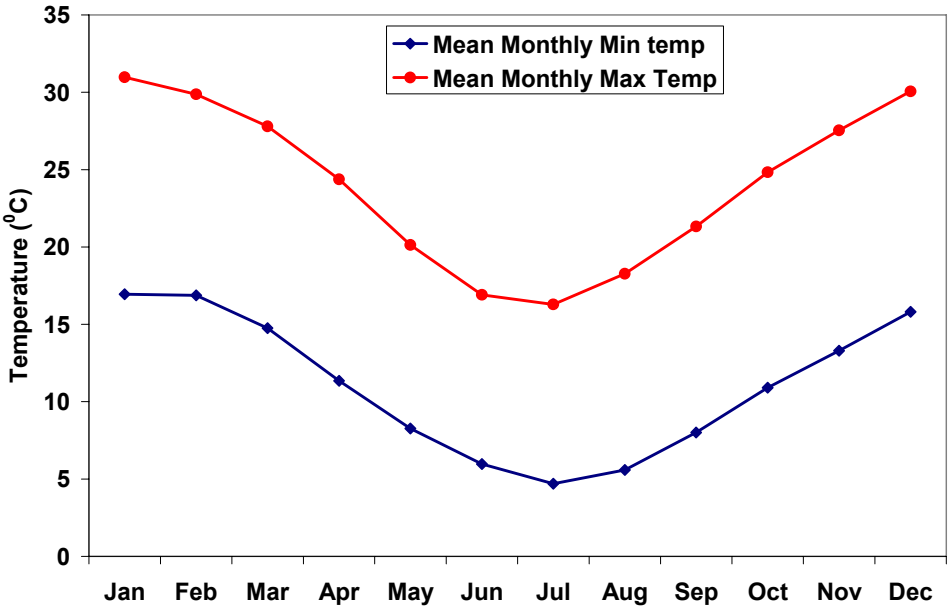


**Figure 3.11** Mean monthly maximum and minimum temperature at Scone (Station # 61089) data from 1955 to 2008

### 3.3.2 Long term Changes in Rainfall

The study has analysed rainfall data from 1903-2008 for observing rainfall trends. A simple linear regression of annual rainfall data suggests that annual rainfall does not have a significant trend over the last 105 years (**Figure 3.12**). However, cumulative residual plot (**Figure 3.13**) shows large, long term variation with rainfall periods of high and low rainfall occurring alternately. In the residual plot, a period of high rainfall occurred in 1904 and then a period of low rainfall occurred in 1907, 1925 and 1946 which was dry year. High rainfall occurred in 1950, 1956, and 1978 and again very low rainfall was in 1965, 1982 and 2006. The total largest extreme annual rainfall occurred in the middle of the twentieth century, in 1950 and the lowest rainfall was in 2006 **(Figure 3.13)**. The general shape of the long-term wetting and drying cycles in rainfall evident in **Figure 3.13** are also evident throughout the Murray-Darling Basin.

Previous studies (Kraus 1955; Pittock 1975; Cornish 1977; Erskine & Bell 1982; Erskine 1986a, b; Nichols & Lavery 1992) also reported a significant (secular) increase in annual rainfall total occurred in some parts of eastern Australia around 1950. Long-term changes in rainfall over the 105 years of the record by taking five-year running averages as shown in **Figure 3.12** were also analysed in order to clarify trends. An inspection of 5-year running mean rainfall generally shows below-average periods from

1903-1911, 1915-1929, 1932-1944, 1957-1958, 1962-1965, 1978-1982 and 2000-2006, and an above-average period from 1912-1914, 1930-1931, 1945-1956, 1959-1961, 1966-1977, 1983-1999, and 2007-2008.

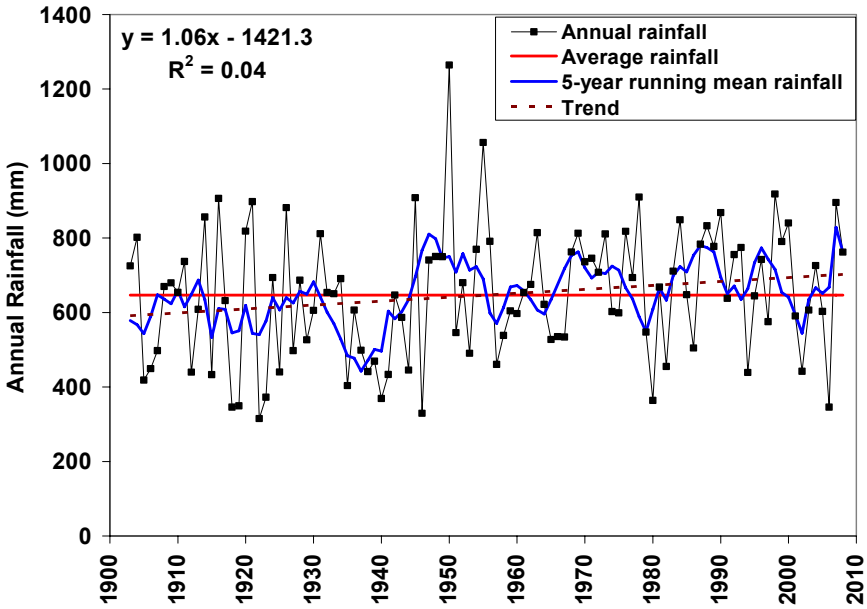


**Figure 3.12** Annual and 5 year running mean rainfall from 1903 to 2008

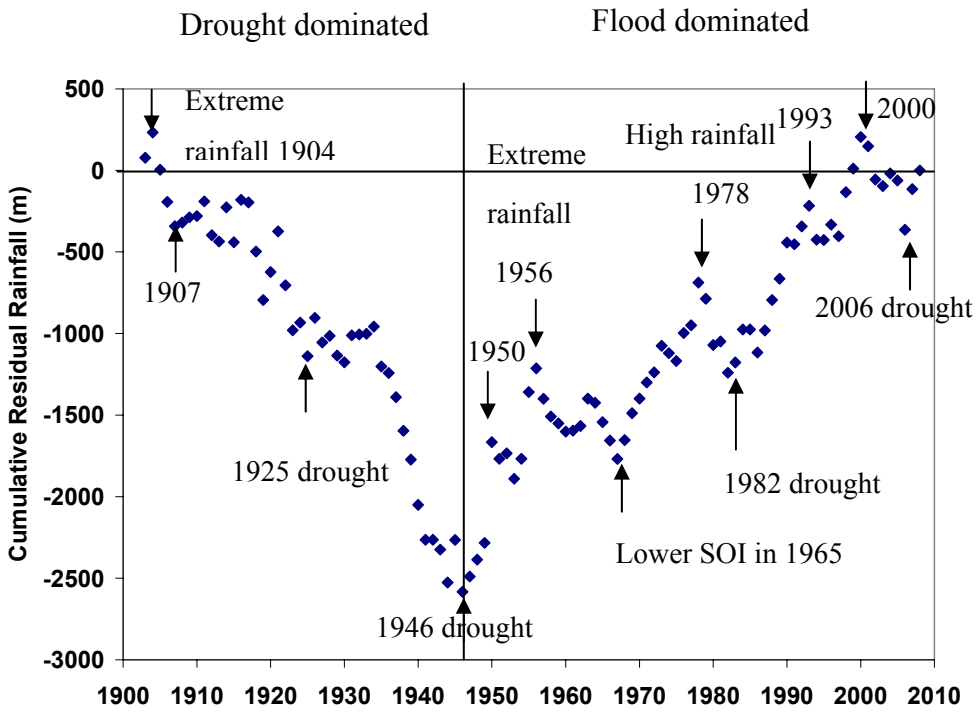


**Figure 3.13** Cumulative residual spatially interpolated rainfalls from 1903 to 2008

Three different trends identified in **Figure 3.13** in catchment rainfall during 1903 and 2008 are shown in **Table 3.4**. The trends were analysed in percent based on the differences between the mean of the earlier periods (Bell and Erskine, 1981). Up to three different periods seem to be present in the cumulative residual plot in **Figure 3.13**. A drying period from 1903 to 1947 with mean annual rainfall 592 mm, a wetting period from 1948-1999 with mean annual rainfall of 681 mm, and the possible start of another drying period from 2000 to 2008 with mean annual rainfall of 572 mm. Comparisons show that 15% of rainfall increases during 1948-1999 against the previous periods of 1903-1947, and 16% of rainfall declines during 2001-2006 against the previous periods of 1948-1999. Gentilli (1971) also documented substantial increases in mean annual rainfall for the period 1911-40, compared with the period 1881-1910, throughout most of coastal NSW. A period of low rainfall defined as drought dominated regimes (DDR) occurred between 1903 and 1947, many floods with high rainfall called as flood dominated regimes (FDR) occurred between 1948 and 1999 and rainfall again declined as of DDR between 2001 and 2006. The results show alternating drought and flood-dominated regimes occurred in these periods. These patterns are similar to those identified the previous studies (Hall, 1927; Pickup, 1976; Riley, 1980, 1981; Erskine and Bell, 1982; Erskine, 1986a; and Erskine and Warner, 1988, 1998).

**Table 3.4** Rainfall statistics for Wybong for different wet and dry periods identified in **Figure 3.13**

| Periods | Mean rainfall | Standard deviation | CV (%) | |
|---|---|---|---|---|
| Dry Period 1903-1947 | 592 | 175 | 29.6 | |
| Wet Period 1948-1999 | 681 | 166 | 24.3 | 15% increase |
| Dry Period 2001-06 | 572 | 196 | 34.3 | 16% decline |

### 3.3.3 Analysis of Droughts

The decile method (Gibbs and Maher, 1967) provides a non-parametric method of examining meteorological and hydrological drought which enables comparisons of rainfalls between different locations. In this section, percentile ranking or monthly decile method was used to identify significant droughts in the Wybong catchment.

The results of the percentile rankings for the previous 12 months rainfalls using data from Wybong gauge are shown in **Figure 3.14(a)** and **(b**). **Table 3.5(a)** shows that twenty three significant droughts occurred in the Catchment from 1900 to 2008 and **Table 3.5(b)** shows eight significant droughts in the period from 1955 to 2008. The percentile rankings of these two time periods differ in drought duration because of the different periods considered. **Table 3.5(b)** will be considered for analysing the impact of catchment yield due to drought.

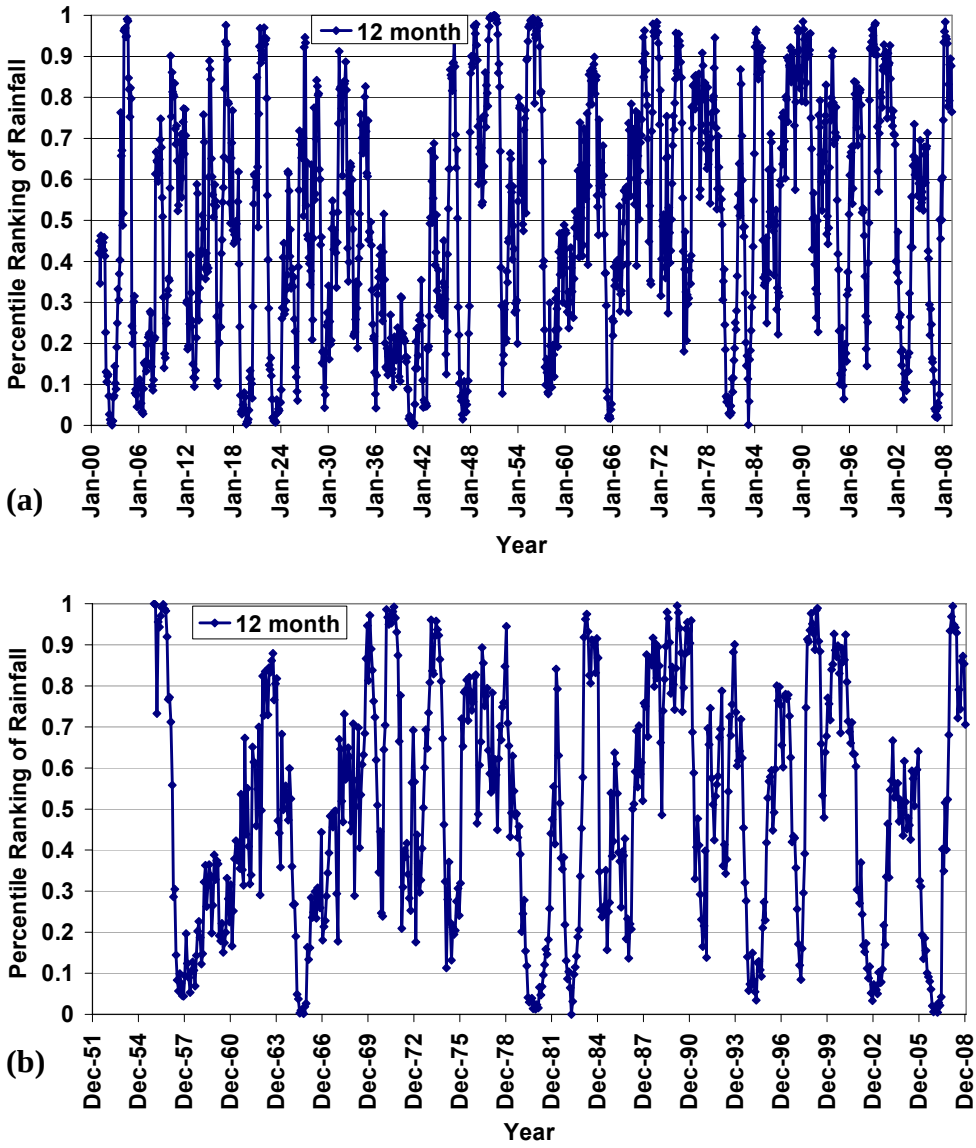


**Figure 3.14** Percentile rankings of rainfall for Wybong catchment Rankings below 10% corresponds to major droughts (a) for 1900 to 2008 (b) for 1955 to 2008

**Table 3.5(a)** Significant meteorological droughts for 12 months rainfall (1900 to 2008)

| Start Date (<10%) | End Date (<10%) | Lowest Percentile (%) | Duration (months) | 12 month rainfall |
|---|---|---|---|---|
| Dec-1901 | Feb-1903 | 0.00 (,Aug-1902)* | 15 | 270 |
| Jul-1905 | Aug-1906 | 2.6 (Jul-1906) | 14 | 334 |
| Sep-1907 | Nov-1907 | 8.5 (Oct-1907) | 3 | 406 |
| Dec-1912 | Feb-1913 | 9.4 (Jan-1913) | 3 | 417 |
| Dec-1915 | Jan-1916 | 9.7 (Jan-1916) | 2 | 419 |
| Nov-1918 | May-1920 | 0.3 (Aug 1919)* | 19 | 288 |
| Oct-1922 | Jan-1924 | 0.7 (Apr 1923)* | 16 | 296 |
| Dec-1925 | Feb-1926 | 6.0 ( Feb- 1926) | 3 | 376 |
| Jun-1929 | Aug-1929 | 4.3 (Jul- 1929) | 3 | 361 |
| Nov-1935 | Feb-1936 | 4.2 (Jan-1936) | 3 | 355 |
| Jan-1938 | Mar-1938 | 9.4 (Mar- 1938) | 3 | 416 |
| Jan-1940 | Dec-1940 | 0.38(Jul 940)* | 12 | 292 |
| Dec-1941 | June-1942 | 4.2(Jan-1942) | 7 | 362 |
| Aug-1946 | Sep-1947 | 2.6(Dec-1946) | 14 | 327 |
| Jan-1952 | Feb-1952 | 7.7 (Jan-1952) | 2 | 401 |
| July-1957 | April-1958 | 7.7(Nov-1957) | 10 | 401 |
| Apr-1965 | Nov-1965 | 1.6(Sep-1965) | 8 | 309 |
| May-1980 | April-1981 | 2.5 (Nov-1980) | 12 | 326 |
| Feb-1983 | May-1983 | 0.15 (Mar-1983)* | 3 | 278 |
| Feb-1995 | April-1995 | 6.0 (April 1995) | 3 | 379 |
| Feb-1998 | Mar-1998 | 9.0 (Mar 1998) | 2 | 455 |
| Oct-2002 | Mar-2003 | 6.3 (Nov-2002) | 6 | 378 |
| Sep-2006 | May-2007 | 1.9 (Feb- 2007) | 9 | 314 |

* Worst drought on record

Not all of these dry periods, which dropped below 10% ranking, can be classed as severe droughts. Among them, 11 out of the 23 very dry periods lasted only 2-3 months below the 10 percentile. The results of the rainfall rankings can be used to compare the severity of droughts for different rainfall periods. This severity can be ranked in three ways; the lowest rainfall percentile ranking, the duration of the drought or the period

rainfall stayed below <10%), and the average ranking over the drought period. Using these criteria together with significantly long droughts in terms of duration are occurred in 1901 to1903, 1905 to 1906, 1918 to1920, 1922-1924, 1940, 1946-1947 and 1980-1981. In case of wet periods the highest percentile ranking >90% are occurred in1956, 1970-1971, 1974, 1984, 1989-1991, 1999 and 2008. Among them the worst drought occurred in 1901 and the drought of 1918 was the longest with having the wettest year of 1956.

**Table 3.5(b)** Significant meteorological droughts (<10% percentile ranked monthly rainfall) for 12 months rainfall at Wybong for the periods of 1955 to 2008

| Start Date (<10%) | End Date (<10%) | Lowest Percentile (%) | Duration (months) | 12 month rainfall |
|---|---|---|---|---|
| June-1957 | Aug-1958 | 4.0 (Nov-1957) | 15 | 401 |
| Apr-1965 | Nov-1965 | 0.15(Sep-1965) | 8 | 309 |
| May-1980 | May-1981 | 1.2 (Nov-1980) | 13 | 326 |
| Dec-1982 | May-1983 | 0.0 (Mar-1983)* | 6 | 278 |
| Oct-1994 | Aug-1995 | 3.0 (April 1995) | 11 | 379 |
| Feb-1998 | Mar-1998 | 8.0 (Mar 1998) | 2 | 455 |
| Aug-2002 | Jun-2003 | 3.0 (Nov-2002) | 11 | 378 |
| Jul-2006 | May-2007 | 0.4(Feb- 2007) | 11 | 314 |
| | | Mean | 9.63 | |
| | | Stand. Deviation | 4.13 | |

* Worst drought on record for the period 1955 to 2008

### 3.3.4 Southern Oscillation Index (SOI) and Rainfall in Wybong

**Figure 3.15** shows that the strongest El Nino events or warm phase, more negative than -10, events during the past 100 years occurred in 1905, 1912, 1914, 1940/1941, 1965, 1977, 1982/1983, 1987, 1991/1992, 1993/1994, 1997. La Niña events (cool phase, greater than +10) occurred in 1910, 1917, 1938, 1950, 1955/1956, 1971/1972, 1974/75, 1989 and 1999. As is true throughout most of eastern Australia, a relatively

weak direct relationship is found between the SOI, a measure of the behaviour of the ENSO phenomenon, and rainfall (McBride and Nicholls 1983; Stone *et al.* 1996).

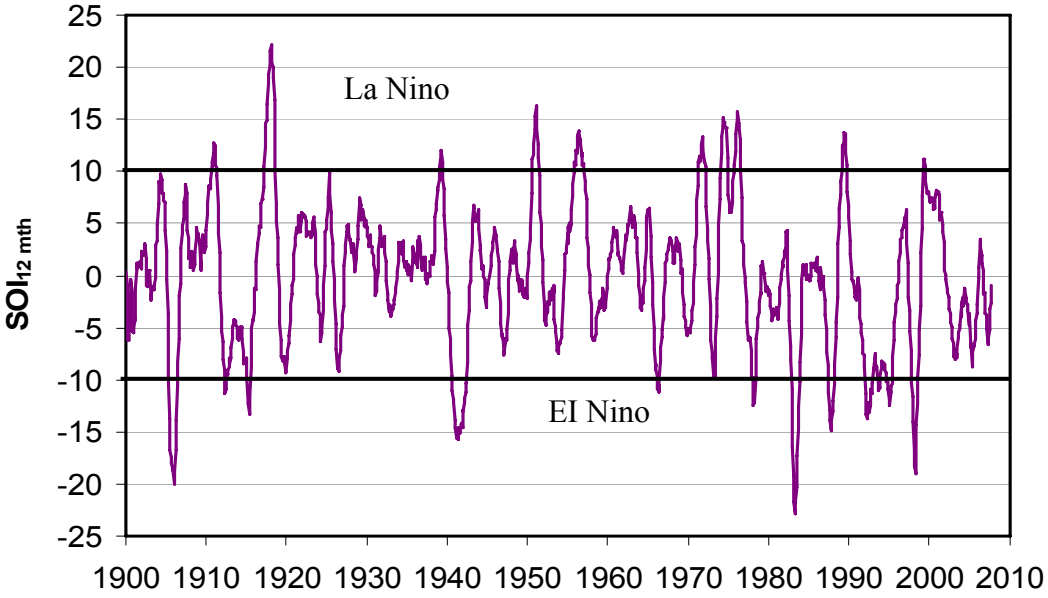


**Figure 3.15** Mean annual SOI from 1900 to 2007 (data from National Climate Centre of the Australian BOM)

**Figure 3.16** shows the relationship between annual rainfall totals and annual average values of the SOI. It shows a similar weak direct relationship between the SOI and rainfall at Wybong. Higher rainfall tends to occur when the SOI is strongly positive (e.g. 1950, 1955), and lower rainfall when it is strongly negative (e.g. 1982). However, the association is weak, since the correlation coefficient is low, 0.15 and some very wet years such as 1961and 1984 and dry years such as 2003 and 2006 occurred with very small SOI close to zero (+0.04, -1.93). The large-scale atmospheric fluctuations measured by the SOI account for only about 15% of inter annual rainfall variability at Wybong.

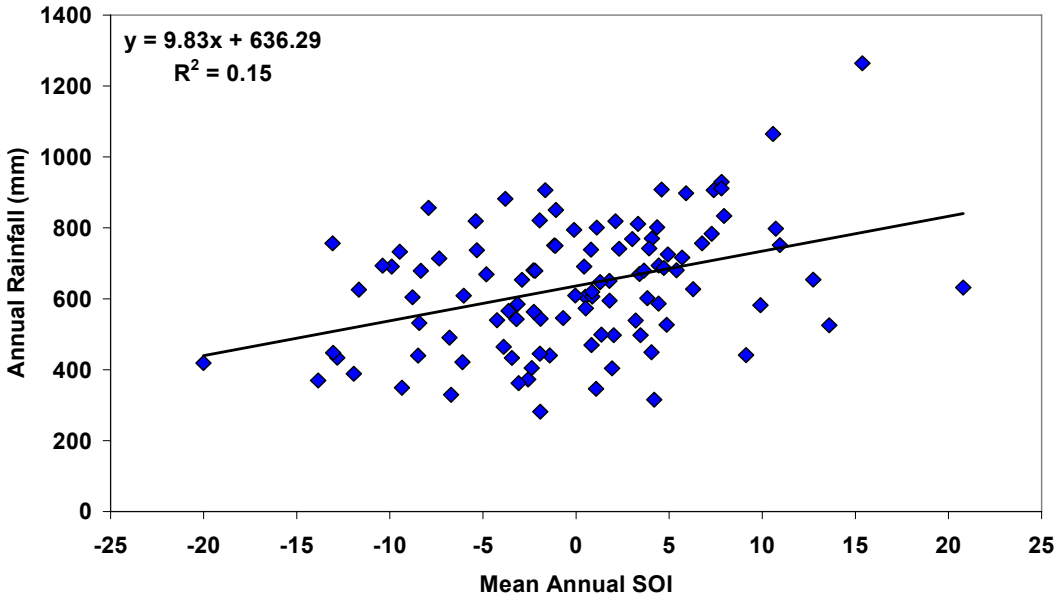


**Figure 3.16** Relationship between Mean annual SOI and annual rainfall from 1903 to 2008

### 3.3.5 Seasonality of Rainfall

Rainfall at Wybong shows clear seasonal fluctuations since the record began in 1903. The data can be divided into summer from December to February, autumn from March to May, winter from June to August and spring from September to November periods. January is the wettest month and August is the driest on average, with a mean difference in rainfall of more than 43 mm between these two months (**Figure 3.17**). The rainfall records in **Figure 3.17**, suggest the data can be divided into wetter and drier seasons. The wetter season is the October through March period "rainy season", and April through September is the drier season. **Table 3.6** lists the seasonal rainfall statistics for Wybong from 1903-2008. Autumn rainfall has the highest CV which could be due to thunderstorms activity.

**Table 3.6** Seasonal rainfall statistics for Wybong from 1903-2008

| Periods | Mean rainfall | Standard deviation | CV |
|---|---|---|---|
| Summer | 74.9 | 4.8 | 0.06 |
| Autumn | 45.6 | 8.1 | 0.18 |
| Winter | 40.6 | 4.0 | 0.10 |
| Spring | 51.0 | 10.3 | 0.20 |

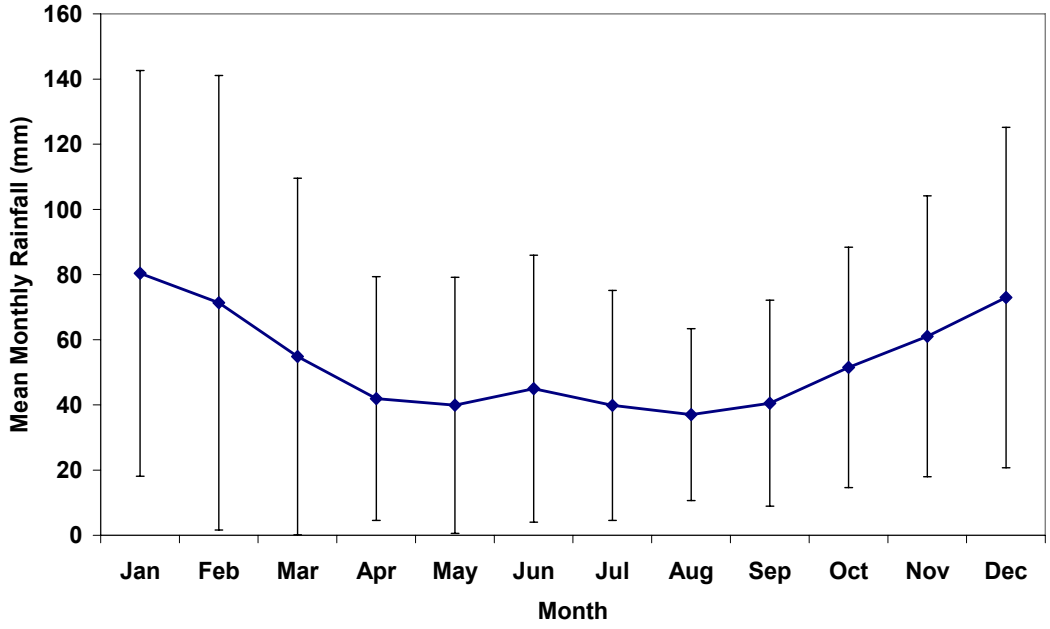


**Figure 3.17** Mean monthly rainfall Wybong from 1903 to 2008

The seasonal rainfall trends show that increase in annual rainfall are largely due to the summer season as shown in **Figure 3.18 and Table 3.6**. Summer rainfall was highest in the years of 1911, 1920, 1953, 1954, 1963, 1968, 1970, 1971, 1976, 1978, 1984, 1991, 1992 and 2004. Winter rainfall was the highest in the year of 1920, 1950 and 2007. A running 5-year mean of summer season rainfall is highest in 1956 and lowest around in the 1940 (**Figure 3.19a**). The cumulative residual curve shows that summer rainfall declines up to 1946 and then rises up to the peak in 1978. Since more than 50 percent of the annual rainfall occurs in the three month summer season, changes in summer season precipitation can have profound effects on the hydrologic system. However, the highest evaporation with lowest soil moisture also occurs in summer and therefore the majority of surface-water runoff and recharge to the ground-water system usually occurs during winter when antecedent soil moisture conditions are high, and surficial aquifer water levels rise.

Autumn rainfall was highest in the years 1913, 1921, 1926, 1932, 1964, 1977, 1979, 1989, 1999 and 2000. The running 5-year mean of autumn season rainfall was highest in 1978 with a lowest in autumn season rainfall in the 1918 (**Figure 3.19b**). However, there is no distinct pattern shown in cumulative residual for autumn except wetter from 1976 to 2003.

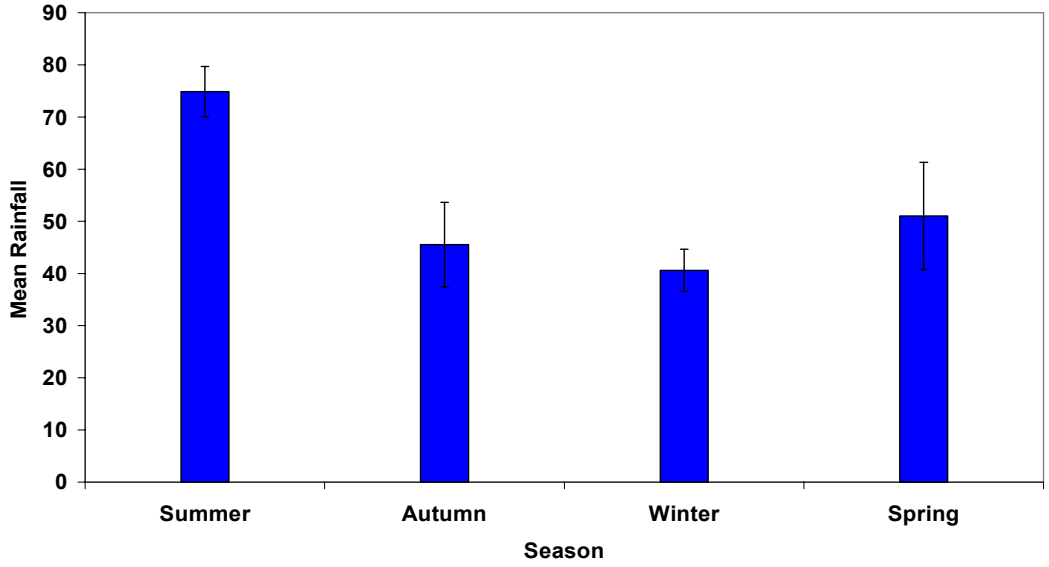


**Figure 3.18** Mean seasonal rainfall from 1903 to 2008

The seasonal rainfall declines during the winter month June, July and August (**Figure 3.18**). The running 5-year mean of winter season rainfall was highest in 1950 and also confirms the reduction in winter season rainfall in 1972 (**Figure 3.19c**). In this graph, the cumulative residual line shows that winter rainfall declines significantly after 1952 and remains low from 1983 to 2006. Factors such as relative intensity and frequency of the ENSO or coupling with the longer term interdecadal Pacific Decadal Oscillation, linked to above-average winter-early spring season rainfall may be responsible for this decline (Timbal, 2009).

However, a high percentage of June rainfall contributes to runoff due to wet antecedent soil conditions.

The years 1903, 1917, 1950, 1961, 1966, 1969, 1973 and 1985 had their highest rainfall in spring. A running 5-year mean of spring season rainfall is highest in 1998 with a lowest in spring season rainfall in the 1920 (**Figure 3.19d**). In this Figure cumulative residual line shows that spring rainfall declines after 1920 and remains low up to 1970.

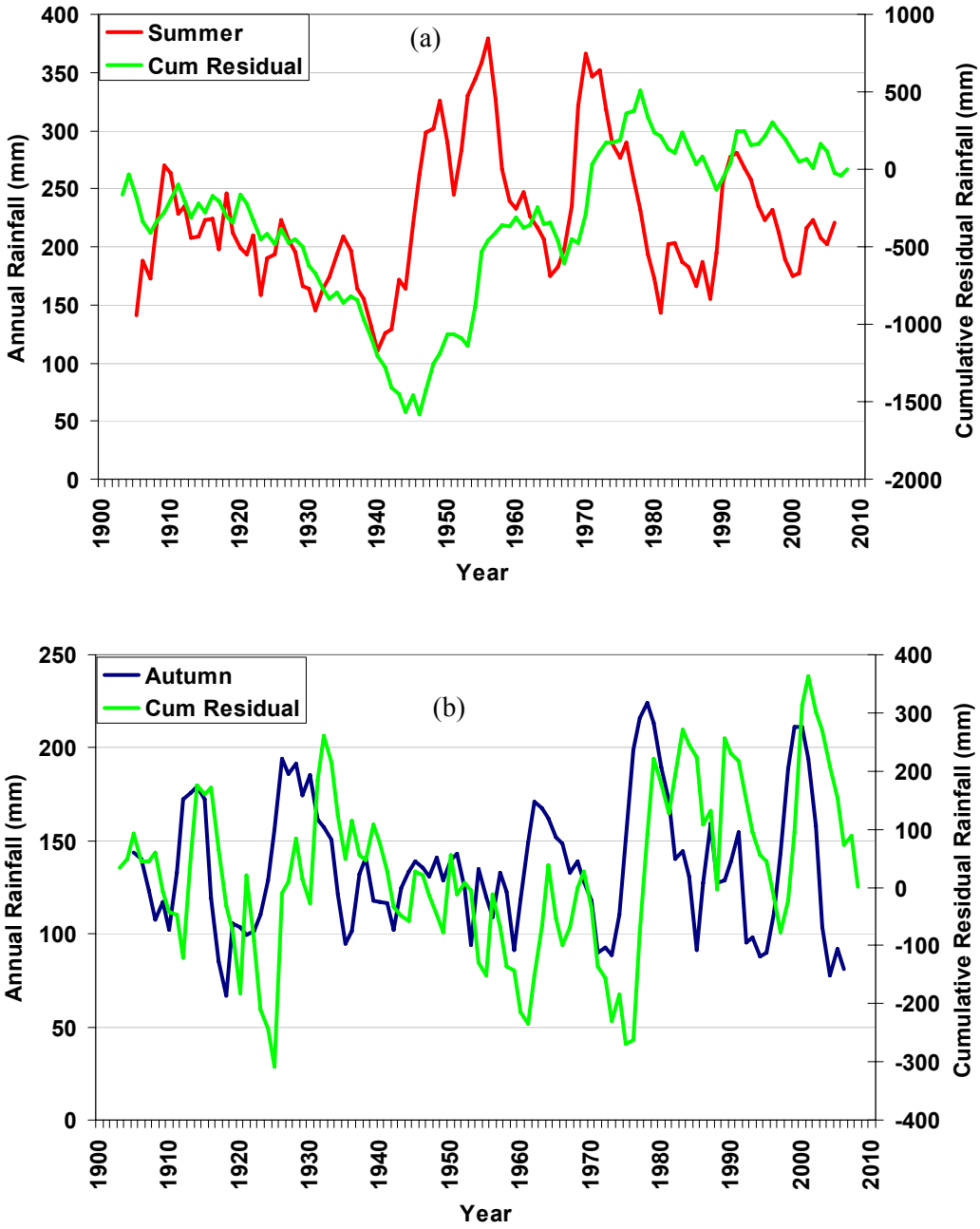


**Figure 3.19 (a)** 5-year running mean seasonal rainfall trends and cumulative residual from 1903 to 2008 **(a)** summer **(b)** autumn

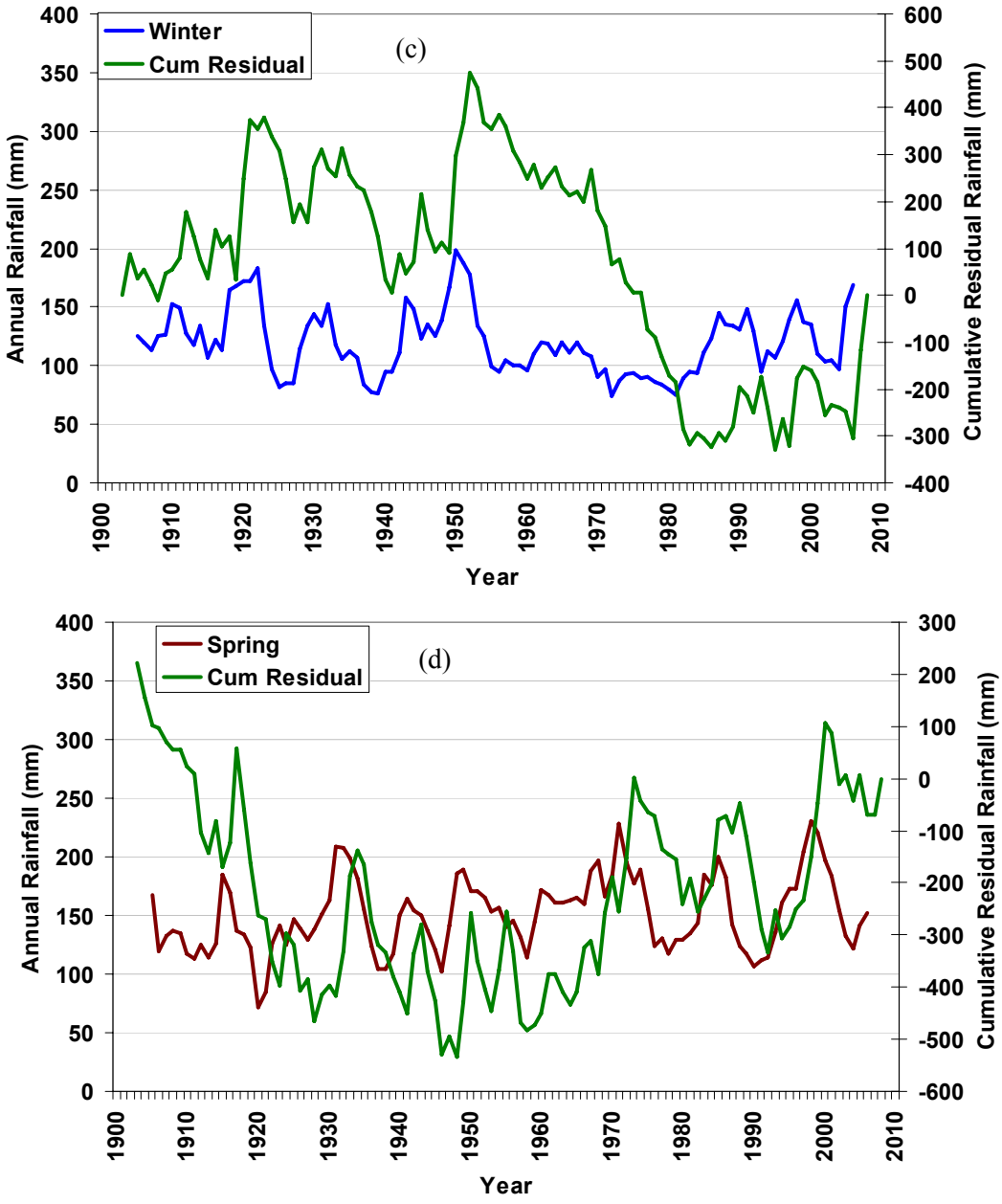


**Figure 3.19** 5-year running mean seasonal rainfall trends cumulative residual from 1903 to 2008 **(c)** winter **(d)** spring

### 3.3.6 Impact on Catchment Yield

Eight significant drought periods occurred between 1955 and 2008: 1957-1958, 1965, 1980-81, 1982-83, 1994-95, 1998, 2002-03 and 2006-07 (**Figure 3.14**). During these droughts changes occurred in the Wybong catchment runoff coefficient during the periods 1981, 1988, 1995 and 2001-June 2007 (**Figure 3.20**). The runoff coefficients between 2001 and 2006 in **Figure 3.20** are significant lower than those in other

droughts. Catchment runoff coefficients are lower than the long-term average in the period 2001-2006. One possible explanation for these abnormal low values could be an increase in water extraction from the catchment during dry period. It is assumed that significant water extraction of both surface and groundwater may have been increased from 2001 due to the large amount of land use for agriculture and other industries. This is also clearly observed from the relationship between cumulative rainfall and runoff in **Figure 3.21**.

**Figure 3.21** and **Figure 3.20** shows that when rainfall occurred during 2001- June 2007 and drought conditions eased there was no corresponding increase in catchment yield or stream flow. It is also observed that in the year of 2006 yield significantly decrease; there was very little run-off during this year.

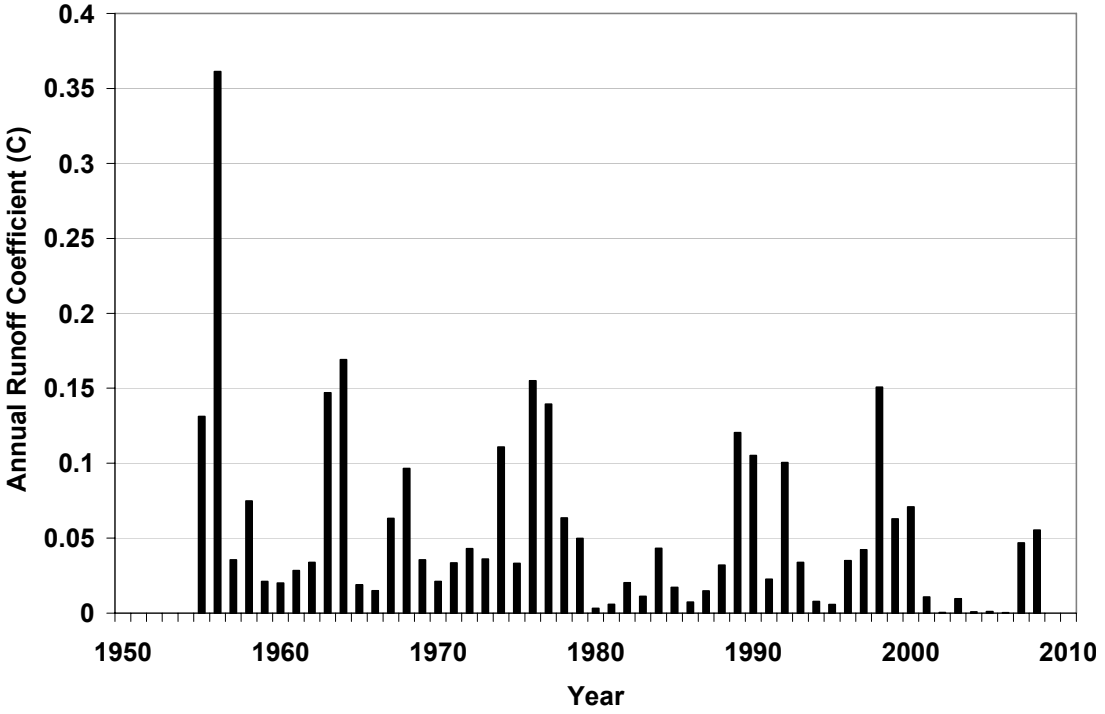


**Figure 3.20** Annual runoff coefficient from 1955 to 2008

Catchment yield was decreased from the mean catchment by 25% in 1957-1958, 93% in 1965, 96% in 1980-1981, 91% in 1982-1983, 97% in 1994-1995, 92% in 2002-2003 and 100% in 2006-June 2007 (**Figure 3.20**). It is instructive to compare the catchment runoff coefficient during drought periods. In the 1957-8 drought the runoff coefficient was 75% of the long-term mean runoff coefficient. This relatively high value

could be due to higher water tables and soil moisture after the flood of 1954. In 1965 the runoff coefficient was only 7% of the low-term mean, while in 1980-1, 1982-3, 1994-5, and 2002-3 droughts it was 4%, 9%, 3% and 8%, respectively of the long-term mean. However, in 2006-June 2007 the runoff coefficient was an unprecedented zero (**Figure 3.20**). Therefore, the yield between 2000 and 2007 may have decreased due to catchment surface and ground water abstraction combined with a decline in soil moisture.

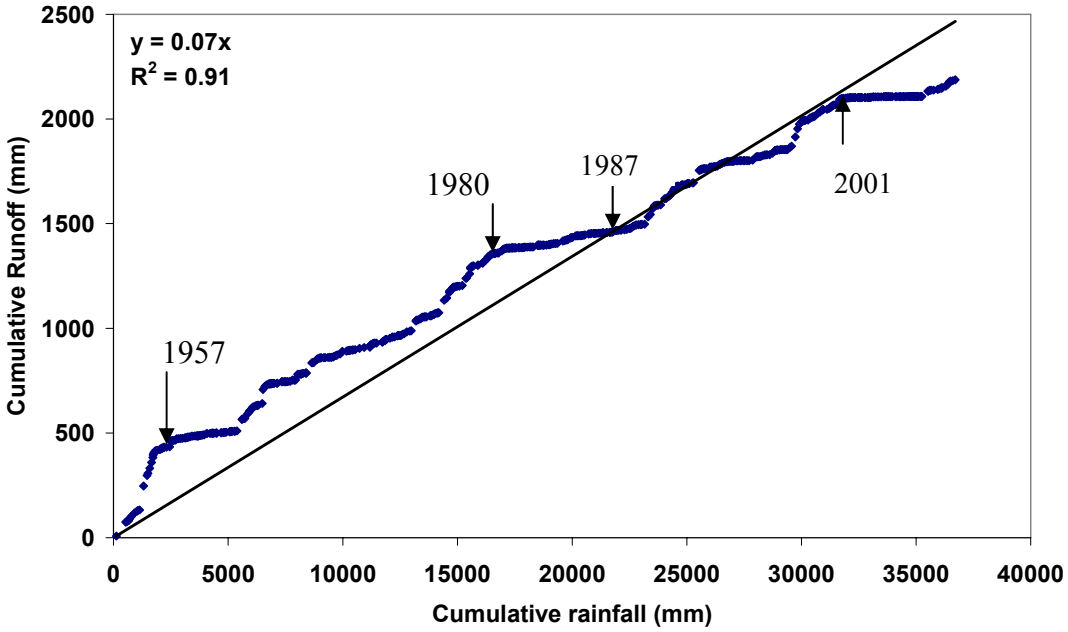


**Figure 3.21** Relationship between cumulative rainfall and cumulative runoff from 1955 to 2008

Runoff changes due to rainfall changes were calculated through runoff and rainfall relationships (**Figures 3.22**). Simple linear regression ($R^2$) was applied to develop an equation that related annual rainfall to runoff. Based on the slope of regression, a correlation was developed between runoff and rainfall. The simple regression analysis assumes a linear relationship between rainfall and runoff. The linear relationship found suggests that minimum annual rainfall needed to generate runoff in the Wybong is about 445 mm/yr (**Figure 3.22**). The $R^2$ value of 0.28 found indicates a poor linear relationship between rainfall-runoff. This is understandable since runoff generation depends on antecedent conditions and rainfall intensity. In real rainfall-runoff processes,

the same amount and intensity of rainfall in two events can lead to higher runoff volumes if antecedent conditions are wetter (higher soil moisture and water table closer to land surface). Therefore, rainfall runoff relationships are highly influenced by other factors such as soil moisture, transmission losses, drainage changes or baseflow loss through ground-water withdrawals.

The rainfall-runoff process may also be influenced by changes in land use/cover, rainfall intensity, water table depth, and antecedent soil moisture conditions. Much of the Wybong catchment has experienced changes in land use due to farming, agriculture, and pri-urbanization (DLWC, 2000). The simple regression models can not account for this situation. In fact, the regression models tend to underestimate runoff changes associated with changes in rainfall.

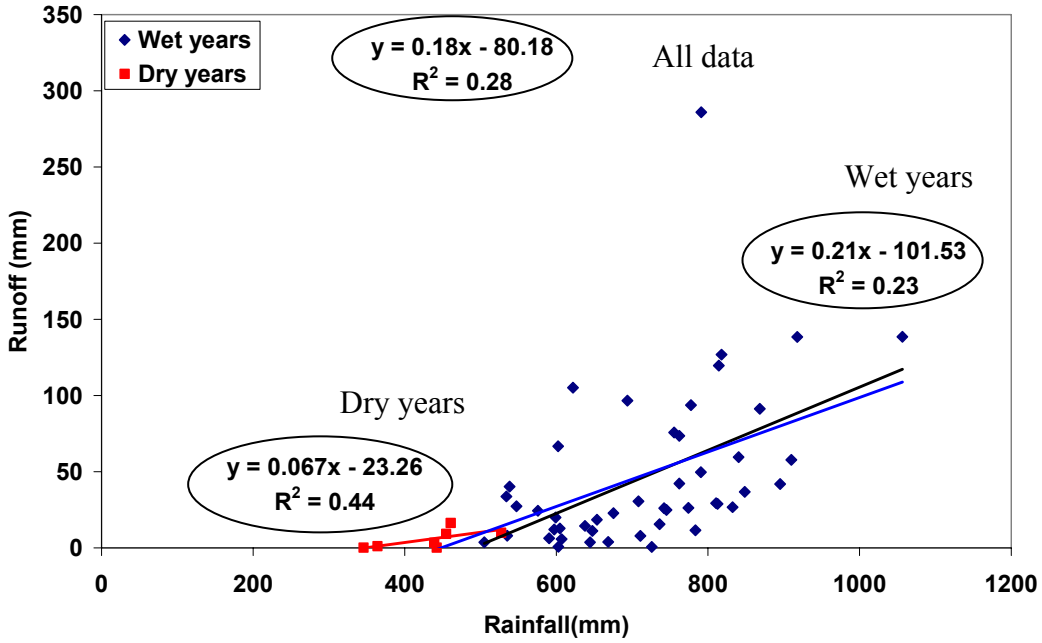


**Figure 3.22** Relation between annual runoff and annual rainfall from 1955 to 2008. Black line all data, red line the 7 Significant 12 month meteorological droughts from Table 3.5b, termed dry years (<10% percentile ranked monthly rainfall). The blue line is the relationship for wet years.

The double mass, cumulative rainfall-runoff plot in **Figure 3.21** illustrates the variability in runoff response to rainfall. It follows the FDR and DDR alternating pattern where runoff was high during FDR and low during DDR. There appears to be a break

point around 1987 where runoff declines. During the period 2006-June 07, dramatic fall in runoff is evident. There is no corresponding increase during 2001-2006 in stream flow with rainfall.

### 3.3.7 Comparison of Percentile Rankings of Runoff and Rainfall

To examine systematic trends in rainfall and runoff data, the percentile ranking of annual runoff against the percentile ranking of annual rainfall for the same year for the Wybong gauging station is plotted in **Figure 3.23**. While there is an approximate trend, the relationship is poor indicating that other factors are important in generating runoff.

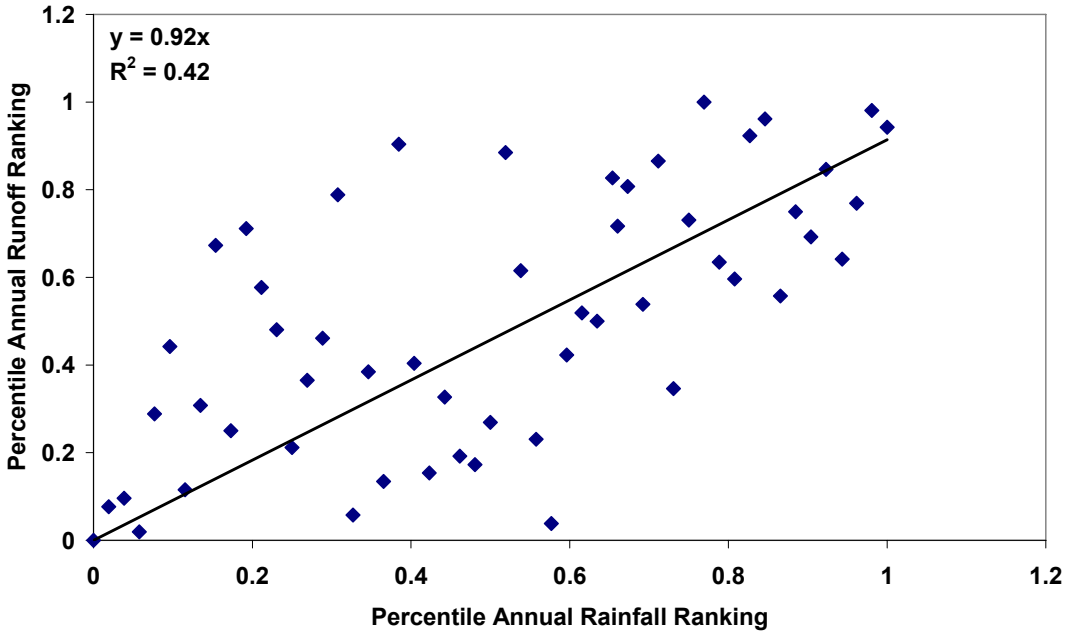


**Figure 3.23** Relation between the percentile rankings of annual runoff and annual rainfall from 1955 to 2008

**Figure 3.24** shows that annual runoff and rainfall rankings were identical for the years 1955-56, 1959-63, 1966, 1968, 1971-73, 1976, 1978, 1986, 1989-1993, 1996, 1998-2001 and 2008. However, there is a considerable scatter for other years. It is assumed that ratios between 1.5 and 0.75 (White *et al*, 2003) represent a reasonably close ranking; then it can be seen that for some years such as 1957-58, 1964-65, 1967, 1969-70, 1974-75, 1979-85, 1987-88, 1994-95, 2002-07, the ratios lie considerably above or below this range. Periods (e.g., 1958, 1974, and 1981) of ratios of more than 1.5 occur due to high rainfall and flood. Since antecedent conditions are wetter, the

same amount of rainfall may lead to higher runoff volumes. The periods (e.g., 1981 and 2002-2006) with ratios lower than 0.75 show that rainfall-runoff processes may be strongly influenced by changes in land use/cover due to agriculture, urbanization, less rainfall intensity and low antecedent soil moisture conditions.

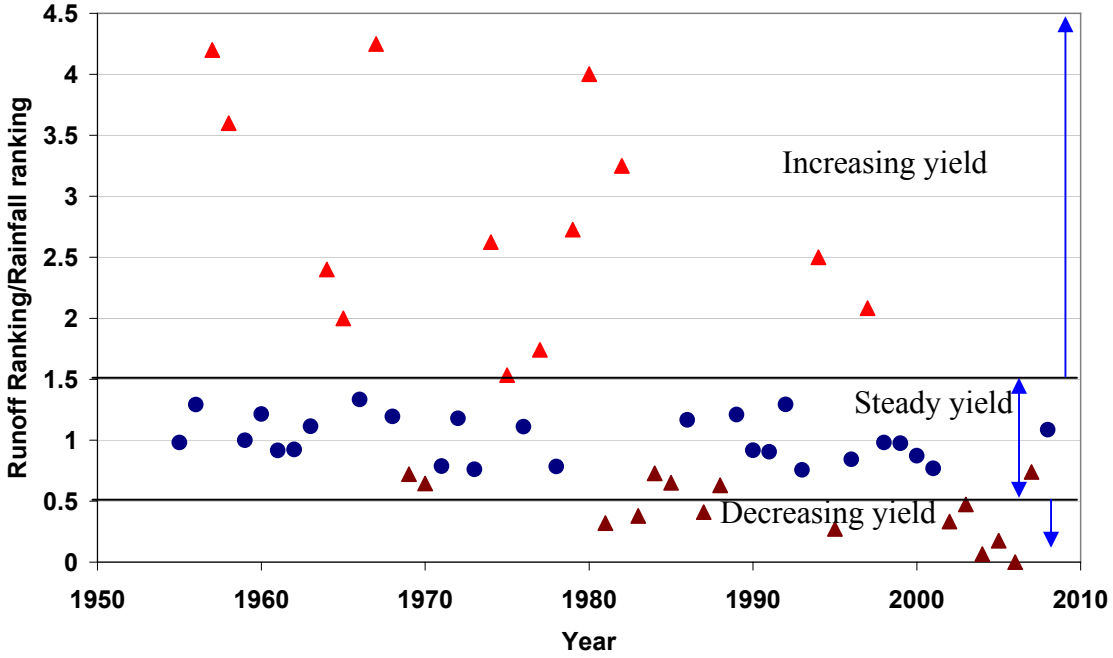


**Figure 3.24** Ratio of annual percentile rankings of runoff to rainfall as a function of the year of ranking data from 1955 to 2008

## 3.4 Conclusion

This chapter has examined the rainfall variability and its impact on runoff in Wybong subcatchment of the Upper Hunter. Meteorological or climatological drought was used in this Chapter to identify climate impact on catchment yield. A digital elevation model of the catchment was used together with tri-variate thin-plate smoothing splines to derive monthly rainfall and pan evaporation surfaces for the catchment. This enabled the monthly, spatial distribution of rainfall and pan evaporation as well as their spatially averaged values to be constructed for a catchment in which there was only one rainfall gauge. Again this work has demonstrated the strength of this procedure for obtaining spatially realistic estimates of the key hydrologic drivers in catchments with limited data.

After filling-in missing data, both rainfall and stream flow data were analysed to examine the variability of rainfall over both long and shorter time scales. The cumulative residual spatially interpolated rainfall showed a generally long drying period from 1903 to 1946 which was followed by a generally wetter period from 1947 to 2000. It is unclear whether the period following 2000 represents the start of another long-term drying period. This 40 to 50 year periods correspond to the drought-dominated and flood-dominated periods identified by Erskine and Bell (1982). These major swings in climate have significant implications for both stream and groundwater hydrology and catchment management.

Non-parametric percentile rainfall ranking method was used to identify of significant droughts in both the FDR and DDR regimes. Rainfall summed over the 12 month time periods, to identify periods of extremely low rainfall or drier periods are the lowest 10 percentile and high rainfall or wetter periods are the highest 10 percentile. It was found over the period 1900 to 2008 that there were 23 droughts in which the rainfall over 12 months dropped below the $10^{th}$ percentile. There were 14 such droughts in the period 1900 to 1946 and 9 from 1947 to 2008. The most severe 12 month meteorological drought on record occurred in August 1902, followed in severity by March 1983 and August 1919. For these droughts the rainfall in the proceeding 12 months was only 270, 278 and 288 mm respectively. The highest 12 month rainfall on record occurred in 1950 when the rainfall in the preceding 12 months was 1264 mm. While this analysis is strictly for meteorological drought it is expected that the use of percentiles for 12 month rainfalls should also identify significant hydrological droughts (White *et al* 1999).

The results of relationships between rainfall in the Wybong catchment and the southern oscillation index found a relatively weak association. This is consistent with previous findings that rainfall throughout most of eastern Australia, is relatively weakly related to SOI, (McBride and Nicholls 1983; Stone *et al.* 1996).

Analysis of the seasonality of monthly rainfall revealed some interesting trends. While the cumulative residual summer rainfall showed the drying trend from 1903 to 1946 and a generally wetter period from 1947 to at least 1978, the winter rainfall showed quite different behaviour. Winter cumulative residual rainfall showed a wetter period from 1903 to about 1974 followed by a major drying out in winter rainfall between 1975 and 2006. This appears to indicate a switch in seasonality of rainfall.

Spring rainfall seems to follow the summer trend while autumn rainfall appears to have no long-term trends. Since winter rainfall is hydrologically important for generating runoff, this switch in seasonality of rainfall has significant implications for runoff.

An examination of catchment yield for the period where stream flow record exists, (1955-2008) shows major variation in the runoff coefficient in line with the extreme droughts and wet periods identified above. While the long term mean runoff coefficient is 0.07, annual runoff coefficients (**Figure 3.20**) varied between a high of 0.36 in 1957 to zero in 2006. Runoff in the period from 2000-2006 appears anomolously low and could be due to excessive water abstraction.

The impacts of droughts and water pumping from the catchment on long-term catchment yield were observed. Catchment yield decreased probably due to water pumping and declined soil moisture during 2001 to 2007 drought. The rainfall-runoff process was highly influenced by other factors such as drainage changes, baseflow loss, etc. through ground-water withdrawals. Therefore, the major and long-term declines in yield were experienced not only due to decrease soil moisture during the drought but also water abstraction. The comparison between percentile rankings of runoff and rainfall also concludes that rainfall-runoff processes are strongly influenced by land use changes due to agriculture, pre-urbanisation and less rainfall during drought. An overall result indicates that catchment water is over allocated against its capacity. The results suggest that total amount of water pumping should be controlled by the local water management authority when flow either decreases or remains constant. It is worthwhile to note that this suggestion is a prediction as water abstraction data was not available for this assessment.

# CHAPTER 4: SALINITY DISCHARGE AND SALT BALANCE IN WYBONG CATCHMENT

This chapter aims to identify salinity processes, sources and salt exports within Wybong Creek study catchment. Stream gauge data analysis can indicate the relative magnitude of groundwater discharge which provides a mechanism for solute discharge. The study used the stream discharge (Q ML/day) and electrical conductivity (EC μS/cm) to estimate salt load, salt output/input ratio and sources of salinity in the catchment. This analysis includes comparisons between stream discharge and salinity, estimating of salt load, baseload salt flux and catchment salt balance. The analysis not only provides a framework for assessing salinity dynamics within this system but also provides indicators of solute sources in the catchment.

## 4.1. Background on Salinity Output/Input Ratios

Salinity is one of the major environmental issues in many parts of the world (Ghassemi *et al*., 1995) and has been a political focus over the past years in Australia. The definition of salinity varies widely. The generally accepted definition is 'the concentration of total dissolved solids in soil and water (Ghassemi *et al*., 1995). Salinity is frequently classified into two types: 'primary salinity'; naturally occurring salinity and 'secondary salinity' or human induced salinity, where perturbation of the hydrologic cycle leads to the redistribution of solutes within the landscape (Peck and Hatton, 2003).

Salinity is also classified according to its association with land use, such as industrial, irrigation, urban and dryland salinity. Dryland salinity is one of the principal secondary salinity issues in Australia and in many locations occurs as a result of increased recharge due to clearance of deep-rooted perennial native vegetation and its replacement with shallow-rooted annual crops and pastures causing increasing groundwater levels. Rising groundwater levels can result in increased discharge of saline groundwater into streams. Dryland salinity draining into catchments is considered to be increasing stream salinities in the Murray–Darling Basin (Jolly *et al*., 1997a, 2001). In areas with high natural storage of salt in the unsaturated zone, increased

recharge from clearance of native vegetation can result in the salinisation of otherwise fresh groundwater in unconfined aquifers (Cook *et al*., 1993; Leaney and Herczeg, 1999). Irrigation salinity, on the other hand, occurs when excess irrigation water infiltrates through the soil, recharging generally saline groundwaters. In streams salinisation, the discharge of salt to stream generally takes place by three mechanisms: direct runoff, groundwater discharge and throughflow discharge (Schofield *et al*. 1988).

A number of salinisation processes are possible in the Hunter catchment, including dryland salinity (Beale *et a*l., 2000), irrigation (Healthy Rivers Commission, 2002), and input from the mining of coal and associated formations (Creelman, 1994). Most industries in the Hunter have some impact on the region's surface and groundwater. The main inputs of salt in the Hunter region are believed to be aeolian deposition of dust, marine-aerosol-origin cyclic salts and parent rock weathering (Kellet *et al*. 1989). Significant deposits of salinity in the Hunter Region appear stored in alternating shallow marine and continental Triassic and Permian sediments (Branagan *et al.,* 1976). Mining of Permian coal measures in the Hunter and use of coal and water in thermal power stations produces significant volumes of saline wastewater. In the past, point-source, wastewater discharges from mines and power station into the Hunter caused serious declines in river water quality. Stream salinity is of particular concern to the region's communities, dryland farmers and irrigators who rely on stream water.

This study focuses on investigating the catchment salinity status using the mass-balance output/input (O/I) ratio which is a key indicator of catchment salinity status (Peck and Hurle, 1973). O/I ratio is also used to identify problems of catchments and relies on determination of salt loads in streams and rainfall (Jolly et al., 1997a; 1997b; 2001). Jolly *et al*. (1997a, 2001) compared estimation of the influx of airborne oceanic salt aerosols (cyclic salts) deposited in rainfall to the calculated salt load exported by streams, using mostly sporadic measurements of stream EC to infer salt loads. In this study the main assumption is that the sources of salt in the stream are marine-aerosol origin cyclic salts, deposited by rainfall, concentrated by evapotranspiration and discharge of stored saline groundwater. Under these assumptions, estimates of the ratio of cyclic salt load exported in streams to that imported in rainfall can be used to infer both catchment salt load output/input ratios (O/I) and the impacts of land use change on stream salinization. In other catchments, however, it has been shown that mineral and

regolith weathering is also an important contribution to stream salt loads (White *et al.*, 2009).

## 4.2. Methods

### 4.2.1 Stream Salt Load

Stream salt load was estimated from gauged measurements of daily stream flow and daily average total dissolved solids concentration (TDS) which was inferred from daily averaged stream electrical conductivity (EC) measurements.

### 4.2.2 Stream Flow and Specific Discharge

Daily stream flow data (Q, $MLday^{-1}$) for the Yarraman gauging station (#210040) in the lower Wybong catchment (see Fig. 1) were sourced from the Pinneena Database (DNR 2008). The area of the catchment above the gauging station is 675 $km^2$. Specific discharge, q ($mm\ day^{-1}$) was calculated by dividing stream flow by this catchment area.

$$q = \frac{Q}{A} \tag{4.1}$$

The flow record began in 1955, but because EC data collection only commenced in 1993, only flow data between 1993 and 2008 were used in this study. In this period there were 260 days of missing flow data due to equipment failure.

### 4.2.3 Filling Missing Flow data

Missing daily flow data were filled in using the IHACRES rainfall-runoff model (Croke *et al.* 2005). The input data for the model are catchment area, pan evaporation and rainfall. The non-linear (LOSS) module converts rainfall into effective rainfall and the linear module transfers effective rainfall to stream discharge. Measurement of fit between observed and modelled stream flow is judged through the value of the coefficient of determination, R**.**

$$R^2 = 1 - \frac{\sum (Q - Q_m)^2}{\sum (Q - \bar{Q})^2} \tag{4.2}$$

where Q is a measured daily flow $\bar{Q}$ is the mean of all measured flow and $Q_m$ is the modelled daily flow value. There are six parameters in the IHACRES model and they

are adjusted to maximise the value of $R^2$**.** The missing Q data were then filled-in with the estimated $Q_m$. The filled-in dataset will be referred to as $Q_i$.

The overall error in specific discharge, in mm per year, was estimated from the Bias, or mean deviation between actual and modelled flow, with

$$Bias = \frac{\sum(q - q_m)}{n} \tag{4.3}$$

where n is the number of measured daily q values.

### 4.2.4 Measured Stream EC

Average daily electrical conductivity (EC, $uScm^{-1}$) at Yarraman EC for 1993 to 2008 were also sourced from the Pinneena Database CD (DNR 2008). The record had 995 missing daily values due to equipment malfunction.

### 4.2.5 Estimation of Total Dissolved Salt Concentration from EC

The total dissolved salt concentration (TDS, mg $L^{-1}$) (Appelo and Postma, 2005) is the summation of the mass concentration of the measured major dissolved ions, $C_i$, $(\text{mg L}^{-1})$:

$$\text{TDS} = \sum \text{C}_\text{i} \tag{4.4}$$

The measured major ion concentrations for stream waters sampled from various locations in the catchment together with the measured EC of the samples were used to calculate a relation between TDS (mg $L^{-1}$) and EC (μS $cm^{-1}$). A simple linear proportionality $\text{TDS} = \text{A} \times \text{EC}$ has often been used as an approximate relationship (e.g. Mackay *et al.,* 1988) but this ignores that fact that the relation is nonlinear at lower salt concentrations as a consequence of the Onsager limiting law (Robinson and Stokes, 1970) and that the proportionality "constant" A changes with changes in ion relative concentrations and ion species (Hem, 1982, 1992). Because of this a power law relation was used to relate TDS to EC (μS $cm^{-1}$) measurements (White *et al*, 2009), which necessarily goes through the origin unlike a simple linear fit with an intercept.

$$\text{TDS} = \text{a.EC}^\text{b} \tag{4.5}$$

### 4.2.6 Filling Missing Salt Load Data

Missing *EC* (μS $cm^{-1}$) data were estimated using the concept of the flow-weighted mean EC (Joly *et al*, 2001). The daily salt flux ($S_i$, tonnes $day^{-1}$) is the product of daily flow $Q_i$ (MLday$^{-1}$) and daily mean TDS estimated from EC. The daily salt flux follows from equation (4.5)

$$S_i = a.10^{-3} EC^b.Q_i \tag{4.6}$$

with the factor $10^{-3}$ required because of conversion of units. $S_i$ was calculated using equation (4.6) where corresponding daily values of $Q_i$ and EC values existed. A power law relationship was then used to fit a relationship between calculated salt load and measured stream flow.

$$S_i = Q_i^c \tag{4.7}$$

Where *c* is a constant Equation 4.7 was used to interpolate all daily salt loads, $S_i$ from the in-filled continuous daily flow data ($Q_i$).

This method assumes that there is no change in catchment weathering with time.

With the flow and salt load data sets filled in, the cumulative stream flow $Q_{cum}$ (ML) is simply

$$Q_{cum} = \sum_{i=1}^{n} Q_i \tag{4.8}$$

and the cumulative salt load $S_{cum}$ (tonnes) is similarly

$$S_{cum} = \sum_{i=1}^{n} S_i \tag{4.9}$$

The mean specific salt load, $S_s$ (tonnes $km^{-2}$ $year^{-1}$) from the catchment is just:

$$S_s = \frac{S_{cum}}{A_c.t} \tag{4.10}$$

where $A_c$ is the catchment area ($km^2$) up to the gauging station and t is the length of the measurement period (years).

### 4.2.7 Rainfall and Salt Inputs to the Catchment

The area-weighted monthly rainfall for the catchment was calculated as discussed in the Chapter 3 in Section 3.2.2.5 and was summed to produce annual rainfall.

#### 4.2.7.1 Estimating the salt deposition rate in the Wybong Catchment

There are two sources of atmospheric inputs of salinity in the Wybong catchment. The first is the meteoric deposition of cyclic salt in rainfall. The second is the dry deposition of dust. The State Pollution Control Committee (SPCC, 1987) reported major ion analyses of rainfall samples collected at the Bunnan meteorological station in normally closed (rainfall only) and always open containers (dust plus rainfall) for each rainfall event during the period 1984-1986. Data on the major ion chemistry of rainfall chemistry is only available for the period 1984-1986. The average rainfall for this period is 667 mm very close to the long term average for the catchment of 670 mm. In this period, 1984 was a wetter year with annual rainfall of 848 mm, this corresponds to the 89 percentile of the annual rainfall record. The year 1986 was a relative dry period with annual rainfall 505 mm, which corresponds to the 38 percentile of the annual rainfall record. While the period chosen does not span the complete variability of the rainfall record it does span the record between the 38 and 89 percentile and the mean lies close to the long term mean. So this period can be considered as reasonably representative. It will be assumed here that this data is relevant to the period 1993 to 2008.

This study will consider one rainfall event, of magnitude P (mm). It is assumed that the area for salt deposition in the normally open and closed containers is the same and equal to $A_s$ cm$^2$.

Let: $C_P$ (mg/L) be the concentration of salt in the normally closed container and is salt deposited by rain and

$C_{P+D}$ (mg/L) be the concentration of salt in the normally open container and is salt deposited by rain (in the same rainfall event) plus dust. It is expected that $C_{P+D} > C_P$.

#### 4.2.7.2 Salt deposited in rainfall

The total volume of rainfall $V_p$ (L) in the closed rainfall container is:

$$V_p = 10^{-4}.P.A \tag{4.11}$$

where the factor $10^{-4}$ converts mm into cm and cm$^3$ into L. The total mass of salt, $M_P$ (mg) deposited in the rain only container is

$$M_P = 10^{-4}.C_P.P.A \tag{4.12}$$

The salt deposition per unit area in this rainfall event is $S_p$ (mg/m$^2$ or kg/km$^2$) is just:

$$S_P = C_P.P \tag{4.13}$$

The salt deposition rate in tonnes per km$^2$ is $10^{-3}.S_P$

The total salt deposited in all rainfalls per unit area over the period 1984-1986, $S_{T_P}$ (tonnes/km$^2$) is:

$$S_{T_P} = 10^{-3}.\sum_{i=1}^{n} S_{P_i} = 10^{-3}.\sum_{i=1}^{n} (C_{P_i}.P_i) \tag{4.14}$$

where n is the total number or rain events and $P_i$ and $C_{P_i}$ are the individual rainfall and corresponding TDS concentration for each separate event. Finally the precipitation-weighted salt deposition rate over the period 1984-86, $\overline{S}_P$ in tonnes/km$^2$/mm rainfall is $S_T$ divided by the total rainfall in the period:

$$\overline{S}_p = \frac{S_{T_P}}{\sum_{i=1}^{n} P_i} = \frac{10^{-3}.\sum_{i=1}^{n} (C_{P_i}.P_i)}{\sum_{i=1}^{n} P_i} \tag{4.15}$$

The total salt deposition (tonnes/km$^2$/y) in annual rainfall is found by multiplying the annual rainfall $P_a$ (mm) by $\overline{S}_P$. The total annual salt input into the whole catchment (relevant to the stream gauge) from rainfall, $\overline{\overline{S}}_p$ (tonnes/y) is

$$\overline{\overline{S}}_p = \overline{S}_p.P_a.A_c \tag{4.16}$$

where $A_c$ (km$^2$) is the catchment area above the stream gauge.

#### 4.2.7.3 Dry deposition of salt

The total mass of salt deposited through dry deposition and rainfall, $M_{P+D}$ (mg) deposited in the always open, rainfall plus dust container (assumed area A) after a rainfall of P is:

$$M_{P+D} = 10^{-4}.C_{P+D}.P.A \tag{4.17}$$

and the total salt deposition per unit area after this rainfall event is $S_{P+D}$ (mg/m$^2$ or kg/km$^2$) is just:

$S_{P+D} = C_{P+D}.P$ If require $S_{P+D}$ in tonnes/km$^2$ then

$$S_{P+D} = 10^{-3}.C_{P+D}.P \tag{4.18}$$

Using equation (4.13) now can estimate the dry deposition of salt by dust, $S_D$ (tonnes/km$^2$) as:

$$S_D = S_{P+D} - S_P = 10^{-3}.P.(C_{P+D} - C_P) \tag{4.19}$$

The total salt deposited in dust per unit area over the period 1984-1986, $S_{T_D}$ (tonnes/km$^2$) is:

$$S_{T_D} = \sum_{i=1}^{n} S_{D_i} = 10^{-3}.\sum_{i=1}^{n}([C_{P+D} - C_P]_i.P_i) \tag{4.20}$$

The total mean salt deposited as dust per year, $\overline{S}_D$ (tonnes/km$^2$/y) is:

$$\overline{S}_D = \frac{S_{T_D}}{t} = \frac{10^{-3}.\sum_{i=1}^{n}([C_{P+D} - C_P]_i.P_i)}{t} \tag{4.21}$$

where t (y) is the time period over which samples were collected (1984-6). The total average annual salt input by dust into the catchment above the stream gauge, $\overline{\overline{S}}_D$ (tonnes/y) is:

$$\overline{\overline{S}}_D = \overline{S}_D.A_c \tag{4.22}$$

#### 4.2.7.4 Total annual salt deposited in the catchment

The total salt inputs into the catchment from meteoric cyclic salt and from dust $\overline{\overline{S}}_T$ (tonnes/y) in any year with annual rainfall $P_a$ is

$$\overline{\overline{S}}_T = \overline{\overline{S}}_p + \overline{\overline{S}}_D \tag{4.23}$$

It has been assumed here that a constant average annual dry deposition of dust occurs across the catchment.

### 4.2.8 Catchment Discharge of Water and Salt

The annual discharge of water from the catchment at the gauging station was calculated for the period 1993 to 2008 by summing the daily in-filled flow data for the Wybong gauging station (Equation 4.9). Annual salt load discharged from the catchment was estimated by summing the in-filled daily salt load (Equation 4.10).

### 4.2.9 Annual Catchment Runoff Coefficient and Salt Output/Inputs Ratios

The annual catchment runoff coefficient was calculated from the ratio of the annual specific discharge from the catchment to annual interpolated rainfall $\left(\sum_{1y}(q)\Big/\sum_{1y}P\right)$.

The annual salt output/input ratio was calculated from the annual stream salt load divided by the estimated annual salt deposition in dust and rainfall for the catchment above the gauging station.

### 4.2.10 Flow and EC Probability

EC and $Q_i$ were ranked in ascending order and assigned a ranking number *m,* starting with 1 for the minimum and maximum flow to *n,* where *n* is the number of flow measurements. The probability *P* that a given flow will be equivalent to

$$P=m/n \tag{4.24}$$

The exceedence E is, $E=1-P$

### 4.2.11 Major Ions in Surface Water

Groundwater and surface water samples were collected during July 2006, a period of low flow. Water samples were taken from 10 sites of the Wybong stream and six bores at locations shown in **Figure 4.1** where stream and groundwater sites are listed in Table 4.2 and Table 4.5, respectively. Stream water samples were collected from near the middle of the stream channel at a depth of approximately 0.6 of the stream depth from the bottom. Groundwater sample were collected from piezometers and bores using an electric submersible pump after suitable purging. At least three well volumes of groundwater were removed from each bore prior to sampling. EC of surface and groundwater samples were measured in the field using a calibrated TPS FLMV-90 meter. Surface water samples were filtered (0.45 μm membrane) immediately after sampling. A 14 ml filtered sample was stored in a polyethylene bottle for laboratory anion IC analyses. Another two 14 ml filtered samples were stored in an acid-washed polyethylene bottle and acidified to pH<2 using nitric acid for cation analyses. After filtration, samples were stored at <5 $^0$C until analysis of major ions using inductively coupled plasma optical emission spectroscopy (ICPOES) at Environmental Analytical

Laboratory (EAL) in Sothern Cross University. Alkalinity was measured in the field on filtered (0.45 µm membrane) triplicate samples using a HACH digital titration kit (Method 8203) with methyl orange indicator.

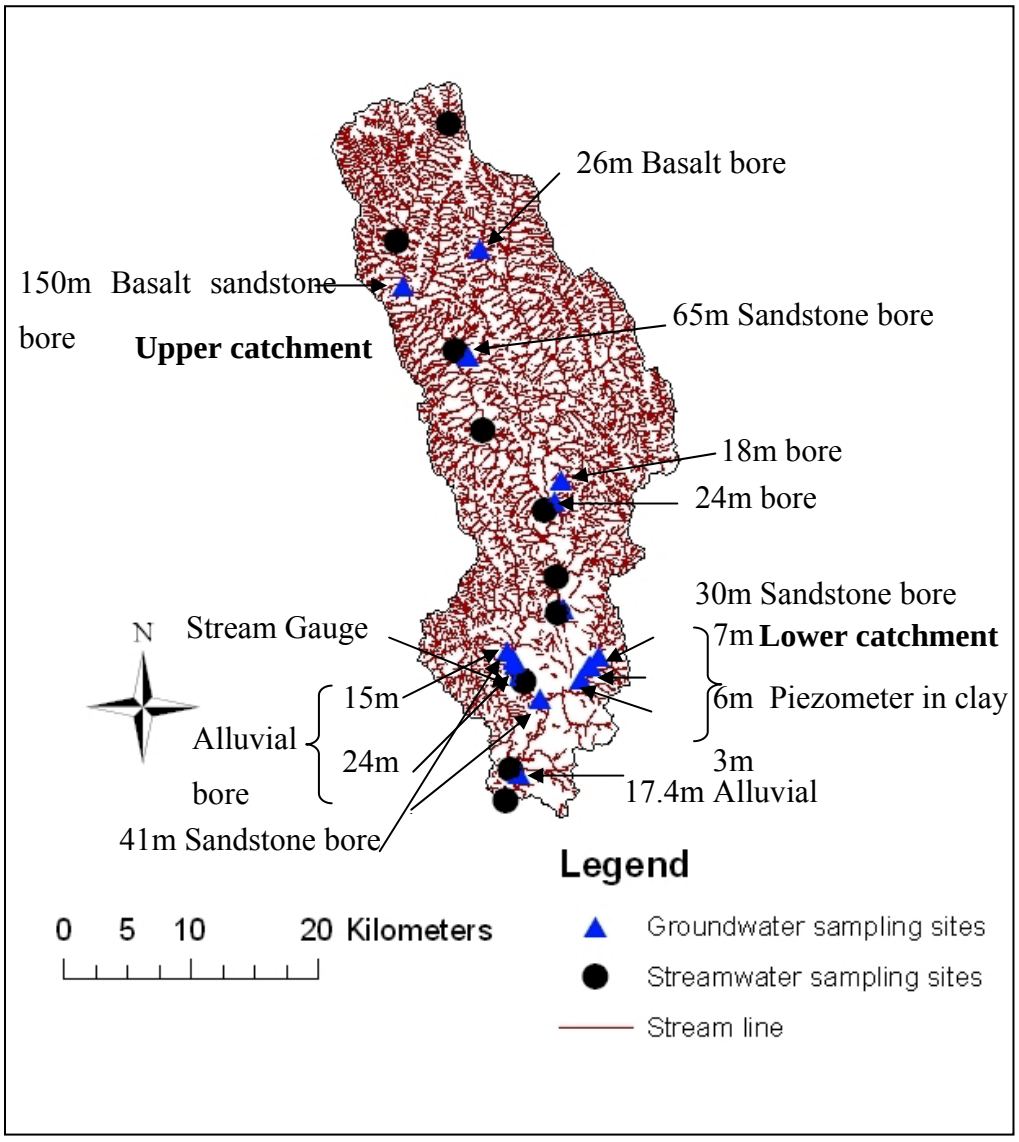


**Figure 4.1** Surface (round) and groundwater (triangular) sampling sites in Wybong catchment

### 4.2.12 Baseload Salt Flux

Baseflow was calculated using Baseflow separation by Lyne Hollick method (Lyne and Hollick, 1979). Details of this method will be discussed in Section 5.2 of Chapter 5**.** The technique was applied for the period 1993 to 2007. The total dissolved salt

concentration (TDS, mg $L^{-1}$) of the bores was calculated using equation 4.4. Baseload salt load $S_b$ (Tonnes $year^{-1}$) was estimated using

$$S_b = 10^{-3}.G_b.Q_b \tag{4.25}$$

where, $G_b$ (mg $L^{-1}$) represents total dissolved salt concentration of groundwater bores, $Q_b$ is the baseflow (ML $year^{-1}$).

## 4.3. Results and Discussion

### 4.3.1 Fitting Flow Data to Fill Missing Values

Flow was predicted using rainfall and evaporation data in the IHACRES rainfall-runoff model. The predicted flow fits the measured flow data, for example 2002-2003, with an $R^2$ of 0.76 and a bias of 0.057 mm/year. The model parameters are listed in **Table 4.1**. This positive bias means that the model under-predicts flow so that using the model to in-fill missing flow data will result in a conservative estimate of salt load. The measured flow is modelled reasonably well but the fit deteriorates over time when rainfall decreases during recession flows when ground water inputs are the source of base flow and the rainfall-runoff relationship gives a poorer fit for stream flow.

**Table 4.1** IHACRES model parameters

| Non linear module Parameters | Values | Linear module Parameters | Value |
|---|---|---|---|
| Drying rate at reference temperature (tw) | 2.00 | Recession rate 1 ($\alpha^{(s)}$) | -0.262 |
| Power on soil moisture (p) | 1.0 | Peak response 1 ($\beta^{(s)}$) | 0.738 |
| Moisture threshold for producing flow (l) | 0.0 | Time constant 1 ($\tau^{(s)}$) | 0.747 |
| Temperature dependence of drying rate(f) | 0.00 | Volume proportion 1 ($v^{(s)}$) | 1.00 |
| Mass balance term (c) | 0.0012 | | |

**Figure 4.2** shows the modelled and measured monthly stream flow over the period 2002 to 2003. **Figure 4.2** illustrates the poorer fit during low flow periods where the total cumulative flow predicted is only about one third of the total flow. These discrepancies do not have a major impact on the estimated salt load since the model under predicts flow at low discharges when salt loads are small. It should be noted that only 260 days of missing flow data out of 5840 days were considered for filling data.

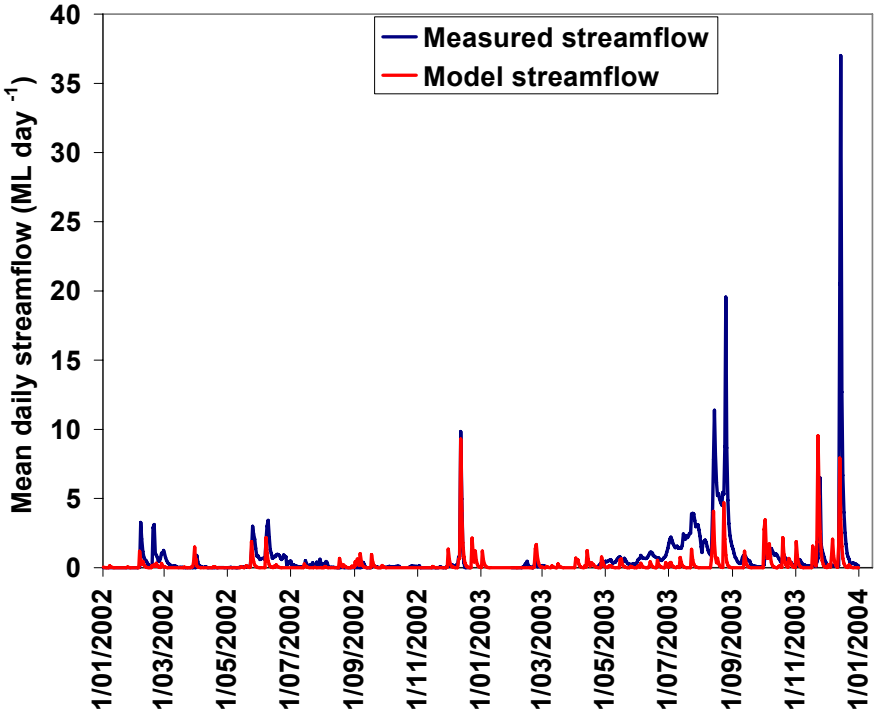


**Figure 4.2** Relationship between model and measured streamflow during 2002-2003

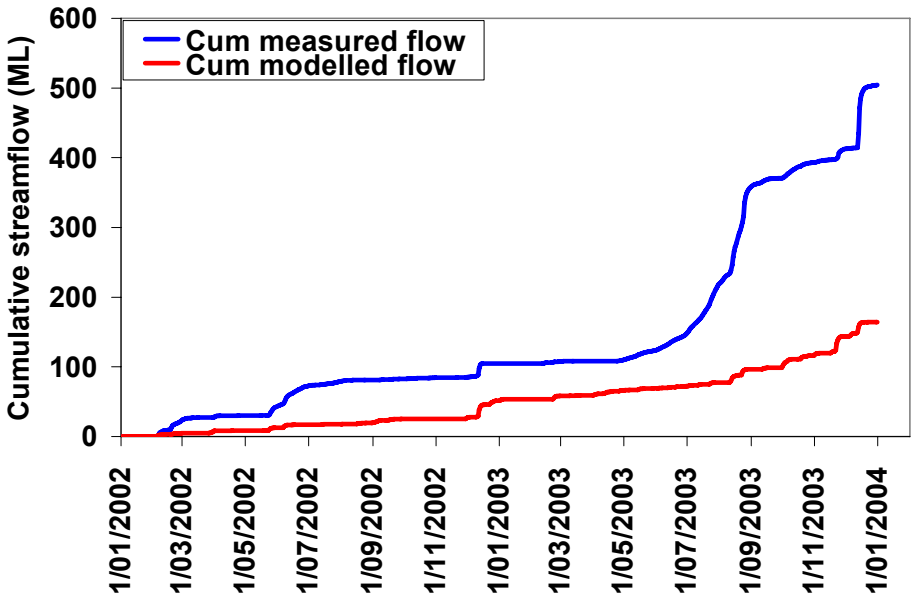


**Figure 4.3** Cumulative measured and modelled streamflow during the dry period January 2002 to December 2003

F**igure 4.3** shows the comparison between the cumulative stream flow and measured stream flow for the longest period of record without missing daily stream flow data. This illustrates the fact that the IHACRES model has difficulties in a stream where bseflow dominates for long periods such as in drought.

### 4.3.2 Relationship between TDS and EC

**Table 4.2** lists the major ion analyses, TDS and measured EC found for the Wybong stream water samples throughout the catchment. The power law between TDS and EC (Equation 4.4) for all the catchment samples gives a=6.75, b=0.70 with a strong coefficient of determination of $R^2$=0.95. When stream data is separated between the upper and lower catchments, quite different relationships are apparent **(Figure 4.4**) for the location-specific samples. The coefficients for equation 4.2 and the $R^2$ values are given in **Table 4.3**. The difference in these coefficients was significant at the 95% confidence level. This possibly suggests that the stream chemistry in the lower catchment is different to that at the upper catchment. The TDS and EC's determined at the stream gauging station in the lower catchment for the calibration in **Figure 4.4** were all measured under lower flow conditions and higher EC conditions in 2005. In order to estimate TDS from the lower EC occurring during higher flow conditions we have assumed that the calibration found for the entire catchment is applicable at the gauging station.

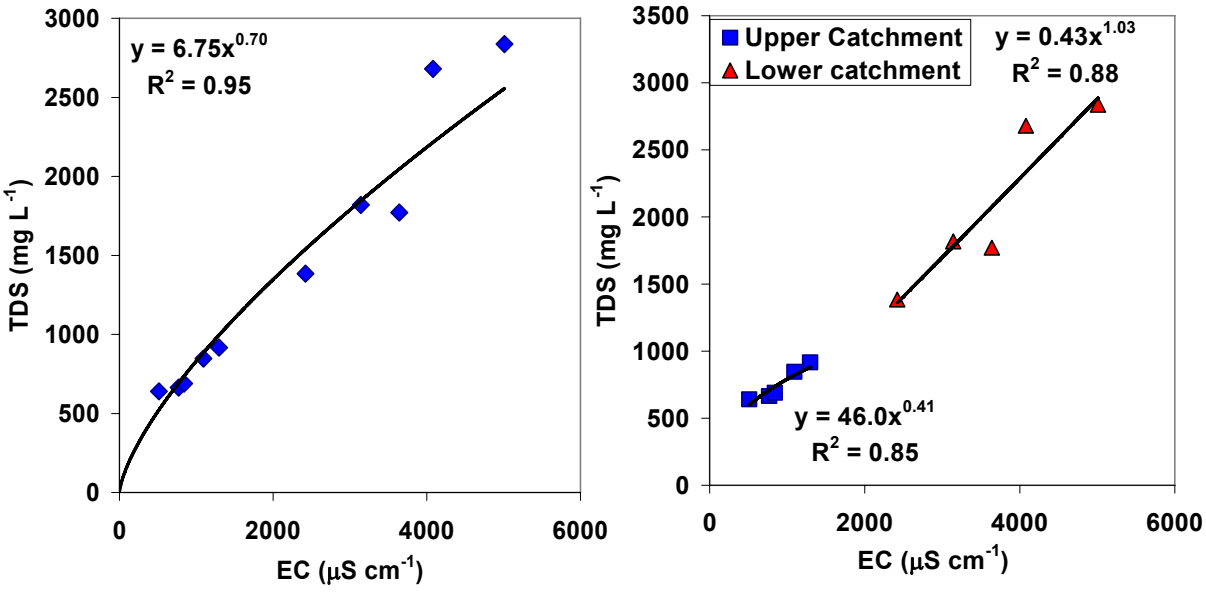


**Figure 4.4** Relationship between TDS and EC for the Wybong catchment.

**Table 4.2** Surface water chemistry for the Wybong catchment in July 2006

| Sampling location | Date | EC ($\mu$S cm$^{-1}$) | Na (mg L$^{-1}$) | K (mg L$^{-1}$) | Ca (mg L$^{-1}$) | Mg (mg L$^{-1}$) | Cl (mg L$^{-1}$) | $HCO_3$ (mg L$^{-1}$) | $SO_4$ (mg L$^{-1}$) | TDS (mg L$^{-1}$) |
|---|---|---|---|---|---|---|---|---|---|---|
| Campground | 21/07/2006 | 768.5 | 53.2 | 0.61 | 48.9 | 50 | 32.4 | 472 | 8.52 | 665 |
| Headwaters | 21/07/2006 | 512 | 50.3 | 0.77 | 28.4 | 28.8 | 23.8 | 478 | 29.6 | 640 |
| Bunnan | 21/07/2006 | 842 | 51.6 | 0.86 | 51.4 | 56.6 | 44.4 | 482 | 2.65 | 689 |
| White Rock | 21/07/2006 | 1092 | 74.7 | 2.88 | 54.9 | 67.2 | 91 | 552 | 3.75 | 847 |
| Dry Ck Rd | 21/07/2006 | 2421 | 224 | 2.72 | 70.3 | 98.3 | 508 | 546 | 26.2 | 1475 |
| Ridgeland | 21/07/2006 | 1296 | 102 | 1.82 | 54.4 | 67.5 | 206 | 476 | 8.18 | 916 |
| Hollydeen | 23/07/2006 | 3640 | 249 | 5.42 | 109 | 142 | 818 | 430 | 18 | 1771 |
| Rockhall Causway | 23/07/2006 | 3140 | 277 | 5.12 | 107 | 143 | 846 | 432 | 8.31 | 1819 |
| Yarraman gauge | 6/01/2007 | 4080 | 350 | 7.3 | 160 | 250 | 1300 | 578 | 35 | 2680 |
| Railway bridge | 23/07/2006 | 5010 | 454 | 5.78 | 178 | 224 | 1496 | 451 | 29.4 | 2837 |

**Table 4.3** Coefficient and $R^2$ for the lower and upper catchment

| Coefficient in Equation 4.5 | a | b | $R^2$ | p |
|---|---|---|---|---|
| Whole catchment | 6.75 | 0.70 | 0.95 | 0.00 |
| Upper catchment | 46 | 0.41 | 0.85 | 0.027 |
| Lower catchment | 0.43 | 1.03 | 0.88 | 0.019 |

### 4.3.3 Fitting Salt Load Data to Fill Missing EC Values

The relation between the log of the calculated daily salt load $\log_{10}(S_0)$ and the log of the measured daily stream flow, where pairs of data existed, is shown in **Figure 4.5**. The data is fitted to Equation 4.6, giving a value of the constant c of c= 0.93 with $R^2$=0.98. This relation was then used to infill the missing salt loads for the period 1993-2008.

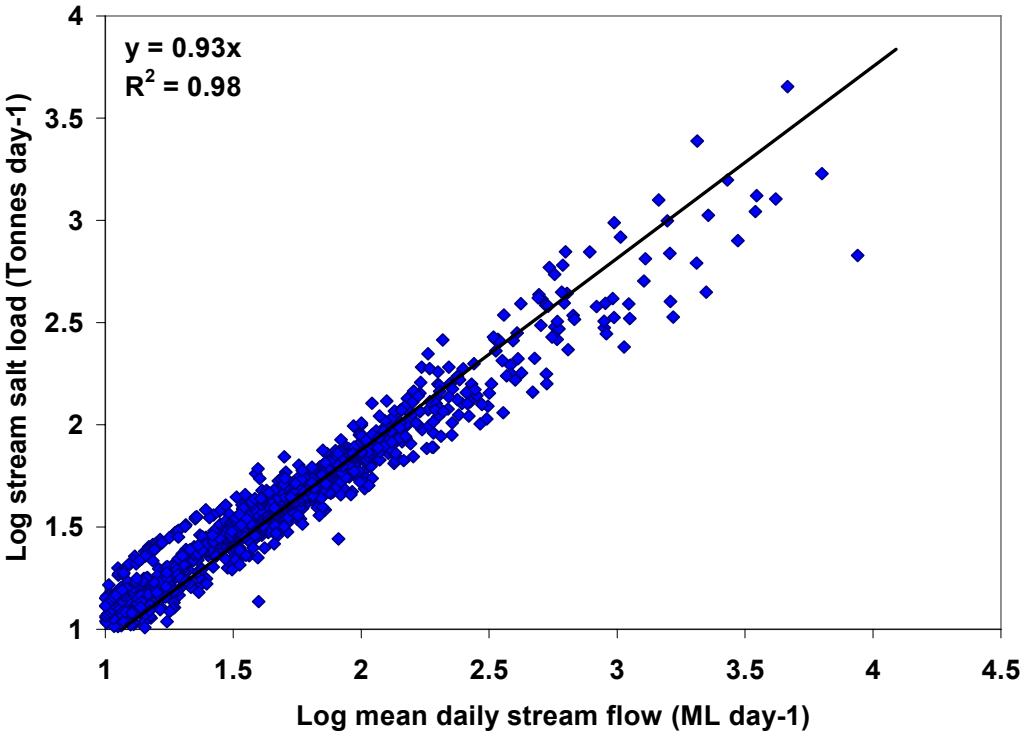


**Figure 4.5** Relationship between log daily salt load and log daily stream flow, at Wybong catchment

### 4.3.4 Relationship between Stream Flow and EC

The relationship between stream flow and EC in **Figure 4.6** appears different over different time periods. During some high flow periods in 1996 to 1997 and 2008, EC increased with stream flow. This may be due to mobilized surface salts deposited during preceding dry periods. It could also be caused by high watertable discharging more saline groundwater. During other periods of high stream flows in 1998 to 2000 and June 2007 EC was lower presumably due to fresher surface runoff during high intensity rainfall events.

Elevated stream salinities were observed during low flow period of 2001-May 2007 due to perhaps the increased contribution of more saline baseflow to the stream. Since 2001, stream flow has been substantially smaller and there was an increasing trend in EC within the catchment until June 2007. The stream salinity is high in the no-flow period from late 2006 to early 2007 possibly due to the predominance of groundwater in the stagnant pools.

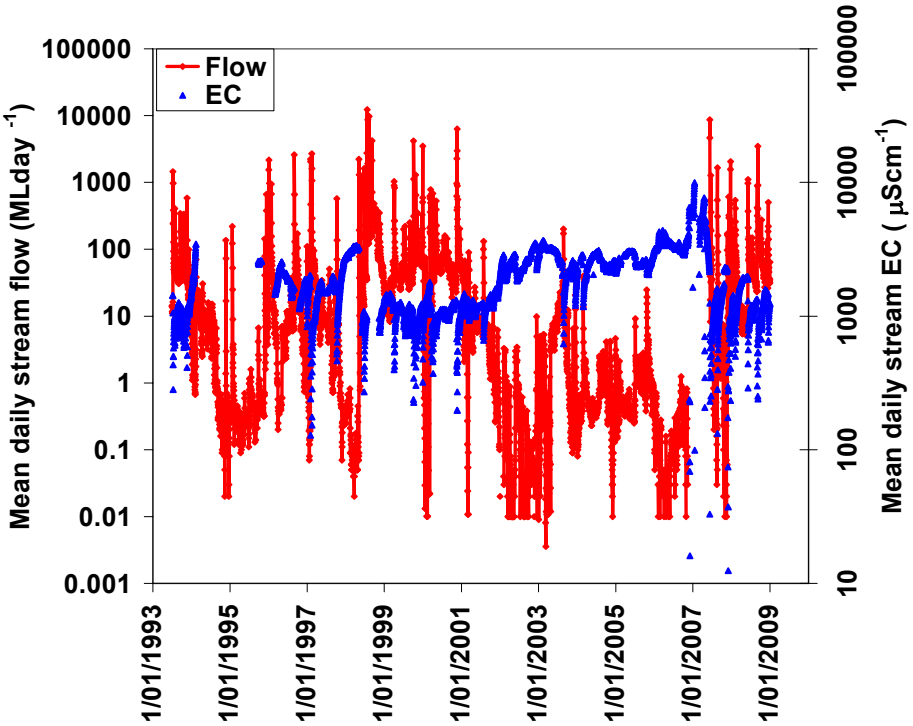


**Figure 4.6** mean daily stream EC and streamflow, Q from 1993 to 2008

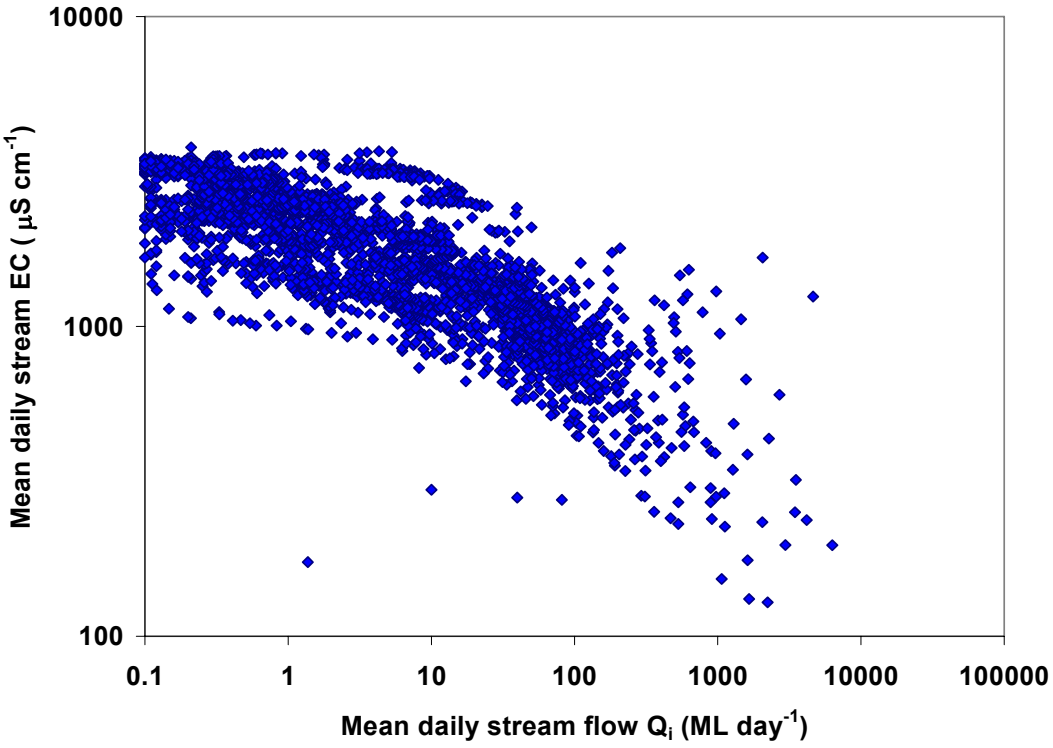


**Figure 4.7** Relationship between mean daily stream EC and streamflow, Q, in the Wybong catchment from 1993 to 2008

The relationship between stream EC and $Q_i$ in **Figure 4.7** shows, on average, that the highest flows have lowest EC however there is considerable variation. The highest EC appear here to occur at flows of 1.76 $MLday^{-1}$, well in excess of the lowest flow of 0.1 $MLday^{-1}$. The mean flow and mean EC are 48 $MLday^{-1}$and 1950 $\mu S\ cm^{-1}$, respectively, over the period of 1993 to 2008. There are also some high EC, such as 1241 $\mu S\ cm^{-1}$, during the highest flow of 4635 $MLday^{-1}$. White *et al*., (2009) also reported variations in EC with flow for annual data in the lower Murray River. Without additional data it is pointless to speculate on the processes causing these variations which could include erroneous data.

### 4.3.5 Cumulative Flow and Salt Load in the Wybong Catchment

**Figure 4.8** shows the relationship between the cumulative salt load and the cumulative streamflow for the period 1993 to 2008. The long term relation between cumulative stream salt load, $S_{cum}$ tonnes, equation 4.9 and cumulative discharge, $Q_{cum}$ $Km^3$ equation 4.8 is:

$$S_{cum} = 0.650 Q_{cum} \tag{4.24}$$

Equation 4.24 is equivalent to saying that the long term mean total dissolved salt concentration at Wybong is $650\,mg\,L^{-1}$.

There appear to be three major variations in the relationship between cumulative salt load and flow in **Figure 4.8**. Dry periods are considered from the significant meteorological droughts (<10% percentile ranked monthly rainfall) for 12 months rainfall at Wybong in Section 3.3.3 in Chapter 3. High discharge periods are considered for the high rainfall periods when flows exceeded the 70 percentile. The period 1993 to 2008 gives three high discharge trends, August 1998 to December 1999, February 2003 to February 2004, and June 2007 to December 2008 that have lower cumulative salt load than the mean trend. It is observed that the salinity in the water decreases with increasing discharge. Cumulative salt load decreases to below the long term trend at higher flows due to more variable salt load and limited occurrence of large events. The drought periods from 1993 to 2008 with three high salinity trends are July 1995 to February 1998, January 2002 to January 2003 and July 2006 to May 2007. The cumulative salt load rose above the long term trend during these drought periods and

this reflects the increased concentration of salt due to the evaporation of the surface waters and the reduction of the dilution of saline ground waters by the stream waters.

The salinity increases just after periods of increasing discharge. It appears that saline groundwaters and the regolith are contributing to stream salt load and the landscape is draining accumulated and stored salts into the stream. Basically the groundwater storage capacity and available soil water storage capacity are close to optimal storage at such times. Similar results for the baseflow contribution to stream salt load were found in the Williamson *et al.* (1987) study on a cleared catchment in the Western Australian Wheatbelt. In that study, the larger proportion of baseflow caused elevated salt loads at lower flows relative to streamflow volume, while at high flows, the larger volume of quickflow reduced the relative contribution of baseflow and thus salt.

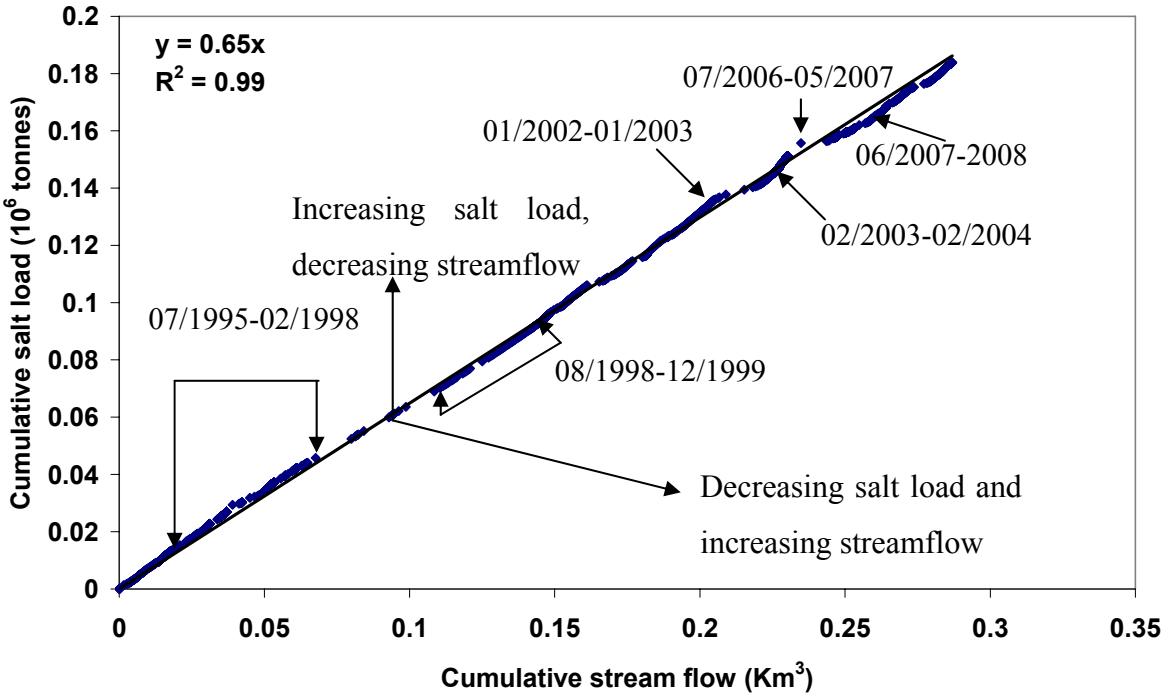


**Figure 4.8** Relationship between cumulative salt load and cumulative flow for Wybong for the period 1993-2008

### 4.3.6. Comparison of Streamflow and EC Exceedance

**Figure 4.9** shows the relationship between flow and exceedence for total record 1993-2008 for the dry period of 2002-2007 and the normal period of 1993-2001. This

dry period is a significant meteorological drought as discussed in Chapter 3. Over the full period, flows of 10 MLday$^{-1}$ were exceeded 34% of the time. In the normal period, flows above 10 MLday$^{-1}$ were exceeded 50% of the time. The tail end of the curve is steep, indicating rapid decline of flow, and the flow between 0.1-0.01 MLday$^{-1}$, may represent base flow during dry times.

During the dry period, flows of 10 MLday$^{-1}$ were exceeded 3% of the time and 0.01 MLday$^{-1}$ is exceeded 78% of the time. Baseflow could constitute 60% of the river flow during the period 2002-2007. During dry periods, EC of 2000 µS cm$^{-1}$ was exceeded 87% of the time. In full and normal periods, EC of 2000 is exceeded 37% and 22%, respectively. High EC values were observed for most of the time during the dry period and this reflects ground water inputs (**Figure 4.10**).

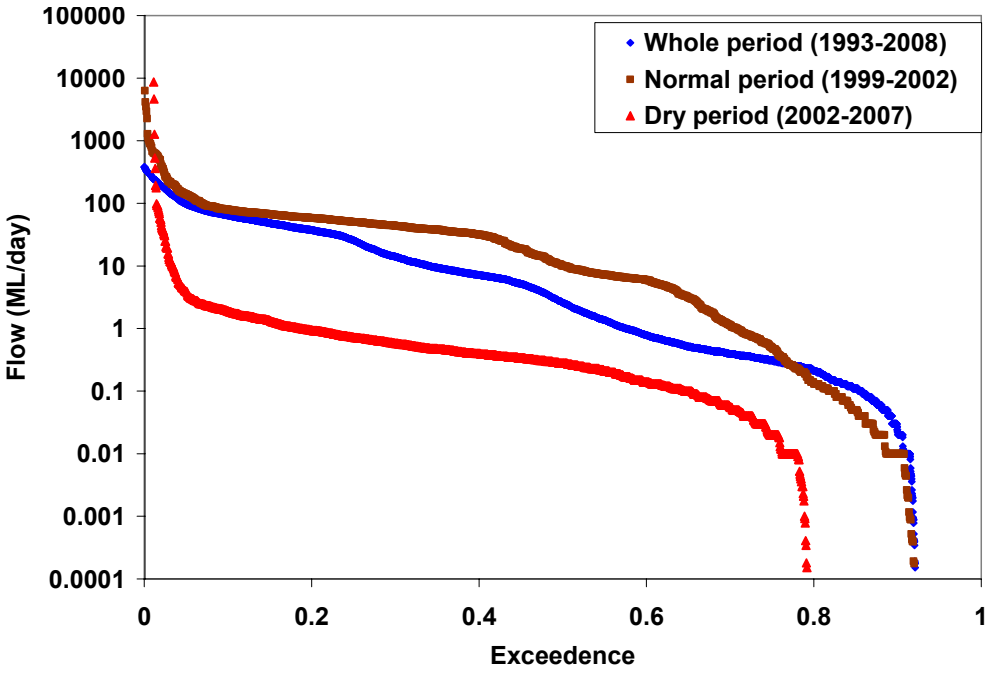


**Figure 4.9** Relationship between streamflow and exceedence

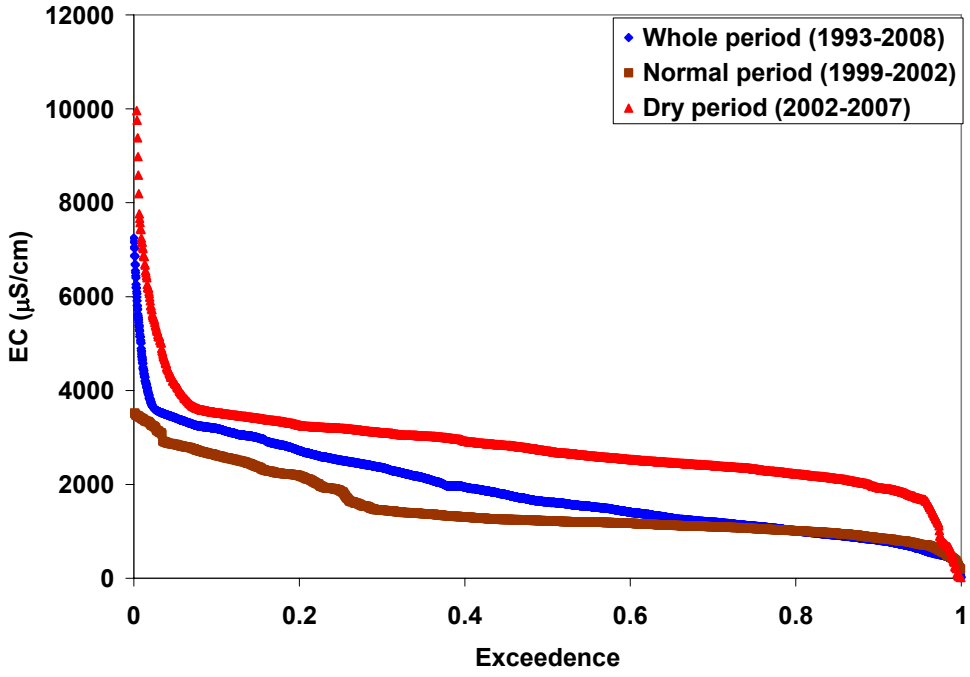


**Figure 4.10** Relationship between EC and exceedence

### 4.3.7 Catchment Salt Balances

From the SPCC data the mean annual dry deposition rate of salt in the catchment was estimated to be 590 tonne year$^{-1}$. Salt O/I balances are used to summarise the catchment's salinity condition and indicates departures from equilibrium condition in the catchment salt balance. Annual salt load O/I ratios during 1993 to 2008 are shown in **Table 4.4**. In many years, such as 1993 to 1994, 1996 to 2001, 2003 and 2007 to 2008, salt outputs are greater than the catchment salt input. In the driest period of 2002 and 2006, the flow was comparatively low and the estimated O/I ratio is 0.1 and the salt output was considerably less than the input. The overall mean O/I ratio of 5.5 in **Table 4.4** suggests that, on average, stored salt is being exported from the catchment. In 8 out of the 16 years in **Table 4.4**, salt O/I ratios are substantially greater that 1. In the dry years, 4 out of the 16 records are substantially less that 1, showing salt storage in the catchment during those years. A further 4 again below average rainfall years have ratios close to 1 indicating equilibrium.

One assumption often made is that it is only stored evaporated cyclic salt that is being exported to the stream during high rainfall periods. It has been assumed here that mean dust salt deposition over the whole catchment is 590 tonnes year$^{-1}$. The largest

recorded event-based dust load in Australia is up to 4.85 Mt which was carried by a dust storm on 23 October 2002 (McTainsh *et al*., 2004). One of the highest dust depositions in Australia is the 94 g $m^{-2}$ $day^{-1}$ measured at Birdsville in the arid Channel Country of the Lake Eyre Basin (McTainsh *et al*., 2006).

**Table 4.4** Estimated annual salt output/input ratios, based on TDS inputs and outputs (C is the runoff coefficient and the mean dry deposition rate is 590 tonnes $year^{-1}$)

| Year | Catchment Rainfall ($MLyear^{-1}$) | Meteoric Cyclic Input Salt ($T\ year^{-1}$) | Total Input Salt ($T\ year^{-1}$) | Stream Discharge ($MLyear^{-1}$) | Output Salt ($T\ year^{-1}$) | C Runoff coeffici-ent | O/I | Mean stream salt con. ($mg\ L^{-1}$) |
|---|---|---|---|---|---|---|---|---|
| 1993 | 520 | 1480 | 2070 | 17680 | 12890 | 0.034 | 6.2 | 730 |
| 1994 | 300 | 840 | 1430 | 2260 | 1980 | 0.008 | 1.4 | 880 |
| 1995 | 440 | 1240 | 1830 | 2500 | 1860 | 0.006 | 1 | 740 |
| 1996 | 500 | 1420 | 2010 | 17580 | 12560 | 0.035 | 6.2 | 710 |
| 1997 | 390 | 1100 | 1690 | 16430 | 10280 | 0.042 | 6.1 | 630 |
| 1998 | 620 | 1760 | 2350 | 93410 | 57570 | 0.151 | 25 | 620 |
| 1999 | 530 | 1520 | 2110 | 33540 | 21170 | 0.063 | 10 | 630 |
| 2000 | 570 | 1610 | 2200 | 43240 | 27550 | 0.071 | 13 | 640 |
| 2001 | 400 | 1130 | 1720 | 3360 | 3040 | 0.011 | 1.8 | 910 |
| 2002 | 300 | 850 | 1440 | 110 | 160 | 0.0003 | 0.1 | 1460 |
| 2003 | 410 | 1160 | 1750 | 2350 | 3260 | 0.010 | 1.9 | 1390 |
| 2004 | 490 | 1390 | 1980 | 400 | 570 | 0.001 | 0.3 | 1430 |
| 2005 | 410 | 1160 | 1750 | 450 | 680 | 0.001 | 0.4 | 1510 |
| 2006 | 230 | 660 | 1250 | 50 | 100 | 0.0002 | 0.1 | 2000 |
| 2007 | 610 | 1720 | 2310 | 28300 | 12260 | 0.047 | 5.3 | 430 |
| 2008 | 520 | 1460 | 2050 | 28460 | 20400 | 0.055 | 9.9 | 720 |
| Mean | 453 | 1281 | 1871 | 18133 | 11646 | 0.03 | 5.49 | 964 |

In the Hunter region, dust generally deposits from mining activity, agricultural, wind erosions (Bridgman, 1992). The work of Nigel Holmes and Associates (1996) shows an increasing trend of dust from 1.7g $m^{-2}$ $month^{-1}$ in 1984 to 2.6g $m^{-2}$ $month^{-1}$ in

1995. It is also considered that dust mobilisation occurs from the Hunter mining work as waste rock piles and dust storms from Central Western Australia which increase the stream salinity. A small portion of the solutes delivered to the catchment via rainfall and dust could recharge the regional aquifers which might then discharge in the catchment. However, this result (**Table 4.4**) may vary because the period taken under consideration for calculating the TDS of rain and dry deposition (1984-1986) was different from the current period (1993-2008).

The estimated average annual salt load exported from the catchment for the period 1993 to 2008 is 17 tonnes $km^{-2}$. In pervious work (Macdonald *et al.* 2009), the long-term average flux (1913-2009) of salt from the Wybong Catchment was estimated to be 3.5 T/$km^2$/yr and 1.6 T/$km^2$/yr was for Goulburn River Catchment. Similar results are found in the work of Jolly (Jolly *et al.*, 1997, 2001) in the Murray–Darling Basin (MDB) where the highest salt imbalances occurred in the upper Murray–Darling Basin and sub-basins of Murrumbidgee, Namoi River and Campspe River with O/I ratios of 2-5.1, 5.1, 9.58 and 14.09 respectively. Jolly (Jolly *et al.*, 1997) also claimed that exported mean annual salt load from the Campspe River at Caliban River@Malmasbury and Murrumbidgee at Muttama Creek@Coolac for the period of 1989-1992 are 28.89 and 20.10 tonnes $km^{-2}$ respectively. Conyers (Conyers *et al.*, 2008) reported that salt delivered to Murrumbidge River from the 17 subcatchments upstream of Wagga Wagga ranging between 4 and 48 tonnes salt/$km^2$/year. The most significant salt imbalance in the Wybong catchment occurred in the high flow year 1998 with O/I ratios of 25 and drought years 2002 and 2006. An average annual salt O/I of 5.5 and the annual O/I in 11 years out of 16 years of greater than 1 indicate that either stored salt is being mobilised or salinity is being produced in the catchment. Catchment salt is in equilibrium in only 1995 and storing cyclic salt occurred in 2002, 2004, 2005 and 2006.

In dry years, O/I are $\leq 1$ when the runoff coefficient is $\leq 0.01$. **Figure 4.11** shows the strong relationship between salt output-input ratio and runoff coefficient. The salt export is clearly dependent on the runoff ratio of the catchment. The O/I rates indicate that discharge of saline groundwater to streams provides the salt load, while rainfall-generated high flow volume is the main driver of salt export. This is similar to the findings of Williamson *et al.* (1987) in the Western Australian Wheatbelt in terms of the total mass of exported salt where the vast majority occurred during periods of high flows generated by high rainfall.

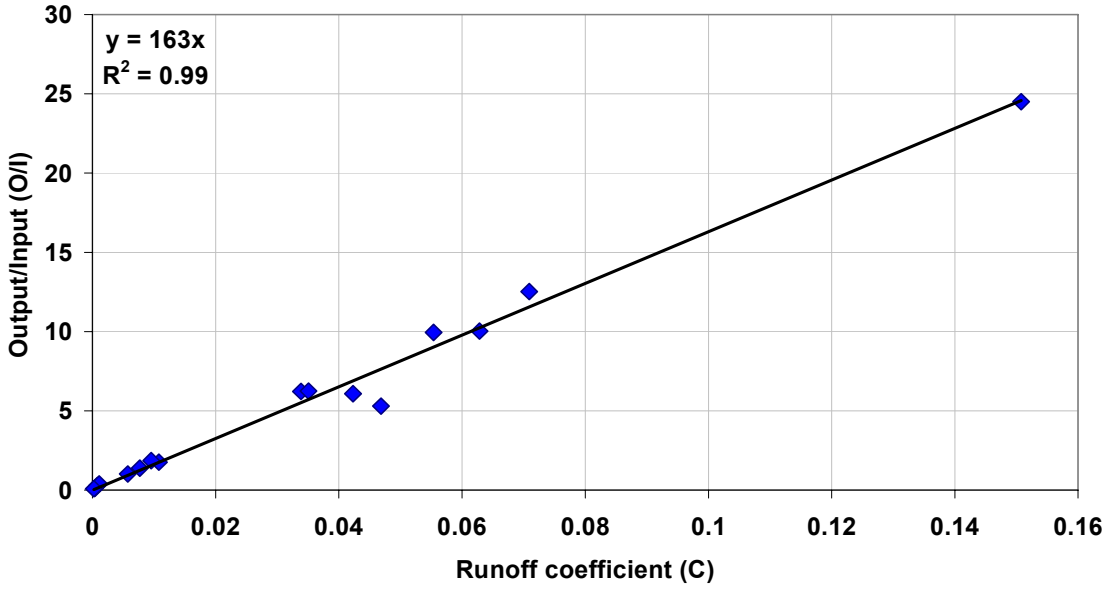


**Figure 4.11** Relationship between salt Output/input ratio and runoff coefficient coefficient

### 4.3.8 Baseload Salt Flux to the Stream

It is assumed here that the baseload salt inputs to the stream are sourced from groundwater whose TDS concentration were as sampled in July 2007. Baseflow salinity is estimated as the mean stream flow salinity for low flow conditions. The most important assumption here is that the solutes in the baseflow are caused by saline groundwater discharge only. The highest value of groundwater TDS (mg/l) is 2471 for bore GW080945, which is near the stream gauge in lower catchment. Other values of groundwater TDS are listed in **Table 4.5**.

**Table 4.5** Groundwater chemistry for the Wybong catchment sample collected on 6th June 2007 (unit of ion chemistry =mg $L^{-1}$)

| Sampling location | EC ($\mu S\ cm^{-1}$) | Na | K | Ca | Mg | Cl | $HCO_3$ | $SO_4$ | TDS (mg $L^{-1}$) | Water level (m) |
|---|---|---|---|---|---|---|---|---|---|---|
| GW080947 | 2790 | 210 | 4.5 | 130 | 150 | 710 | 523 | 24 | 1752 | 11.64 |
| GW080945 | 3310 | 430 | 5.2 | 88 | 170 | 650 | 1108 | 20 | 2471 | 11.9 |
| GW080946 | 2530 | 310 | 5.6 | 92 | 110 | 600 | 458 | 28 | 1604 | 12.14 |

Baseload groundwater input salts to the stream throughout the years considered which are shown in **Table 4.6**. Estimated average annual groundwater discharge and mean annual salt input for Wybong catchments are 4874 ML $y^{-1}$ and 6546 (T $year^{-1}$), respectively. Major export of salinity from the catchment occurred during high flows and the highest groundwater salt input also occurred during high rainfall period of 1998 (**Table 4.6**). The groundwater input salt is almost same as the output salt in the years of 1993-1994, 1999-2001 and 2007, and the highest value is 94% obtained in 2005 and the lowest value is 4% achieved in 2007 due to high flood in this year with respect to stream discharge.

**Table 4.6** Estimated baseload groundwater salt input using the TDS (mg/L) of three sampled bores (**Table 4.5**)

| Year | Annual Groundwater input (ML/Y) | Annual Salt Input (T $year^{-1}$) for GW080946 | Annual Salt Input (T $year^{-1}$) for GW080945 | Annual Salt Input (T $year^{-1}$) for GW080947 | Mean GW Salt Input (T $year^{-1}$) | Salt % of Stream Discharge |
|---|---|---|---|---|---|---|
| 1993 | 7509 | 12046 | 18557 | 13157 | 14587 | 83 |
| 1994 | 1073 | 1722 | 2653 | 1881 | 2085 | 92 |
| 1995 | 346 | 556 | 856 | 607 | 673 | 27 |
| 1996 | 4043 | 6485 | 9991 | 7084 | 7853 | 45 |
| 1997 | 3545 | 5687 | 8761 | 6211 | 6886 | 42 |
| 1998 | 25431 | 40792 | 62841 | 44556 | 49397 | 53 |
| 1999 | 14094 | 22608 | 34828 | 24694 | 27377 | 82 |
| 2000 | 14406 | 23108 | 35598 | 25240 | 27982 | 65 |
| 2001 | 1569 | 2517 | 3877 | 2749 | 3048 | 91 |
| 2002 | 27 | 43 | 67 | 47 | 52 | 48 |
| 2003 | 146 | 236 | 363 | 257 | 285 | 12 |
| 2004 | 153 | 247 | 380 | 269 | 299 | 75 |
| 2005 | 214 | 344 | 529 | 375 | 416 | 94 |
| 2006 | 21 | 34 | 52 | 37 | 41 | 76 |
| 2007 | 532 | 854 | 1315 | 932 | 1034 | 4 |

## 4.4 Conclusion

This chapter has investigated salinity dynamics, stream salt load and salt exports of the Wybong catchment. Procedures were employed to fill in missing streamflow and stream salinity date to synthesise a complete record. Stream salt loads, sources of salinity and salt output/input ratios (O/I) were estimated using stream flow, electrical conductivity and geo-chemical data. Stream EC and TDS analysis suggest that the stream chemistry in the lower catchment is different from that in the upper catchment. This suggests there are different sources of salinity in the upper and lower catchment.

The results of stream discharge and EC analysis indicated that the relative magnitudes of groundwater and salt discharge to the stream. Groundwater discharge appears to be the predominat source of salinity discharge in the Wybong.

The results of cumulative stream discharge and cumulative salt load show stream salt load was increased due to accumulated salt discharge into the stream from the regolith, soil landscape draining and contribution of saline groundwater. The cumulative salt load rose above the long term trend during drought periods due to the reduction of the dilution of saline ground waters by the stream waters. This study determined the long term mean total dissolved salt concentration at Wybong is 650mg/L.

The results of O/I ratios show that on average the catchment exports more salt that is deposited on it. The most significant salt export from the Wybong catchment occurred in the high flow periods generated by high rainfall and lowest salt export occurred in the drought years and salt was concentrated in the catchments during dry periods. The salt O/I ratio, in most of the years, is greater than 1 which emphasises that the catchments is not at equilibrium.

Salt-load and catchment salt export analysis for catchments could provide practical information to identify areas of high salinity at which to target further investigations and develop the level of understanding necessary for management. This is particularly important for determining the distribution, volume and number of water abstraction licences.

# CHAPTER 5: SOURCES OF SALINITY IN THE WYBONG CATCHMENT

Stream salinity as discussed in Chapter 4. Two different trends of EC and TDS relationships for upper ($TDS=0.43EC^{1.03}$) and lower catchments ($TDS=0.46EC^{0.41}$) were found in **Figure 4.4** in Section 4.3.2, which indicated different chemical compositions of salinity in the upper and lower catchments.

This Chapter aims to identify solute sources and develop a salinity model for the Wybong catchment. Hydrochemistry data are used to investigate the role of groundwater discharge to streams and sources of salinity. This chapter also includes analyses of major ion chemistry and major ion ratios to determine whether the solute sources are from Permian rock and/or basalt weathering in the catchment. Stable isotope composition of groundwater and surface water are also used to investigate evaporation and the groundwater contribution to streamflow. These processes are important for water salinity and catchment management and policy development in this region of the Hunter.

## 5.1 Introduction

Several studies of ground and surface water in the Hunter catchment have concluded that geology is the principal control of water chemistry (Griffen, 1960; Kellet *et al*, 1989; Crelman, 1994). The geology essentially consists of Tertiary basalts, Triassic sandstones and Permian coal and shale deposits. The Permian stratigraphy formed under fluvial/deltaic conditions, although connate marine salts characterise the deltaic units. The saline ground water is believed to be sourced from highly permeable coal aquifers (AGC, 1984; Crelman, 1994; Griffen, 1960; Kellet *et al*, 1989) rather than the fractured rock aquifers. It has been hypothesized that the principal pathway through which saline water enters the Hunter River and its tributaries is via fault lines (Crelman, 1994) and rising water tables (Beale *et al*. 2000). The main sources of salt in the Hunter region are believed to be aeolian deposition of dust, marine-aerosol-origin cyclic salts and parent rock weathering (Kellet *et al*. 1989). Kellet *et al* (1989) also proposed that Permian rocks were the sources of most saline water in the Hunter and that Tertiary

basalt contributed salt to the headwaters of the many creeks where silicate weathering provides an abundant supply of bicarbonate to base flow water.

## 5.2 Methods

### 5.2.1 Groundwater and Surface Water Sampling and Analysis

Groundwater and surface water samples were collected during July and April 2006, June and July 2007 and July 2008. The collection of surface and groundwater samples and their analyses were described in Section 4.2.11. Groundwater and surface water samples were also collected during July 2005 to analyse for oxygen and hydrogen isotopes. Winter was chosen as a sampling period, because water is readily available in stream then. Surface water and groundwater samples were collected over the length of Wybong Creek and also at bores and piezometer locations in **Figure 5.1. S**tream water sampling sites in the upper and lower catchments are also listed in **Table 5.1**.

**Table 5.1** Surface water sampling location

| Sampling site name | Location | Easting | Northing |
|---|---|---|---|
| Headwaters | Upper catchment | 271397 | 6471098 |
| Campground | Upper catchment | 267288 | 6461916 |
| Bunnan | Upper catchment | 271937 | 6453299 |
| White Rock | Upper catchment | 274178 | 6447018 |
| TSR | Upper catchment | 279906 | 6435501 |
| Ridgeland | Upper catchment | 279002 | 6440694 |
| Dry Ck Rd | Lower catchment | 280029 | 6432618 |
| Rockhall casuway | Lower catchment | N/A | N/A |
| Yarraman gauge | Lower catchment | 277347 | 6427310 |
| Wybong Bridge | Lower catchment | 278550 | 6425917 |
| Hollydeen | Lower catchment | 276340 | 6420345 |
| Railway bridge | Lower catchment | 275979 | 6417927 |

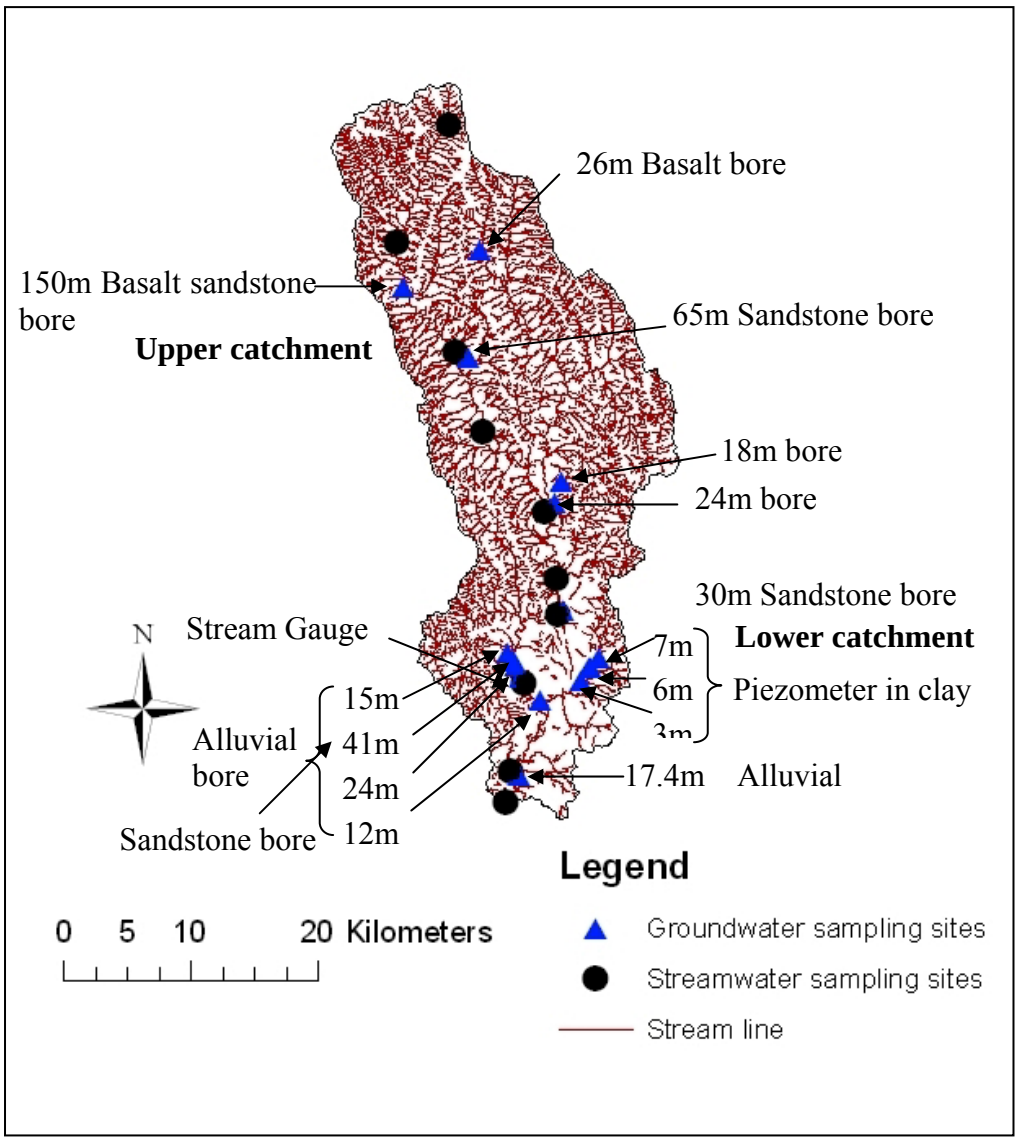


**Figure 5.1** Surface (round) and groundwater (triangular) sampling sites in Wybong catchment

Groundwater samples were collected from various piezometers in the lower catchment. These are Roberts-1, Morgans, and Big Flat Creek (BFC)-TSR, and from alluvial bores of Rockhall-riverflats and Frenchies and are listed in **Table 5.2**. Groundwater samples were also collected from deeper aquifer bores in upper catchment at Ethers#1, Ethers#2, GW017391 and Queen Street as well as Roberts House Bore, GW080948, Hannahs bore and GW080947 in the lower catchment. Bore details, locations, water level, depth of bores, water bearing zone and lithology are all given in **Table 5.2.** Groundwater samples were collected from sites with different soils, geology

and from different aquifers in order to identify soil and geological signatures of the water chemistry. The groundwater geochemistry data for the Fassifern Coal seam were supplied by Mackie Environmental Research (2006) as given in **Table 5.3**.

**Table 5.2** Bore names, locations, water level, depth, water bearing zone and lithology of groundwater sample

| BoreID | Name | Location in catchment | Aquifer type | Northing | Easting | Water depth (m) | Depth of the bores (m) | Water bearing zone (m) | Lithology |
|---|---|---|---|---|---|---|---|---|---|
| 080434 | Wybong Road | Lower | Unconsolidated unconfined | 6420011 | 276924 | 14.2 | 17.4 | 14-17.4 | Topsoil,Clay, clay-sand, gravel |
| 080944 | Ridgelands Rd. | Lower | Consolidated semi-confined | 6433278 | 280484 | 6.7 | 30 | 24-26 | Topsoil, clay, sandstone, pyroclastic, conglomerate |
| 080945 | Rockhall | Lower | Consolidated unconfined | 6428921 | 276746 | 11.9 | 24 | 16-18 | Topsoil, clay, gravel, clay |
| 080946 | Rockhall | Lower | Consolidated unconfined | 6427767 | 277053 | 12.14 | 19.46 | N/A | Smectite clay |
| 080947 | Rockhall | Lower | Consolidated semi-confined | 6429075 | 276604 | 11.64 | 60 | N/A | N/A |
| 080948 | Rockhall | Lower | Consolidated semi-confined | 6429734 | 276107 | 8.45 | 41 | 27-29 | Clay, gravel, clay, sandstone |
| Piezos | Roberts_1 | Lower | N/A | 6428684 | 281846 | 3.3 | 5.98 | N/A | Clay |
| Piezos | Morgans | Lower | N/A | 6429324 | 283206 | 4.3 | 5.97 | N/A | Clay |
| 049877 | Roberts HouseBore | Lower | N/A | 6428598 | 282482 | 4.8 | 30 | N/A | Clay, sandstone |
| Piezos | BFC TSR deep | Lower | N/A | 6427710 | 281900 | 3.5 | 12 | N/A | Clay |
| Piezos | BFC_TSR shallow | Lower | N/A | 6427519 | 281802 | 3.5 | 6.97 | N/A | Clay |
| 040960 | Frenchies | Lower | N/A | 6428684 | 276924 | 10 | 14 | N/A | Clay, gravel |
| 200417 | Yarraman Bore | Lower | N/A | 6427499 | 275711 | 35.5 | | N/A | Permian coal |
| 035173 | Yarraman Wall | Lower | N/A | 6428008 | 276775 | N/A | | N/A | Gravel and clay |

| | | | | | | | | | |
|---|---|---|---|---|---|---|---|---|---|
| 025789 | Googe's Well | Lower | N/A | 6437059 | 279858 | 9.2 | N/A | N/A | Gravel and clay |
| 061136 | QueenSt | Upper | Consolidated | 6453006 | 272980 | 61.3 | 64 | 54.9-61 | Smectite clay, basalt, sandstone |
| | Ethers #2 | Upper | N/A | 6453515 | 271737 | | 150 | N/A | Basalt, sandstone |
| 080595 | Ethers #1 | Upper | N/A | 6458419 | 267813 | 2 | 150 | 14.5-97 | Topsoil, clay bands, gravel, sandstone |
| 038293 | Roachs#1 | Upper | Consolidated | 6443108 | 280333 | 7.7 | 18.2 | 11-12.1 | Soil Clay sandstone |
| 080943 | Roachs#2 | Upper | N/A | 6441641 | 279919 | 13.41 | 24 | 18-20 | Topsoil, Shale, sandstone |
| 017391 | Wicks(kar springs) | Upper | Fractured (Basalt water supply) | 6461393 | 273820 | 6.8 | 26.21 | 3.1-26.21 | Soil, basalt |

**Table 5.3** Fassifern Coal seam data (Mackie Environmental Research, 2006)

| Site name | Ca (meq/l | Mg (meq/L) | Na (meq/L) | K (meq/L) | $HCO_3$ (meq/L) | $SO_4$ (meq/L) | Cl (meq/L) |
|---|---|---|---|---|---|---|---|
| Fassifern seam | 195 | 122 | 567 | 17 | 793 | 30 | 977 |
| Fassifern seam | 358 | 314 | 543 | 16 | 758 | 238 | 1572 |
| Measure coal seam | 67 | 54 | 1194 | 11 | 519 | 558 | 1439 |
| Fassifern seam | 106 | 75 | 458 | 10 | 817 | 21 | 568 |
| Fassifern seam | 254 | 112 | 341 | 15 | 470 | 183 | 817 |
| Fassifern seam | 384 | 313 | 503 | 21 | 644 | 336 | 1581 |
| Fassifern seam | 238 | 338 | 822 | 30 | 559 | 643 | 1741 |
| Fassifern seam | 106 | 156 | 1393 | 24 | 1266 | 110 | 1883 |

Filtrated (0.45 μm membrane) surface water and groundwater samples were stored at <5 $^0$C and delivered to Research School of Biological Sciences (RSBS) at the ANU for deuterium (δD) and oxygen-18 ($\delta^{18}O$) analysis. Stable isotopes were measured at the RSBS using a Micromass Isoprime CF-IRMS (Continuous-Flow Isotope-Ratio Mass Spectrometer). Oxygen isotope ratios of the water were determined by equilibration

with carbon dioxide. Approximately 250ml of water was pipetted into a screw top glass vial. A mixture of air and 5% CO2 was then gently flowed into the remaining space and a screw top with a PTFE lined, butyl rubber septum immediately fitted. The sealed samples were held in the mass spectrometer room at a temperature held constant at +/- 0.5 degrees Celsius for about 48 hours. Samples of standard waters with values spanning the anticipated analytical values were treated in a similar way. At the end of this period two needles were inserted through the septum (helium carrier gas in and out) and using a loop valve. The sample was carried through a magnesium perchlorate moisture scrubber and a Porapak QS GC column which separated the carbon dioxide from the other gases in the helium carrier stream. The carbon dioxide $\delta^{18}O$ was then measured in the mass spectrometer with a value normalised against a reference gas pulse. The precision for the $\delta^{18}O$ runs is typically between 0.06 and 0.1 o/oo. At the end of the run the analysed values of the carbon dioxide equilibrated with the standard waters were used to calculate a slope and offset to correct the analytical results to the VSMOW scale.

Hydrogen isotope values were calculated using the chromium method in which water is reduced on hot chromium metal to liberate $^{2}H$. Aliquots of sample waters and standards were placed in 2 ml septum topped bottles (as above) leaving a minimal air-space. The bottled samples and standards were then placed in the rotary carousel of a Fisons AS800 autosampler. The sampler sits atop a furnace which maintains a chromium-packed quartz column at 1000 degrees Celsius, with helium carrier flowing down through the column. Approximately 0.75 ml of sample was picked up by the auto sampler and injected through the septum above the reaction column and onto the hot chromium. The chromium in the column binds the oxygen in the water as chromium oxide and releases the $^{2}H$ to be carried down through the column by the He carrier. The carrier gas passes through a magnesium perchlorate scrubber to dry it and then through a Porapak QS GC column to separate the hydrogen from traces of other gases and shape the peak. The gas then flows into the mass spectrometer through a capillary system and its ratios are determined. Each sample peak is placed between a large and a small reference pulse, permitting normalisation of the results and calculation of the $H^{3+}$ correction. Typically each sample is run 2 or 3 times so that memory effects from one sample to the next are minimised. The precision for the $\delta^{2}H$ runs it is typically between

0.3 and 0.6 o/oo. Finally the slope and offset for the standard waters is determined and the results all corrected to the VSMOW scale.

The Bores GW080944, GW080945, GW080946, GW080947, GW080948 and GW080434 (**Table 5.2**) are very close and their bases are deeper than the stream. Comparison of groundwater levels and the stream height show that groundwater level is higher than the stream bed. This suggests that the aquifer is connected to the stream. This will be examined in more detail in Chapter 6, Section 6.3.1.

### 5.2.2 Ion Ratios as Indicators of Catchment Weathering Processes

The ratio bicarbonate to chloride $HCO_3$/Cl (concentrations in meq $L^{-1}$) provides important information for identifying the sources of salt from mineral weathering relative to cyclic salts sourced from rainfall (Mackay *et al*., 1988; Herczeg *et al*., 2001). Other ratios such as (Ca+Mg)/Cl and (Na+K)/Cl (in meq $L^{-1}$) also provide additional information about the input of ions from mineral weathering (White *et al*., 2009).

### 5.2.3 Reactions Associated with the Weathering Processes

Typical rock type e.g., granite, volcanic rocks (rhyolite and Basalt) may contain plagioclase phenocrysts in a feldspar-rich groundmass composed of olivine, clinopyroxene, ilmenite, magnetite, chlorophaeite and apatite. Qlivine, albite and augite minerals are commonly found in basalt. Water–rock reactions, controlling basalt hydrochemistry are the dissociation of olivine, and the weathering of augite, albite and anorthite to kaolinite, and albite to montmorillonite, with the subsequent release of ions to solution (Locsey and Cox 2002).

The significant water-rock reactions associated with the weathering of these minerals to clays are:

Olivine dissociation

$$(Fe,Mg)SiO_4 + 4CO_2 + 4H_2O \rightarrow Fe^{2+} + Mg^{2+} + H_4SiO_4 + 4HCO_3^-$$

Albite- Kaolinite

$$2NaAlSi_3O_8 + 2CO_2 + 11H_2O \rightarrow Al_2Si_2O_5(OH)_4 + 2Na^+ + 4H_4SiO_4 + 2HCO_3^-$$

Anorthite-Kaolinite

$$CaAl_2Si_2O_8 + 2CO_2 + 3H_2O \rightarrow Al_2Si_2O_5(OH)_4 + 2Ca^{2+} + 2HCO_3^-$$

Augite- Kaolinite

$$[Ca_{1.15}MgAl_{0.3}Si_{1.7}]O_6 + 4.3CO_2 + 5.25H_2O \rightarrow 0.15Al_2Si_2O_5(OH)_4 + 1.15Ca^{2+} + Mg^{2+} + 1.4H_4SiO_4 + 4.3HCO_3^-$$

Albite-Montmorillonite

$$3NaAlSi_3O_8 + Mg^{2+} + 4H_2O \rightarrow 2Na_{0.5}Al_{1.5}Mg_{0.5}Si_4O_{10}(OH)_2 + 2Na^+ + 4H_4SiO_4$$

Albite-Gibsite

$$NaAlSi_3O_8 + CO_2 + 8H_2O \rightarrow Al(OH)_3 + Na^+ + 3H_4SiO_4 + HCO_3^-$$

$$CO_2 + H_2O \rightarrow H^+ + HCO_3^-$$

Geochemically, carbon dioxide and its dissolved equivalents are important constituents of groundwater. The carbon dioxides' partial pressure within the soil/regolith zone is significantly higher than atmospheric, due to generation by biological processes such as organic decay and soil respiration. Dissolved carbon dioxide ($CO_2$) is a driving mechanism for dissolution of the basalt minerals, with the presence of carbonic acid forming relatively to low pH conditions.

Furthermore, weathering reactions also take place in silicate rocks or sandstones percolated with groundwater. It is noted that all silicate weathering reactions are acid consuming and therefore they have a pH buffer effect. Carbonic acid is the most important source of protons, and as indicated by the last equation of the water-rock reactions, bicarbonate is produced during weathering of silicates by the presence of dolomite. Sodium is mainly derived from weathering of Na-feldspar like albite and anorthite (Ca-feldspar). Plagioclase weathering release in addition $Ca^{2+}$, although also weathering of amphibols, pyroxenes, etc., may contribute to the $Ca^{2+}$ and $Mg^{2+}$ concentration (Appelo and Postma, 2005). Calcite also occurred as graincutan on marine and continental Permian sediments. As Kellett (Kellett *et al.*, 1989) mentioned, calcite replaces sodic plagioclase and rock fragments in the Permian coal measures and feldspars and pyroxene in the dolerite intrusions.

#### 5.2.4.1 Estimating the Fraction of Stream Salt load due to Mineral Weathering (White *et al.*, 2009)

One of the key questions examined in this work is the source of stream salinity. An important aspect of this is the fraction of stream salt load that can be attributed to

mineral weathering. Poulsen *et al*. (2006) and White and Blum (1995) described a method for quantifying the supply of solutes from mineral weathering to groundwater by estimating the weathering index. Their method, however assumes that weathering is relative to seawater. In the Wybong catchment it is assumed that cyclic salt, rather than marine origin salt should be important in the upper catchment.

An alternatly method for examining the contribution of weathering is to estimate the contribution of mineral weathering to the stream salt load. In this method it is assumed that chloride is a conservative tracer and is sourced from cyclic salt deposited by rainfall in the catchments and concentrated by evapo-transpiration. It is considered that other ions in the river or groundwater are sourced either from concentrated cyclic salts and dust in the catchment or from mineral weathering. For other ions it is assumed that they are concentrated in the same proportion to chloride as in rainfall, that is that the ion ratios relative to chloride do not change as rainwater cyclic salts are concentrated by evapotranspiration. The mean value of chloride concentration (in mg/L) and TDS (in mg/L) at the river or groundwater sites is assumed representative of the long term average composition in the river.

### 5.2.4.2 Estimating Weathering Fraction in Areas with Cyclic Salt

With the above assumptions, the total dissolved solids estimated to come from cyclic salt due to concentration of cyclic salts in the catchment and discharge into the river, $TDS_{cyc}$ :

$$TDS_{cyc} = [Cl]_{riv} \times \left( \left| \frac{[Na+K]}{[Cl]} \right|_{rain} + \left| \frac{[Ca]}{[Cl]} \right|_{rain} + \left| \frac{Mg}{Cl} \right|_{rain} + \left| \frac{[SO_4]}{[Cl]} \right|_{rain} + \left| \frac{[HCO_3]}{[Cl]} \right|_{rain} + 1 \right) \quad (5.1)$$

Where $[Cl]_{riv}$ and $TDS_{riv}$ are the mean value of chloride concentration and TDS in the river. The total dissolved solids due to weathering, $TDS_{weath}$ is:

$$TDS_{weath} = TDS_{riv} - TDS_{cyc} \quad (5.2)$$

It follows that the fraction of total dissolved solids due to weathering, $WF$ is:

$$WF = \frac{TDS_{weath}}{TDS_{riv}} = 1 - \frac{TDS_{cyc}}{TDS_{riv}} \quad (5.3)$$

The same reasoning holds for groundwater where the amount of chloride in the groundwater is $[Cl]_{gw}$ and total dissolved solids measured in the groundwater, $TDS_{gw}$ .

### 5.2.4.3 Estimating Weathering Fraction in Areas with Marine Origin Waters

In upper Hunter catchments there is the possibility that sources of salt in stream and groundwaters may be sourced from marine origin waters. Exactly the same reasoning as above can be used to estimate the contribution of mineral weathering to waters where there are marine origin waters (White, private communication, August 2010).

This approach assumes that Chloride is a conservative tracer and is sourced from marine origin groundwaters discharging into streams or groundwater. Additionally it assumes that the processes of deposition and evaporation of the marine origin waters and its subsequent discharge has not altered the ratios of major ions to chloride from the value for the ratios in seawater. With these assumptions the total dissolved solids in river water, $TDS_{MO}$ is:

$$TDS_{MO} = [Cl]_{riv} \times \left( \left| \frac{[Na+K]}{[Cl]} \right|_{sea} + \left| \frac{[Ca]}{[Cl]} \right|_{sea} + \left| \frac{Mg}{Cl} \right|_{sea} + \left| \frac{[SO_4]}{[Cl]} \right|_{sea} + \left| \frac{[HCO_3]}{[Cl]} \right|_{sea} + 1 \right) \quad (5.4)$$

and the total dissolved solids due to weathering, $TDS_{weath}$ is just the difference between the actual total dissolved solids measured in the river $TDS_{riv}$ and $TDS_{MO}$:

$$TDS_{weath} = TDS_{riv} - TDS_{MO} \quad (5.5)$$

and the fraction of total dissolved solids in the stream due to weathering, $WF_{MO}$ is just

$$WF_{MO} = \frac{TDS_{weath}}{TDS_{riv}} = 1 - \frac{TDS_{MO}}{TDS_{riv}} \quad (5.6)$$

Again, precisely the same arguments hold for groundwater where the amount of chloride in the groundwater is $[Cl]_{gw}$ and total dissolved solids measured in the groundwater, $TDS_{gw}$.

## 5.3 Results and Discussion

### 5.3.1 EC and pH in Surface and Groundwater

Surface water samples collected over the length of Wybong Creek have ECs from 512 to 5010 µS cm$^{-1}$ and from 517 to 1142 µS cm$^{-1}$ during the 2006 dry periods and 2008 wet periods, respectively (**Table 5.4** and **Table 5.5**). Higher EC during dry periods appears due to the discharge of saline groundwater in baseflow which dominates during the dry periods (**Figure 5.2a**). Lower EC obtained in 2008 are due to runoff dominating

during wet period in 2008 (**Figure 5.2b**). Groundwaters in the lower catchment have high salinity and the highest EC of 12580 μS $cm^{-1}$(BFT shallow piezometer) is shown in **Figure 5.2b**. The water chemistry of this piezometer is similar to that in the coal measures and is considered to be sourced from Permian coal. Groundwater within the coal measure is generally saline with ECs in the range of 853-12508 μS/cm and an average value of 4904 μS/cm (Mackie Environmental Research, 2006). The stream salinity increases downstream (**Figure 5.2)** and this appears due to groundwater discharge from the Permian deposits.

The pH values measured in the Wybong catchment (**Table 5.4** and **Table 5.5**) are in the range of 7.5–8.3 which are generally common in the basalt and granite sourced groundwaters (Langmuir, 1997). However, the maximum pH value observed for the basalt groundwaters in the upper catchment is 8. Such elevated pH values generally occur where groundwater chemistry is dominated by minerals such as silicates, aluminosilicates and bicarbonate, which increase the pH (Langmuir, 1997). Therefore, it is possible that elevated pH values in the groundwaters are also sourced from the silicate minerals.

**Table 5.4** Surface and groundwater sampling data during July 2006

| Surface water Sampling site | EC (μS $cm^{-1}$) | pH | Distance D/S (km) | Groundwater Sampling site | EC (μS $cm^{-1}$) | pH | Distance D/S(km) |
|---|---|---|---|---|---|---|---|
| Headwaters | 512 | 7.7 | 5 | Morgans piezo | 6920 | 7.3 | 43.4 |
| Campground | 768.5 | 8.3 | 11 | Roberts_1 piezo | 7470 | 7.5 | 43.7 |
| Bunnan | 842 | 8.3 | 28.2 | BFCTSR Deep piezo | 5100 | 7.8 | 44.8 |
| White Rock | 1091.5 | 8.3 | 35.7 | GW080434 Wyb-brid | 1115 | 7.5 | 51.4 |
| Ridgelands | 1296 | 8.3 | 45.9 | GW049877 -RHB | 4065 | 7.6 | 43.9 |
| Dry Ck Rd | 2420.5 | 7.8 | 60 | GW080946Rhockhall | 2380 | 7.6 | 43.7 |
| RockhallCauswa | 3140 | 6.8 | 67 | GW040960-Frenchie | 3090 | 7.3 | 42.8 |
| Yarraman | 4080 | N/A | 72 | GW080943-Roach#2 | 1789 | 7.5 | 30.7 |
| Hollydeen | 3640 | 8.1 | 83 | GW038293-Roach#1 | 2440 | 7.1 | 29.4 |
| Railwaybridge | 5010 | 7.4 | 89 | GW061136 QueenSt | 1228 | 7.2 | 18.3 |
| | | | | GW080595-Ethers#1 | 707.5 | 8.0 | 13.2 |
| | | | | GW017391 -Wicks | 799 | 7.9 | 10.0 |

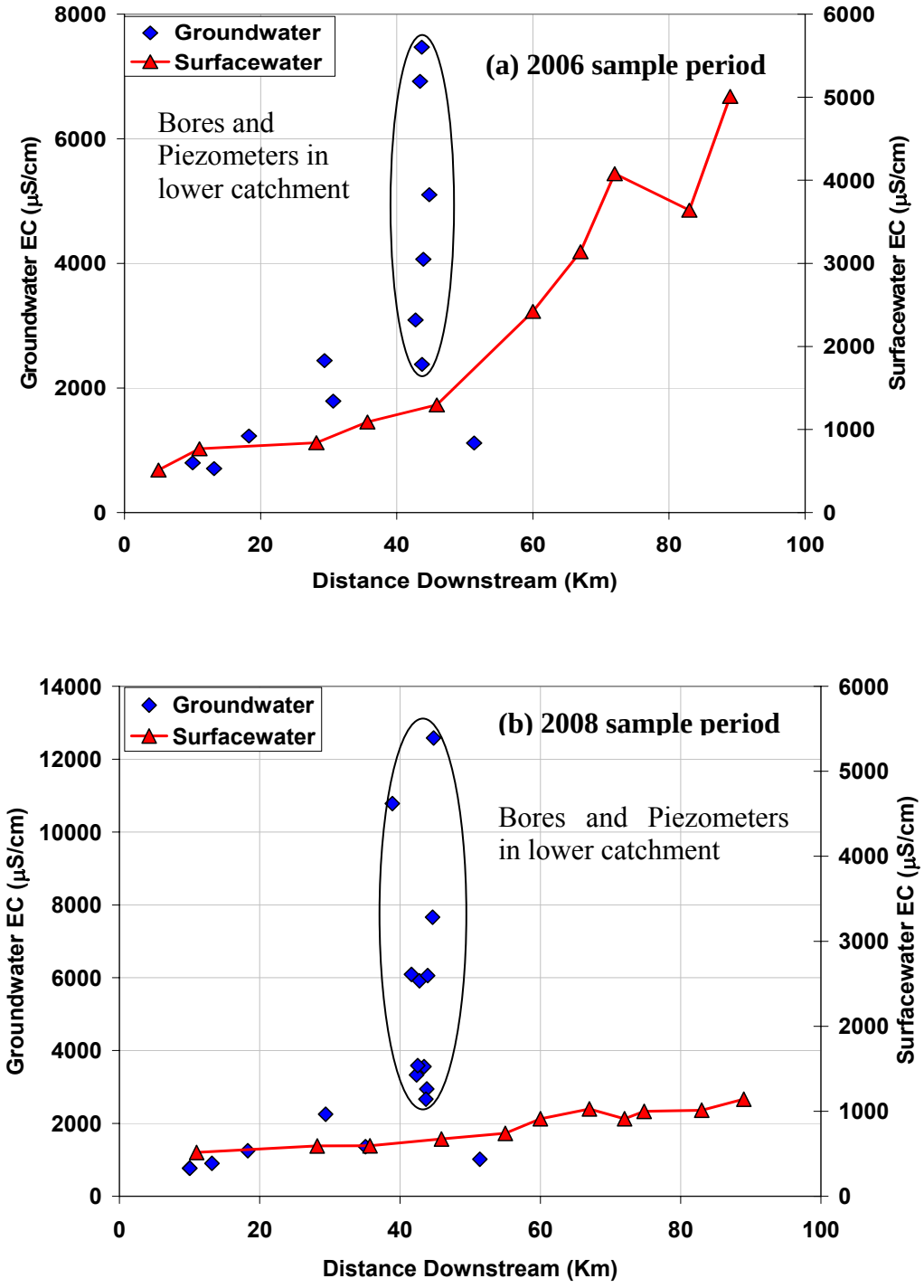


**Figure 5.2** The relationship between EC and distance downstream from the head of the river during sampling periods **(a)** 2006 and (**b**) 2008

**Table 5.5** Surface and groundwater sampling data July 2008

| Surfacewater Sampling site | EC (μS cm$^{-1}$) | pH | Distance D/S (km) | Groundwater Sampling site | EC (μS cm$^{-1}$) | pH | Distan D/S (km) |
|---|---|---|---|---|---|---|---|
| Campground | 517 | 8.3 | 11 | GW017391 | 773 | 7.5 | 10.00 |
| Bunnan | 592 | 8.3 | 28.2 | Ethers #2 | 768 | 7.8 | 10.03 |
| White Rock | 595 | 8.4 | 35.7 | GW080595 | 905 | 7 | 13.18 |
| Ridgelands | 674 | 8.5 | 45.9 | GW061136 | 1252 | 7 | 18.28 |
| TSR | 740 | 8.6 | 55 | GW038293 | 2252 | 7.4 | 29.38 |
| Dry Ck Rd | 911 | 8.7 | 60 | GW025789 | 1364 | Nil | 35.07 |
| RockhallCauswa | 1029 | Nil | 67 | GW080944 | 10780 | 7.1 | 38.90 |
| Yarraman Gauge | 911 | 8.6 | 72 | GW080948 | 6090 | 6.9 | 41.63 |
| Wybong Bridge | 999 | 8.5 | 74.8 | GW080947 | 3330 | 7.2 | 42.34 |
| Hollydeen | 1012 | 8.5 | 83 | GW080945 | 3590 | 7.7 | 42.51 |
| Railwaybridge | 1142 | 8.5 | 89 | GW040960 | 5920 | 7.3 | 42.77 |
| | | | | GW035173 | 3560 | 7.3 | 43.42 |
| | | | | GW080946 | 2668 | 7.4 | 43.70 |
| | | | | GW200417 | 2945 | 7.3 | 43.81 |
| | | | | GW049877 | 6060 | 7.6 | 43.92 |
| | | | | BFC TSR deep | 7660 | 7.7 | 44.64 |
| | | | | BFC TSR shallow | 12580 | 8.3 | 44.78 |
| | | | | GW080434 | 1019 | 7.5 | 51.39 |

### 5.3.2 Major Ion Chemistry in Surface and Groundwater

Surface and groundwater chemistry during July 2006-June 2007 and July 2007-July 2008 periods are listed in **Table 5.6, Table 5.7, Table 5.8 and Table 5.9,** respectively.

The major ion chemistry analyses in surface water samples show that the upstream is dominated by bicarbonate and the downstream is dominated by chloride ions **(Figure 5.3**). In the majority of groundwater samples magnesium and sodium are the dominant cations with some proportion of calcium, with bicarbonate and chloride the dominant anions **(Figure 5.4)**.

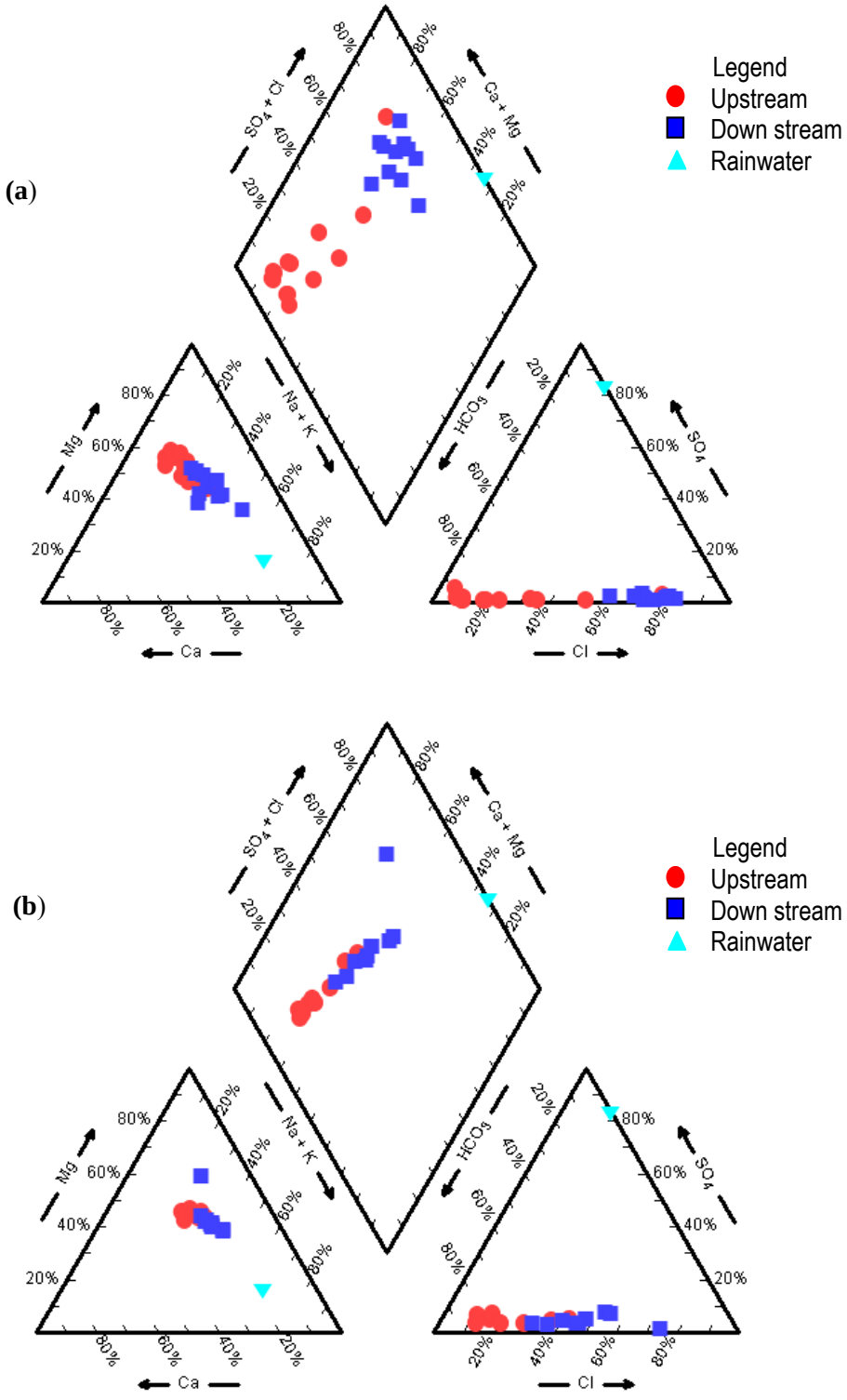


**Figure 5.3** Piper diagrams for stream chemistry in the Wybong catchment data during **(a)** July 2006-June 2007 **(b)** July2007-July2008 sampling periods

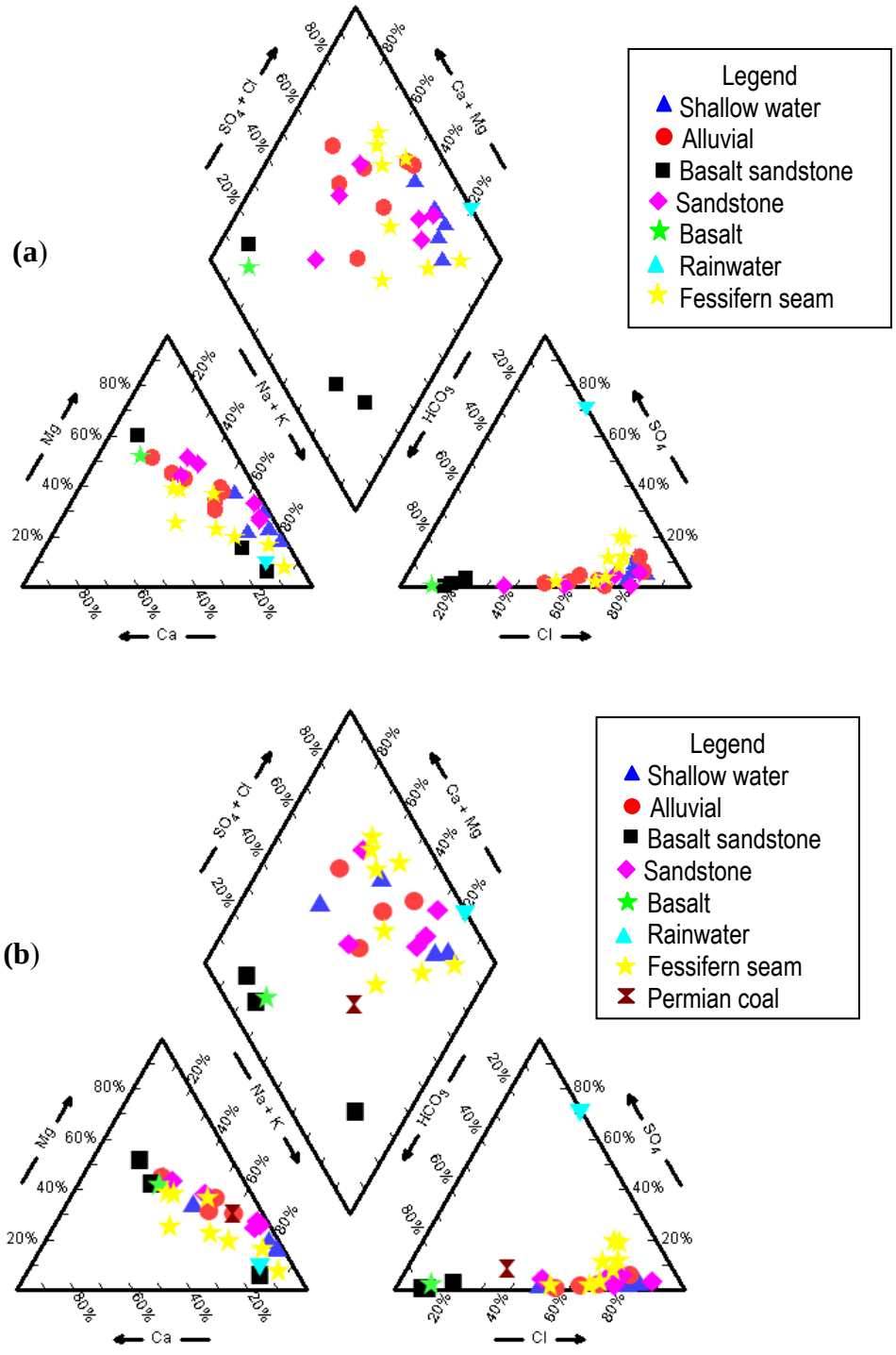


**Figure 5.4** Piper diagrams for groundwater chemistry in the Wybong catchment data during **(a)** July 2006-June 2007 and **(b)** July 2008 sampling periods

Basalt-sandstone and basalt bores in the fractured rock aquifer in the upper catchment are dominated by bicarbonate. Both surface and groundwater in the upper catchment is dominated by bicarbonate possibly derived from basalt and sandstone

(**Figure 5.3** and **Figure 5.4**). Kellet *et al*. (1989) also found that Tertiary basalt contributed to the salt to the headwaters of the Creeks in the Hunter.

The shallow groundwater is dominated by Na, Ca, Mg and Cl. Magnesium probably derives from exchange process relating to the ubiquitous presence of smectite (tuffaceous sandstones, smectite produced by weathering of basalt) and or volcanic clasts within the conglomerates (Mackie Environmental Research, 2006). Shallow groundwaters from piezometers, and alluvial and clay-sandstones bores in the lower catchment are mostly dominated by Cl and Na.

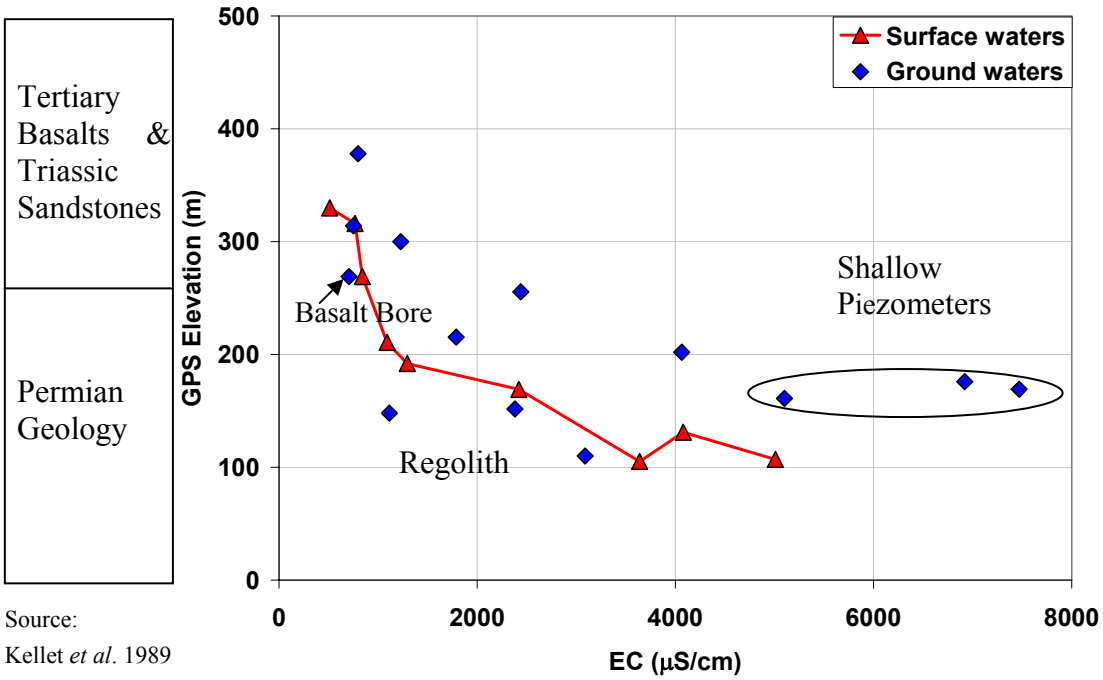


**Figure 5.5** The relationship between GPS elevation, geological unit and surface and ground water EC during 2006 sampling periods

The sandstone groundwater samples move from chloride to bicarbonate as shown in **Figure 5.4**. Saline, Na-Cl dominated groundwater occurs in the sandstone (GW049877) and fractured conglomerate of the Narrabeen Group (Hannahs bore GW080944). The water chemistry of this bore is similar to the coal measures and has a high EC of 10780 µS $cm^{-1}$. The lower catchment is dominated by Cl derived from Permian Coal (**Figure 5.3** and **Figure 5.4**). Kellet *et al*. (1989) identified the Permian Coal Measures as the source of salinity in the lower Wybong Creek catchment. The

lower catchment is characterised by saline Permian coal geologies which are reflected in the change in surface and ground water chemistry (**Figure 5.5**).

**Table 5.6** Surface water sampling data during July 2006 and June 2007

| Sampling Site | location | Ca (meq/l | Mg (meq/L) | Na (meq/L) | K (meq/L) | $HCO_3$ (meq/L) | $SO_4$ (meq/L) | Cl (meq/L) |
|---|---|---|---|---|---|---|---|---|
| Headwaters | Upstream | 2.84 | 4.74 | 2.20 | 0.04 | 10.28 | 0.62 | 0.67 |
| Campground | Upstream | 4.89 | 8.09 | 2.33 | 0.03 | 10.28 | 0.19 | 0.91 |
| Bunnan | Upstream | 5.13 | 9.31 | 2.25 | 0.04 | 10.62 | 0.06 | 1.25 |
| White Rock | Upstream | 5.48 | 11.05 | 3.26 | 0.15 | 11.97 | 0.09 | 2.57 |
| Ridgelands | Upstream | 5.43 | 11.10 | 4.45 | 0.09 | 1.62 | 0.19 | 5.81 |
| Campground | Upstream | 4.48 | 9.15 | 2.35 | 0.01 | 9.98 | 0.17 | 0.91 |
| Bunnan | Upstream | 4.49 | 9.65 | 2.31 | 0.05 | 10.20 | 0.05 | 1.26 |
| White Rock | Upstream | 5.04 | 11.50 | 3.49 | 0.16 | 11.79 | 0.06 | 2.65 |
| Ridgelands | Upstream | 5.34 | 11.93 | 4.75 | 0.08 | 10.25 | 0.15 | 5.14 |
| WhiteRock | Upstream | 3.34 | 6.58 | 3.96 | 0.10 | 12.19 | 0.06 | 3.67 |
| BunnanBridge | Upstream | 2.84 | 4.85 | 2.31 | 0.03 | 11.05 | 0.18 | 1.30 |
| CampGround | Upstream | 2.74 | 4.61 | 2.52 | 0.06 | 10.62 | 0.18 | 1.02 |
| Ridgelands | Upstream | 2.94 | 5.67 | 4.31 | 0.06 | 10.68 | 0.08 | 5.92 |
| TSR | Upstream | 3.59 | 7.07 | 5.22 | 0.08 | 8.90 | 0.13 | 9.59 |
| DryCreekRoad | Downstream | 4.99 | 11.51 | 16.09 | 0.10 | 9.92 | 1.10 | 24.82 |
| Hollydeen | Downstream | 8.48 | 18.09 | 17.40 | 0.17 | 8.88 | 0.88 | 36.67 |
| Railbridge | Downstream | 4.59 | 9.05 | 8.26 | 0.43 | 6.68 | 0.13 | 16.64 |
| Yarraman | Downstream | 7.98 | 20.56 | 15.22 | 0.19 | 9.47 | 0.73 | 36.67 |
| Dry Ck Rd | Downstream | 7.02 | 16.18 | 9.77 | 0.14 | 9.48 | 0.48 | 14.32 |
| Railwaybridge | Downstream | 17.76 | 36.83 | 19.81 | 0.30 | 9.07 | 0.68 | 42.19 |
| Hollydeen | Downstream | 10.92 | 23.30 | 10.90 | 0.28 | 9.24 | 0.51 | 23.07 |
| RockhallCaus | Downstream | 10.71 | 23.56 | 12.08 | 0.26 | 9.30 | 0.35 | 23.86 |
| Dry Ck Rd | Downstream | 8.58 | 17.11 | 12.67 | 0.20 | 9.53 | 0.61 | 20.77 |
| Hollydeen | Downstream | 13.35 | 20.85 | 15.74 | 0.34 | 9.62 | 0.24 | 29.19 |
| Railwaybridge | Downstream | 18.04 | 24.05 | 20.38 | 0.44 | 10.31 | 0.55 | 39.93 |
| Yarraman | Downstream | 7.98 | 20.56 | 15.22 | 0.19 | 9.48 | 0.73 | 36.67 |
| Rain water | Bunnan | 0.01 | 0.01 | 0.03 | 0.00 | | 0.03 | 0.01 |

**Table 5.7** Groundwater sampling data during July 2006 and June2007 *(Basalt and Sandstone=Basalt & Sst.)

| Sampling Site | Sample ID | Ca (meq/l | Mg (meq/L) | Na (meq/L) | K (meq/L) | $HCO_3$ (meq/L) | $SO_4$ (meq/L) | Cl (meq/L) |
|---|---|---|---|---|---|---|---|---|
| Roberts_1 | Shallow | 5.03 | 30.08 | 99.75 | 2.21 | 14.96 | 12.76 | 89.59 |
| Morgans | Shallow | 18.53 | 33.94 | 105.42 | 4.20 | 19.88 | 12.24 | 121.03 |
| BFC_TSR | Shallow | 3.09 | 21.28 | 70.53 | 1.92 | 13.25 | 3.47 | 59.88 |
| BFC_TSR_1B | Shallow | 1.40 | 12.34 | 56.55 | 0.87 | 16.34 | 1.88 | 62.05 |
| Morgans_1 | Shallow | 13.47 | 58.41 | 87.00 | 1.84 | 21.16 | 12.50 | 112.83 |
| Roberts_1A | Shallow | 2.40 | 32.91 | 78.30 | 1.10 | 14.97 | 4.58 | 95.90 |
| Rockhall Riv | Alluvial | 7.31 | 13.98 | 11.28 | 0.29 | 6.21 | 0.01 | 15.27 |
| Wybong_Brdg | Alluvial | 8.64 | 15.07 | 5.73 | 0.11 | 6.88 | 0.86 | 11.54 |
| Frenchies | Alluvial | 16.90 | 27.74 | 46.67 | 1.10 | 9.43 | 9.39 | 63.51 |
| Rockhall old | Alluvial | 4.39 | 13.98 | 18.70 | 0.13 | 18.16 | 0.42 | 18.33 |
| Rockhall -Riv | Alluvial | 4.59 | 9.05 | 13.48 | 0.14 | 7.51 | 0.58 | 16.92 |
| Wybong_Brdg | Alluvial | 4.64 | 7.98 | 5.22 | 0.06 | 7.95 | 0.31 | 11.28 |
| Frenchies | Alluvial | 10.98 | 35.37 | 43.50 | 0.90 | 12.75 | 6.04 | 81.80 |
| Roberts_HB | Sandstone | 2.10 | 19.90 | 37.36 | 1.81 | 8.61 | 0.00 | 33.93 |
| Roberts_HB | Sandstone | 2.69 | 16.45 | 40.89 | 0.92 | 8.61 | 3.13 | 47.95 |
| Roachs#1 | Sandstone | 3.68 | 11.98 | 8.91 | 0.22 | 12.44 | 0.03 | 7.00 |
| Roachs#2 | Sandstone | 6.57 | 19.45 | 11.93 | 0.26 | 9.68 | 0.02 | 12.67 |
| Rockhall North | Sandstone | 6.49 | 12.34 | 9.13 | 0.12 | 8.57 | 0.50 | 20.03 |
| Rockhall Hays | Sandstone | 3.09 | 16.45 | 42.63 | 1.30 | 15.41 | 2.71 | 47.95 |
| Ethers #1 | Basalt & Sst. | 1.67 | 1.52 | 6.71 | 0.32 | 6.72 | 0.08 | 1.45 |
| QueenSt | Basalt & Sst. | 7.48 | 15.02 | 2.57 | 0.08 | 11.74 | 0.01 | 2.25 |
| Ethers#2 | Basalt & Sst. | 1.00 | 0.47 | 6.52 | 0.18 | 6.37 | 0.25 | 1.83 |
| Wicks | Basalt bore | 5.44 | 8.34 | 2.47 | 0.01 | 7.90 | 0.03 | 1.01 |

**Table 5.8** Surface water sampling data during July 2007 and July 2008

| Sampling Site | location | Ca (meq/l | Mg (meq/L) | Na (meq/L) | K (meq/L) | $HCO_3$ (meq/L) | $SO_4$ (meq/L) | Cl (meq/L) |
|---|---|---|---|---|---|---|---|---|
| Campground | Upstream | 1.60 | 2.47 | 1.52 | 0.03 | 5.11 | 0.38 | 0.71 |
| Bunnan | Upstream | 2.20 | 3.37 | 1.83 | 0.03 | 6.97 | 0.40 | 1.02 |
| WhiteRock | Upstream | 1.90 | 3.37 | 1.96 | 0.05 | 6.17 | 0.35 | 1.30 |
| Ridgelands | Upstream | 2.25 | 4.44 | 3.00 | 0.08 | 6.73 | 0.48 | 4.23 |
| TSR Wybong | Upstream | 2.35 | 4.36 | 3.35 | 0.08 | 6.02 | 0.52 | 4.80 |
| Campground | Upstream | 1.65 | 2.30 | 1.48 | 0.02 | 2.94 | 0.27 | 0.62 |
| White Rock | Upstream | 1.90 | 2.88 | 1.74 | 0.04 | 5.22 | 0.20 | 0.76 |
| Ridgelands | Upstream | 1.85 | 3.13 | 2.04 | 0.05 | 5.45 | 0.23 | 1.47 |
| TSR Wybong | Upstream | 2.00 | 3.45 | 2.48 | 0.05 | 5.55 | 0.25 | 2.31 |
| DryCreekRoa | Downstream | 2.30 | 4.28 | 3.44 | 0.08 | 6.61 | 0.52 | 4.80 |
| Yarraman | Downstream | 2.45 | 4.44 | 4.00 | 0.09 | 6.14 | 0.60 | 6.21 |
| WybongBridge | Downstream | 2.40 | 4.52 | 4.05 | 0.08 | 6.11 | 0.63 | 6.21 |
| Hollydeen | Downstream | 2.25 | 4.52 | 4.78 | 0.13 | 5.14 | 0.92 | 6.77 |
| Railway Bridge | Downstream | 2.50 | 4.77 | 5.22 | 0.15 | 5.11 | 0.90 | 7.33 |
| Dry Creek RD | Downstream | 2.00 | 3.62 | 2.61 | 0.05 | 5.46 | 0.27 | 2.57 |
| Causeway -2 | Downstream | 4.34 | 15.63 | 6.52 | 0.05 | 3.87 | 0.21 | 11.56 |
| Yarraman | Downstream | 2.20 | 3.87 | 3.18 | 0.06 | 5.77 | 0.27 | 3.38 |
| Hollydeen | Downstream | 2.45 | 4.36 | 4.05 | 0.07 | 5.50 | 0.35 | 5.08 |
| Railway Bridge | Downstream | 2.59 | 4.61 | 4.35 | 0.07 | 5.72 | 0.33 | 5.08 |

### 5.3.3 Ion Ratios of Stream and Groundwater

The ion ratios for surface and groundwater chemistries are plotted against the reciprocal of Cl in **Figure 5.6** and **Figure 5.7** in order to plot rainwater and seawater on the same graph. A simple mixing model appears to describe the $HCO_3$ /Cl chemistry with high ratios in the upper catchment dropping to values below rainwater in the lower catchment. The results shown in the Figures, also demonstrate that [Ca+Mg]/[Cl] and [Na+K]/[Cl] are high in the upper catchment indicative of mineral weathering. Samples with [Na+K]/Cl and [Ca+Mg]/[Cl] greater than the ratios for rainwater and sea water indicate that the mineral weathering contributing solute to the stream water.

**Table 5.9** Groundwater sampling data in July 2008 (SW=Shallow water)

| Site Name | Sample ID | Ca (meq/l | Mg (meq/L) | Na (meq/L) | K (meq/L) | $HCO_3$ (meq/L) | $SO_4$ (meq/L) | Cl (meq/L) |
|---|---|---|---|---|---|---|---|---|
| BFC TSR SW | SW | 3.49 | 22.20 | 91.34 | 0.66 | 22.28 | 2.06 | 95.90 |
| BFC TSR deep | SW | 1.60 | 11.51 | 60.90 | 0.82 | 11.83 | 1.92 | 70.52 |
| Yarraman Wall | SW | 7.49 | 11.51 | 15.22 | 0.12 | 7.75 | 0.67 | 25.67 |
| Googe's Well | SW | 3.79 | 6.25 | 3.96 | 0.05 | 6.83 | 0.14 | 7.05 |
| | Alluvial | 4.89 | 13.98 | 19.14 | 0.14 | 16.59 | 0.31 | 21.15 |
| | Alluvial | 4.64 | 8.22 | 13.48 | 0.14 | 7.61 | 0.52 | 18.90 |
| Wybong Bridg. | Alluvial | 5.49 | 9.05 | 5.65 | 0.07 | 6.85 | 0.29 | 12.69 |
| Frenchies | Alluvial | 5.49 | 17.27 | 33.93 | 0.51 | 8.70 | 3.33 | 45.13 |
| | Sandstone | 7.98 | 13.98 | 10.44 | 0.12 | 7.39 | 0.52 | 24.26 |
| Hannahs | Sandstone | 3.24 | 28.78 | 73.95 | 1.05 | 9.85 | 3.33 | 93.08 |
| | Sandstone | 3.19 | 14.80 | 40.89 | 1.36 | 13.93 | 2.71 | 42.31 |
| Roachs Bore | Sandstone | 3.79 | 9.05 | 10.87 | 0.21 | 10.95 | 1.02 | 11.56 |
| Roberts House | Sandstone | 1.80 | 15.63 | 42.19 | 1.07 | 10.92 | 3.33 | 45.13 |
| Ethers#1 | Basalt & Sst. | 3.34 | 4.36 | 2.48 | 0.20 | 8.77 | 0.03 | 0.99 |
| Ethers #2 | Basalt & Sst. | 1.05 | 0.46 | 6.52 | 0.17 | 6.11 | 0.23 | 1.52 |
| Queen St. | Basalt & Sst. | 4.34 | 7.15 | 2.35 | 0.06 | 11.92 | 0.05 | 1.61 |
| GW017391 | Basalt | 2.45 | 3.45 | 2.35 | 0.01 | 7.03 | 0.18 | 1.02 |
| Yarraman Bore | Permiancoal | 3.29 | 9.87 | 18.70 | 1.00 | 13.72 | 2.08 | 8.46 |

**Figure 5.6** and **Figure 5.7** show these slopes appear to be differ of the ion ratio versus 1/Cl in the upper and lower catchment. Ion ratios increase as 1/Cl increases with high values upstream. The low-chloride component appears to be due to mineral weathering from upstream water and surface runoff. In **Figure 5.7** the July 2008 data, taken after heavy rains shows that rainwater is the end member for $HCO_3$ /Cl but not for (Na+K)/Cl or (Ca+Mg)/Cl which still show a weathering component possible due to soil runoff.

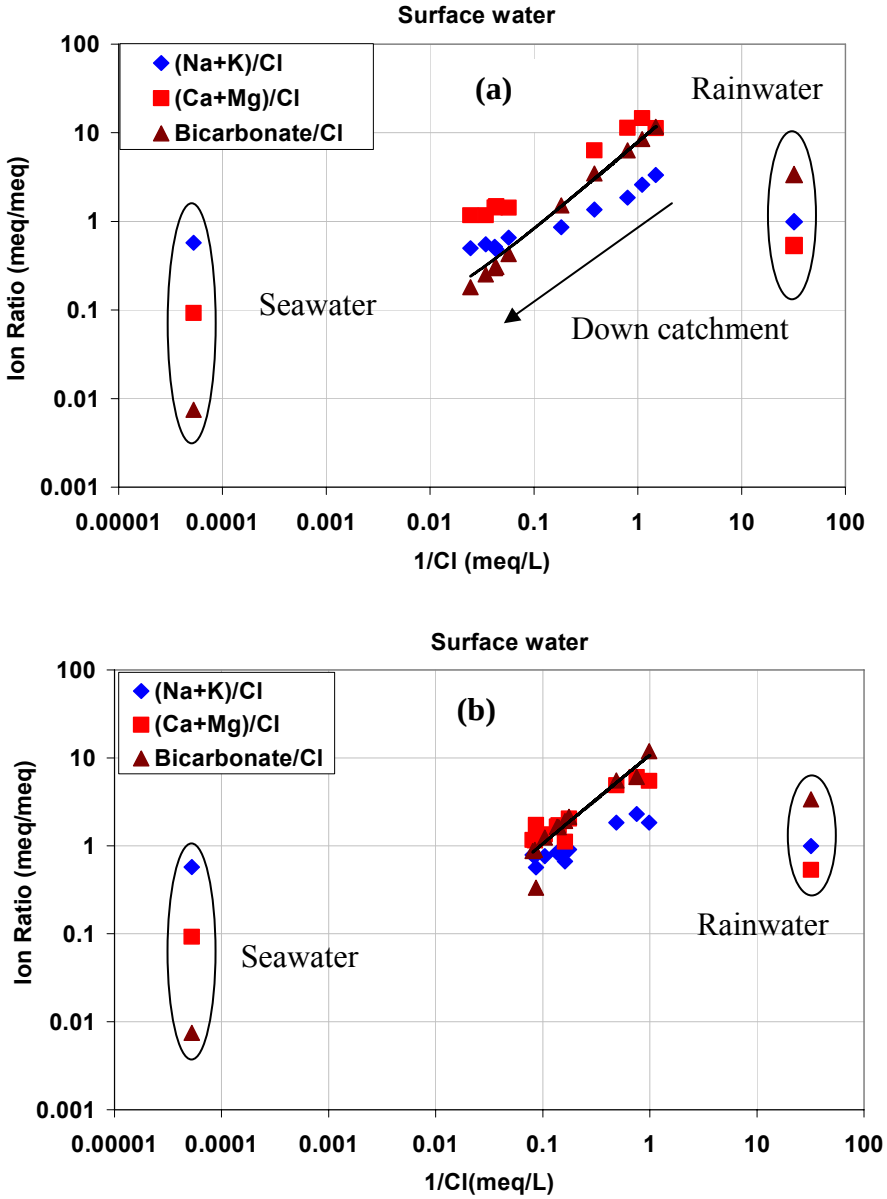


**Figure 5.6** Relation between ion ratios versus the reciprocal chloride concentration for stream water data during **(a)** July 2006 **(b)** July 2007-July 2008 sampling periods

**Figure 5.8** shows profiles of the ion ratios of $HCO_3$ /Cl, (Ca+Mg)/Cl and (Na+K)/Cl with distance downstream. These results show systematic progression of water from the upstream catchment with higher ion to Cl ratios to those downstream. The relative $HCO_3$ concentration is higher in the upper catchment and appears sourced from weathering of the silicate dominated Liverpool Range Volcanics and the

sandstones and conglomerates of the Narrabeen Group which are also silica dominated. With weathering of both these rock types produce $HCO_3$ dominated water as does soil respiration. It is clear from these ion ratio profiles that the stream chemistry below about 45 km downstream is radically different from the upstream.

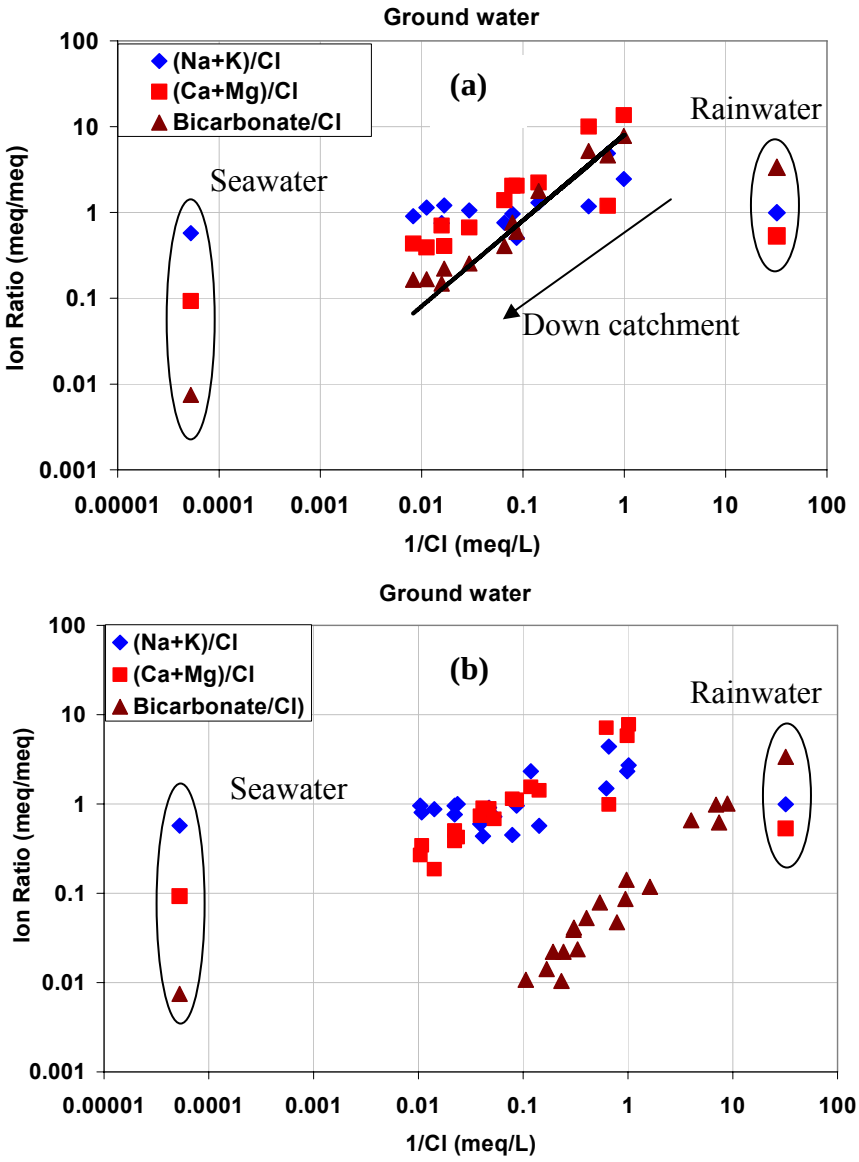


**Figure 5.7** Relation between ion ratios versus the reciprocal chloride concentration for groundwater data during **(a)** July 2006 **(b)** July 2008 sampling periods

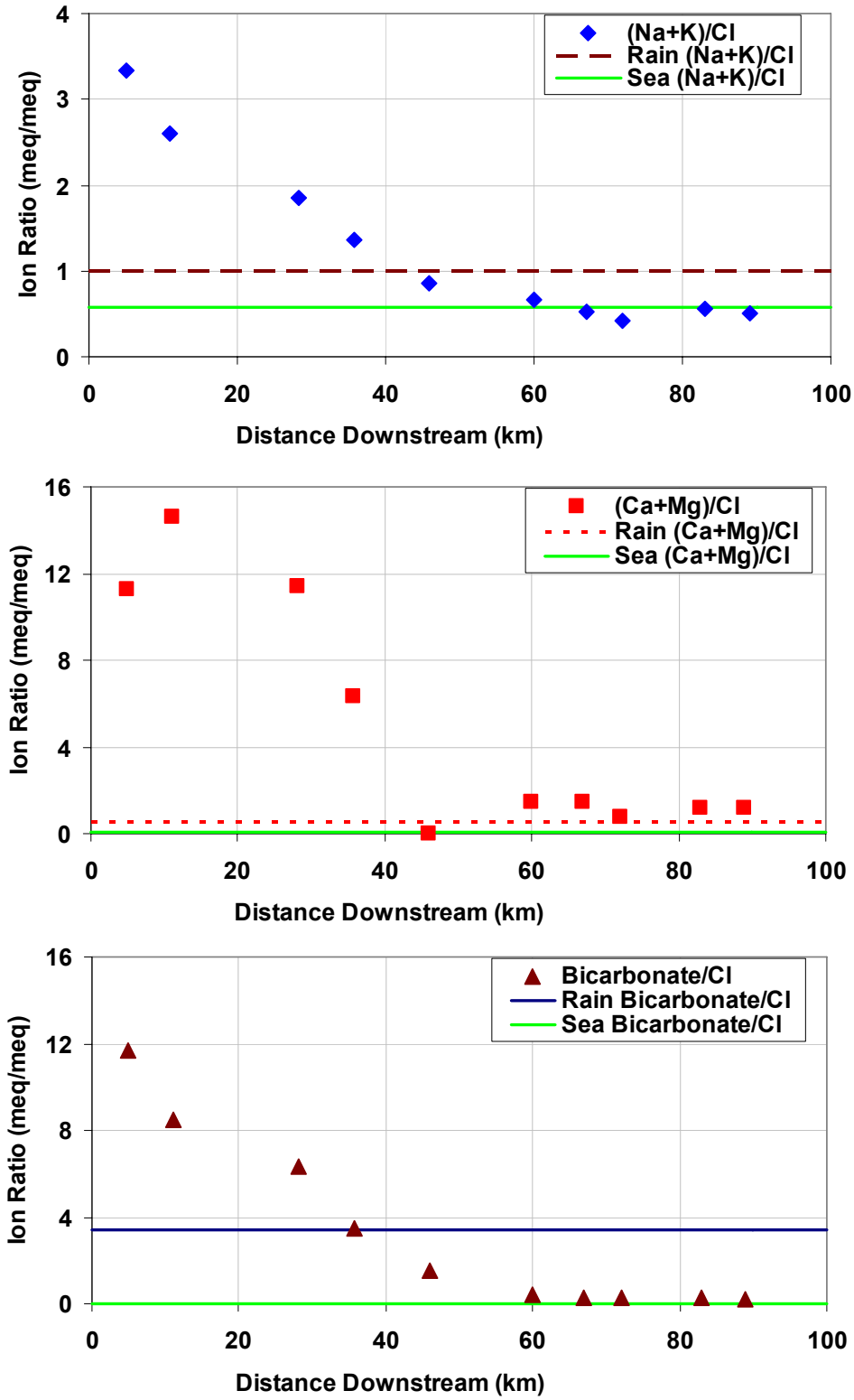


**Figure 5.8a** Profiles of ion ratios of mineral weathering products downstream from the head of the river for the July 2006 sampling period

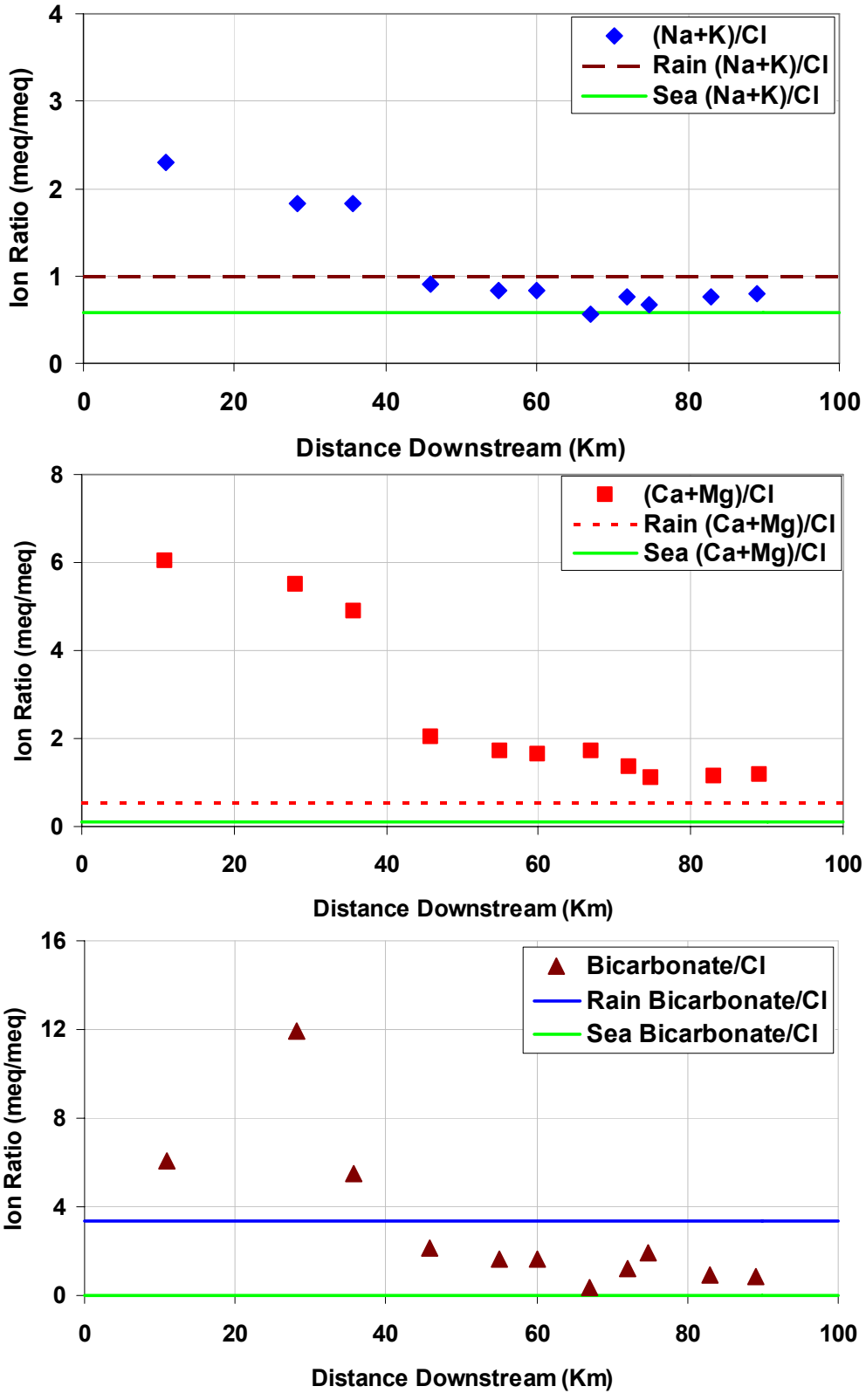


**Figure 5.8b** Profiles of ion ratios of mineral weathering products downstream from the head of the river for the July 2007-July 2008 sampling period

The groundwater samples appear to fall into two groups. Those with higher TDS where the ratios of Na/(Ca+Na), Na/(Mg+Na) and Cl/(Cl+ $HCO_3$) are close to 1 and those with low TDS where the ratios are less than 1 (**Figure 5.9**). Samples with TDS greater than 2000mg/L generally show relatively low concentrations of Ca and $HCO_3$ in solution relative to Na and Cl. The weathering of augite releases $Ca^{2+}$ and $HCO_3^-$ ions to solution, resulting in an increase in pH observed in upper catchment. The distribution of TDS vs Na/(Mg+Na) and TDS vs Na/(Ca+Na) (**Figure 5.9a** and **5.9b**) represent a larger proportion of cations (Mg and Ca, respectively) at lower TDS suggesting that basaltic and granitic weathering in the Liverpool Ranges provide $Mg^{2+}$ and $Ca^{2+}$ and $Na^+$ to the solution. $Ca2^+$, $Mg^{2+}$, $Na^+$ and $HCO_3^-$ concentrations are the highest in the basalt groundwaters and these ions are released from the weathering of aluminosilicate minerals (Locsey and Cox 2000).

Linear relationships between bicarbonate and major cations (calcium, magnesium and sodium) have been used as evidence for the release of these ions from weathering of a basalt host. These are plotted as indicated in **Figure 5.10**. A relationship has been used in the previous studies as evidence of the concomitant release of these ions from the weathering of basalt (Locsey and Cox 2002; Cook *et al.* 2001). On the basis of the stoichiometry of the reactions associated with the weathering of pyroxene and feldspars to kaolinite and gibbsite, the theoretical ratio of sodium to bicarbonate is 1:4.3 (**Figure 5.10a**). Samples close or parallel to this trend are dominated by these weathering processes. The excess of sodium relative to bicarbonate, originate from the marine salt influence within the shallow groundwater system. It is clear for **Figure 5.10** that while some of the shallow groundwater samples do not fall on these predicted linear relations for basalt dissolution, there is a possible linear trend in the deeper upstream groundwater samples suggested that some of the $HCO_3$ is sourced from basalt weathering in the upper catchment.

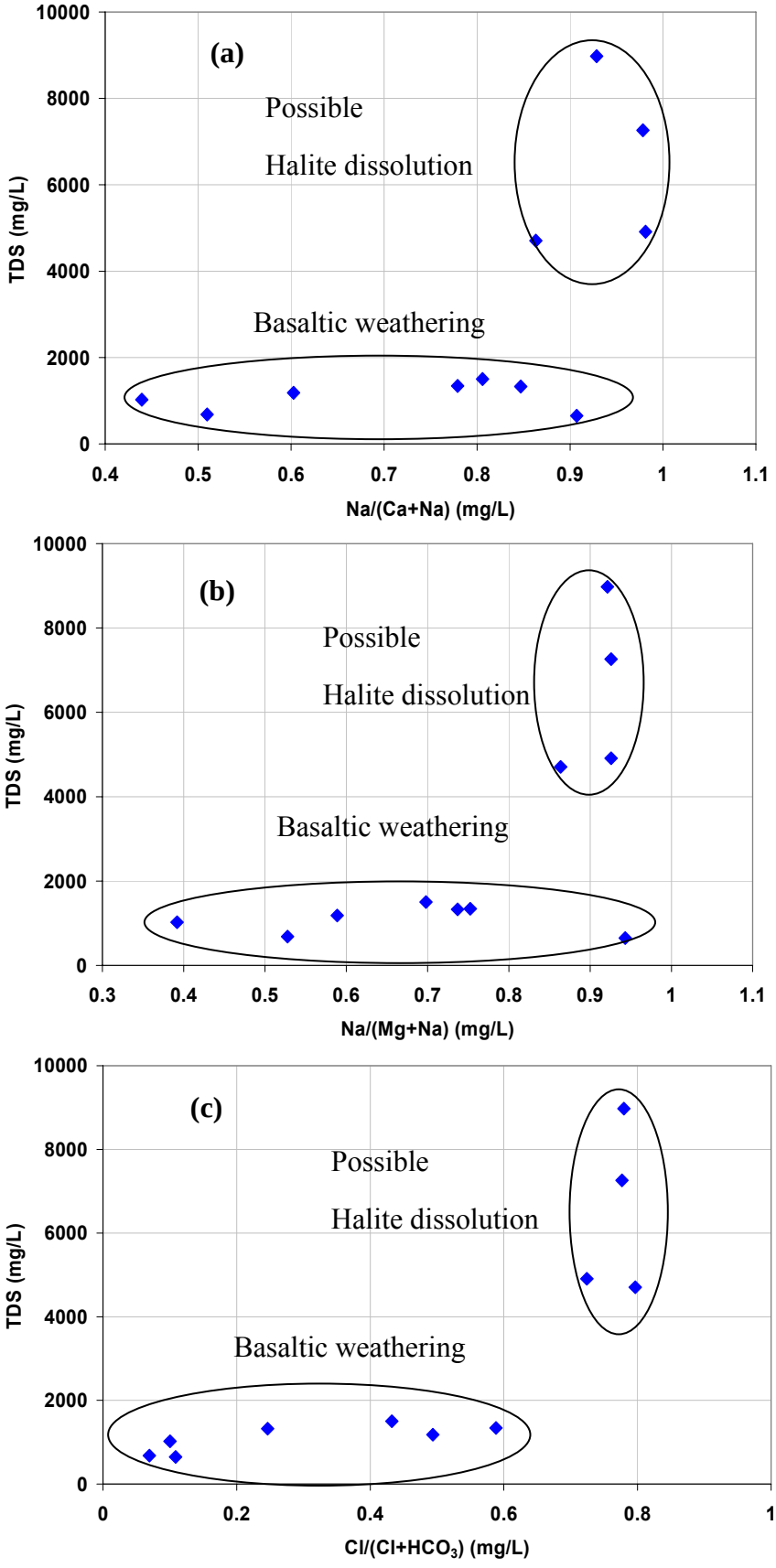


**Figure 5.9** The relationship between TDS and **(a)** Na/(Ca+Na) **(b)** Na/(Mg+Na) v and **(c)** Cl/(Cl+$HCO_3$) for groundwater samples during July 2006 sampling periods

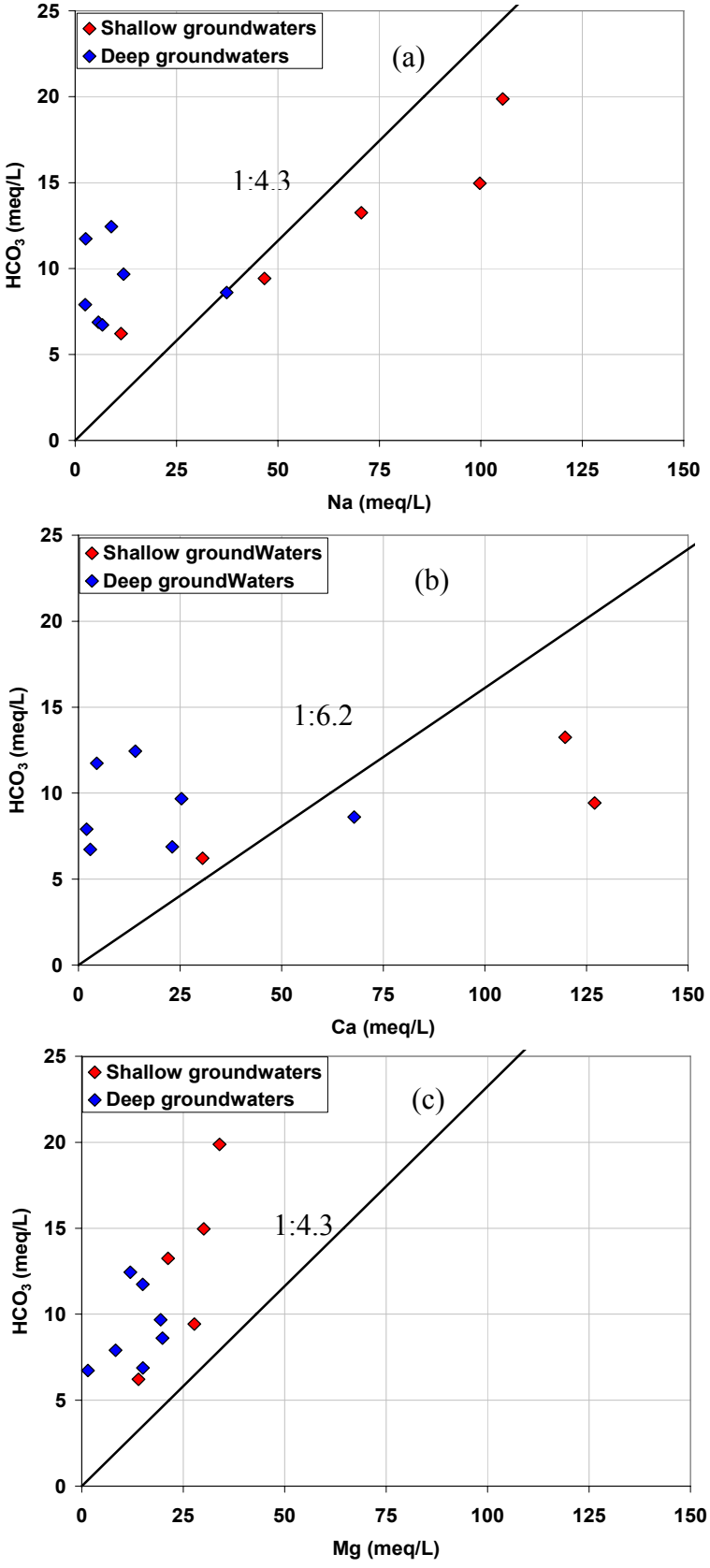


**Figure 5.10** Major ion **(a)** Na versus $HCO_3$ **(b)** Ca versus $HCO_3$ (c) Mg versus $HCO_3$ for groundwater sample

### 5.3.4 Sources of $Ca^{2+}$, $Mg^{2+}$ in Stream and Groundwater

The major ion to chloride ratios in Section 5.3.3 show that the lower catchment the stream water shows a significant influence of marine origin waters, while in the upper catchment those ratios exceeded those of marine origin waters and this was attributed to mineral weathering. In this and the following sections we examine potential sources of major ions in the catchment.

The relationship between $Ca^{+2}$ +$Mg^{+2}$ and $HCO_3^-$ concentration shown in **Figure 5.11** is used to examine the sources of calcium, magnesium in the surface water sampling during July 2006, June 2007 and July 2008 and in the groundwater during July 2006, June 2007 and July 2008. Dissolution of carbonate and silicate minerals results in an increase in $Ca^{2+}$, $Mg^{2+}$ and $HCO_3^-$ , and $Na^+$, $K^+$, and Si concentrations (Sarin *et al*., 1989; Bartarya, 1993; Harris *et al*., 1998; Singh and Hasnain, 1998; Singh *et al*., 1998a; Galy and France-Lanord, 1999; Pandey *et al.*, 1999) in soil water and ground water relative to infiltrating of rainfall.

**Figure 5.11a** shows that one surface water sample at Railway Bridge, at the lowest sampling point in the stream and lies close to 2:1 line. **Figure 5.11c** shows surface water sample at Rockhall Causway which lies above the line. **Figure 5.11b** shows that surface water sample at TSR in upper catchment, Yarraman gauge, Wybong Bridge, Hollydeen and Railway Bridge in lower catchment all lie close to the 2:1 line. These results suggest carbonate dissolution at these sample sites and sampling times. In general, however, the surface water samples in **Figure 5.11** lie below the carbonate dissolution line suggesting that other mineral weathering processes or groundwater sources such as marine origin water are contributing to the $Ca^{2+}$ and $Mg^{2+}$ in the stream.

Groundwater samples at the bores GW080946, GW080434 lie close to the 2:1 line and that at Frenchies bore lies above the line as shown in **Figure 5.11d**. In **Figure 5.11e**, none of the samples lie on the 2:1 line, although two samples, Roberts_1A piezometer and Roberts_House Bore lie above the line. In **Figure 5.11f,** groundwater samples at bores GW080946 and GW080434 lie close to the 2:1 line and GW080947 and Frenchies bore again lies above the line. While some groundwater samples could be consistent with carbonate dissolution the majority suggest that other mineral weathering or groundwater sources are responsible for the $Ca^{2+}$ and $Mg^{2+}$ in the surface and groundwater samples.

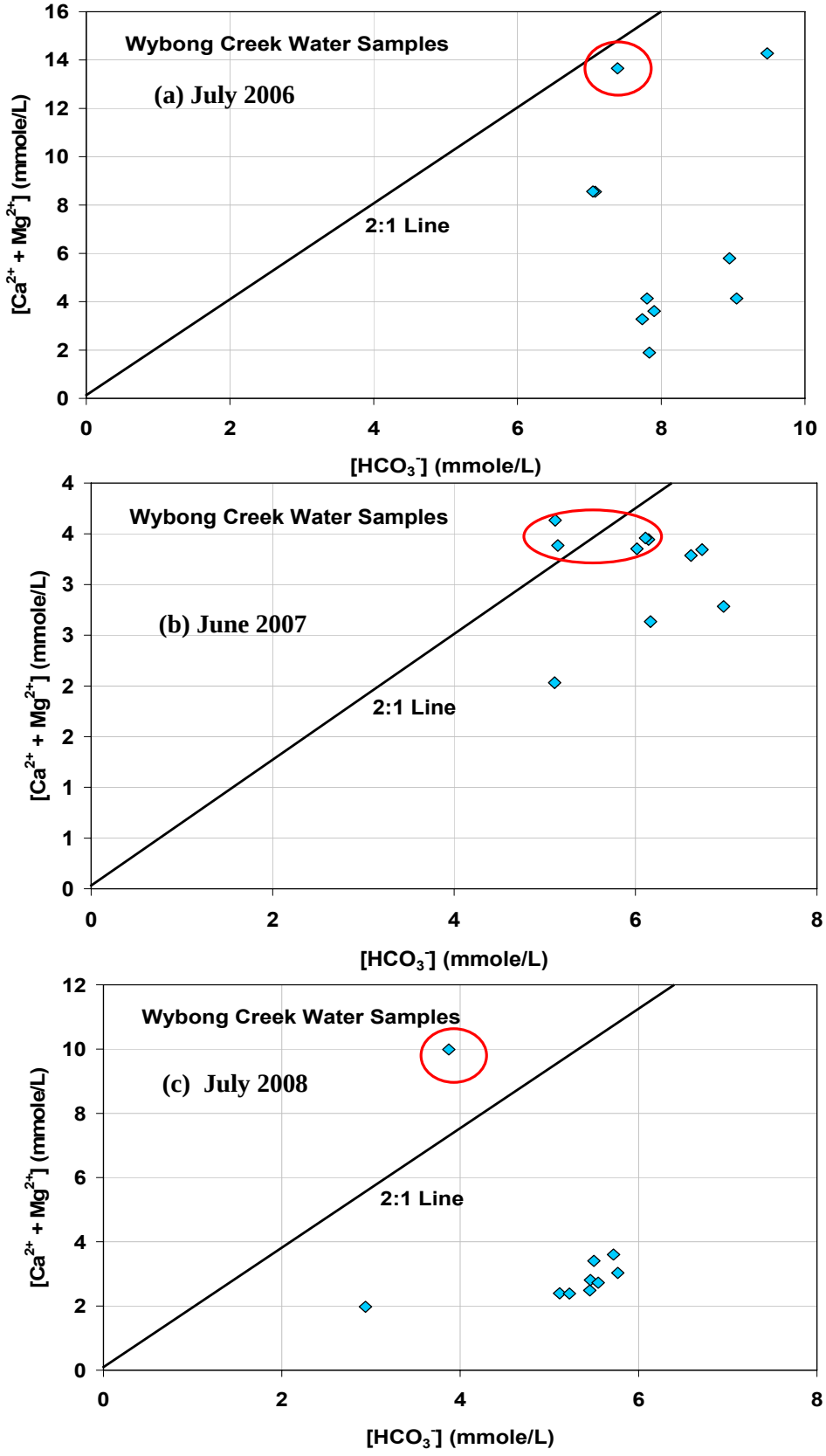


**Figure 5.11** Relationship between Ca +Mg concentrations as a function of [$HCO_3$] of the surface water data during **(a)** July 2006,**(b)** June 2007 and **(c)** July 2008 sampling periods

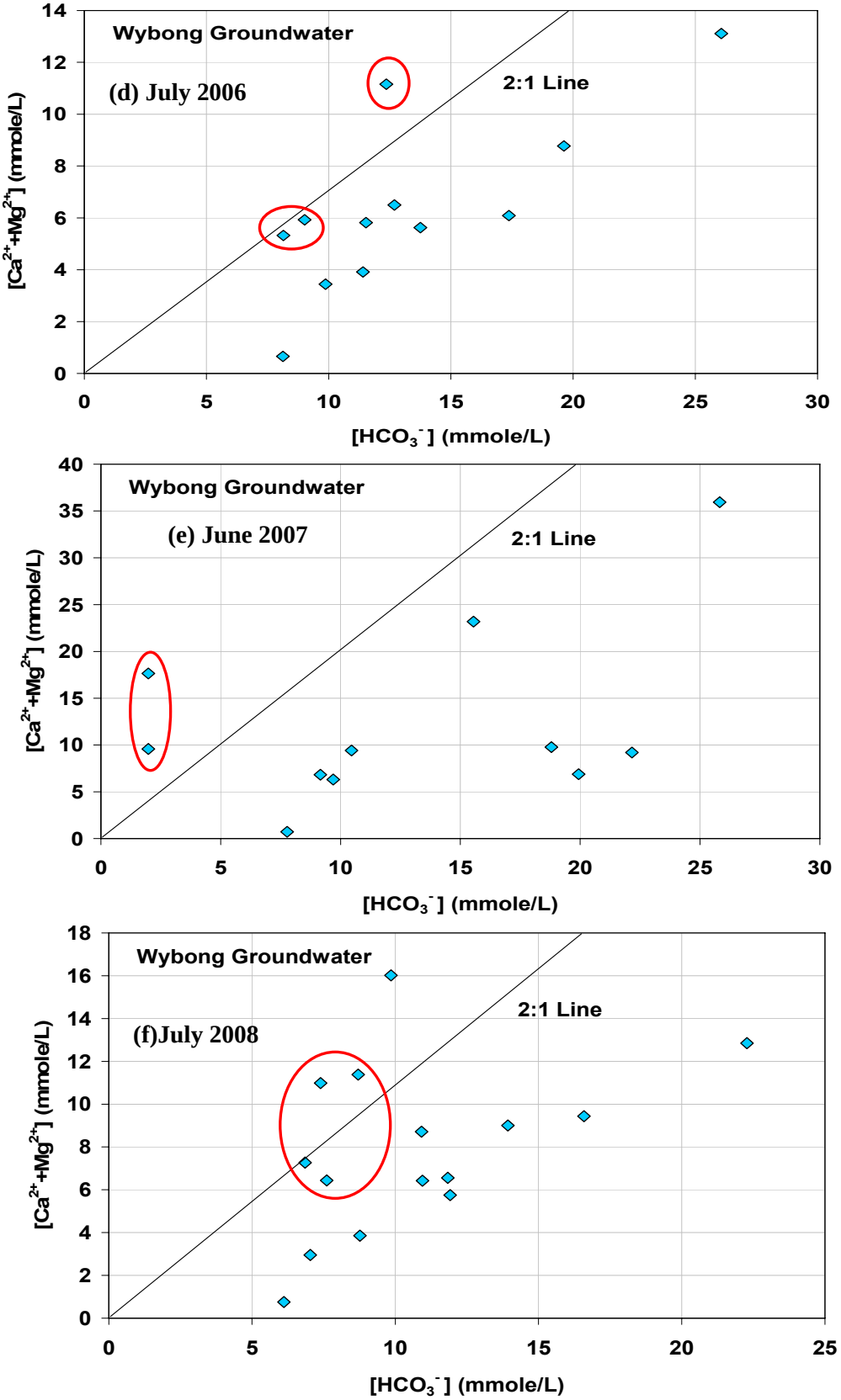


**Figure 5.11** Relationship between Ca +Mg as a function of $HCO_3$, of the groundwater data during **(d)** July 2006 and **(e)** June 2007 and **(f)** July 2008 sampling periods

In general, these results suggest that the sources of $Ca^{2+}$ and $Mg^{2+}$ in the upper catchment are not from carbonate dissolution and are possibly from basaltic and granitic weathering of the Liverpool Range Volcanics. In the lower catchment some sites may possibly be sourced either from carbonate dissolution or from deeper, marine origin groundwaters as inferred in section 5.3.3.

### 5.3.5 Sources of $Na^+$, $Ca^{2+}$, $HCO_3^-$ and $SiO_2$ in Stream and Groundwater

Analysis of the molar ratios of dissolved Na/Ca and $HCO_3/SiO_2$ are useful for examining the relative dominance of silicate versus carbonate weathering (Jacobsen *et al.,* 2002) as shown in **Figure 5.12.** Jacobsen *et al.* (2002) compared these ratios in streams in the Himalayas with the ratios found for stream water samples in the Sierra Nevada (Garrels and Mackenzie, 1967) and Rocky Mountains (Mast *et al.,* 1990) (both silicate weathering) and in the French Alps (Sarazin and Ciabrini, 1997) (carbonate weathering). Those results are also shown for comparison in **Figure 5.12** where the ratio for seawater is also shown**.** The surface water results for Wybong Creek in **Figure 5.12a, b, c** fall well above carbonate weathering (French Alps) and below that for seawater. The surface water samples also fall considerably to the left of the region expected for silicate weathering suggesting other sources of $HCO_3^-$, which could be soil respiration **Figure 5.12d, e, f** shows that some of the groundwater samples fall within the general area of seawater. Some of the groundwaters have higher Na/Ca ratios than those of silicate weather consistent with the influence of marine origin waters as inferred in Section 5.3.3.

The Na/Ca versus $HCO_3/SiO_2$ for Wybong surface water in **Figure 5.12a and 5.12e** suggest that some of the sources of major ions in the upper catchment could be ion exchange with the clays in the regolith while in the lower catchment Na appears to be sourced from marine origin waters. Surface water samples at Campground Bunnan and White Rock appear to fall on a mixing line similar to the Sierra Nevada results as shown in **Figure 5.12b** and **5.12c**. Groundwater samples at Wicks and Queen Street bore, GW080947 and Ethers #1 bore also appear to fall on a mixing line similar to the Sierra Nevada (**Figure 5.12d** and **5.12f)**. These results indicate that the sources of major ions in upper catchment surface and groundwater samples are from silicate weathering.

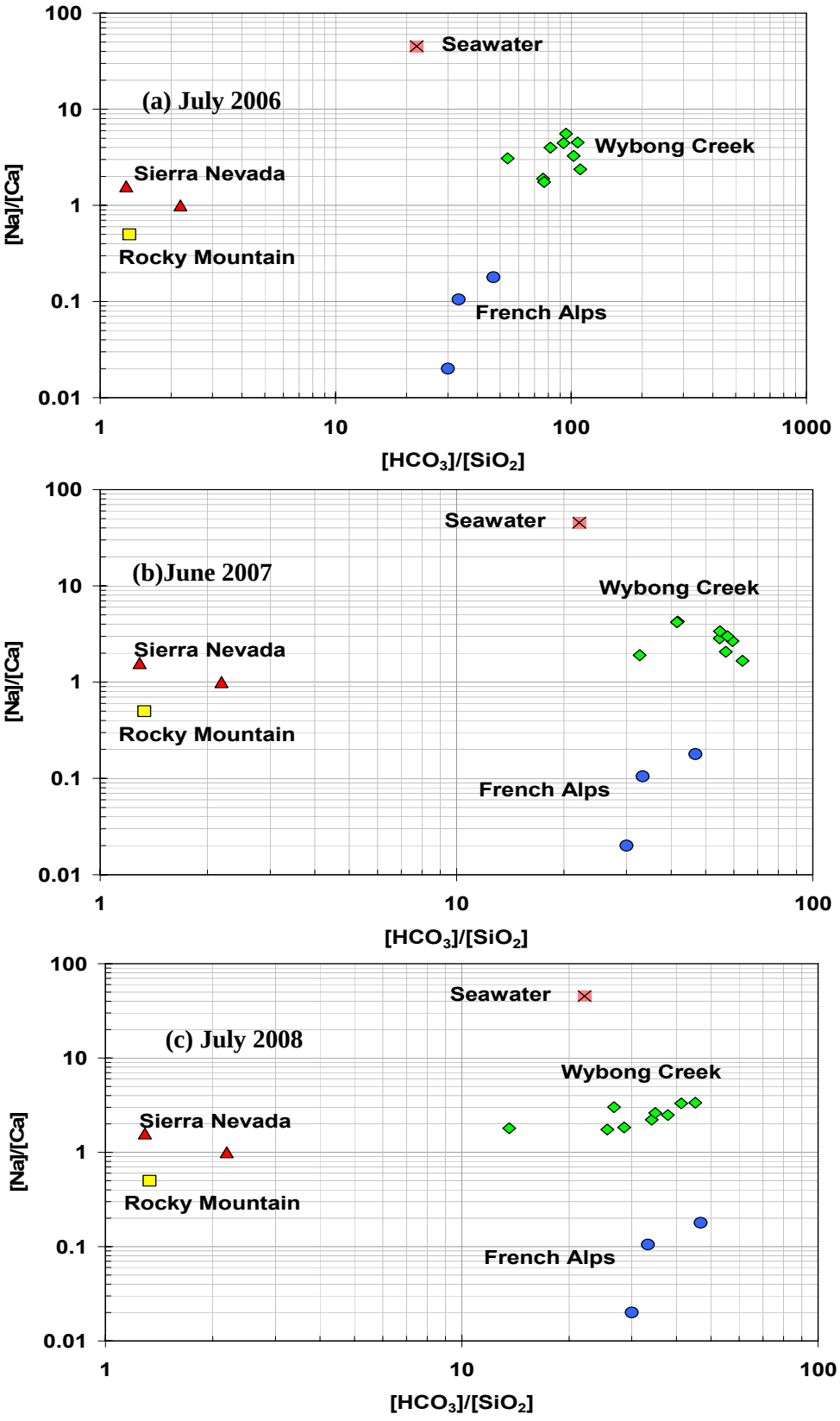


**Figure 5.12** Relationship between Na/Ca vs $HCO_3/SiO_2$, of surface water in Wybong Creek during **(a)** July 2006, **(b)** June 2007 and **(c)** July 2008 sampling periods. Values for mountain streams are from Jacobsen (2002).

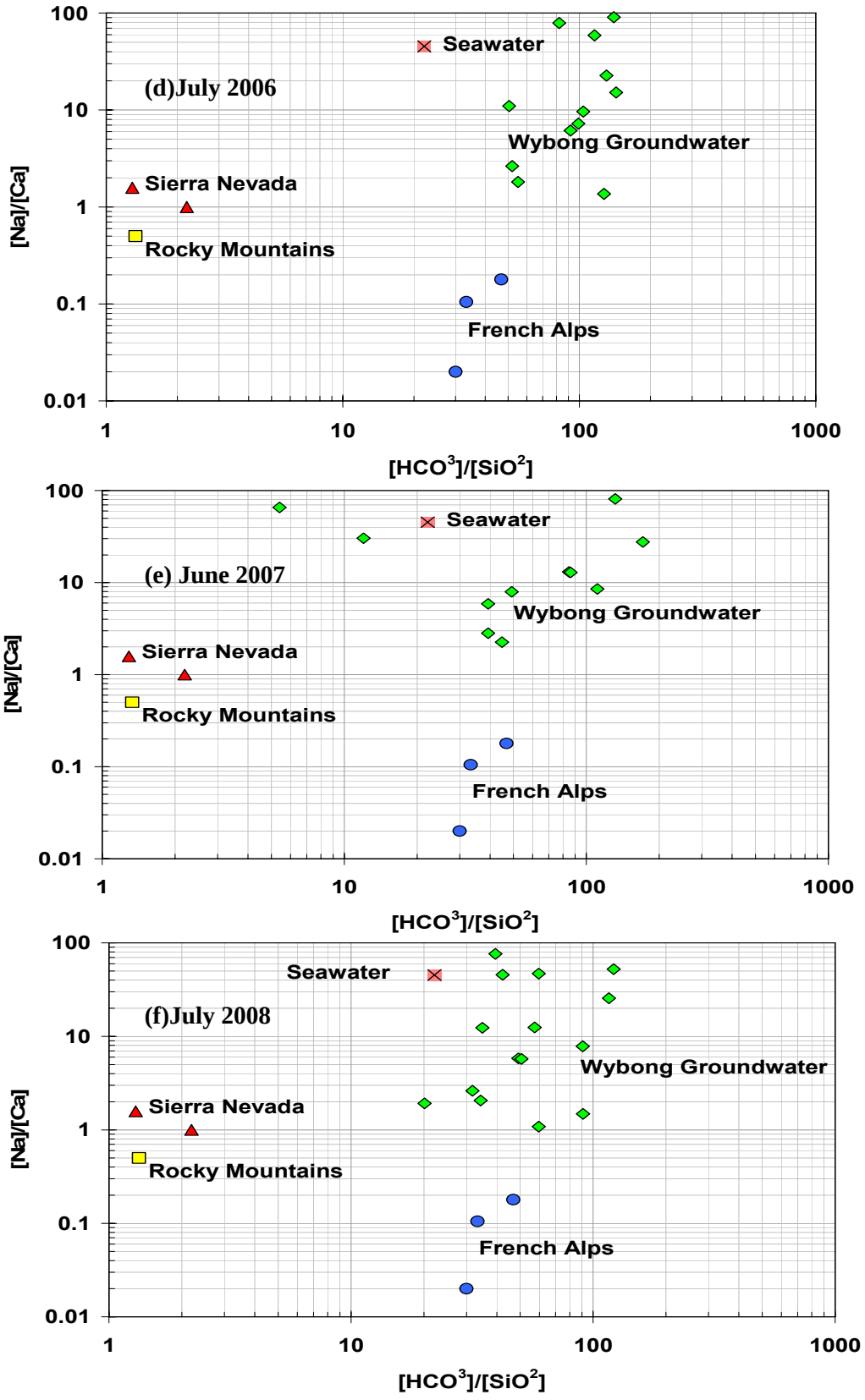


**Figure 5.12** Relationship between Na/Ca vs $HCO_3/SiO_2$, of the groundwater samples during **(d)** July 2006, **(e)** June 2007 and **(f)** July 2008 sampling periods. Values for mountain streams are from Jacobsen (2002).

### 5.3.6 Calcium and Strontium in Stream and Groundwater

The calcium to strontium ratio can be used to examine potential sources of dissolved ions in surface and groundwaters (Jacobsen *et al.*, 2002). **Figure 5.13** shows the relationship between Ca/Sr and distance downstream of the Wybong Creek. **Figure 5.13** shows that the ratio decreases generally to downstream except for the Headwaters (for July 2006 only). There is a clear break in decreasing trend between Ridgeland and Dry Creek Road. However it is noted that there is a continual change from Campground to Dry Creek which suggests continual mixing until Dry Creek Road. This mixing could be due the recharge of groundwater systems in the Liverpool Ranges and discharge in the adjacent upper Wybong Creek valley.

The approximate Ca/Sr ratio for igneous rocks is 215, for sandstones 1749, for shales 170 and for carbonates 964 (Hem, 1992). The plots of $[Ca^{+2} + Mg^{+2}]$ versus $[HCO_3^-]$ in **Figure 5.11** showed that carbonates were not a major source of Ca in the upper catchment. The values of Ca/Sr shown in **Figure 5.13a** for surface water are quite high particularly for July 2006, ranging between 248 to 595, 134 to 445 (**Figure 5.13b**) and 282 to 416 (**Figure 5.13d**). In addition values of [Ca]/[Sr] of 2206 and 124 were found for the ground water at Wick bore; 1131 and 826 are for Queen Street bore; and 457 for Ether #1 during July 2006 and 2008 sampling period. Wick bore located in basalt has the largest value of the [Ca]/[Sr]. The high values of [Ca]/[Sr] in the upper catchment surface and groundwater suggest that source of weathering in some of these bores may be the sandstones and conglomerates of the Narrabeen Group where weathering produces high Ca/Sr ratios and also $HCO_3$ dominated water.

In order to examine whether the trend in Ca/Sr ratio downstream in Wybong is due to a mixing process values of the ratio[Ca]/[Sr] versus 1/[Cl] are plotted in **Figure 5.14a, b, c.** The streamwater results, apart from the result at Headwater, in **Figure 5.14a, b, c** seem to fall on a mixing line between seawater composition and a large value of the ratio at low chloride concentrations which perhaps could be a sandstone or conglomerate source. One possible reason for the anomalous Headwaters value could be the local geology.

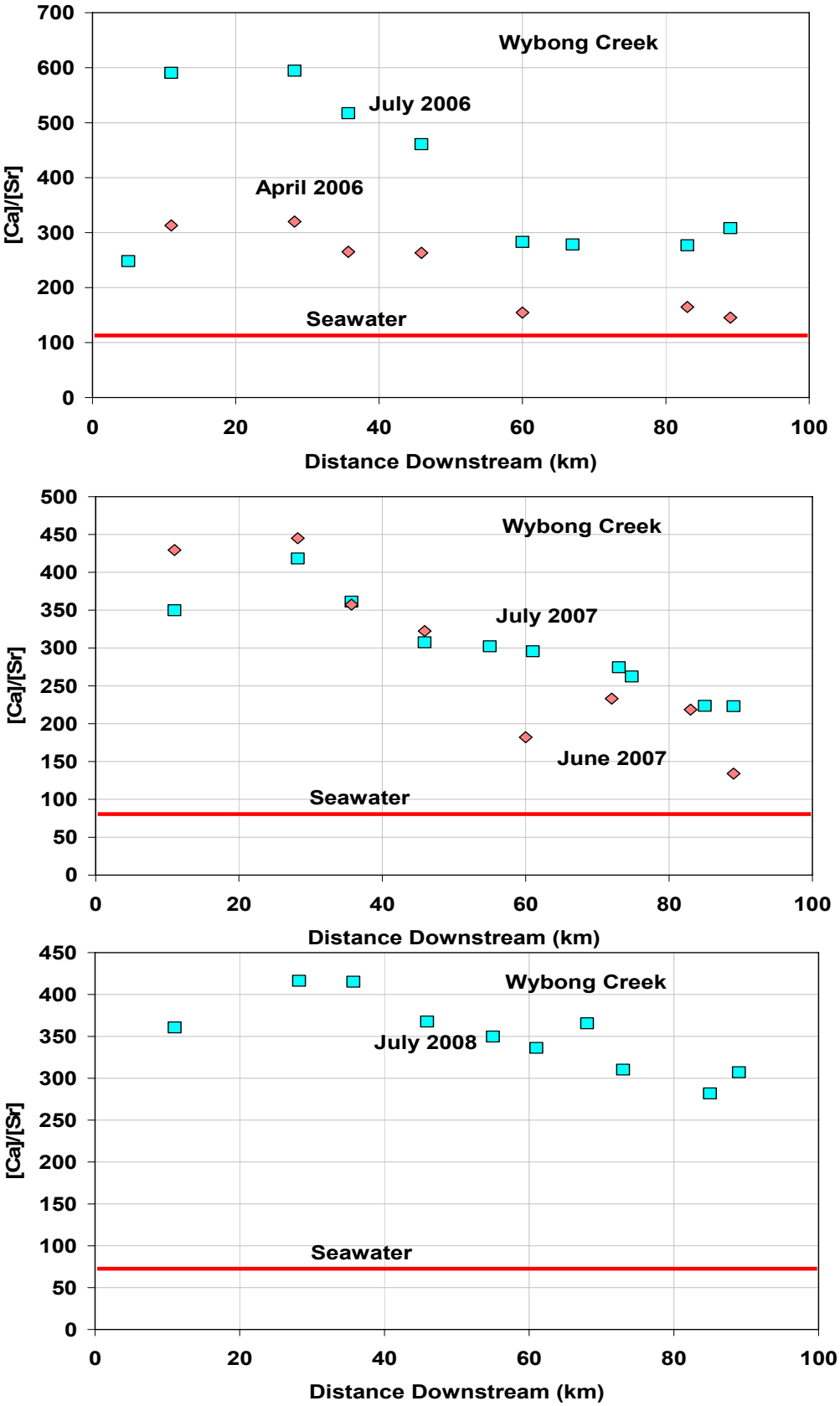


**Figure 5.13** Relationship between Ca/Sr vs Distance downstream for stream water during **(a)** 2006, **(b)** 2007 and **(c)** 2008 sampling periods

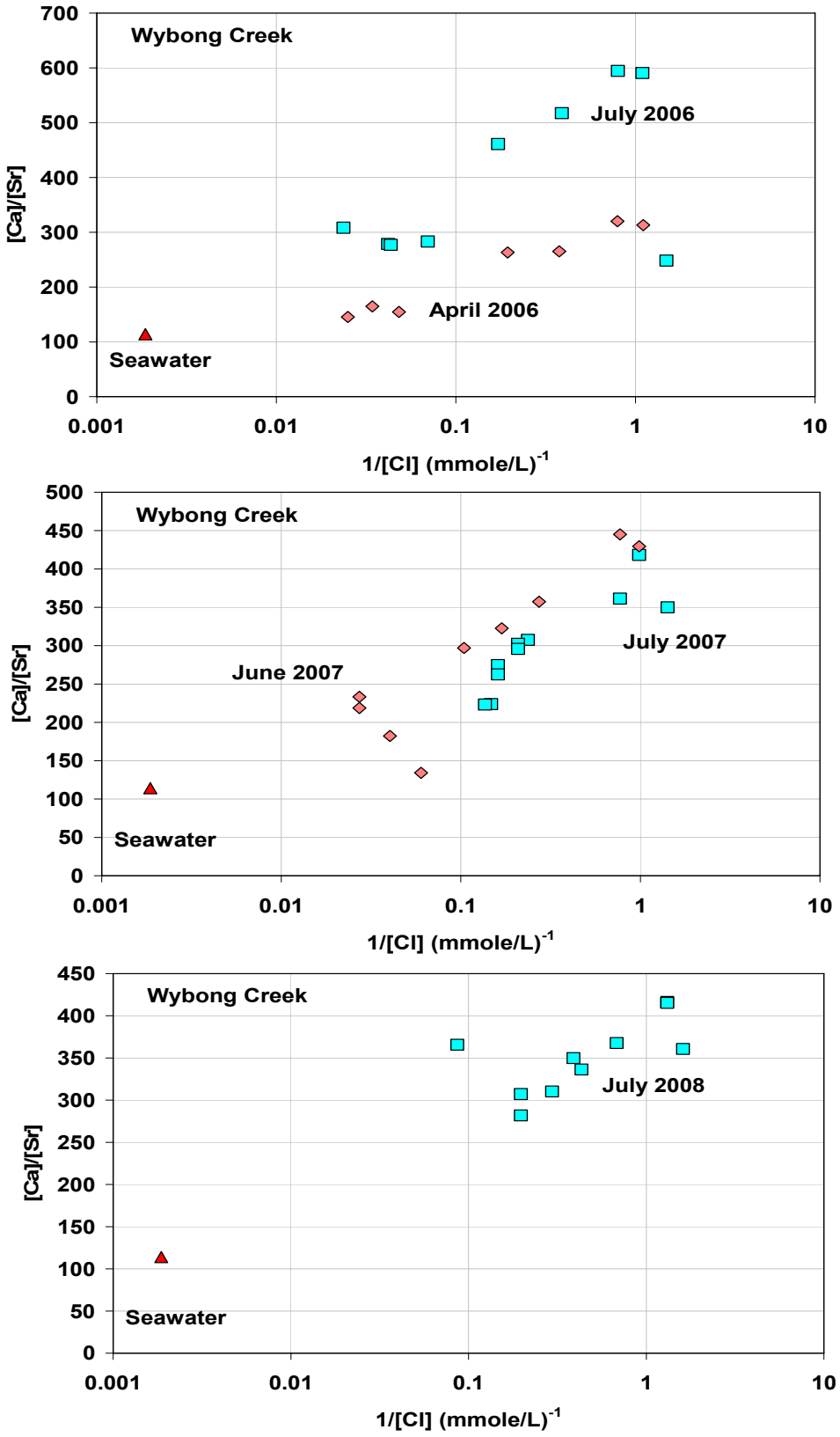


**Figure 5.14** Relationship between [Ca/Sr] and 1/[Cl] for stream water during **(a)** 2006, **(b)** 2007 and **(c)** 2008 sampling periods. Seawater values are from Hem (1992).

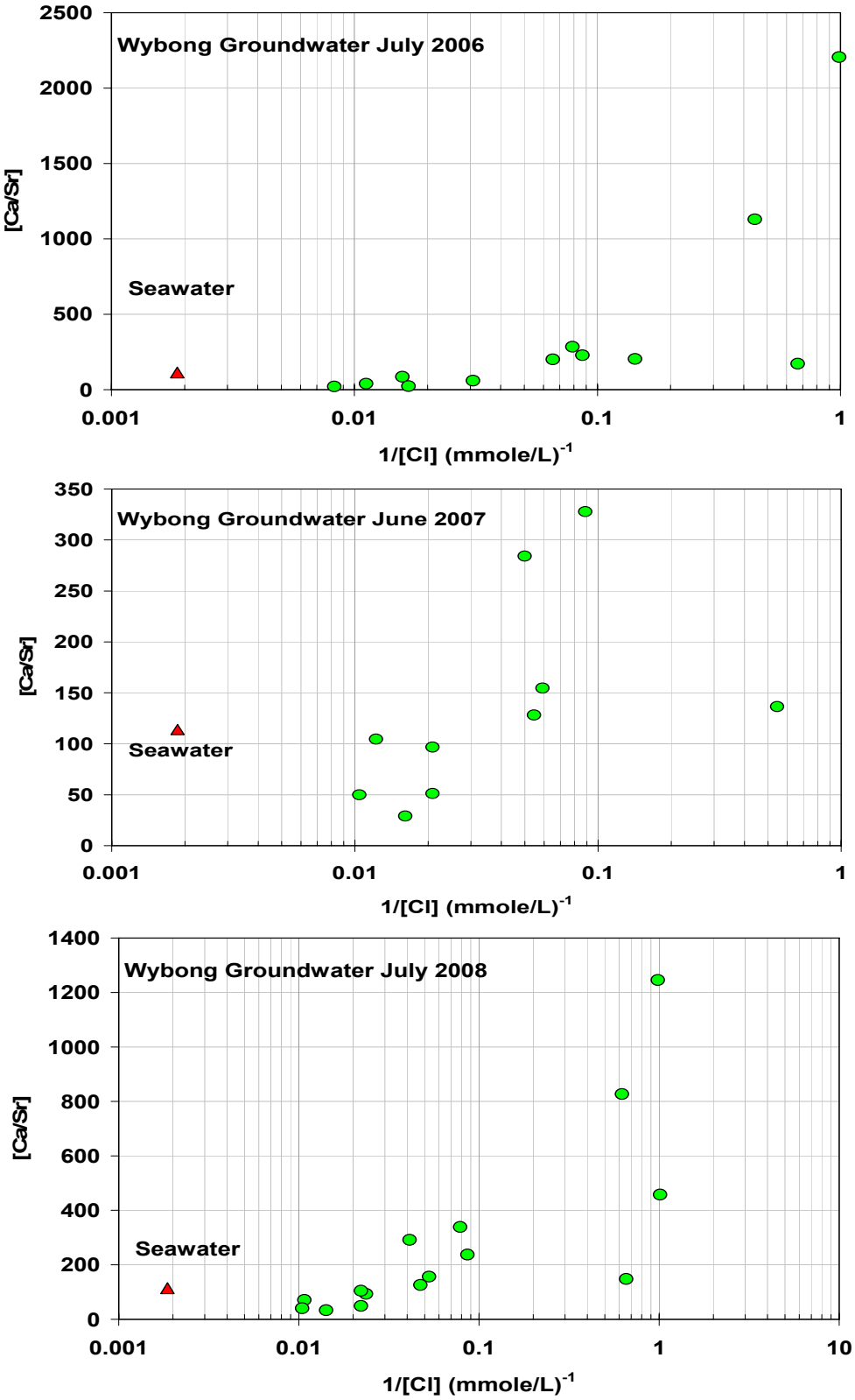


**Figure 5.14** Relationship between Ca/Sr vs 1/Cl for groundwater during **(d)** 2006, **(e)** 2007 and **(f)** 2008 sampling periods. Seawater values are from Hem (1992)

The groundwater results in **Figure 5.14d, e, f** show a general trend from very high values at low chloride concentrations, as for surface water although this trend is less clear for groundwater as there is considerable scatter of results. Some samples with higher chloride content have values of [Ca]/[Sr] that are less than that of seawater. One question which arises from the groundwater samples is the location in the regolith of the groundwater sampled by the bores and wells. One approximate surrogate for that is depth to groundwater.

The EC of the groundwater appears to decrease markedly with increasing groundwater depth as shown in **Figure 5.15**. Groundwaters in the shallow piezometers in lower catchment have high salinity that sourced from Permian Coal Measures. High salinity groundwater occurs in the Narrabeen Group fractured conglomerate (bore GW080944) and the sandstone (bore GW080948). The Narrabeen Group is extensively fractured at the surface, with faults and fractures provide conduits for saline groundwater to move from the Permian Coal Measures into surface water and soil throughout the Hunter Valley ( see e.g. Kellet *et al*., 1989).

The decrease in EC with groundwater depth is also partly reflected in the increase in [Ca]/[Sr] ratio with depth shown in **Figure 5.16.** Ethers #2 bore is an outlier at 150 m depth. It perhaps indicates confined groundwater at this depth. The [Ca]/[Sr] ratio are smaller than seawater in the shallow bores. This may be could be due to ion exchange between Ca, Sr and clays in the regolith that may lower the dissolved Ca/Sr ratio.

**Figure 5.17** shows the interaction between the [Ca]/[Sr] for surface and groundwater as a function of 1/[Cl] during the 2006, 2007 and 2008 sampling periods. The comparison shows some overlapping values indicating the exchange between stream water and groundwater.

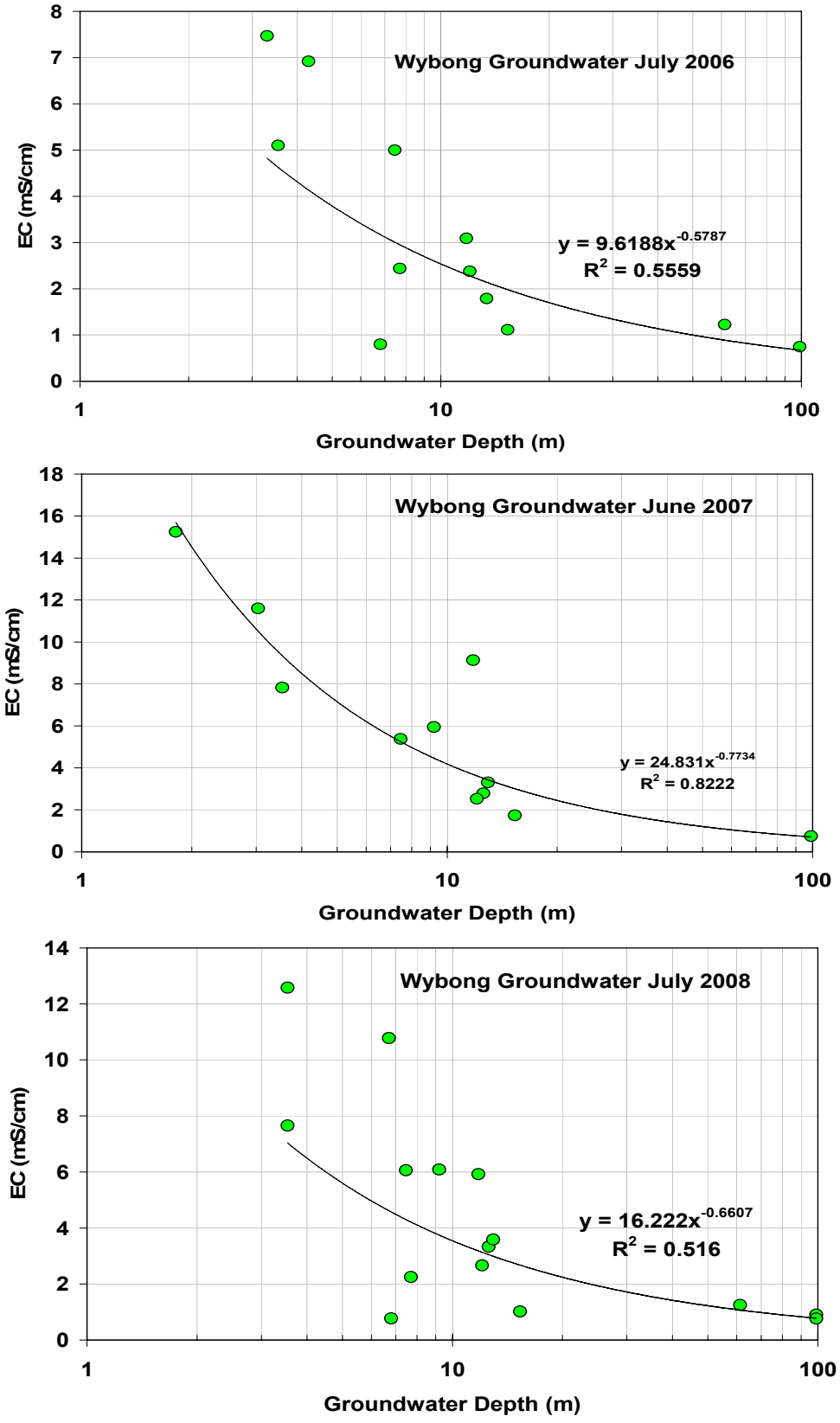


**Figure 5.15** Relationship between EC(mS/cm) vs groundwater depth for **(a)** 2006, **b)** 2007 and **(c)** 2008 sampling periods

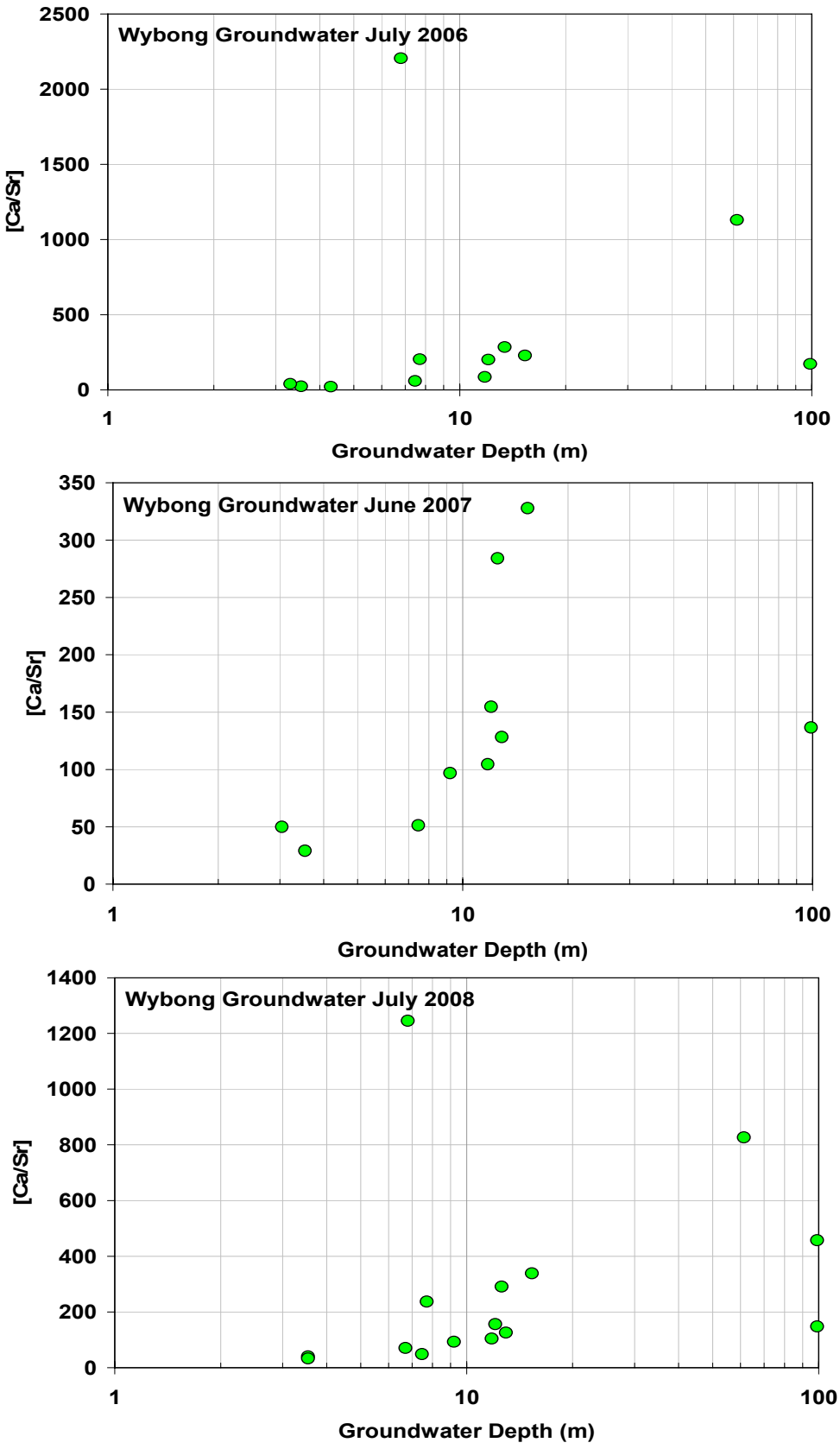


**Figure 5.16** Relationship between Ca/Sr vs groundwater depth during **(a)** 2006, **(b)** 2007 and **(c)** 2008 sampling periods

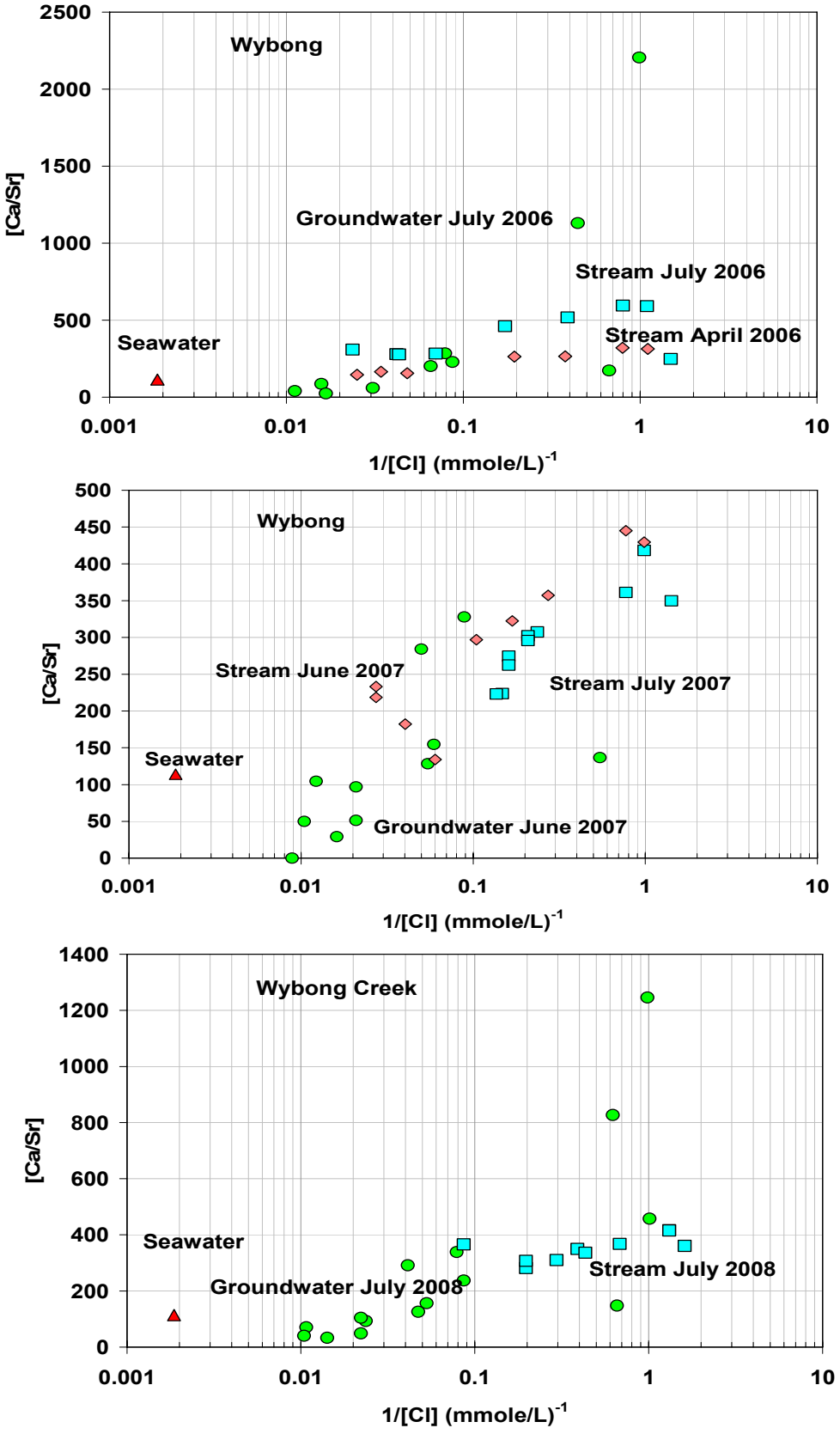


**Figure 5.17** Relationship between Ca/Sr vs 1/Cl of surface and groundwater Samples during July **(a)** 2006, **(b)** 2007 and **(c)** 2008 sampling periods

### 5.3.7 Na/Cl Ratios of Stream and Groundwater

Molar ratios of Na/Cl are used to determine sources of Na ions and identify geochemical processes that affect Na concentrations (Cartwright *et al.,* 2004). Halite contains Na and Cl in equal concentrations. If halite dissolution is the primary source of sodium and chloride within the Wybong catchment then it would expect a 1:1 ratio between $Na^+$ and $Cl^-$ within the surface and ground waters. **Figure 5.18** shows such a relationship for the groundwaters and few samples in the surface waters of upper catchments. Since, however, marine waters also have Na:Cl molar ratio close to 1, this plot does not differentiate between salt sourced from halite weathering and salt sourced from marine water mixing in the coal measures.

The relationship between Na/Cl and Cl shows (**Figure 5.19**) that the lowest salinity (<5 mmol $L^{-1}$) surface water have high Na/Cl ratios (up to 3.3) while surface water with Cl concentrations of >15 mmol $L^{-1}$, has Na/Cl ratios from 0.5 to 0.84 that are close to the oceanic ratio (0.86) and probably similar to the rainfall in Wybong (0.89). The high Na/Cl ratios in the low salinity stream water may be explained by Na being derived predominantly from rock weathering possible weathering of pyroxene and plagioclase which could supply Na. A similar result has been obtained for groundwater. However the lowest salinity (<20 mmol $L^{-1}$) ground water has high Na/Cl ratios (up to 4.7) while ground water with Cl concentrations of >20 mmol $L^{-1}$, has Na/Cl ratios from 0.73 to 0.86 that are close to the oceanic ratio of (0.86). The surface and ground waters in the lower catchment are probably influenced by halite dissolution or seawater and evaporation (**Figure 5.19**). The bores with Cl > 60 mmol are shallow surface piezometers, which are strongly influenced by evaporation, and Cl dominated groundwater are sourced from deeper groundwater.

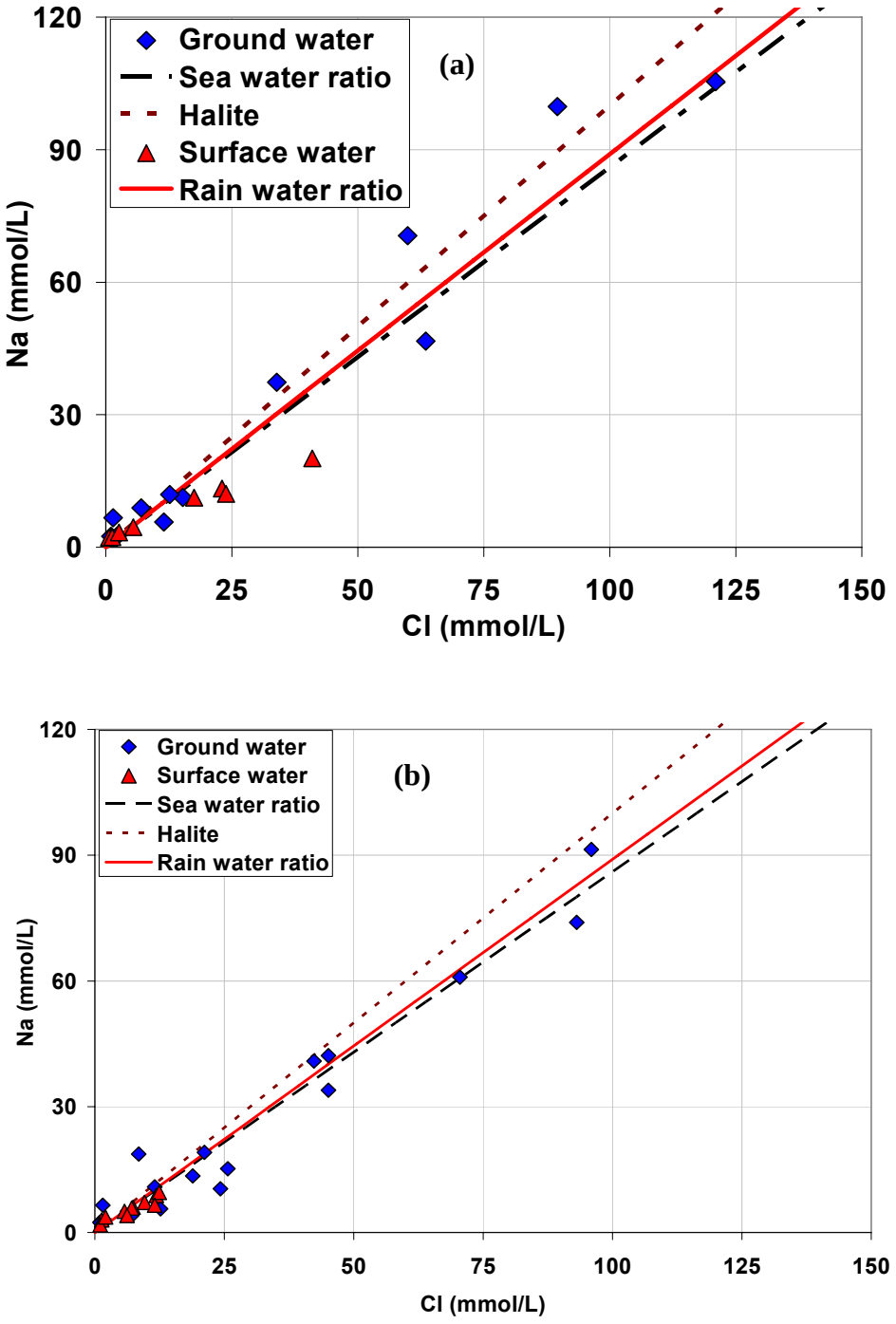


**Figure 5.18** Relationship between Cl and Na of the surface and ground waters data during **(a)** July 2006 and **(b)** July 2007-July 2008 sampling periods

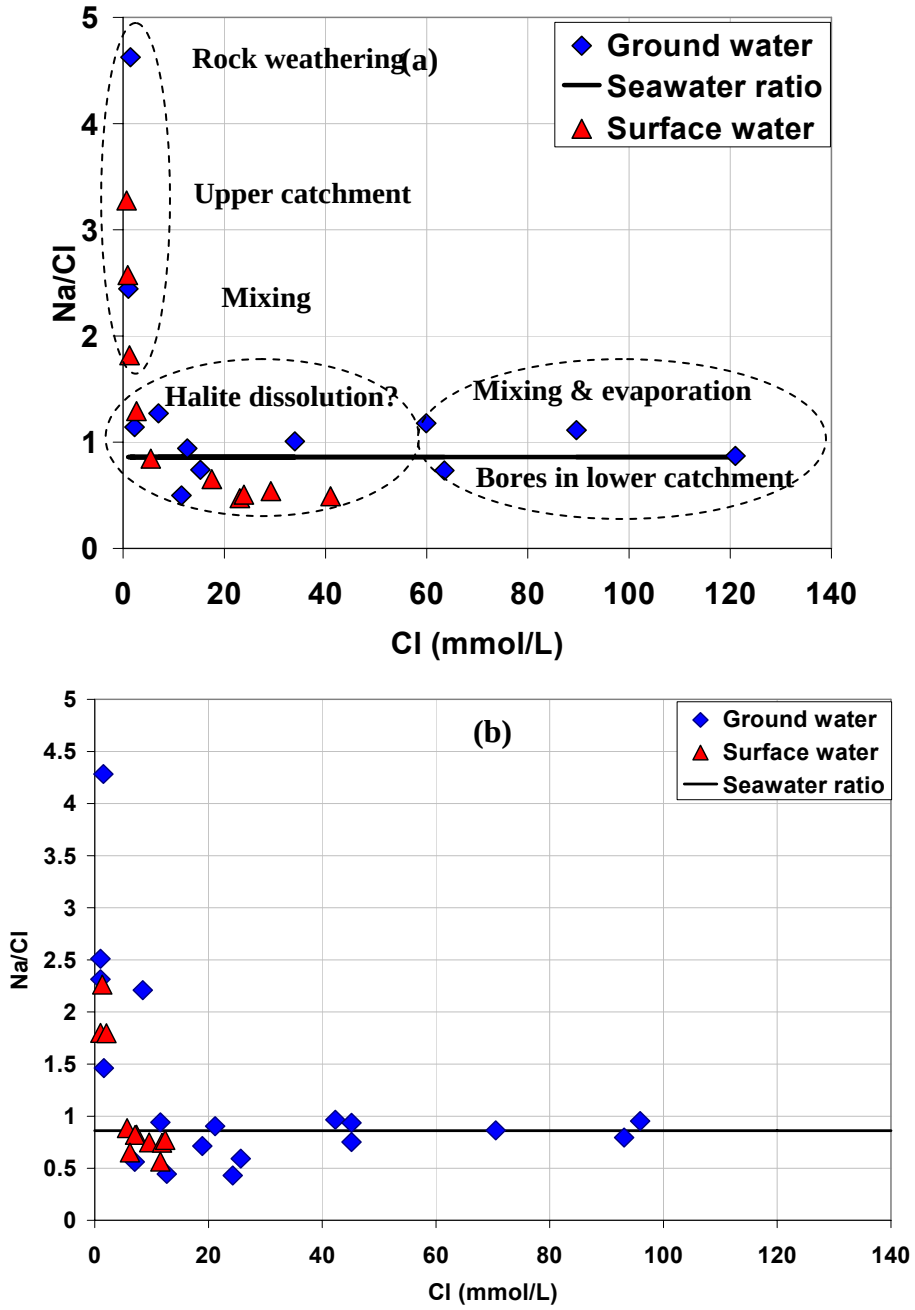


**Figure 5.19** Relationship between Na/Cl and Cl, and of the surface and ground waters data during **(a)** July 2006 and **(b)** July 2007-July 2008 sampling periods

### 5.3.8 Cl/Br Ratios of Stream and Groundwater

The Cl/Br ratio is commonly used to identify halite dissolution contributing Cl to groundwater (Cartwright *et al.,* 2004). The Cl/Br ratios determined here and plotted in **Figure 5.20** show systematic variation of surface and groundwater. It has been shown

that groundwater samples with <20 mmol/L Cl have a range of Cl/Br ratios from 321 to 1510 where surface water range is from 406 to 4620. In general, more saline groundwater has been shown to have a more restricted range of Cl/Br ratios 600–900 that are close to or above the oceanic ratio of 650 (Cartwright *et al.,* 2004, 2006, Davis *et al*., 1998, Davis *et al*., 2001). The lowest Cl/Br ratios are 321-650 of the groundwater represent that local rainfall water recharges the aquifer system.

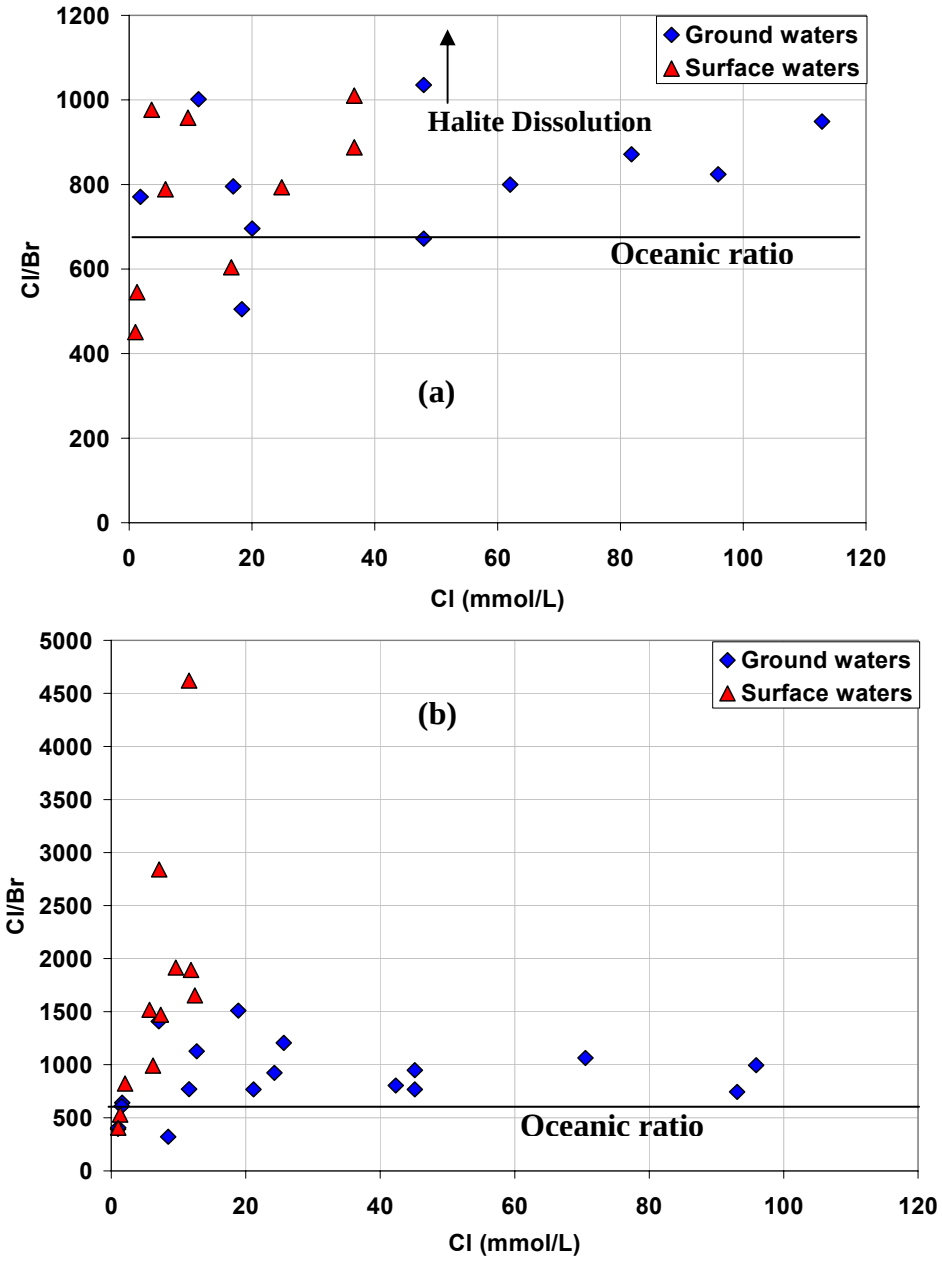


**Figure 5.20** Relationship between Cl/Br and Cl, of the surface and groundwater data during **(a)** June 2007 and **(b)** July 2007-July 2008 sampling periods

The highest Cl/Br ratios occur in groundwater with Cl concentrations of <20 mmol/L (**Figure 5.20**) probably dissolution of halite. Cl/Br ratios of halite may be ~$10^4$. Dissolution of halite is locally present in the soils, clay, shale and organic debris is the most likely mechanism to increase Cl/Br ratios. However, moderate Cl/Br ratios are observed in groundwater with Cl concentrations of >20 mmol/L. The Cl/Br ratio in the Wybong Creek trends to a value of ~600–1000 which reflects the composition of the rainfall and the degree of halite dissolution that occurs during recharge. The Cl/Br ratios of some samples are lower than seawater but much higher than halite indicating that evaporated dissolution or rock weathering contributed a small amount of solute in the water. **Figure 5.21** shows a Na/Cl verses Cl/Br plot with Cl concentration on which the major controls on groundwater chemistry (rock weathering, halite dissolution, mixing and evaporation) are indicated.

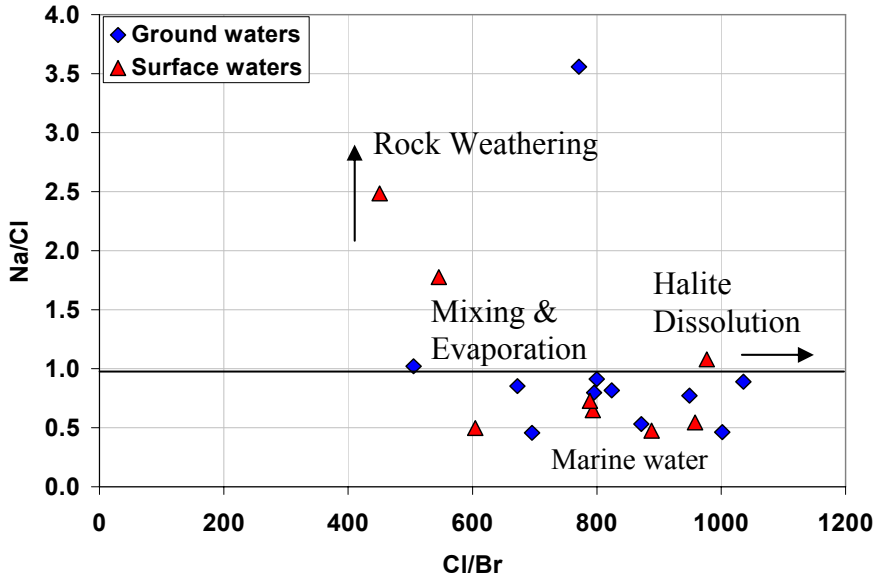


**Figure 5.21** Relationship between Na/Cl and Cl/Br of the surface and groundwater data during June 2007 sampling periods

### 5.3.9 Stable Isotope Composition of Surface Water and Groundwater

The $\delta^2$H and $\delta^{18}$O (‰) signatures of continental rainfall derived from oceanic moisture generally fall close to the Global Meteoric Water Line (GMWL, Craig 1961).

$$\delta^2 H = 8.\delta^{18} O + 10 \qquad (5.7)$$

Rainwater samples collected in the Wybong fell on a local meteoric line, LMWL ($R^2$ =0.987):

$$\delta^2 H = (7.4 \pm 0.6).\delta^{18} O + (11 \pm 5) \quad (5.8)$$

which is close to the GMWL. Surface water samples in a transect of Wybong Creek fell on a quite different relationship to both the GMWL amd the LMWL ($R^2$ = 0.978):

$$\delta^2 H = (4.1 \pm 0.6).\delta^{18} O - (7.9 \pm 2.3) \quad (5.9)$$

Groundwater isotope samples from the Tertiary and Permian sediments in the catchment fell with more scatter on a similar but slightly more evaporated relationship than the surface water samples in equation 5.10 ($R^2$ = 0.771):

$$\delta^2 H = (4.7 \pm 1.5).\delta^{18} O - (9.4 \pm 7.9) \quad (5.10)$$

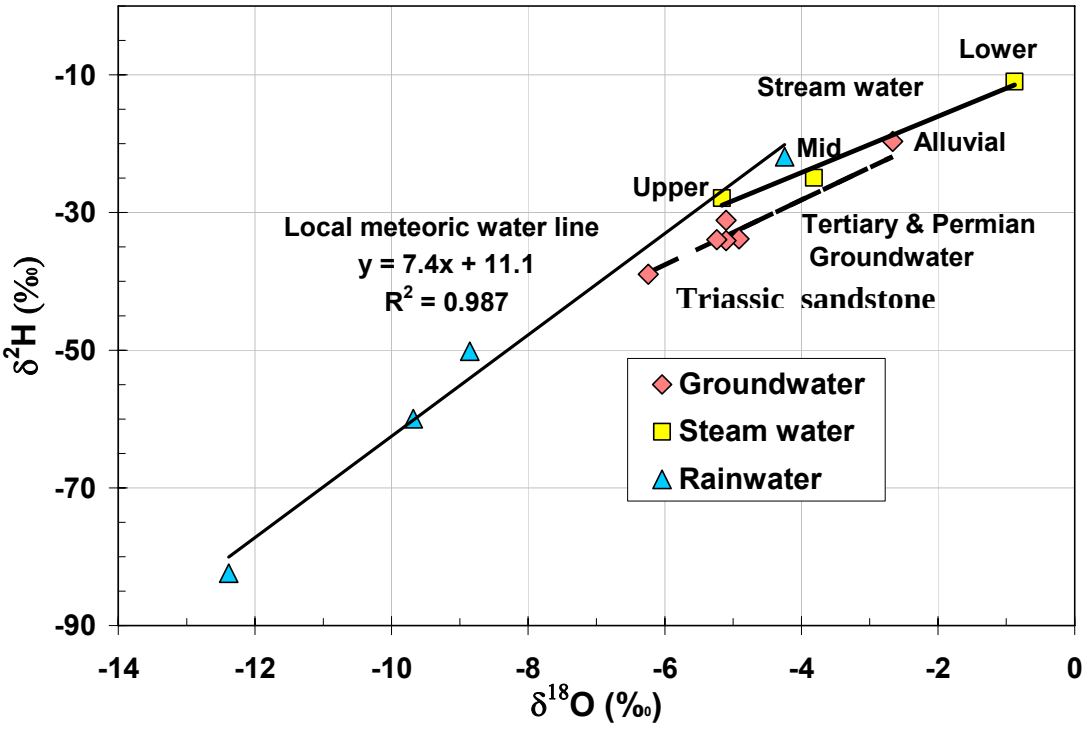


**Figure 5.22** Stable isotope relations for rainwater, stream water and alluvial and deeper groundwater in the Wybong Creek catchment data during 2005 sampling periods

The results are plotted in **Figure 5.22** where it can be seen that the stream water sample in the upper catchment falls on the LMWL. The downstream water isotopes, however, progressively deviate below the LMWL. There are two possible explanations for this: progressive evaporation of the surface water or mixing with groundwater. Since the Permian and Tertiary groundwater samples lie approximately parallel to the stream water samples it appear that mixing with evaporate groundwater is the dominant process.

The isotopic signatures of deeper groundwater samples from the Tertiary and Permian sediments in **Figure 5.22** fall below the LMWL indicating evaporation of recharge water. These also fall slightly below the stream water relation in the upper catchment, although an alluvial groundwater sample taken in the lower catchment falls on the stream water relation, indicating intimate mixing between alluvial and stream water. The deeper groundwater results suggest that the stream water isotopic line is a result of progressive mixing of evaporated surface and interflow with deeper groundwater.

### 5.3.10 Weathering Fractions in Surface and Groundwater

The ion ratio results in section 5.3.3 and 5.3.6 suggest that there are salt in both surface and groundwaters are sourced from weathering products in the upper catchment and marine-origin water in the lower catchment. In order to estimate the contribution of mineral weathering to waters in which both cyclic salt and marine origin salt contribute to salt loads, the approaches outlined in Section 5.2.4.2 and 5.2.4.3 are used.

**Tables 5.10, 5.11, 5.12** and **5.13** show salt loads and weathering fraction due to cyclic salt (rainwater ion ratios are from Murray darling Basin and Bunnan) and marine origin salt estimated by assuming chloride as a conservative tracer sourced from rainwater and marine origin waters in the surface and groundwater, respectively.

Results listed in **Table 5.10** show that Headwaters, Campground, Bunnan, White Rock and Ridgeland sites in upper catchment all show significant mineral weathering fractions of between 0.86 to 0.27 relative to cyclic salt. In the lower catchment, from Dry Creek Road to the Railway Bridge sites, the weathering fractions are negative. This strongly suggests input of waters with ion ratios substantially different from cyclic salt. The cyclic salt ion ratios (**Table 5.10b**) measured in the Hunter region in the 1980's had a distinct contribution from $SO_4$. Because sulphur removal from Hunter coal-burning

fire stations has improved in the last 25 years, cyclic salt ion ratios from nearby in the Murray-Darling Basin have also been used here (**Table 5.10a)**. Comparison of the weathering fractions estimated from either cyclic salt data sources (**Tables 5.10a and 5.10b**) show only a small change in weathering fractions and the overall conclusion of significant weathering in the upper catchment and another source of salt in the lower catchment remain unaltered.

**Table 5.10a** Salt loads and weathering fraction in Wybong Creek due to cyclic salt estimated by assuming chloride as a conservative tracer sourced from rainwater (rainwater ion ratios are from Murray darling Basin).

| Site name | Distance down stream (km) | Max $Cl_{riv}$ (mg/L) | Max $TDS_{riv}$ (mg/L) | $TDS_{cyc}$ (mg/L) | $TDS_{wea}$ (mg/L) | WF |
|---|---|---|---|---|---|---|
| Headwaters | 5 | 23.78 | 639.9 | 91 | 549 | 0.858 |
| Campground | 11 | 36 | 864 | 137 | 727 | 0.841 |
| Bunnan | 28.2 | 46 | 898.6 | 175 | 723 | 0.805 |
| White Rock | 35.7 | 130 | 1119 | 495 | 624 | 0.557 |
| Ridgeland | 45.9 | 210 | 1095 | 800 | 295 | 0.269 |
| Dry Ck Rd | 60 | 880 | 2152 | 3353 | -1201 | -0.558 |
| Rockall Causeway | 67 | 845 | 1820 | 3220 | -1400 | -0.769 |
| Yarraman gauge | 72 | 1300 | 2680 | 4953 | -2273 | -0.848 |
| Hollydeen | 83 | 1300 | 2681 | 4953 | -2272 | -0.848 |
| Railway bridge | 89 | 1496 | 2823 | 5700 | -2877 | -1.019 |

When it is assumed that the salts in Wybong Creek is due to marine origin water **Table 5.11** shows that mineral weathering contributes to the salt load all the way down the stream to above Railway Bridge although the contribution is relatively small at and below Dry Creek Road. At Railway Bridge the results suggest that the streamwater is straight diluted marine origin water. If we assume that the marine origin water has the same TDS as seawater, the dilution ratio of $TDS_{riv}/TDS_{sw}$ is equal to 0.081 or about a 1 to 12.3 dilution factor. Of course the dilution factor could be larger if the marine origin source water is more evaporated than seawater.

**Table 5.10b** Salt loads and weathering fraction in Wybong Creek due to cyclic salt estimated by assuming chloride as a conservative tracer sourced from rainwater (rainwater ion ratios are from Bunnan).

| Site name | Distance down stream (km) | Max $Cl_{riv}$ (mg/L) | Max $TDS_{riv}$ (mg/L) | $TDS_{cyc}$ (mg/L) | $TDS_{wea}$ (mg/L) | WF |
|---|---|---|---|---|---|---|
| Headwaters | 5 | 23.78 | 639.9 | 98 | 542 | 0.847 |
| Campground | 11 | 36 | 864 | 148 | 716 | 0.829 |
| Bunnan | 28.2 | 46 | 898.6 | 189 | 709 | 0.789 |
| White Rock | 35.7 | 130 | 1119 | 535 | 584 | 0.522 |
| Ridgeland | 45.9 | 210 | 1095 | 864 | 231 | 0.211 |
| Dry Ck Rd | 60 | 880 | 2152 | 3622 | -1470 | -0.683 |
| Rockall Causeway | 67 | 845 | 1820 | 3477 | -1657 | -0.911 |
| Yarraman gauge | 72 | 1300 | 2680 | 5350 | -2670 | -0.996 |
| Hollydeen | 83 | 1300 | 2681 | 5350 | -2669 | -0.996 |
| Railway bridge | 89 | 1496 | 2823 | 6157 | -3334 | -1.181 |

When it is assumed that the source of salts in the groundwater in the Wybong catchment is due to cyclic salt, the results listed in **Table 5.12** shows that bores GW080943 and GW038293 in upper catchment have water that is almost identical to the cyclic salt ion ratios with weathering fractions close to zero. This suggests that the salt in these two bores is from evaporated rainwater. If so, the TDS from these two bores can approximately be used to estimate the annual recharge, R, from the mass balance $_{ann}x\{TDS\}_{rain} = Rx\{TDS_{gw}$, since $\{TDS\}_{rain}$ is approximately 5.3 mg/L, and $\{TDS\}_{gw}$ is 1686 and 1571 mg/L for the two bores so that R = 0.0031 to 0.0033x $P_{ann}$. The value of rainfall for the 12 months prior to the groundwater sample is being taken to estimate the recharge but it suggests that if we take 647 mm as the long term average P for Wybong, then R is approximately 2.0 to 2.2 mm/year for the groundwater in these two bores.

**Table 5.11** Salt loads and weathering fraction in Wybong Creek due to marine-origin salt estimated by assuming chloride as a conservative tracer sourced from marine-origin waters.

| Site name | Distance downstream (km) | Max $Cl_{riv}$ (mg/L) | Max $TDS_{riv}$ (mg/L) | $TDS_{cyc}$ (mg/L) | $TDS_{wea}$ (mg/L) | WF |
|---|---|---|---|---|---|---|
| Headwaters | 5 | 23.78 | 639.9 | 43 | 597 | 0.933 |
| Campground | 11 | 36 | 864 | 65 | 799 | 0.924 |
| Bunnan | 28.2 | 46 | 898.6 | 83 | 815 | 0.907 |
| White Rock | 35.7 | 130 | 1119 | 236 | 883 | 0.789 |
| Ridgeland | 45.9 | 210 | 1095 | 381 | 714 | 0.652 |
| Dry Ck Rd | 60 | 880 | 2152 | 1597 | 555 | 0.258 |
| Rockall Causeway | 67 | 845 | 1820 | 1533 | 287 | 0.158 |
| Yarraman gauge | 72 | 1300 | 2680 | 2359 | 321 | 0.120 |
| Hollydeen | 83 | 1300 | 2681 | 2359 | 322 | 0.120 |
| Railway bridge | 89 | 1496 | 2823 | 2714 | 109 | 0.039 |

The results listed in for the weathering fractions in groundwater **Table 5.12** show that all other bores in the upper catchment have the weathering fraction between 0.67 to 0.84. These show that there is significant weathering occurring in these bores with up to 84% salt present due to mineral weathering in the upper catchment. In the lower catchment the results listed in **Table 5.12** that all piezometers and bores, together with bores GW080943 and GW038293 in the upper catchment have negative values of weathering fractions. This suggests a different source of salt in these bores such as marine origin waters since the sum of its ion ratios is less than that for rainwater.

If we assume that the source of salt in groundwater is marine origin water then the weathering fraction results listed in **Table 5.13**, for the piezometers BFC TSR deep and the bore GW080944 in the lower catchment have weathering fractions close to zero indicating they are close to straight diluted marine origin waters. If we assume that the marine origin waters has the TDS of seawater then the dilution ratio of these two bores is approximately the ratio of the TDS of the groundwater to that in seawater, for BFC TSR deep the ratio is 1 part seawater to 13.9 parts freshwater and for bore GW080944 1 part seawater to 10.5 parts freshwater, both indicating a substantial marine origin flux.

This is also close to the values of dilution ratio found for stream water in lower catchment at Railway Bridge.

**Table 5.12a** Salt loads and weathering fraction in groundwater due to cyclic salt estimated by assuming chloride as a conservative tracer sourced from rainwater (rainwater ion ratios are from Murray darling Basin).

| Site name | Distance down stream (km) | Max $Cl_{Gw}$ (mg/L) | Max $TDS_{Gw}$ (mg/L) | $TDS_{cyc}$ (mg/L) | $TDS_{wea}$ (mg/L) | WF |
|---|---|---|---|---|---|---|
| Roberts_1 | 43.7 | 3176 | 7545 | 12102 | -4557 | -0.604 |
| Morgans | 43.4 | 4290 | 9355 | 16346 | -6991 | -0.747 |
| BFC TSR shallow | 44.78 | 3400 | 7324 | 12955 | -5631 | -0.769 |
| BFC TSR deep | 44.8 | 2500 | 4918 | 9526 | -4608 | -0.937 |
| GW080434 | 51.4 | 409 | 1312 | 1558 | -246 | -0.188 |
| GW049877 | 43.9 | 1600 | 3664 | 6097 | -2433 | -0.664 |
| GW080946 | 43.7 | 670 | 1668 | 2553 | -885 | -0.531 |
| GW040960 | 42.8 | 2251 | 4883 | 8577 | -3694 | -0.757 |
| GW080945 | 42.51 | 750 | 2490 | 2858 | -368 | -0.148 |
| GW080947 | 42.34 | 860 | 1911 | 3277 | -1366 | -0.715 |
| GW080948 | 41.63 | 1500 | 3717 | 5716 | -1999 | -0.538 |
| GW080944 | 38.90 | 3300 | 6217 | 12574 | -6357 | -1.023 |
| GW080943 | 30.7 | 449 | 1686 | 1711 | -25 | -0.015 |
| GW038293 | 29.4 | 410 | 1571 | 1562 | 9 | 0.006 |
| GW061136 | 18.3 | 80 | 1246 | 305 | 941 | 0.755 |
| GW080595 | 13.2 | 50 | 817 | 191 | 626 | 0.767 |
| Ethers #2 | 10.03 | 54 | 621 | 206 | 415 | 0.669 |
| GW017391 | 10.0 | 36 | 831 | 137 | 694 | 0.835 |

**Table 5.12b** Salt loads and weathering fraction in groundwater due to cyclic salt estimated by assuming chloride as a conservative tracer sourced from rainwater (rainwater ion ratios are from Bunnan).

| Site name | Distance down stream (km) | Max $Cl_{Gw}$ (mg/L) | Max $TDS_{Gw}$ (mg/L) | $TDS_{cyc}$ (mg/L) | $TDS_{wea}$ (mg/L) | WF |
|---|---|---|---|---|---|---|
| Roberts_1 | 43.7 | 3176 | 7545 | 13070 | -5525 | -0.732 |
| Morgans | 43.4 | 4290 | 9355 | 17655 | -8300 | -0.887 |
| BFC TSR shallow | 44.78 | 3400 | 7324 | 13992 | -6668 | -0.910 |
| BFC TSR deep | 44.8 | 2500 | 4918 | 10288 | -5370 | -1.092 |
| GW080434 | 51.4 | 409 | 1312 | 1683 | -371 | -0.283 |
| GW049877 | 43.9 | 1600 | 3664 | 6585 | -2921 | -0.797 |
| GW040960 | 42.8 | 2251 | 4883 | 9264 | -4381 | -0.897 |
| GW080946 | 43.7 | 670 | 1668 | 2757 | -1089 | -0.653 |
| GW080945 | 42.51 | 750 | 2490 | 3087 | -597 | -0.240 |
| GW080947 | 42.34 | 860 | 1911 | 3539 | -1628 | -0.852 |
| GW080948 | 41.63 | 1500 | 3717 | 6173 | -2456 | -0.661 |
| GW080944 | 38.90 | 3300 | 6217 | 13581 | -7364 | -1.184 |
| GW080943 | 30.7 | 449 | 1686 | 1848 | -162 | -0.096 |
| GW038293 | 29.4 | 410 | 1571 | 1687 | -116 | -0.074 |
| GW061136 | 18.3 | 80 | 1246 | 329 | 917 | 0.736 |
| GW080595 | 13.2 | 50 | 817 | 206 | 611 | 0.748 |
| Ethers #2 | 10.03 | 54 | 621 | 222 | 399 | 0.642 |
| GW017391 | 10.0 | 36 | 831 | 148 | 683 | 0.822 |

All other piezometers and bores in the lower catchment in **Table 5.13** show some mineral weathering relative to marine origin water. So there is some addition of salt to groundwater by mineral weathering and all bores in the upper catchment show significant mineral weathering relative to marine origin water. This is because GW080943 and GW038293 are essentially evaporated rainwater and bores GW080595,

Ethers #2; GW017391 and GW061136 are all actively weathering with respect to rainwater.

The results here show that mineral weathering does contribute to stream salt loads especially in the upper catchment where some bores show essentially evaporated rainwater signatures. In the lower catchment there is a significant input of marine origin water, with stream water at the lowest sampling site Railway Bridge, essentially being diluted marine origin waters.

**Table 5.13** Salt loads and weathering fraction in groundwater due to marine-origin salt estimated by assuming chloride as a conservative tracer sourced from marine-origin waters.

| Site name | Distance down stream (km) | Max $Cl_{Gw}$ (mg/L) | Max $TDS_{Gw}$ (mg/L) | $TDS_{cyc}$ (mg/L) | $TDS_{wea}$ (mg/L) | WF |
|---|---|---|---|---|---|---|
| Roberts_1 | 43.7 | 3176 | 7545 | 5762 | 1783 | 0.236 |
| Morgans | 43.4 | 4290 | 9355 | 7783 | 1572 | 0.168 |
| BFC TSRshallow | 44.78 | 3400 | 7324 | 6169 | 1155 | 0.158 |
| BFC TSR deep | 44.8 | 2500 | 4918 | 4536 | 382 | 0.078 |
| GW080434 | 51.4 | 409 | 1312 | 742 | 570 | 0.434 |
| GW049877 | 43.9 | 1600 | 3664 | 2903 | 761 | 0.208 |
| GW040960 | 42.8 | 2251 | 4883 | 4084 | 799 | 0.164 |
| GW080946 | 43.7 | 670 | 1668 | 1216 | 452 | 0.271 |
| GW080945 | 42.51 | 750 | 2490 | 1361 | 1129 | 0.454 |
| GW080947 | 42.34 | 860 | 1911 | 1560 | 351 | 0.184 |
| GW080948 | 41.63 | 1500 | 3717 | 2721 | 996 | 0.268 |
| GW080944 | 38.90 | 3300 | 6217 | 5987 | 230 | 0.037 |
| GW080943 | 30.7 | 449 | 1686 | 815 | 871 | 0.517 |
| GW038293 | 29.4 | 410 | 1571 | 744 | 827 | 0.526 |
| GW061136 | 18.3 | 80 | 1246 | 145 | 1101 | 0.884 |
| GW080595 | 13.2 | 50 | 817 | 91 | 726 | 0.889 |
| Ethers #2 | 10.03 | 54 | 621 | 98 | 523 | 0.842 |
| GW017391 | 10.0 | 36 | 831 | 65 | 766 | 0.921 |

## 5.4 Conclusions

This chapter sought to examine salt sources and salinity trends in the Wybong catchment using the hydro and geochemistry of surface and groundwater samples. This included examining EC, pH, major ion chemistry, major ion ratios and stable isotope compositions and the weathering fraction of the water samples. Potential sources of salts considered included evapotranspiration-concentrated cyclic salts, halite dissolution, marine-origin groundwaters within the Permian sediments and mineral weathering.

The pH of waters in the upper catchment was consistent with that of groundwater in contact with basalt and suggests that aluminosilicates may be weathering to produce dissolved silica and bicarbonate. The transects of EC taken during dry periods (2000-2007), when groundwater discharge dominates, shows an increasing trend downstream. There is a marked increase in salinity between 46 to 60 km downstream, between the Ridgeland and Dry Creek Road sites, which continues, increasingly downstream. This suggests intersection of the stream with groundwater from the Permian coal measures which is known to be saline (AGC, 1984; Crelman, 1994; Griffen, 1960; Kellet *et al*, 1989). **Figure 5.5** shows this occurs below a stream elevation of between about 170 to 190 m AHD.

The difference between the upper and lower catchment, revealed by the pH and EC measurements are reflected in the major ion chemistry of surface and groundwaters. These showed that the upper catchment is dominated by bicarbonate, Na, Ca and Mg while the lower catchment is dominated by Cl and Na ions, suggesting again that solute sources in the upper catchment was from mineral weathering possibly from basalt while those in the lower catchment are consistent with marine origin groundwaters from the Permian coal measures.

The major ion ratios to chloride were used to further investigate mineral weathering. Ion ratios decrease fairly consistently downstream in the catchment. The ion ratios in the upper catchment were significantly above those for rainwater, indicating that mineral weathering is a dominant source of salts in the upper catchment. The major ion compositions suggest mineral weathering in the silicate dominated Liverpool Range Volcanics and the sandstones and conglomerates of the Narrabeen Group in the upper catchment. Depletion of calcium and magnesium relative to

bicarbonate indicate that Tertiary basalt contributes to sources of stream salinity in the upper catchment.

Further downstream in the catchment, the ion ratios approach that of seawater. Plots of the ion ratios as a function of 1/Cl (**Figures 5.6** and **5.7**) suggest that seawater or possibly halite is an end member for most of the major ions in both stream and groundwater. These plots also generally show that rainwater is not an end member at low Cl concentrations, which is attributed to mineral weathering. The downstream profiles of ion ratios (**Figures 5.8** and **5.9**), however, show that there appears to be some mixing with marine origin water occurring down the catchment with a final transition to marine origin water at about 46 km downstream.

The relationship between $Ca^{2+}$ + $Mg^{2+}$ and $HCO_3^-$ showed that the sources of $Ca^{2+}$ and $Mg^{2+}$ in the upper catchment are not from carbonate dissolution and are possibly from basaltic and granitic weathering of the Liverpool Range Volcanics. In the lower catchment some sites may possibly be sourced either from carbonate dissolution or from deeper, marine origin groundwaters.

Analysis of the molar ratios of dissolved Na/Ca and $HCO_3/SiO_2$ were used to examine the relative dominance of silicate versus carbonate weathering and generally showed that the source of major ions in upper catchment surface and groundwater samples is from silicate weathering. The Ca/Sr ratios suggested that seawater was one end member for these ions in the lower catchment and that the end member in the upper catchment has a very high Ca/Sr ratio possibly suggesting sandstone of conglomerate source.

The chemistry of the lowest salinity (<20 mmol $L^{-1}$) surface and ground waters with high Na/Cl ratios and variable Cl/Br ratios of ~600–1000 were attributed to rock weathering which is possible weathering of pyroxene and plagioclase, halite dissolution or seawater, and mixing and evaporation. Stable isotope analysis suggested that stream water isotopic line is due to the progressive mixing of evaporated groundwater with the evaporated rainwater.

An estimation of the weathering fraction of surface and groundwaters has been made in this chapter. These were based on either evaporated rainwater or evaporated seawater as the water source. For either water source, significant weathering fractions were observed in the upper catchment above 60 km downstream at Dry Creek Road. Two groundwater samples had weathering fractions relative to cyclic salt close to zero

suggesting that the samples where essentially evaporated cyclic salt. From these samples it was estimated that the annual groundwater recharge was between 2 and 2.2 mm/yr. When it is assumed that marine origin water is the major source of water it appears that some mineral weathering still contributes to salinity to about 89 km downstream at the Railway Bridge site. Two groundwater bores in the lower catchments had weathering fractions close to zero relative to seawater suggesting that they were diluted seawater with dilution ratios between 1/10 and about 1/14, close to the dilution factor at the Railway Bridge site. It is noted here that the analysis of weathering fractions assumes that ion ratios of rainwater or seawater do not change on evaporation or dilution.

The results in this Chapter can be used to develop a conceptual model of the sources of salinity in the Wybong Creek catchment. In the upper catchment, the sources of stream and groundwater salinity are mineral weathering of basalts, Triassic Vocanics, sandstones and conglomerates. In the lower catchment, below 60 km downstream, marine origin groundwater, most probably from the Permian coal measures is the source of salinity. The results here suggest that the shallow ground and surface water in dry periods have a salt to freshwater mixing ratio of between 1/10 and 1/14. The system is not one of simply two salt sources. Rather the profiles of salinity show that progressive mixing occurs in the upper catchment between weathering solutes and marine origin water since seawater is generally an end member of mixing curves. An issue raised by these results is the time period over which saline groundwater has been discharging from the Permian and the time necessary for the depletion of the saline groundwater.

# CHAPTER 6

# SURFACE AND GROUNDWATER INTERACTIONS

The interaction of surface and groundwater has significant implications for both water quantity and quality, and its quantification is important for water resource management and allocation. In this chapter, the Lyne and Hollick (1979) filter method and frequency analysis techniques (Brodie *et al,* 2006) are used for investigating stream and aquifer connectivity. Streamflow, rainfall, stream height and groundwater elevation data are employed for investigating the dynamics of groundwater input into the stream. The analysis includes stream height and groundwater elevation comparison and use the baseflow separation technique to estimate the groundwater contribution to streamflow during drought and non-drought periods. This chapter also compares streamflow percentiles with relevant rainfall percentile curves to provide insights into the nature of groundwater-surface water interactions in catchments.

## 6.1 Overview

It is crucial to understand and quantify the exchange processes and pathways between groundwater and surface water in order to protect and manage surface and groundwater resource. Various techniques used to investigate groundwater-surface water interaction include seepage meters (Cherkauer and McBride, 1998; Brodie *et al.,* 2005), river bed piezometers (Baxter *et al.,* 2003), time-series temperature measurements (Stonestrom and Constanz, 2004) and environmental tracers (Herczeg *et al.,* 2001; Baskaran *et al.,* 2004). Scanlon *et al.* (2002) presented an overview of techniques for quantifying groundwater recharge from streams at different spatial and temporal scales. Some of these methods can equally be applied to measure groundwater discharge to streams and recharge through the streambed. Landon *et al*. (2001) compared in-stream methods for measuring hydraulic conductivity aimed at determining the most appropriate techniques for use in sandy streambeds. Other methods for investigating the surface and ground water exchange include mass balance approaches, water flux, heat tracer methods and methods based on Darcy's Law (Kalbus *et al*., 2006).

The groundwater contribution to streamflow can be estimated by separating a stream hydrographs into the different components, such as baseflow, interflow and quickflow (Hornberger *et al*., 1998; Davie, 2002; Poulsen *et al*., 2006; Even *et al*., 2007), and then assuming that baseflow represents groundwater discharge into the stream (Hannula *et al.*, 2003). The validity of the underlying assumptions of the separation techniques is critical in using hydrograph separation to determine groundwater-surface water interactions (Halford and Mayer, 2000).

Analysis of the baseflow component of the stream hydrograph has a long history since the early theoretical and empirical work of Boussinesq (1904), Maillet (1905) and Horton (1933). Many reviews mapping this development have been written such as Nathan and McMahon (1990), Tallaksen (1995), Furey and Gupta (2001) and Smakhtin (2001). The methods that have evolved can be categorized into two basic approaches of baseflow separation: frequency analysis and recession analysis. Baseflow analysis is mainly an application of recursive digital filters to remove the high-frequency quickflow signal. Many known filters algorithms which have been developed and implemented including Lyne and Hollick (1979), Chapman (1991), Boughton (1993), Jakeman and Hornberger (1993), Chapman and Maxwell (1996) and Furey and Gupta (2001). Brodie derived (Brodie *et al,* 2006, 2008) relationship between streamflow magnitude and frequency which is considered one of the most common applications of the flow duration curve (FDC). In case of recession analysis, streamflow recession curves are individually or collectively analyzed to gain an understanding of discharge processes.

## 6.2 Methods and Data Sources

Groundwater level data from bores GW080946, GW080948 and GW080434 in the Wybong catchment were obtained from the DNR database (see **Figure 5.1**). **Figure 6.1** shows Wybong stream gauge (station #210040), Warkworth stream gauge (station #210004) in Wollombi Brook and Coggan stream gauge (station #210006) in Goulburn River from which stream flow and stream height data were also collected. Daily rainfall data were collected from Bunnan rainfall station #61007, Cessnock rainfall station #61242 and Denman rainfall station #61007. In order to investigate the groundwater contribution to stream for longer time periods, Coggan stream flow data from 1913 to

2007 and Warkworth streamflow data from 1958 to 2007 were also considered, since stream flow data for Wybong was only available from 1955 to 2008.

The streamflow data of Wybong from 2000 onwards during the drought appears to be heavily influenced by excessive abstraction and that has been ignored in the frequency analysis but not in the streamflow separation analysis. The data before 1972 has excessive numbers of missing days and it has been excluded from the frequency analysis. Therefore, data from 1970 to 2000 has been used in the frequency analysis.

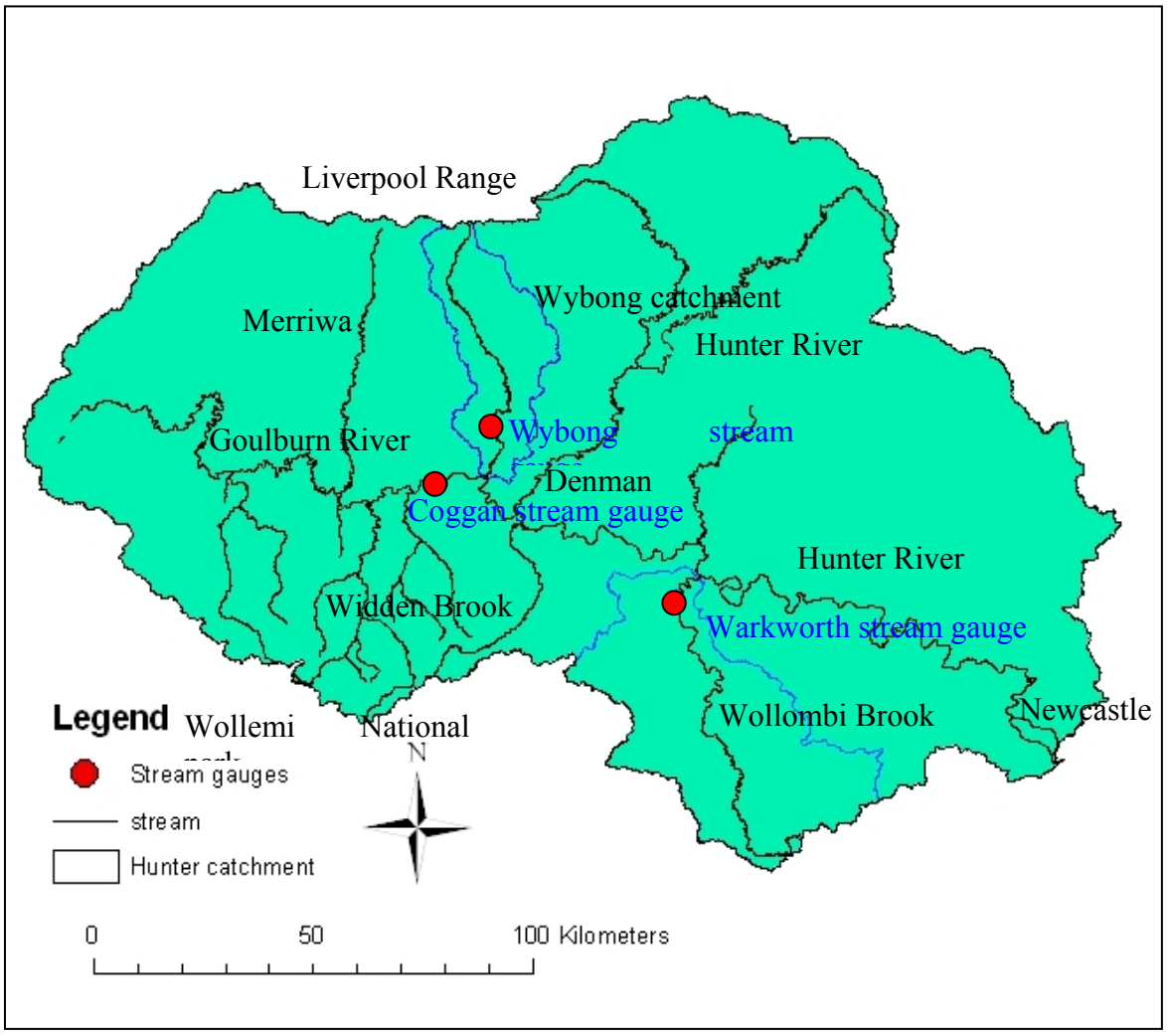


**Figure 6.1** Location of Wybong, Warkworth and Coggan streamflow gauge in the Hunter catchment

### 6.2.1 Baseflow Separation Methods

Daily stream hydrographs from the Wybong Creek were separated into baseflow and quickflow components in order to determine the contribution of groundwater to streamflow. Baseflow was defined as the slow response of groundwater discharge from the saturated and unsaturated subsurface zones, while quickflow was defined as the rapid response of rainfall-generated surface runoff and flow through the unsaturated subsurface zone. **Table 6.1** outlines some of the digital filters that have been applied to smoothing hydrographic data. The hydrograph separation technique is a subroutine (HYBASE) in the time series data management program HYDSYS (1992), which applies the recursive digital filter algorithm of Lyne and Hollick (1979). An evaluation of automated hydrograph separation techniques (Nathan and McMahon 1990) found the Lyne and Hollick filter to be a fast and objective method of continuous baseflow separation, producing similar results to the traditional graphical techniques.

This filter algorithm has been widely applied to daily streamflow data and is cited in much of the Australian rainfall-runoff modelling literature (Grayson *et al,*. 1996). Based on the fundamental signal processing theory, the procedure separates the streamflow hydrograph into low frequency (baseflow) and high frequency (quickflow) components using a digital filter of the form:

$$f_{(k)} = \alpha f_{(k-1)} + (\frac{1+\alpha}{2})(y_k - y_{k-1}) \qquad (6.1)$$

where $f_{(k)}$ is the filtered quickflow response of streamflow at the *kth* sampling instant, $f_{(k-1)}$ is the filtered quickflow for previous sampling instant, $y_k$ is the original streamflow measurement, $y_{k-1}$ is the original streamflow for previous sampling instant and $\alpha$ is the filter parameter. The filtered baseflow component of streamflow is thus defined as $y_k - f_k$. Using data from 186 catchments in south-eastern Australia, Nathan and McMahon (1990) showed that the most acceptable baseflow separation was achieved with a filter parameter $\alpha$=0.925, although acceptable results were obtained in the range of 0.9–0.95. The filter parameter affects the degree of attenuation, while the number of passes of the filter determines the degree of smoothing. The original work of Lyne and Hollick (1979) and the subsequent evaluation by Nathan and McMahon (1990) showed that three filter passes (forward, backward and forward again) produced the best results.

**Table 6.1** Recursive digital filters used in base flow analysis (Grayson *et al,* 1996; Chapman, 1999; Furey and Gupta, 2001)

| Filter Name | Filter Equation | Source | Comments |
|---|---|---|---|
| One-parameter algorithm | $q_{b(i)} = \frac{K}{2-K} q_{b(i-1)} + \frac{1-K}{2-K} q_{(i)}$ | Chapman and Maxwell (1996) | $q_b(i) \leq q(i)$ Applied as a single pass through the data. |
| Boughton two-parameter algorithm | $q_{b(i)} = \frac{K}{1+C} q_{b(i-1)} + \frac{C}{1+C} q_{(i)}$ | Boughton (1993) Chapman and Maxwell (1996) | $q_b(i) \leq q(i)$ Applied as a single pass through the data Allows calibration against other baseflow information such as tracers, by adjusting parameter *C* |
| IHACRES three-parameter algorithm | $q_{b(i)} = \frac{K}{1+C} q_{b(i-1)} + \frac{C}{1+C}(q_{(i)} + \alpha_q q_{(i-1)})$ | Jakeman and Hornberger (1993) | Extension of Boughton two-parameter algorithm |
| Lyne and Hollick algorithm | $q_{f(i)} = \alpha q_{f(i-1)} + (q_{(i)} - q_{(i-1)}) \frac{1+\alpha}{2}$ | Lyne and Hollick (1979) Nathan and McMahon, (1990) | $q_f(i) \geq 0$ α value of 0.925 recommended for daily stream data filter recommended to be applied in three passes Baseflow is $q_b = q - q_f$ |
| Chapman algorithm | $q_{f(i)} = \frac{3\alpha-1}{3-\alpha} q_{f(i-1)} + \frac{2}{3-\alpha}(q_{(i)} - \alpha q_{(i-1)})$ | Chapman (1991) Mau and Winter (1997) | Baseflow is $q_b = q - q_f$ |
| Furey and Gupta filter | $q_{b(i)} = (1-\gamma) q_{b(i-1)} + \gamma \frac{C_3}{C_1}(q_{(i-d-1)} - q_{b(i-d-1)})$ | Furey and Gupta (2001) | Physically-based filter using mass balance equation for baseflow through a hillside |
| Eckhardt | $q_{b(i)} = \frac{(1-BFI_{\max}) a q_{b(i-1)} + (1-a) BFI_{\max} q_i}{1 - aBFI_{\max}}$ | Eckhardt (2005) | general formulation that can devolve into several of the commonly used one-parameter filters |

In **Table 6.1**

$q_{(i)}$ is the original streamflow for the $i^{th}$ sampling instant

$q_{b(i)}$ is the filtered baseflow response for the $i^{th}$ sampling instant

$q_{f(i)}$ is the filtered quickflow for the $i^{th}$ sampling instant

$q_{(i-1)}$ is the original streamflow for the previous sampling instant to $i$

$q_{b(i-1)}$ is the filtered baseflow response for the previous sampling instant to $i$

$q_{f(i-1)}$ is the filtered quickflow for the previous sampling instant to $i$

$k$ is the filter parameter given by the recession constant

$\alpha$, $\alpha_q$ are filter parameters

$C$ is a parameter that allows the shape of the separation to be altered

$\gamma$, $c_1$, $c_3$ are physically based parameters

$BFI_{max}$ is the maximum baseflow index (which is the ratio of aggregated baseflow to total streamflow)

### 6.2.2 Streamflow Hydrograph Analysis

The streamflow data of the Wybong catchment (station #210040) was used to investigating the dynamics of groundwater input into the stream. **Figure 6.2** plots the available daily streamflow data for Wybong from 1972 to 2000.

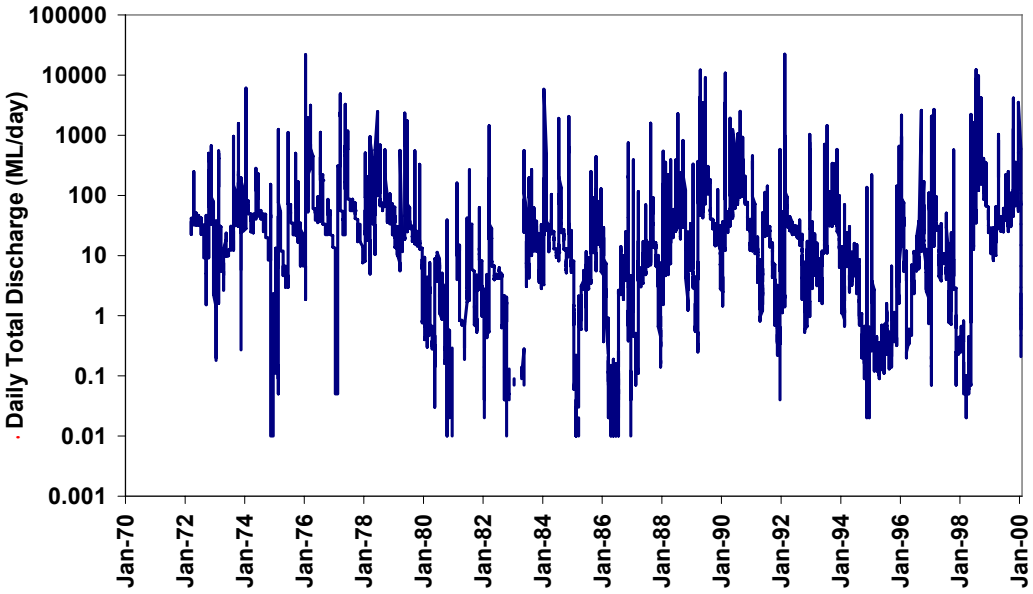


**Figure 6.2** Daily stream flow records for Wybong Creek (station#210040) from 1972 to 2000

**Table 6.2** shows the hydrological characteristics of the Wybong catchment. The status of the catchment as a dominantly gaining stream is indicated by a high baseflow index (BFI, which is the ratio of aggregated baseflow to total streamflow), high Q90/Q50 ratio (ratio of 90% exceedance flow to 50% (median) flow for daily streamflow record), a shallow slope for the frequency distribution curve (FDC), small percentage of zero-flow days and a relatives low ratio between mean and median flows.

**Table 6.2** Hydrological parameters of Wybong catchment, Wollombi Brook and Goulburn River over a period of 1972–2000, 1958-2007 and 1913-2007 respectively.

| Parameter | Description | Wybong | Warkworth | Coggan |
|---|---|---|---|---|
| Catchment area | Area of catchment above the stream gauging station ($km^2$) | 675 | 1848 | 3340 |
| Mean flow | Average daily stream flow (ML/d) | 74.96 | 374.80 | 236.27 |
| Baseflow index (BFI) | Long term ratio of derived baseflow to total flow, applying Lyne and Hollick (1979) filter ($\alpha$ = 0.925) on daily streamflow data. Gaining streams have high BFI (0.5~0.9). | 0.539 | 0.439 | 0.622 |
| Mean/median ratio | Ratio of mean flow to median flow for streamflow record. High values indicates large fluctuation in streamflow | 4.7 | 17.0 | 5.9 |
| Q90/Q50 | Ratio of 90% exceedance flow to 50% (median) flow for daily streamflow record. Gaining streams have high ratio due to persistent low flows | 0.29 | 0.04 | 0.28 |
| FDC slope | Slope of linear regression of frequency distribution curve between Q80 and Q20. FDC derived from daily streamflow data normalised against average flow over period. High baseflow streams have shallow slope (Growns and Marsh, 2000) | 12 | 65.47 | 11.52 |
| % Zero-flow | Percentage of streamflow record with zero flows. Intermittent (losing) streams have relatively high number of zero-flow days | 3.3 | 11.7 | 2.1 |

### 6.2.3 Frequency Analysis Method

A new hydrographic analysis technique is applied in this study which was developed by Brodie (Brodie *et al*., 2007). In this frequency analysis approach, the streamflow data can be presented in an entirely different format to the traditional time-series approach, as used in **Figure 6.2**. A significant advantage of this method is that because it uses non-parametric percentiles, transformation of data to normal distributions is not required.

Daily percentiles of the stream flow data were calculated by:

(i.) assigning each daily streamflow record to its appropriate day of the year (1-365).

(ii.) deriving flow statistics for each daily population of streamflow data. Flow percentiles for each day were generated on a 5% incremental basis from Q5 to Q95, with the extreme flows of Q1 and Q99 also calculated for each day of the calendar year.

The Q50 represents median conditions where 50% of the flow record for that particular day is above this value. The Q5 percentile represents the very high flow condition on a daily basis, where only 5% of the flow record for that particular day is above this value. In contrast, the Q95 percentile represents the very low flow condition on a daily basis, where 95% of the flow record for that particular day is above this value. It is generally considered that the high flow regime (>Q50) is influenced by quickflow, with the low-flow regime (<Q50) more influenced by baseflow processes (Brodie *et al,* 2006).

The daily percentiles rainfalls for the Bunnan rainfall station #61007 were calculated using the above procedure for the each day of the year. The upper half of the rainfall record is represented as percentiles R50, R20, R10 and R5. This is because the daily median rainfall (R50) is typically zero. Basically, about 60% of the daily rainfall records are non-rain days. The R20 percentile is where 20% of the rainfall record for the particular day lie above this value whilst the R10 represent a 10% threshold value. A smoothed 7-day moving average R10 rainfall percentile (7daysR10) was calculated to facilitate better comparison against the streamflow percentiles. Since streamflow integrates previous rainfalls.

The time lags used to shift the streamflow percentiles to provide a better match with the rainfall 7daysR10 percentile were calculated statistically by cross-correlation analysis (Davis, 1986). Such an approach has been used to define time lags between

rainfalls and recharge affecting the groundwater level (Moon *et al*, 2004). In this study, the daily 7daysR10 record is compared with a series of data sequences produced by incrementally shifting the streamflow percentile record by one day at a time. For each of the 364 shifts in the streamflow record, the cross-correlation or 'goodness of fit' is calculated using:

$$r_m = \frac{COV_{1,2}}{S_1 \times S_2} \tag{6.2}$$

where $COV_{1,2}$ is the covariance of the two data sequences (i.e. the daily 7daysR10 sequence and a shifted daily Q90 streamflow sequence) and $S_1$ and $S_2$ are the standard deviations of these sequences. The shifted streamflow data sequence with the maximum cross-correlation ($r_m$) has statistically the best fit with the 7daysR10 data. The closer $r_m$ is to +1 the better the correlation between the two data sequences.

## 6.3 Results and Discussion

### 6.3.1 Stream Height and Water Table Elevation

**Figure 6.3** shows that the Wybong groundwater levels are higher than the stream levels so that the groundwater gradient is towards the stream. The standard deviation of groundwater level data of the bores near the river is higher (0.34m for bore#080946) compared to the further away bores (0.2m for bore #080434). Bore #80434 (0.17m Figure **6.3a)** which is located 7.31km directly downstream from the stream gauge and adjacent to the stream bed. In this bore, the water bearing zone is a gravel layer between 14m and 17.4m. The bore #080946 is very close, 0.5 km from the stream gauge and water bearing zone is Smectite clay. Standing water level is about 12m and above the stream level (**Figure 6.3b**). The bore #080948 is 2.72 km from the stream gauge and is monitoring water hosted within Permian sandstone and water bearing zone has an elevation of 27-29m below the ground surface. Groundwater pressure is relatively constant throughout the measurement periods and standing water level is about 8.5m and above the stream level (**Figure 6.3c**). The distances of Bores #080945, #080947 and #080944 are 1.7 km, 1.9 km and 6.7 km respectively from the stream gauge and their water level are above the stream height (**Figure 6.3d**, **Figure 6.3e** and **Figure 6.3f**). Since ground water levels are higher than the stream height, this suggests that groundwater has the potential to flow from higher aquifers units to the stream.

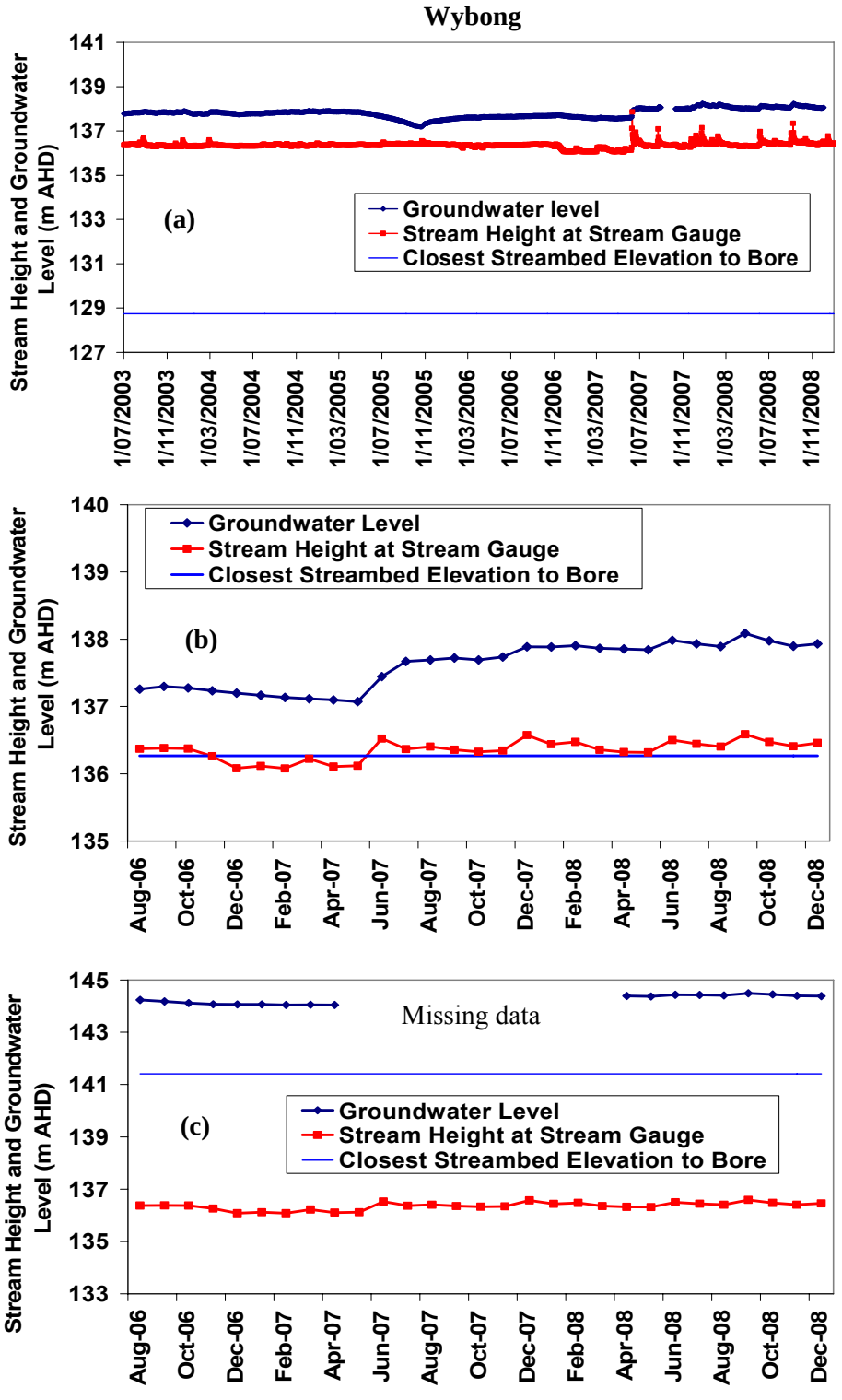


**Figure 6.3** Relationship between groundwater level and stream height for the bores **(a)** #080434 (standard deviation=0.21m) **(b)** #080946 (standard deviation=0.34m) **(c)** #080948 (standard deviation=0.17m

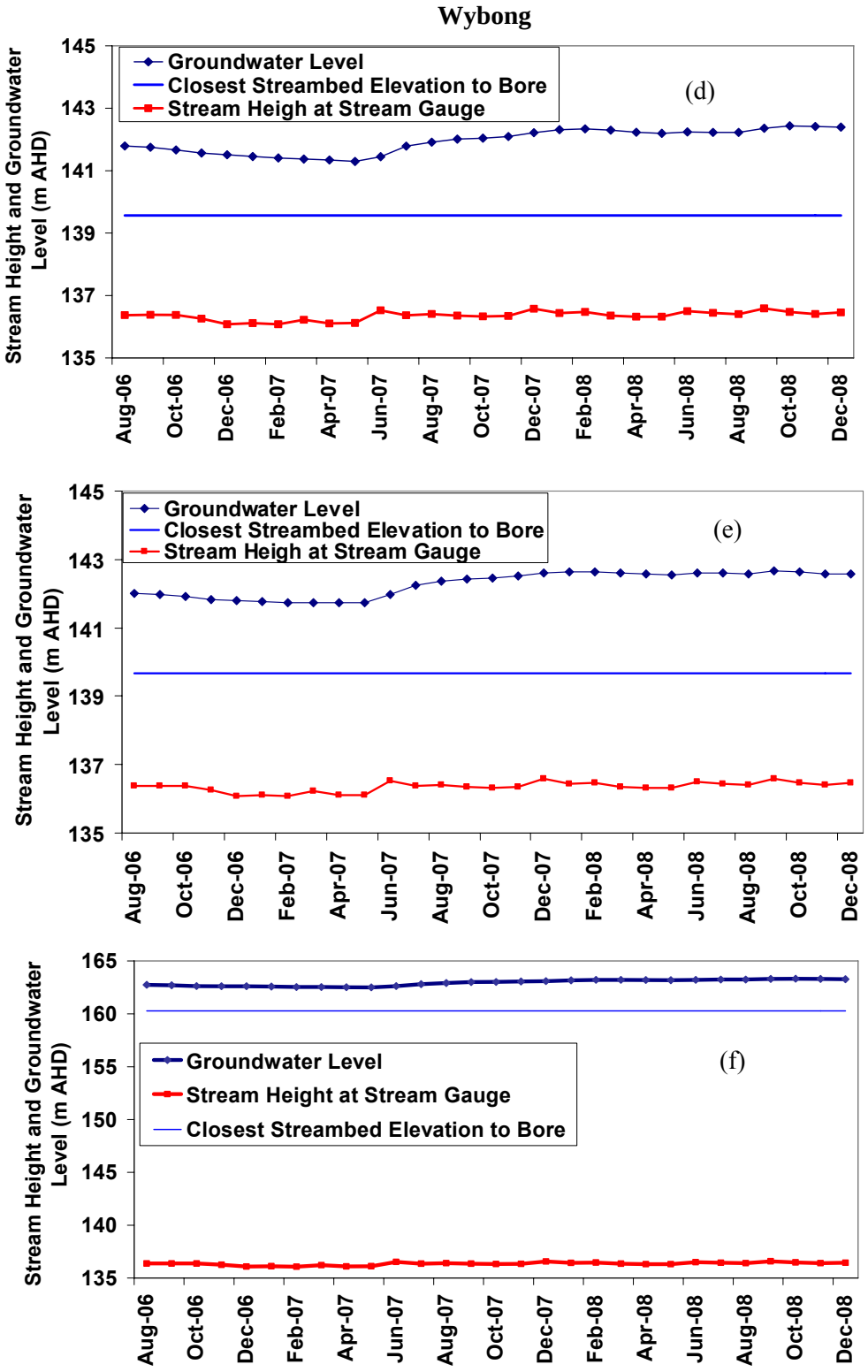


**Figure 6.3** Relationship between groundwater level and stream height for the bore **(d)** GW080945 **(e)** GW080947 (**f)** GW080944

### 6.3.2 Streamflow Hydrograph Separations

The Lyne and Hollick filter was applied to the Wybong streamflow data, using the significant drought years (rainfall <10% percentile) of 1980-1981, 1982-1983, 1994-1995, 2002-2003 and 2006-2007 and wet years of 1956, 1978, 1993, 1998 and 2000. The results of the baseflow separation are shown in Appendix C. Since 2000 has moderate baseflow among the dry years, the results of 2002 are only discussed in this section. A recursive filter was passed three times over the streamflow data in 2002 (**Figure 6.4**) using a filter parameter of 0.925. The output was constrained so the separated baseflow and quickflow components were not negative or greater than the original streamflow.

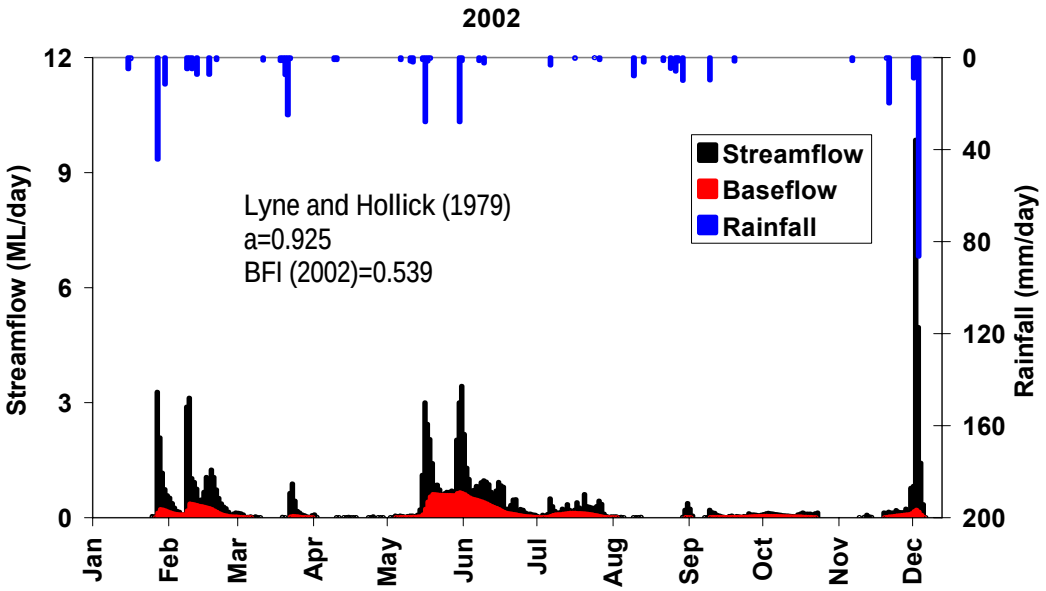


**Figure 6.4** Baseflow separation of Wybong for 2002 calendar year using recursive filter

The results of Lyne and Hollick filter are highly sensitive to small changes in the single parameter α. The use of such recursive filter is inherently arbitrary and requires confirmation with other information such as field observations (Nathan and McMahon 1990). **Figure 6.4** highlights the variability of the derived baseflow signal. This is also shown in the variability of the calculated baseflow index (BFI) which is the ratio of aggregated monthly baseflow to total streamflow, and ranges from 0.10 to 0.43 for 2002. All maximum BFI of the drought and wet years are listed in **Table 6.3**. The

maximum BFI is 0.83 in the dry year of 1982 and the minimum occurs during the dry periods of 2002-2007 with the lowest values of 0.22 occurs in 2007. The calculated maximum BFI is 0.53 from 1972 to 2000 suggesting that maximum 53% of streamflow is baseflow during this period.

**Table 6.3** Maximum baseflow indexes for Wet and drought periods (Dry and wet years are marked as black and blue colours respectively)

| Period | Month | Maximum BFI |
|---|---|---|
| 1972-2007 | September | 0.516 |
| 1972-2000 | September | 0.539 |
| 1980-1981 | April | 0.804 |
| 1980 | April | 0.773 |
| 1981 | April | 0.817 |
| 1982-1983 | April | 0.675 |
| 1982 | July | 0.845 |
| 1983 | October | 0.661 |
| 1994-1995 | May | 0.650 |
| 2002-2003 | July | 0.548 |
| 2002 | June | 0.432 |
| 2003 | June | 0.612 |
| 2006 | June | 0.572 |
| 2007 | October | 0.229 |
| 1956 | November | 0.934 |
| 1978 | August | 0.884 |
| 1993 | August | 0.751 |
| 1998 | December | 0.737 |
| 2000 | June | 0.836 |

However, a common feature of the derived baseflow signals in **Figure 6.4** is the strong build up of baseflow following the successive rainfall events of February to March, May to June and December. The initial rain events in February (44mm) have small recessions and then significant recessions occurred in response to rainfall events later in the May and June (28mm and 28mm). A significant proportion of these early

rains in February and March infiltrates and provides aquifer recharge. With replenishment of soil and groundwater storages, the later rainfall events in May and June provide the impetus for a major recession phase. Only a slight recession was observed follows the significant 86mm rainfall in December. This may be due to high evapo- transpiration or groundwater pumping during this month.

### 6.3.3 Frequency Analysis

#### 6.3.3.1 Frequency Analysis for Wybong

**Figure 6.5** shows the daily percentile rainfall for the Bunnan rainfall station #61007. In focusing on the low-flow regime (**Figure 6.6a**), daily rainfall percentiles were smoothed to facilitate better comparison. A 7-day moving average R10 rainfall percentile from the Bunnan rainfall station was used as the comparison against the streamflow percentiles. This smoothed the data but importantly there is no shift in the timing of fluctuations so that a smoothed R20 peak corresponds with a smoothed R5 peak (**Figure 6.5**). **Figure 6.6(b)** shows the variability of the high-flow regime on the basis of daily percentiles over the calendar year, ranging from the Q5 percentile to the Q50 percentile, with **Figure 6.6(a)** showing the lower half of the flow regime spanning from Q50 down to Q95.

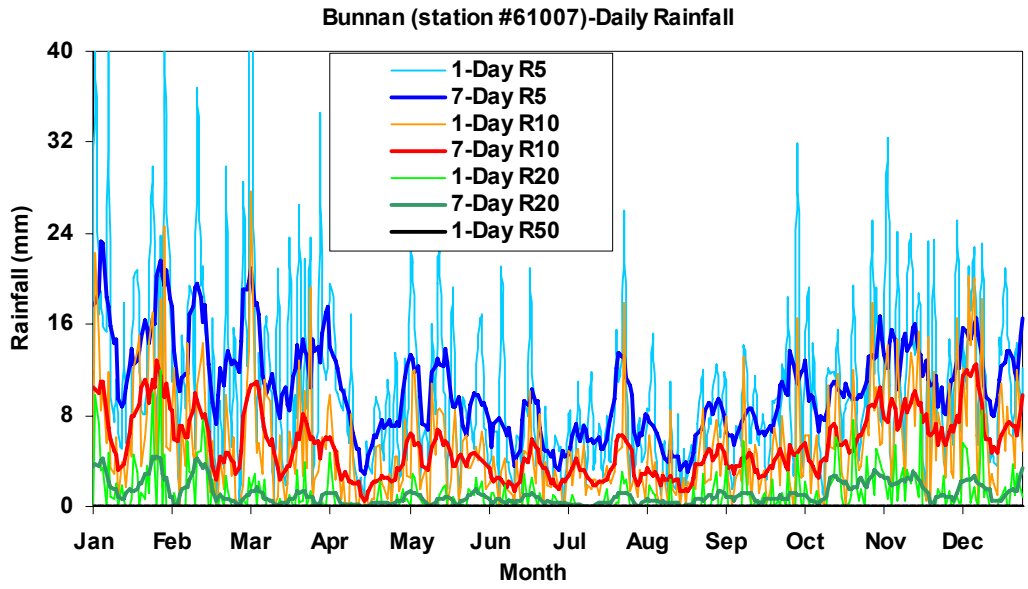


**Figure 6.5** Daily rainfall percentile for Bunnan (station #61007) from 1972-2000

The 7dayR10 rainfall percentile for Bunnan is plotted with the various Wybong streamflow percentiles in **Figure 6.6**. The low-flow regime (**Figure 6.6a**) appears to be a significant lag between the streamflow peak (June to September) and the rainfall peak (December to February). The higher flow percentiles (**Figure 6.6b**) become progressively more variable as well as higher in magnitude. This is because the highest percentiles (e.g., Q5) are dominated by the flood events that occur sporadically throughout the record (January to April and May to August). In a general sense, the lag between rainfall and streamflow in these percentiles is not as apparent as in the low-flow regime (**Figure 6.6a**).

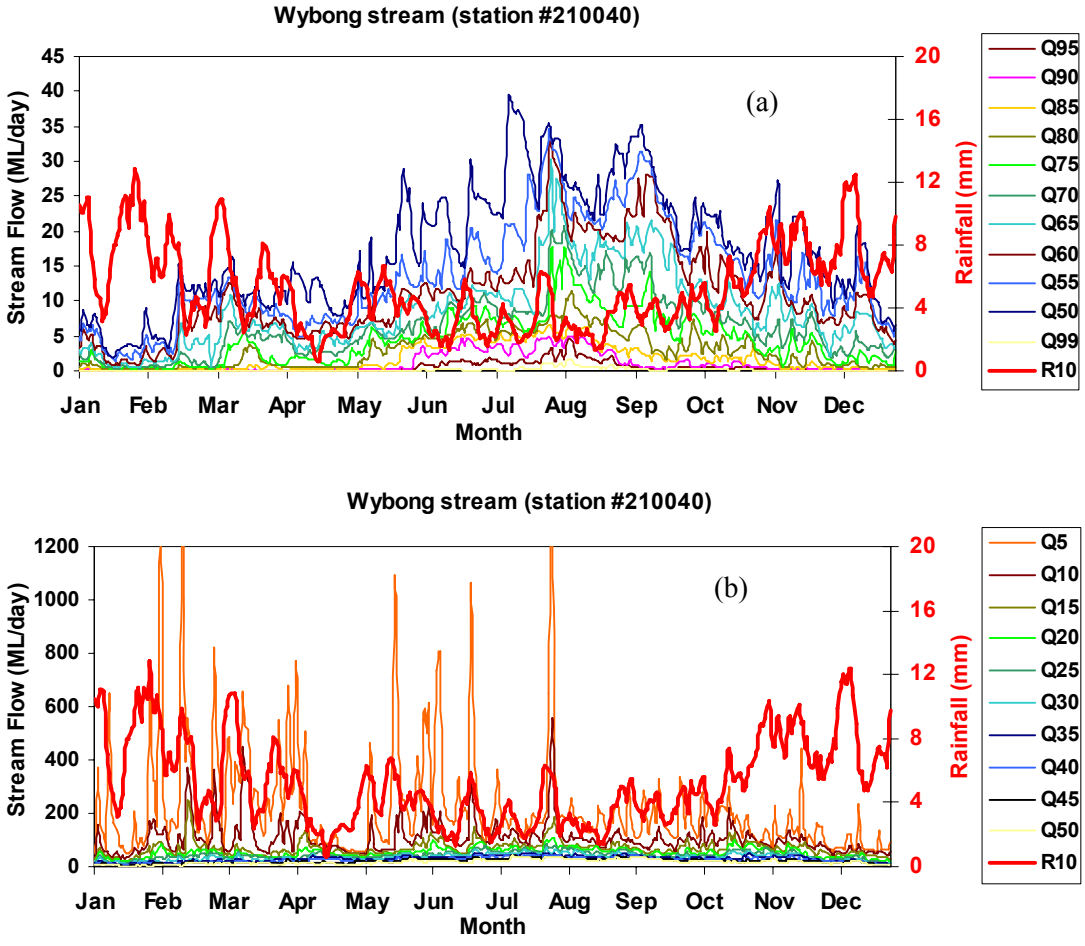


**Figure 6.6** Daily discharges for various percentiles for the Wybong stream (station #210040) compared with 7dayR10 percentile rainfall for Bunnan (station #61007) **(a)** low flow Q50-Q95 **(b)** high flow Q5-Q50.

In **Figure 6.7** the selected flow percentile curves are plotted individually against the 7dayR10 rainfall percentile curve. As an example, the Q90 streamflow percentile is plotted against the 7dayR10 rainfall percentile (**Figure 6.7a**). The Q90 streamflow percentile is taken to be representative of low-flow conditions dominated by baseflow contributions from natural storages such as the shallow groundwater system. The 7day R10 rainfall percentile is considered to be representative of the significant rainfall events that generate run-off and also recharge to aquifers (Brodie *et al,* 2006). There are several important features to this plot of **Figure 6.7a**. Firstly, the distinct time lag between the seasonal 7dayR10 rainfall peak (in December-February) and the Q90 streamflow peak (in June-September)**.** This provides the frequency analysis method with its name of Q-Lag (Brodie *et al*., 2007). When the streamflow data is shifted back by 206 days (plotted as light gray), the second feature of the plot becomes more evident, that is the similarity between the general shape of rainfall and shifted streamflow pattern.

For the Q10 streamflow (**Figure 6.7c**), the lag between streamflow and rainfall is not as long, with a delay of 147 days instead of 206 days to shift the streamflow record. The lag time decreases with higher-flow regimes, with a shift of only 64 days for the Q1 flow percentile (**Figure 6.7d**). The corresponding trends of increasing noise in the streamflow data are also apparent in these plots, making it more difficult to interpret relationships between streamflow and rainfall.

The Q1 data suggests that the lag between this high-flow percentile and rainfall is relatively small lag with 64 days. Plots e, f and g of **Figure 6.7** show the various flow percentile curves plotted individually against the 7dayR5 rainfall percentile curve. At Q90 streamflow (**Figure 6.7e**), the lag between streamflow and rainfall is 179 days to shift the streamflow record where 206 days lag is found for 7dayR10. There is no lag time for high-flow regime Q1 flow percentile and 7dayR5 rainfall percentile curve. This is expected as the Q1 percentile is dominated by quickflow processes such as direct runoff and interflow.

**Figure 6.8** shows the results of the cross-correlation analysis for the daily Q90 data with showing that the maximum $r_m$ and thereby the best fit is provided when the streamflow data is shifted by 206 days. This shift is represented in the plot of **Figure 6.7a**.

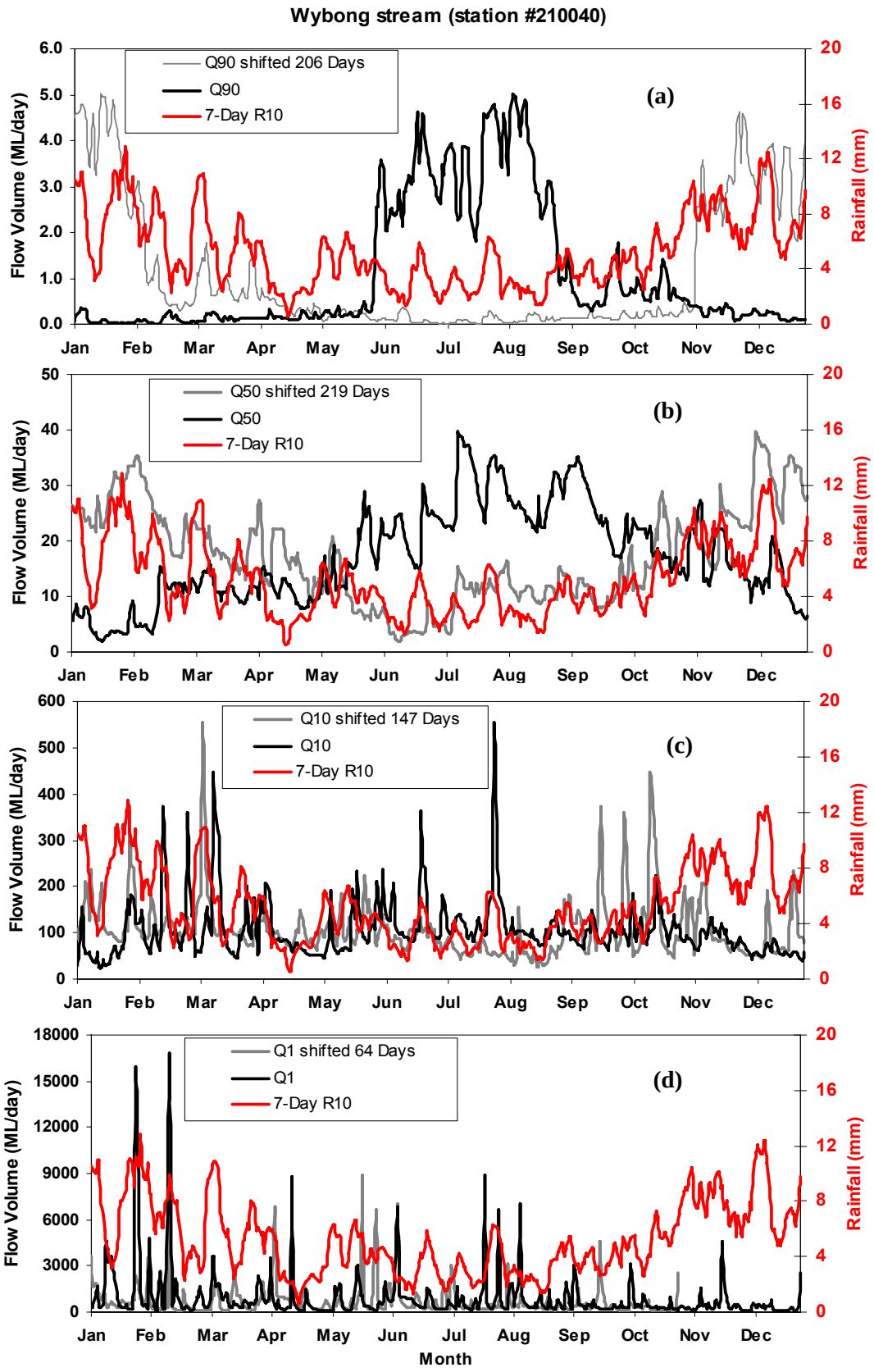


**Figure 6.7** Comparison of various daily stream flow percentiles for Wybong stream gauge (station #210040) with moving 7-day average of daily rainfall percentile (R10) for Bunnan rainfall (station #61007)

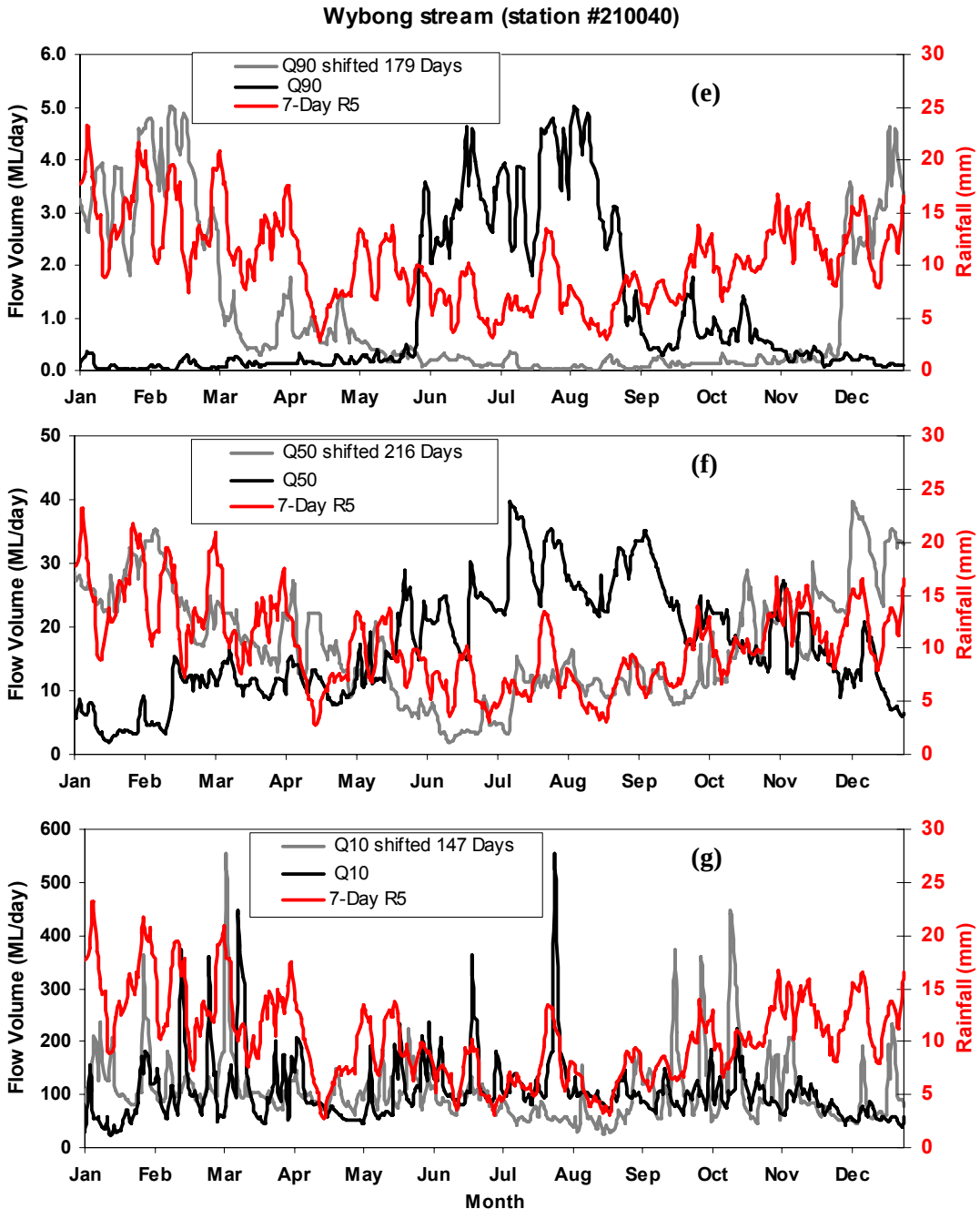


**Figure 6.7** Comparison of various daily stream flow percentiles for Wybong stream gauge (station #210040) with moving 7-day average of daily rainfall percentile (R5) for Bunnan rainfall (station #61007)

**Figure 6.9** shows the results of the cross correlation analysis of the flow percentiles calculated for Wybong streamflow and with respect to Bunnan rainfall. The lag between rainfall and streamflow increases in the low-flow regime (**Figure 6.9a**) and remains steady from Q20-Q99, with a mean of 223 days. In general, the correlation is

good, with the maximum cross-correlation typically ranging from 0.7-0.9. In this analysis the maximum fit $r_m$ is 0.72 (**Figure 6.10a**) during 1972-2000. The maximum fit $r_m$ of 0.78 (**Figure 6.10b**) is achieved in the longer period of 1955-2008 which is better than the period 1972-2000. For the high flow percentiles of Q5 and Q1 (lag only 64 days), the data are relatively noisy (**Figure 6.7d)**, so comparison against the 7dayR10 rainfall sequence is more difficult and seems better suited to comparison with 7dayR5.

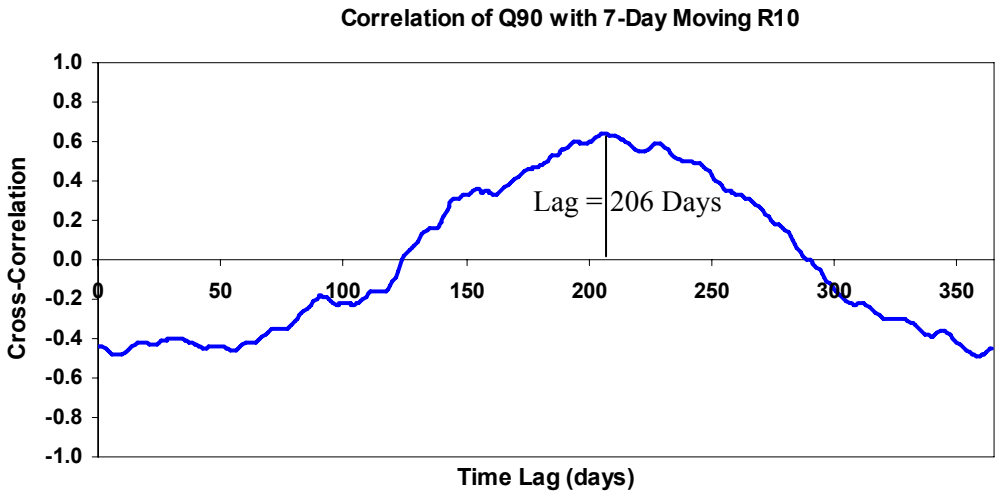


**Figure 6.8** Derivation of time lag between Wybong stream flow Q90 and Bunnan rainfall 7dayR10 using cross-correlation. The calculated time lag is the day shift that gives the maximum cross correlation $r_m$, in the case of 206 days during 1972-2000

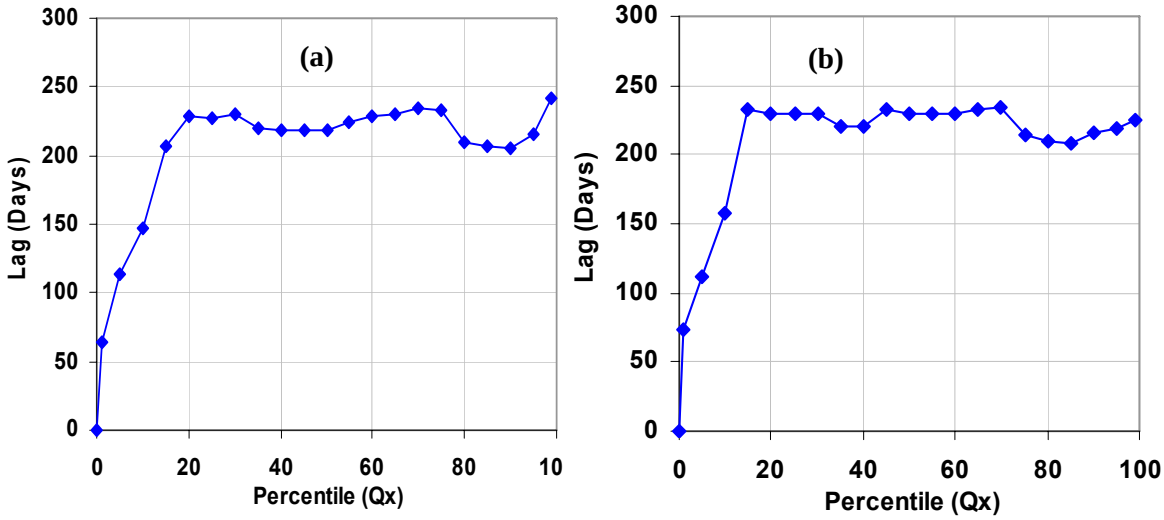


**Figure 6.9** Relation between lag and flow percentiles for Wybong stream flow percentiles (Qx) and Bunnan rainfall 7R10 percentile **(a)** during 1972-2000 **(b)** during 1955-2008

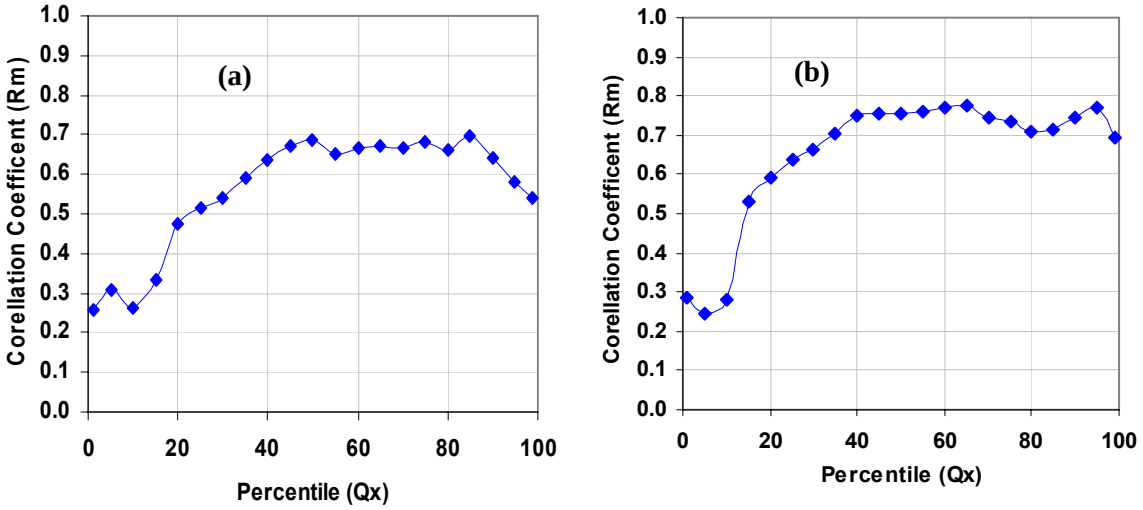


**Figure 6.10** Relationship between maximum cross correlation $r_m$ and flow percentiles for Wybong stream flow percentiles (Qx) and Bunnan rainfall 7R10 percentile **(a)** during 1972-2000 **(b)** during 1955-2008

The flow percentile ratio of Q90/Q50 is commonly used as an indicator of the relative proportion of baseflow (Nathan and McMahon, 1990). As plotted in **Figure 6.11**, this ratio confirms that the baseflow component is more dominant during months of June to August. This appears to reflect the lower average rainfall over winter coupled with lower average evaporation leading to higher groundwater recharge.

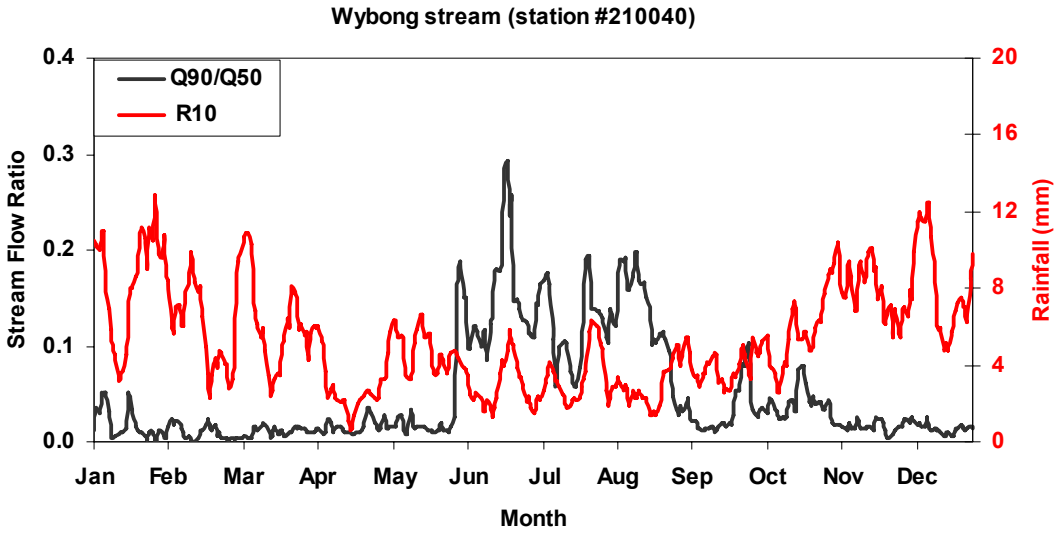


**Figure 6.11** Stream flow percentile ratios Q90/Q50 for Wybong stream gauge compared with Bunnan 7R10 data from 1972-2000

### 6.3.3.2 Land Use Impacts

Runoff of the Wybong catchment was decreased by 20% relative to the long term average during 2001-2006. Rainfall-runoff processes can be strongly influenced by land use changes due to agriculture and water extraction during the drought year of 2001-2006. It is possible that significant water extraction of both surface and groundwater may have taken place from 2001 due to large amount of land use for irrigated agriculture. To explore the impact of increased water extraction, daily percentile analysis was undertaken on Wybong streamflow data. The record was split into a "pre-drought and minor water uses" period of 1972–2000 and a "post-drought and major water uses" period of 1979– 2007 and separately analyzed. The lag distributions for these time periods are quite different (**Figure 6.12**). The lags associated with the "pre-drought and minor water uses" period are shorter than the lags for the "post-drought and major water uses" period up to Q20 and then follows similar trend up to low flow Q90. However, there are some minor differences observed between them after Q20.

The increased lag evident for lower flow percentiles (**Figure 6.9**) reflects groundwater contributions from the deeper aquifers with longer flow paths. The trends in lags observed in **Figure 6.12** can also be explained in this way. Since 2001, water extraction has mostly been from in-stream pumping and groundwater extraction from the shallow unconfined aquifer. This represents a relative loss from in-stream and near-stream storage that is associated with quick response times and short flow paths. This means that groundwater discharge derived from storages with longer flow paths to the stream network become more dominant, as represented in the overall lengthening of lags.

The impact of increased consumptive use is also evident when the pre and post-drought and major water uses flow percentiles are directly compared, as in the case for Q90 and rainfall (**Figure 6.13**). The two 7R10 rainfall percentile curves are somewhat similar except for some differences such as the position of the rainfall maxima. The peaks in the relevant streamflow percentiles are not at these rainfall maxima. The pre-drought and minor water uses Q90 percentiles in the winter months are not similar to the post- drought and major water uses periods. Pre-drought and minor water uses period flows are higher during the winter months when irrigation water demand is limited. Post- drought and major water uses periods flows are relatively depleted in the remaining months when extraction for irrigation occurs.

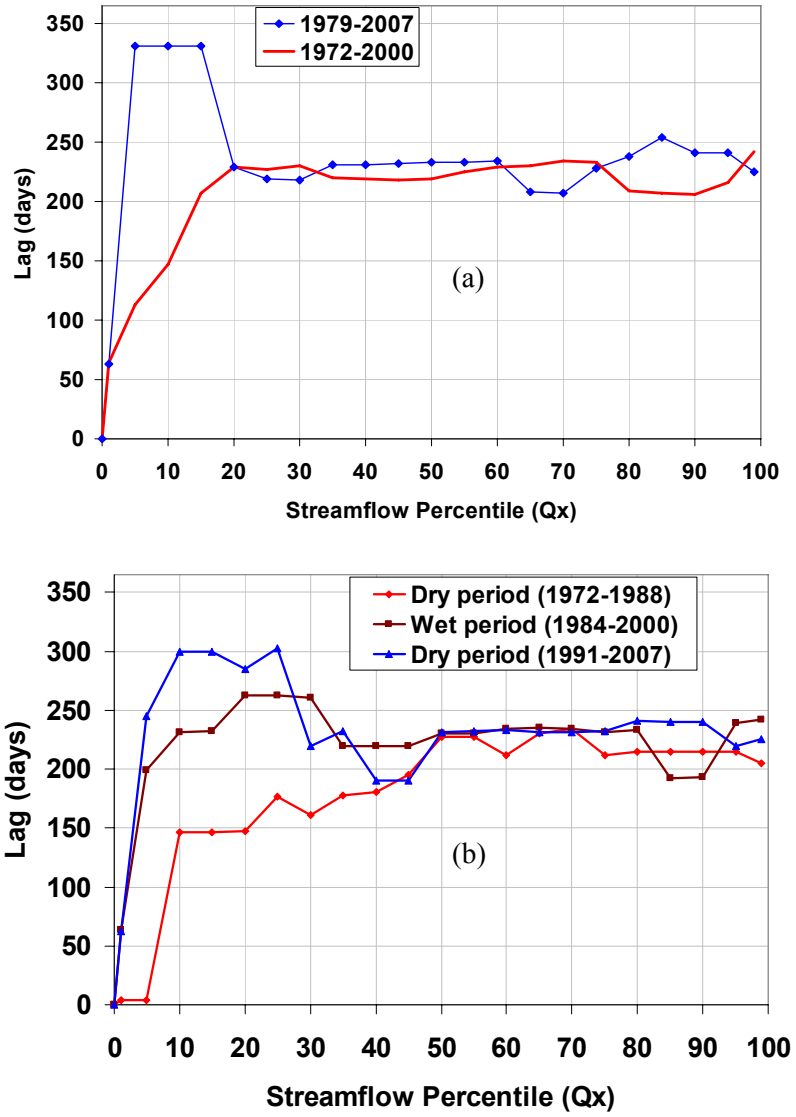


**Figure 6.12** Daily percentile analysis showing relationship between lag and streamflow percentiles for Wybong using (**a)** pre-drought and minor water uses period of 1972–2000 and a post-drought and major water uses period of 1979– 2007 and **(b)** dry and wet periods

The general similarity in the rainfall 7dayR10 percentiles for these two periods also suggests that these flow differences are not related to rainfall differences. The impact of water extraction during the summer lowflow period is also reflected in the apparent streamflow deficit relative to rainfall. This summer pumping is a water management priority for the catchment and is dominated by demand from the irrigation. This

extraction has decreased the magnitude of summer flows and increased the duration of critical low flow events. Furthermore, the ratio of Q90/Q50 flow (baseflow) in post-drought and major water uses periods lower than the pre-drought and minor water uses (**Figure 6.11** and **Figure 6.14**) is also evident for impact of water abstraction during post-drought and major water uses period.

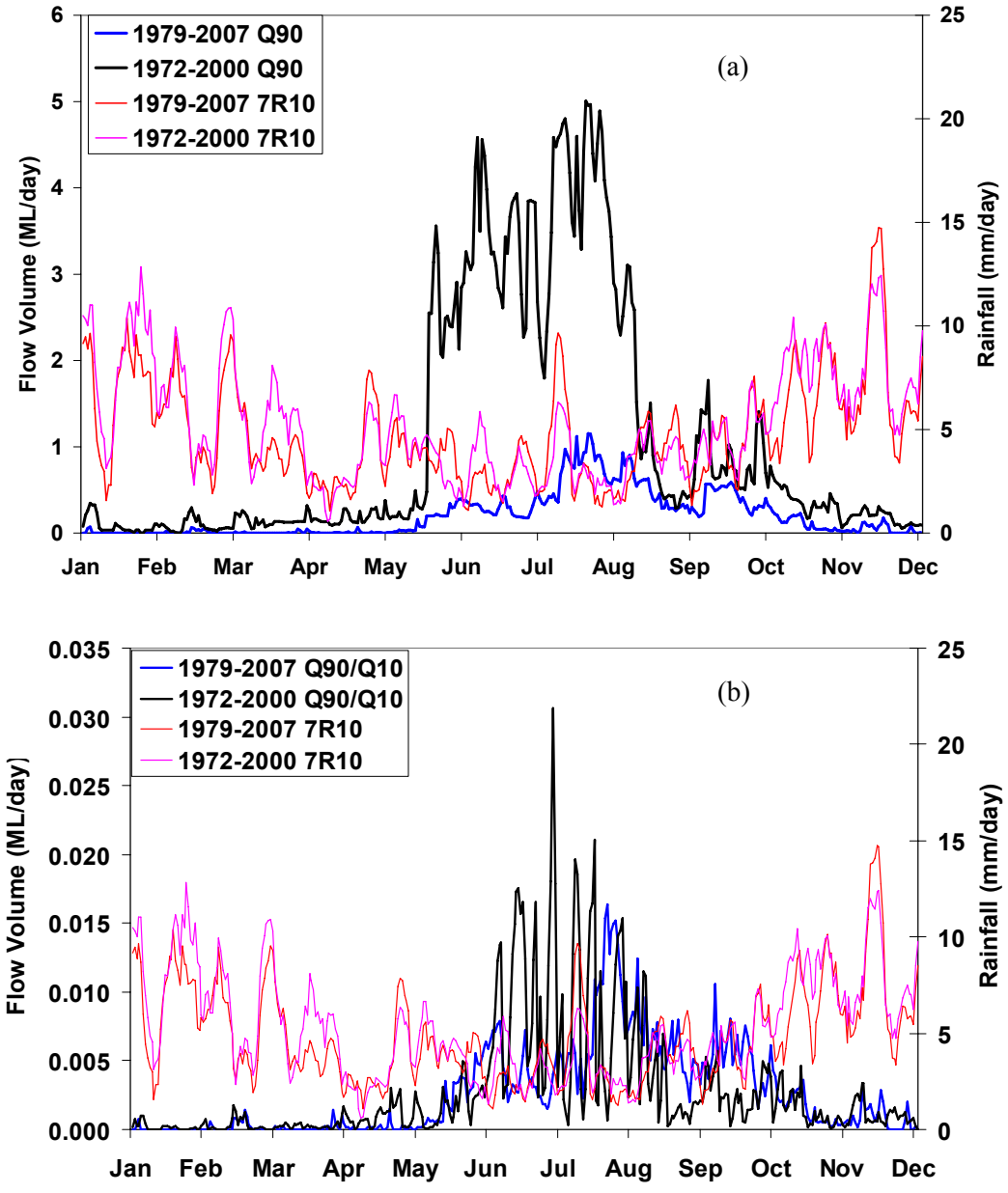


**Figure 6.13** Comparison of pre and post **(a)** Q90 flow percentiles and 7 day R10 rainfall percentiles **(b)** Q90/Q10 flow percentiles and 7 day R10 rainfall percentiles for Wybong

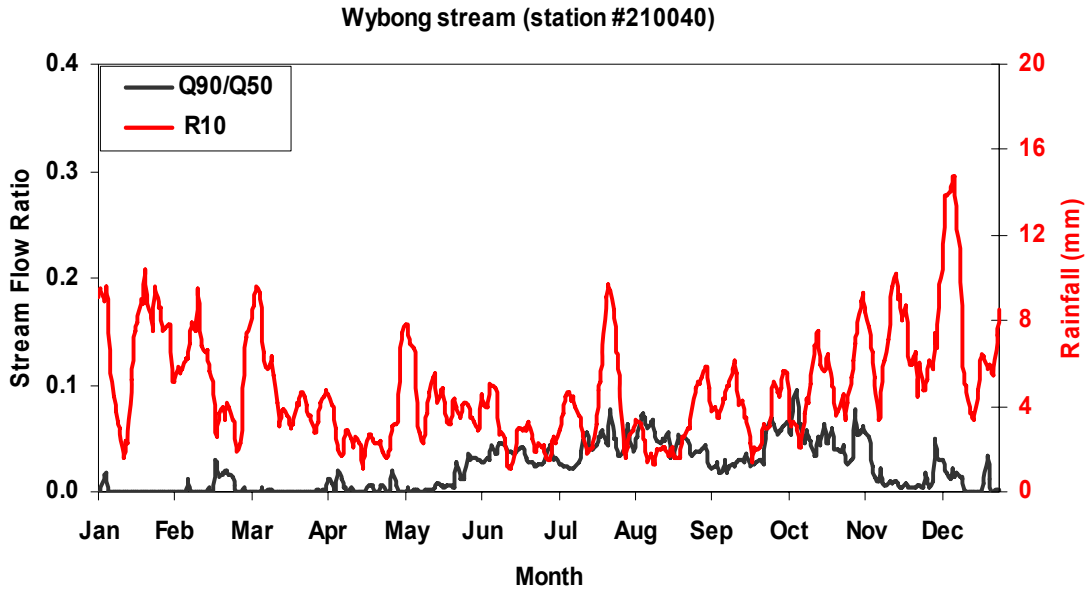


**Figure 6.14** Stream flow percentile ratios Q90/Q50 for Wybong stream gauge compared with Bunnan 7R10 data from 1979-2007

### 6.3.4 Gaining Stream – Wollombi Brook at Warkworth

In this section the Q Lag method is used to investigate flows in another tributary of the Hunter River, Wollombi Brook with longer streamflow record. The lags between the rainfall and streamflow percentiles clearly depend on the catchment properties such as geology, soils and the magnitude and regularity of rainfall events, as well as hydrogeology of aquifer and catchment size. Analysis of daily percentiles was performed on streamflow data from the Wollombi Brook at Warkworth, and compared with the 7dayR10 rainfall percentiles for the Cessnock rainfall station during 1958 to 2007. **Figure 6.15** presents the relationship between the reference rainfall percentile curve and various flow percentiles, including the shifted flow record as calculated by cross-correlation. The lag between the streamflow and rainfall maxima is particularly evident for the lower flow percentiles. The associated time lags are112 and 132 days for Q10 and Q90 percentiles respectively (**Figure 6.17)**.

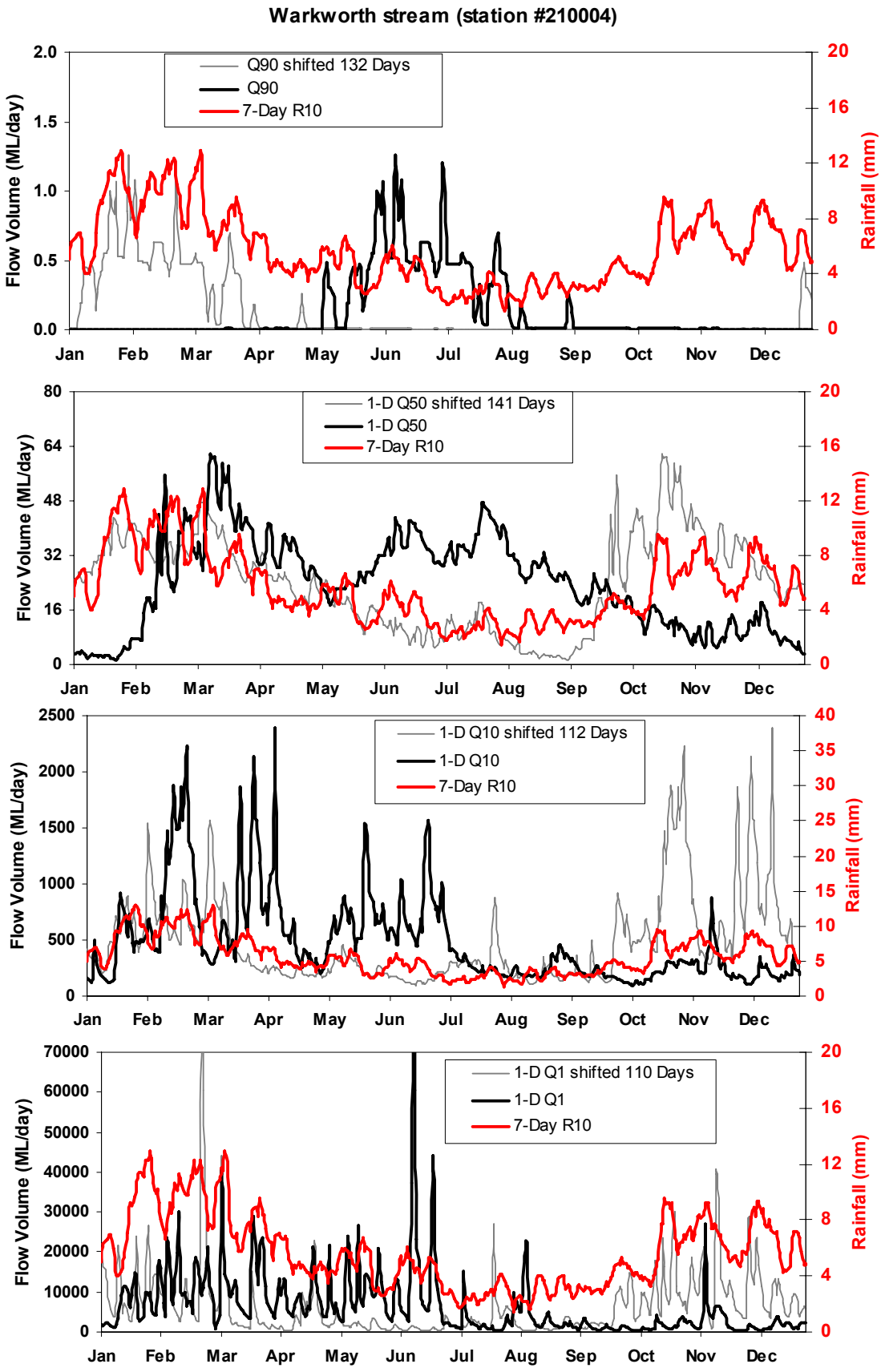


**Figure 6.15** Comparison of various daily stream flow percentiles for Warkworth stream gauge (station #210004) with moving 7-day average of daily rainfall percentile for Cessnock rainfall (station #61242)

**Figure 6.16** shows the results of the cross-correlation analysis for the daily Q90 percentile data, showing that the maximum $r_m$ found when the streamflow data is shifted by 132 days. This shift is depicted in **Figure 6.15**. **Figure 6.18** shows the outcome of cross correlations of the flow percentiles calculated for Warkworth streamflow with respect to Cessnock 7dayR10 rainfall. The lag between rainfall and streamflow increases with the low-flow regime (**Figure 6.17**). The maximum correlation is strong with the maximum fit value of 0.83 in **Figure 6.17** as Wollombi brook stream is dominantly a gaining groundwater system**. Figure 6.19** also shows that the flow percentile ratio of Q90/Q50, the baseflow component, is high during months of May to August, covering the late autumn-winter period. It is noted that the Q90/Q50 ratio for Wollombi Brook at Warkworth (**Figure 6.19**) is almost an order of magnitude lower than that for the Wybong (**Figure 6.14**) or the Goulburn River at Coggan (**Figure 6.23**), reflecting the markedly different distribution of flow in Wollombi Brook.

The match between the shifted Q90 flow percentiles and 7dayR10 rainfall percentiles is visually good (132 days lag) comparing with the equivalent plots for the Wybong Catchment (**Figure 6.7**).

It is interesting to note that in **Figure 6.17** at Qx below 20 percentile there is not a marked decrease in lag as occurs in Wollombi Brook (**Figure 6.15**). This may be due to the generally flatter topography around the Warkworth streamflow gauge compared with that around the Wollombi gauge.

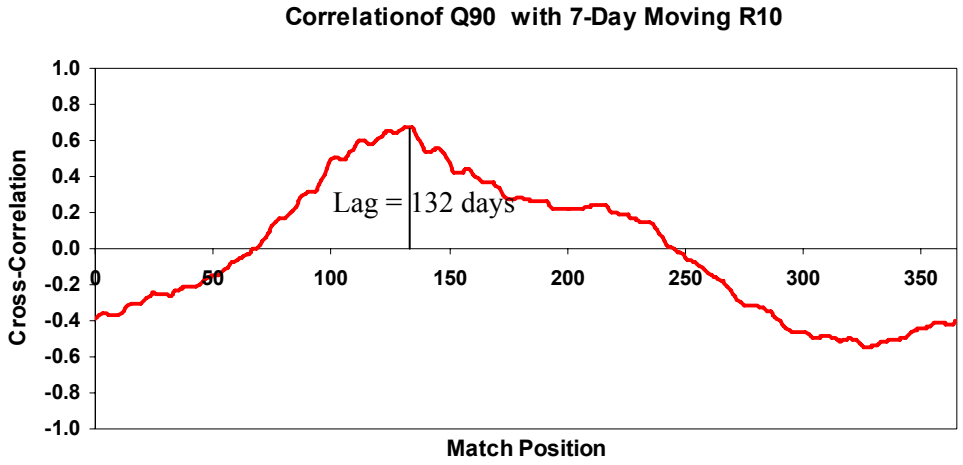


**Figure 6.16** Determination of time lag with the maximum cross-corelation between Warkworth stream Q90 and Cessnock rainfall 7R10 during the period 1958 to 2007

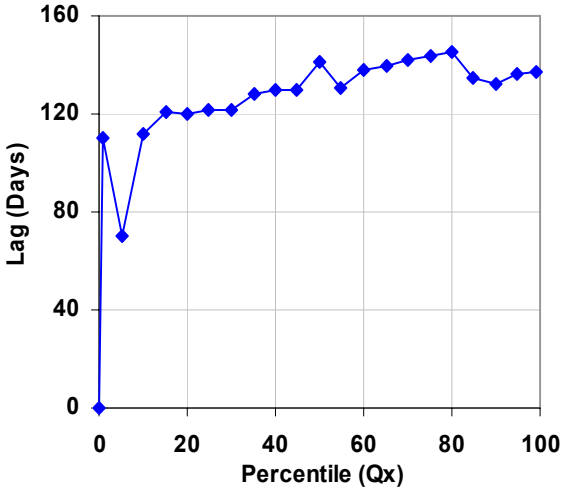


**Figure 6.17** Relation between lag and flow percentiles for the Warkworth stream gauge and Cessnock rainfall 7R10 percentile during 1958 to 2007

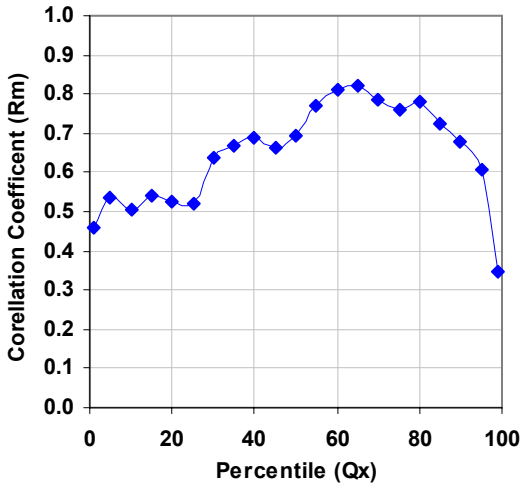


**Figure 6.18** Relationship between maximum cross correlation $r_m$ and flow percentiles for the Warkworth stream gauge and Cessnock rainfall 7R10 percentile

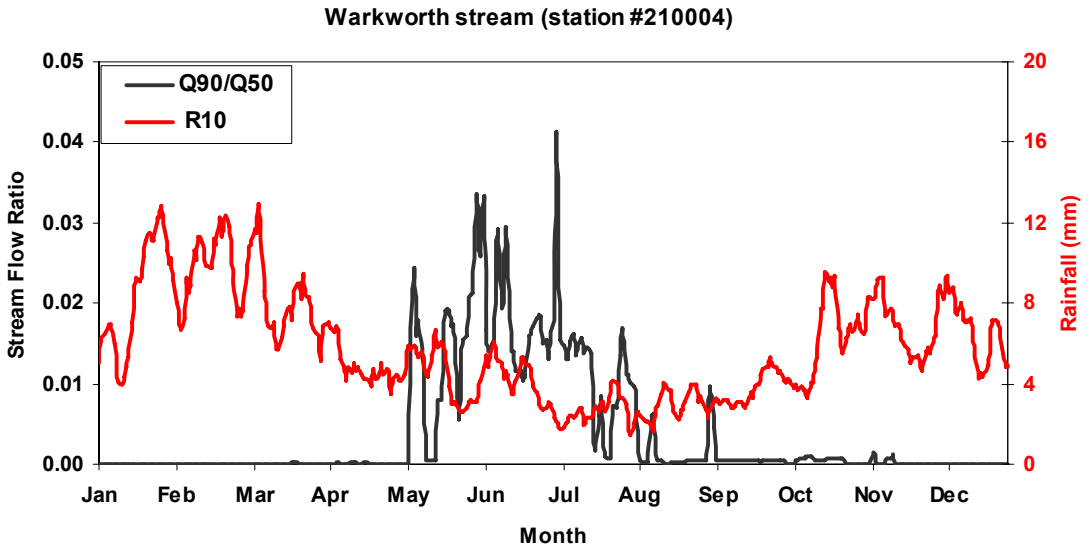


**Figure 6.19** Stream flow percentile ratios Q90/Q50 for Warkworth stream gauge compared with Cessnock rainfall 7R10 during 1958 to 2007

### 6.3.5 Gaining Stream – Goulburn River at Coggan

In this section the Q Lag method is applied to a large catchment, the Goulburn River at Coggan. For the Coggan stream gauge, the lags between the rainfall and streamflow percentile curve is also investigated. Longer time periods without missing flow data are only available for Coggan stream gauge. Analysis of daily percentiles was undertaken on streamflow data from the Goulburn River at Coggan and compared with the 7dayR10 rainfall percentiles for the Denman rainfall station from 1913 to 2007. **Figure 6.20** presents the relationship between the 7dayR10 rainfall percentile curve and various flow percentiles, including the shifted flow record as calculated by cross-correlation. The lag between the streamflow and rainfall maxima is particularly evident for the lower flow percentiles. The associated time lags are 23 and 214 days for Q1 and Q90 percentiles and have a reasonable correlation ($r_m$ = 0.8) as shown in **Figure 6.21 and Figure 6.22** respectively. **Figure 6.23** shows the flow percentile ratio of Q90/Q50 (baseflow) which is high during months of May to August and November to February. However, baseflow occurs all over the year unlike Wollombi. The maximum correlation of 0.8 and high baseflow all over the year demonstrate that the Goulburn River stream is dominantly gaining stream.

The match between the shifted Q90 flow percentiles and 7dayR10 rainfall percentiles is visually resonable (214 days lag) comparing with the equivalent plots for the Wybong Catchment (**Figure 6.7**). For the Goulburn River at Coggan it is noted that for $Qx \leq 10$, the time lag are considerably shorter than those for Qx>20. This differs from Wollombi Brook at Warkworth and may result the generally steeper catchment around the Coggan rain gauge.

To explore the impact of increased water extraction during drought periods, daily percentile analysis was undertaken by splitting the record into drier years of 1913 to 1947, 1973 to 2007 and wetter years of 1948 to 1999, considered a drought dominated regimes (DDR) and floods dominated regimes (FDR) in Chapter 3 Section 3.3.2. The associated time lags are 236, 209 and 236 days for Q90 percentiles with rainfall percentiles where the correlation $r_m$ = 0.53, 0.72 and 0.8 with corresponding time lags as shown in **Figure 6.24, Figure 6.25 and Figure 6.26**. The impact of water extraction during drought periods is reflected in the apparent streamflow deficit relative to rainfall and poor correlations. In addition, the behaviour of the lags for Qx<10 is quite different in the dry period 1973 to 2007 then in the dry period 1913 to 1947.

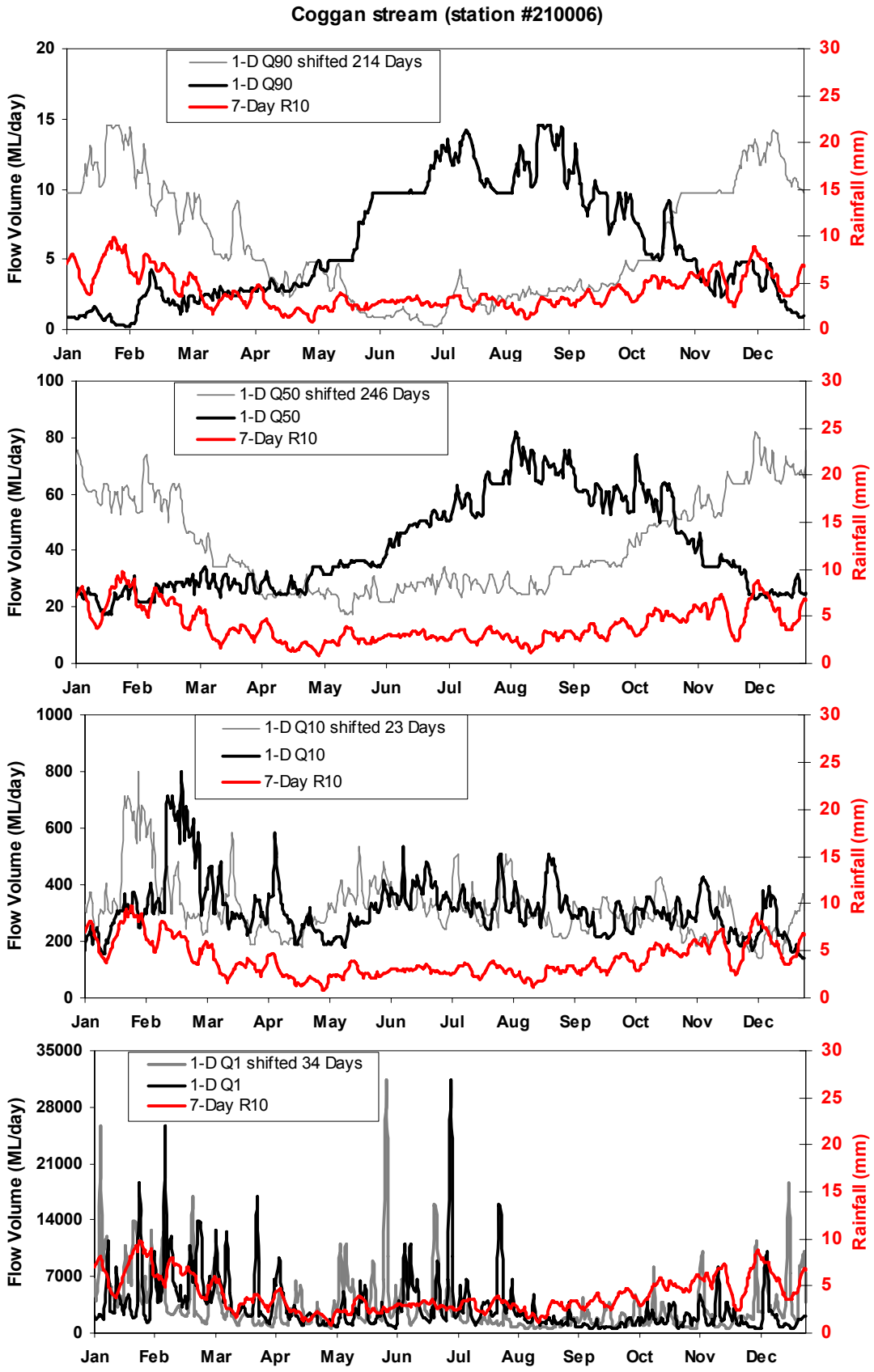


**Figure 6.20** Comparison of various daily stream flow percentiles for Coggan stream gauge (station #210006) with moving 7-day average of daily rainfall percentile for Denman rainfall (station #61007) during 1913 to 2007

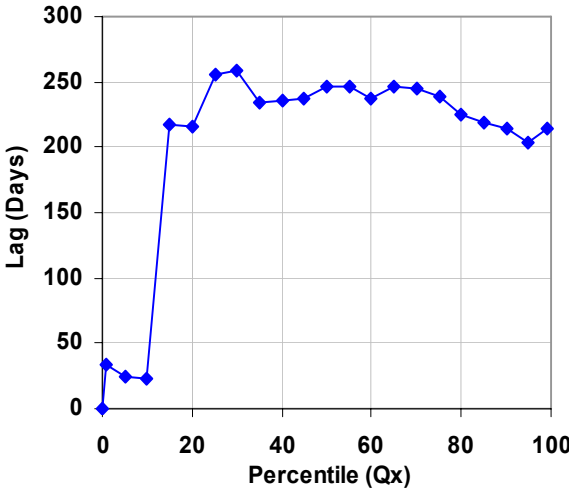


**Figure 6.21** Relation between lag and flow percentiles (Coggan stream flow percentiles Qx and Denman rainfall 7R10 percentile) during 1913 to 2007

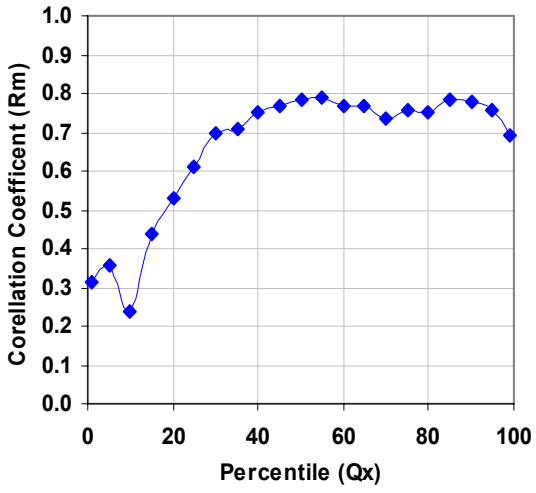


**Figure 6.22** Relationship between maximum cross correlation $r_m$ and flow percentiles (Coggan stream flow percentiles Qx and Denman rainfall 7R10 percentile)

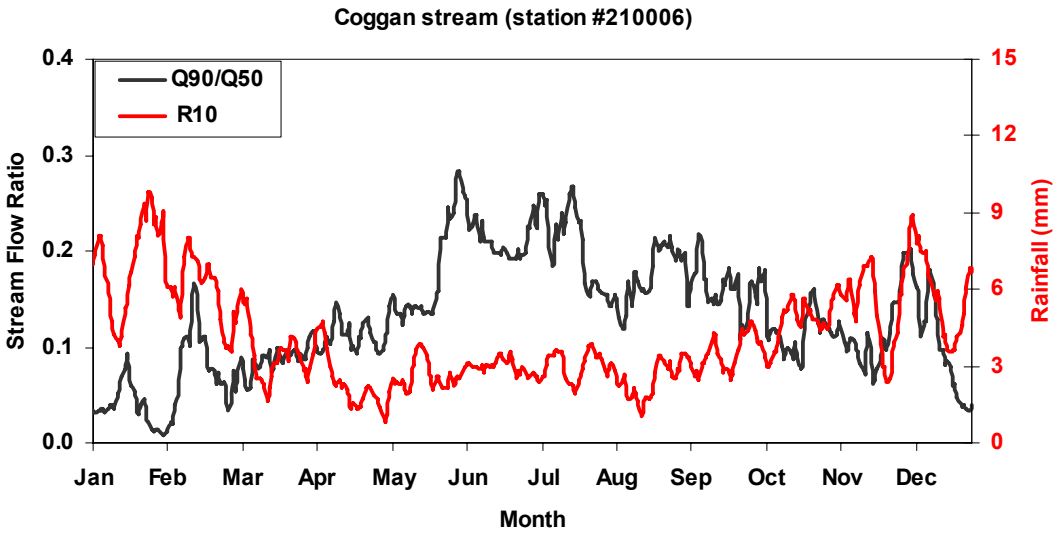


**Figure 6.23** Stream flow percentile ratios Q90/Q50 for Coggan stream gauge compared with Denman rainfall 7R10 during 1913 to 2007

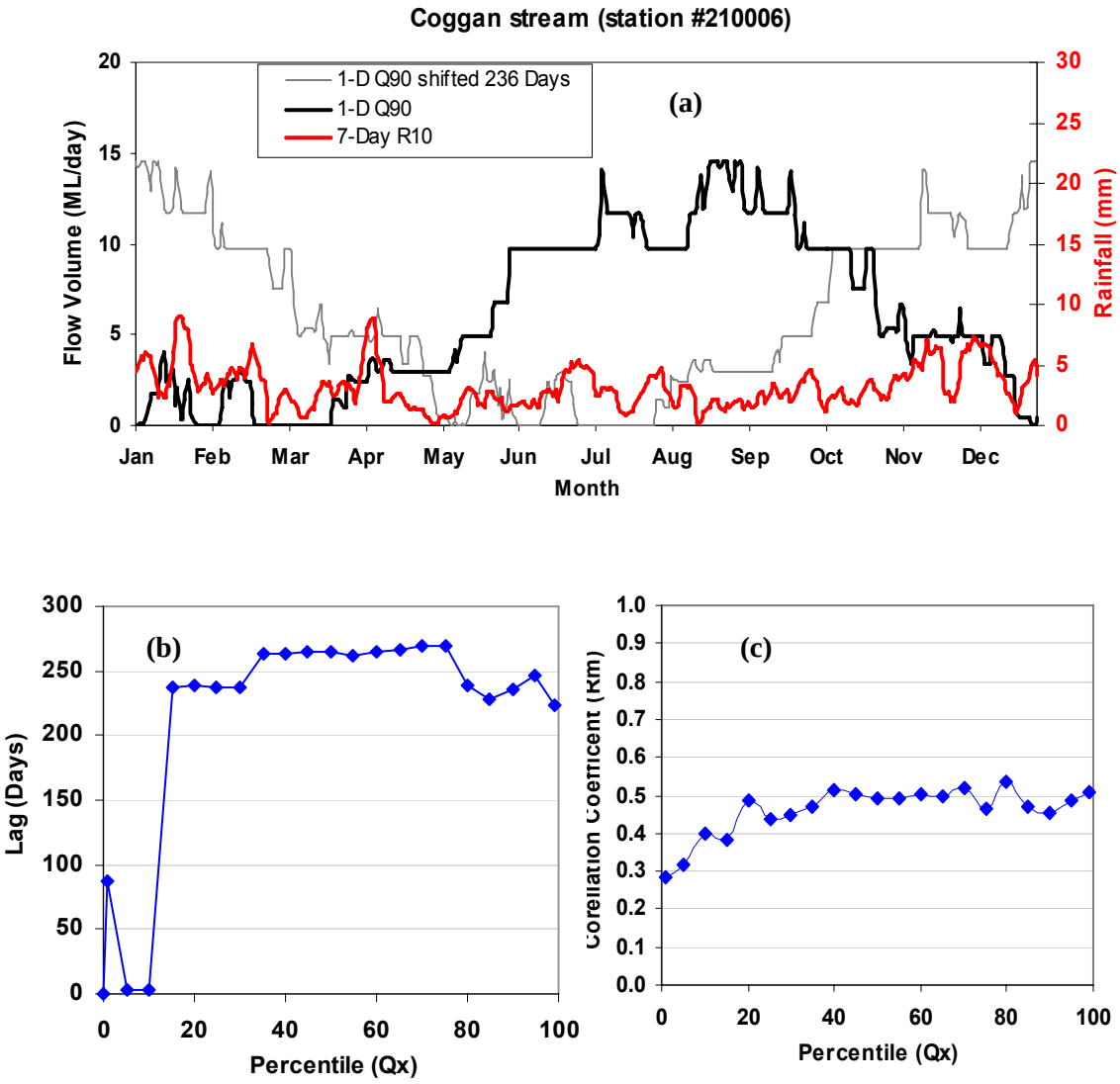


**Figure 6.24 (a)** Comparison of various daily stream flow percentiles **(b)** Lag days and **(c)** $r_m$ for Coggan stream gauge (station #210006) with moving 7-day average of daily rainfall percentile for Denman rainfall (station #61007) during the drier period 1913 to 1947

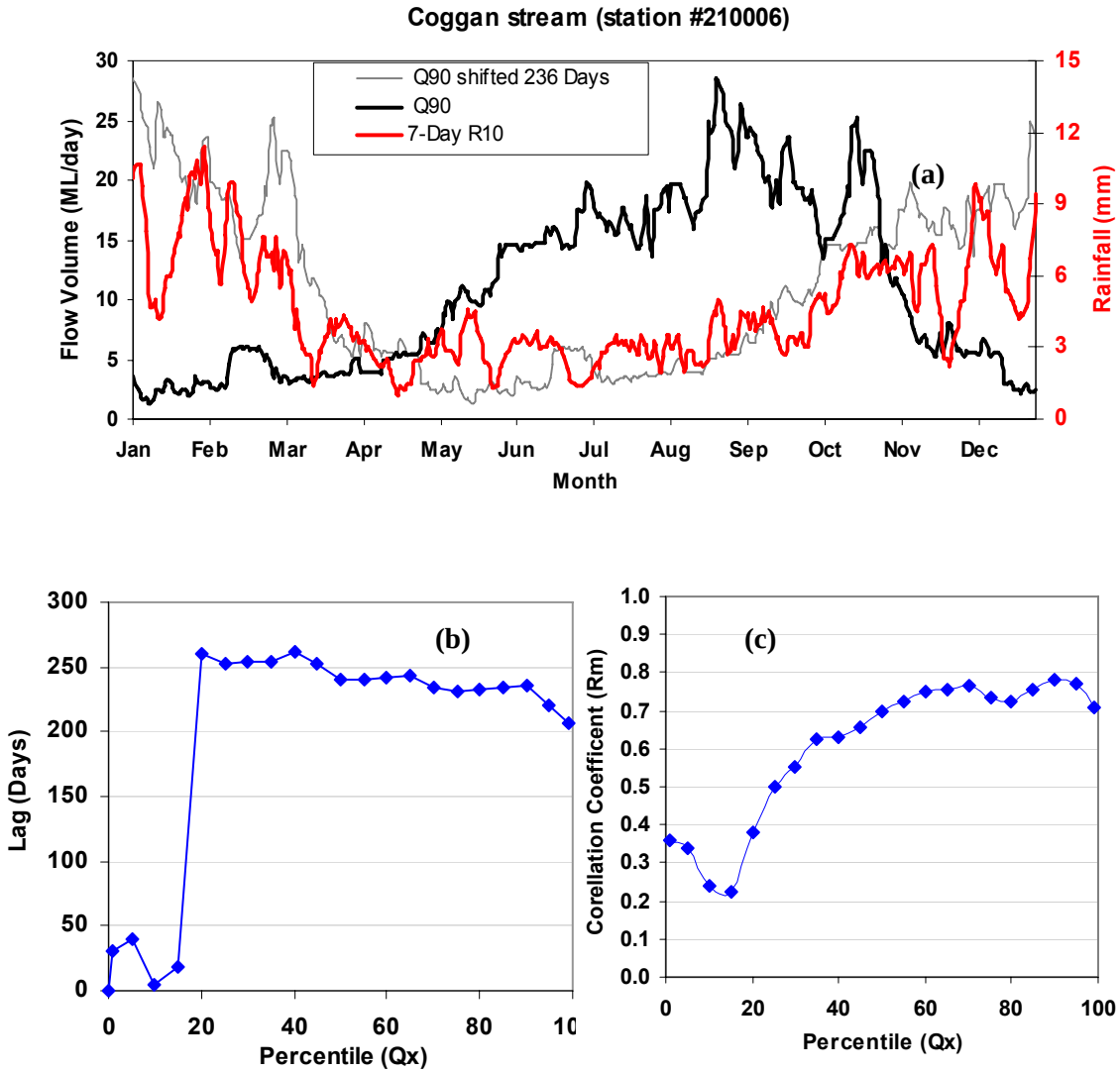


**Figure 6.25 (a**) Comparison of various daily stream flow percentiles **(b)** Lag days and **(c)** $r_m$ for Coggan stream gauge (station #210006) with moving 7-day average of daily rainfall percentile for Denman rainfall (station #61007) during wetter period 1948 to 1999

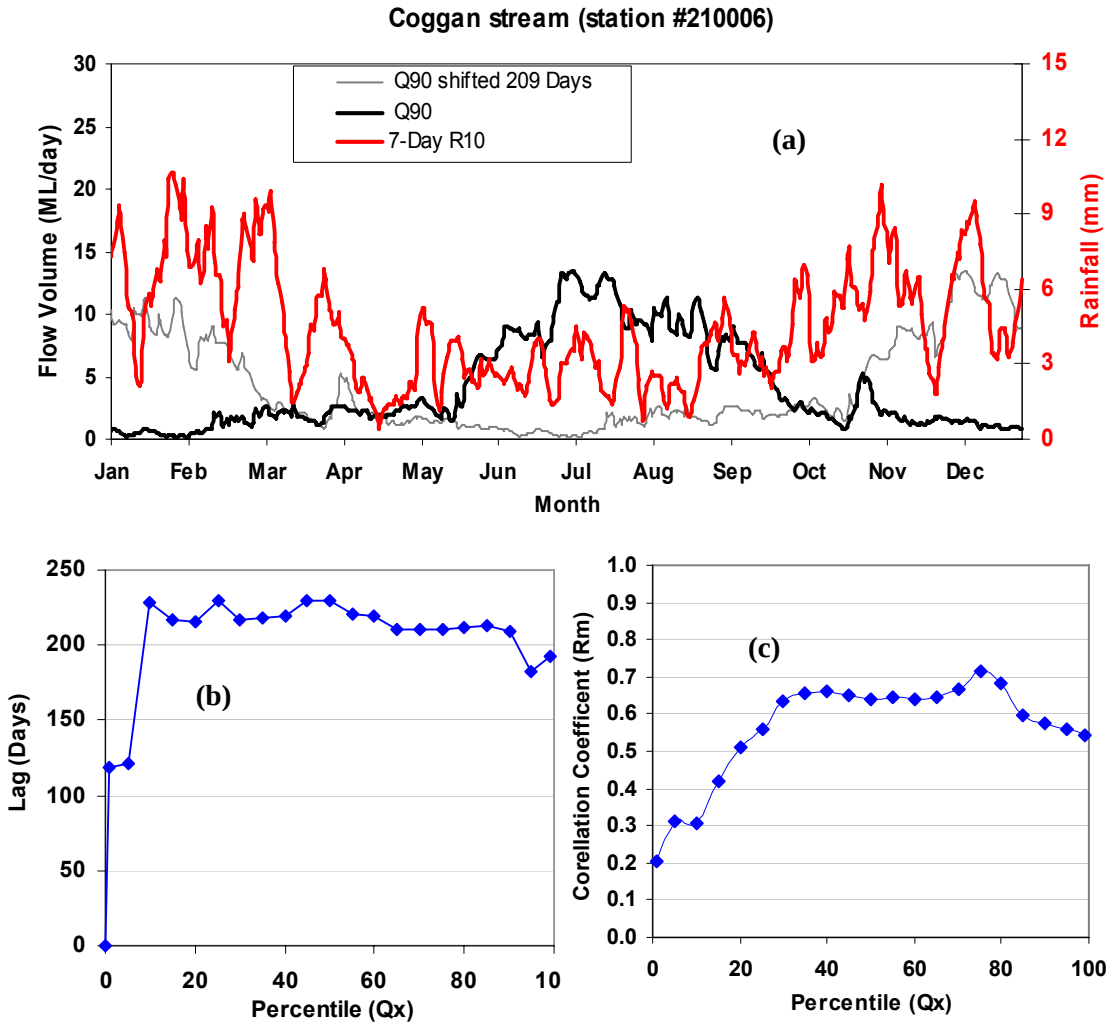


**Figure 6.26 (a)** Comparison of various daily stream flow percentiles **(b)** Lag days and **(c)** $r_m$ for Coggan stream gauge (station #210006) with moving 7-day average of daily rainfall percentile for Denman rainfall (station #61007) during 1973 to 2007

In order to compare the results of daily percentile analysis, it is noted that three stream gauges for Wybong, Warkworth and Coggan with 29, 50 and 94 years of data along with of catchment areas, 675 $km^2$, 1848 $km^2$ and 3340 $km^2$ respectively, were considered. As mentioned, $R_m$ and the Lag between Q90 flow percentiles and 7R10 rainfall percentiles of the stream gauges are 0.72, 0.8 and 0.83 with rlags of 206, 132 and 214 days, respectively. The results demonstrate that longer period's data for Coggan give a better fit than shorter period data.

When same time period (1972-2000) is considered for the catchments, Wybong and The Goulburn at Coggan show almost same lag behaviour and maximum correlation. This is interesting to note since the Goulburn at Coggan has almost 5 times the upstream catchment area to that at the Wybong gauging station. Both catchments have similar climate. The results suggest that the streams of Wybong and Coggan which are highly connected with groundwater aquifer respond in similar ways despite the difference in catchment area. This scale dependence of groundwater lag times is worthy of more research. In contrast, Wollombi Brook has a much shorter time lag response (Figure 6.27) during the same period. Since the characteristics of rainfalls differ only slightly over the catchments the comparison of lags between the rainfall and streamflow percentile curves between the three catchments show that the groundwater systems in Wollombi Brook are more responsive. This may be a due to the much larger shallow-watertable sandy floodplain in the lower Wollombi Brook Catchment.

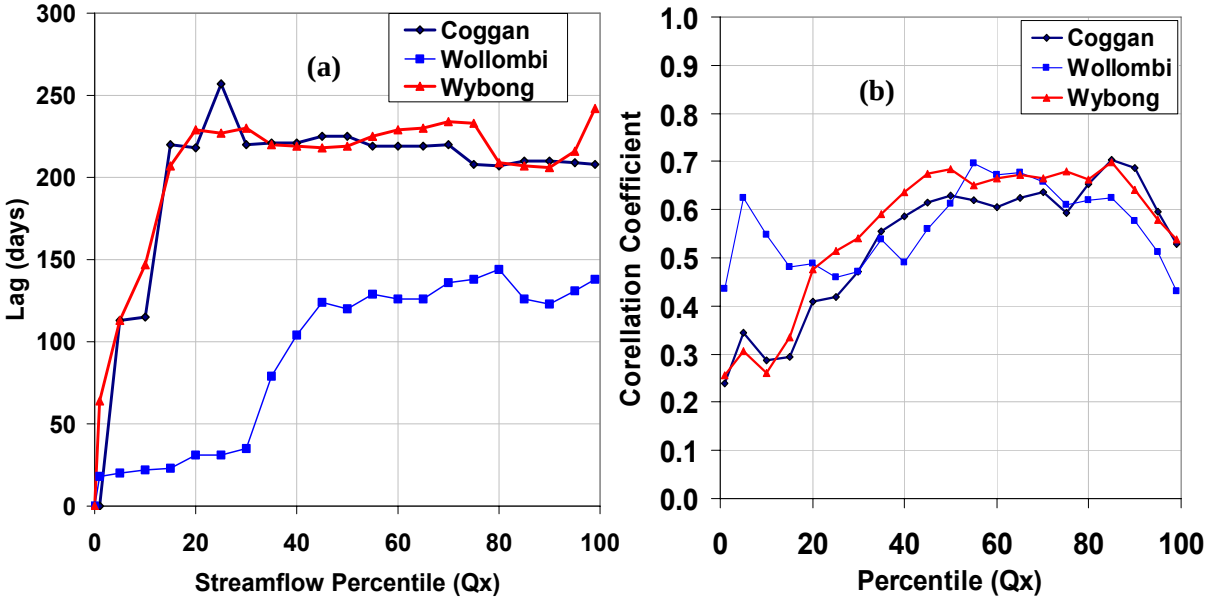


**Figure 6.27** Cross-correlation analysis stream flow percentiles (Qx) and rainfall 7R10 percentile during 1972 to 2000 for Wybong, Coggan and Wollombi **(a)** relationship between lag and flow percentiles **(b)** relationship between maximum cross correlation ($r_m$) and flow percentiles.

## 6.4 Conclusion

Groundwater-surface water interactions have been investigated in this chapter for three different catchments. Stream height and groundwater elevation comparison, frequency analysis and baseflow separation technique have employed for investigating the dynamics of groundwater input into the stream during drought and non-drought periods in Wybong Creek. The results of Wybong stream height and ground water level comparison show that groundwater gradient is towards the stream and hence there is a significant potential discharge.

The Lyne and Hollick filter method of baseflow separation analysis was used to estimate baseflow contribution to the stream and found that about 53% of streamflow is baseflow. Significant recessions occurred in the winter months of May and June, and very low recession occurred in December presumably due to influence of evapo-transpiration and groundwater higher. Low BFI during the dry years of 2002 to 2007 appears due to the high evapo-transpiration and excessive water pumping during this period.

Comparison of streamflow percentiles with relevant rainfall percentile curves has also provided insights into the nature of groundwater-surface water interactions in catchments. This is summarised by the comparison of the relationships between the Q90 percentile flow and the 7dayR10 rainfall percentile curve for the study areas. Analysis of the Wybong, Wollombi and Coggan streamflow record demonstrate dominantly gaining stream.

A lag was found between the seasonal peak in the low-flow percentile curves and the seasonal peak in the smoothed daily rainfall percentile curve. This shift gives this frequency analysis method its name of Q-Lag. Use of cross-correlation between the time-shift required allowed the best fit between the streamflow and rainfall percentile curves to be calculated for identifying the lag period. When the streamflow percentile data is shifted accordingly, the goodness of fit between the rainfall percentile curves and the shifted streamflow percentile curve is good ($r^2$>0.7) for the gaining stream example.

In case of the Wybong, much of the rainfall's recharge component returns to the stream as groundwater discharge over the year. It reflects a good correlation ($r_m$=0.78) between the shifted flow percentile curves and the reference rainfall percentile curve. The lags represent the processes of firstly replenishing catchment storage such as soil moisture and groundwater, and subsequent discharge to the stream. The lag of 206 days

found between streamflow percentiles and rainfall was attributed to catchment hydrogeology as well as climate (notably the magnitude and regularity of rainfall events).

The impact of water extraction has also recognized in this analysis. Differences in rainfall–streamflow correlation represent losses from the water budget with respect to the stream. These losses can be occurred due to either natural processes, such as evapotranspiration or leakage to aquifers, or human processes such as consumptive use. The apparent deficit in streamflow related to the rainfall curve during the non-winter months is assumed to be of surface and groundwater extraction.

In summary, the analyses used to provide guidance on whether the stream is dominantly gaining or losing relative to the groundwater system. For gaining streams, changes in the magnitude of the lags between streamflow percentiles and rainfall can provide insights into the catchment storages that contribute to streamflow. Overall, Q-Lag analysis, baseflow separation and stream height and groundwater level analysis showed that Wybong stream was highly connected with groundwater aquifer and differed in character to Wollombi Brook which had much shorter lag times. This was attributed to difference in aquifer properties.

# CHAPTER 7

# MODEL FOR GROUNDWATER DYNAMICS

Better knowledge of the interactions between groundwater and streamflow in catchments is required to improve water resources management. Recent water sharing plans in New South Wales have highlighted the need to manage surface and ground water as a connected system. In this chapter the use of a simple monthly, conceptual model is explored to assess its usefulness for predicting simultaneously groundwater levels and streamflow in the Wybong Creek and Wollombi Brook catchments of the Hunter River. Streamflow, groundwater level, rainfall and evaporation data are employed to assess the stream and groundwater dynamics in the catchments. The analysis includes a water balance model, and descriptions of monthly streamflow and groundwater models which are modified and extended. The approach appears to be of use in Hunter water management initiatives.

## 7.1 Overview

Groundwater levels fluctuate due to groundwater recharge, discharge and extraction (Olin and Svensson, 1992) and a variety of other influences. These include variability of precipitation, evaporation, temperature, atmospheric pressure especially in the case of swelling soils, transpiration by vegetation, tidal effects near the sea (Shih and Lin, 2002), earthquakes (Wang *et al.*, 2004) and artificial recharge. A wide range of analytical models have been applied for simulating groundwater level fluctuations in response to changes in river stage (Narayan *et al.*, 1993; Jolly *et al.*, 1998). Such models distribute floodplain groundwater discharge as seepage at the break of slope, evapotranspiration across the floodplain and as groundwater flow into and out of the river. Regional scale groundwater models are widely used to estimate the flux of groundwater entering near-surface and surface systems (Narayan *et al.*, 1993).

Groundwater recharge can be estimated from a wide varity of techniques including estimates of the water location chemical or isotopic tracer data and climatic data (Jellett, 2005). Changes in soil water storage can also be used to infer groundwater recharge (Chapman and Malone, 2002). Direct measurement of groundwater levels is essential in order to understand the groundwater systems and to test the predictive capability of

models. Modelling of groundwater levels and streamflow provides a way of investigating the effects of land use, climate change and change management regime.

Monthly water balance models (Makhlouf and Michel, 1994) have widely been used for long-term management of water resources, reservoir design and reservoir operation. Thornthwaite and Mather (1955) developed a set of deterministic monthly water balance models, in which only two parameters were used. In developing an index of meteorological drought, Palmer (1965) suggested a model that divides the soil moisture storage into two layers, each with its own soil moisture capacity as the model's two parameters. Both the Thornthwaite and Palmer models used the concept that runoff and recharge do not occur until the soil moisture capacity threshold is reached. This assumption tends to underestimate runoff during summer and autumn, as runoff can still occur over a range of soil water contents when rainfall intensities are sufficiently high, such as in summer and autumn thunderstorms. Alley's (1984) review of the water balance models concluded that prediction errors were similar among the models. Gleick (1987) developed a monthly water balance model specifically for climate impact assessment and addressed the advantages of using water balance type models in practice. In the 1990s, monthly water balance models were developed for studying the impact of climate change on the hydrological balance and for general water resources planning and management (Mimikou *et al*., 1991; Guo *et al.* 2002; Guo, S. 1992; Guo and Yin, 1997; Xu and Singh, 1998; Xiong and Guo, 1997). Vandewiele and Elias (1995) used a spatial surface model to fit parameter values to estimate runoff from ungauged catchments.

Most models are over-parameterized leading to interactions between parameters and correlation between parameter estimates (Jakeman and Hornberger, 1993). A conceptual model with few parameters is required for reducing the computational complexity. A simple, two parameter monthly water balance model was developed by Xiong and Guo (1999) and applied to seventy subcatchments located in the south of China for runoff simulation. Jellett (2005) employed this model for predicting stream flow and modified it for predicting unconfined groundwater level in Orroral Valley in the Australian Capital Territory after he found that many standard hydrological models were considered to be statistically inadequate. The advantage of the model developed by Jellett (2005) includes its statistically sound testing procedures which are used to find the model parameters efficiently. Measurement of the hydraulic conductivity of the

alluvial aquifer is not required in the modified XG model. Jellett (2005) demonstrated that the XG recharge model can predict stream flow accurately after being calibrated on a limited subset of groundwater level data. This is particularly useful because the model can be used to estimate recharge in areas where there are stream flow data but insufficient ground water level data. In this study the usefulness of the modified two parameter (evapotranspiration and runoff parameter) monthly water balance model in predicting groundwater levels and streamflow in the Hunter Catchment is examined.

## 7.2 Water Balance Model

Water balance models are particularly important for forecasting catchment water balance components including groundwater levels (Walker and Zhang, 2002). Water balance models ensure that the amount of water coming into, being stored and flowing out of the reference area or catchment is explicitly conserved using an appropriate water balance equation. The input water consists of rainfall, and output water includes losses via evapotranspiration, runoff and seepage to ground water. Standard one-dimensional water balance models express all of the catchment water quantities in volume per unit area or length units, frequently millimeters so that properties of catchments with different areas can be compared.

The processes in a simple water balance model at the Earth's surface are shown in **Figure 7.1**. Precipitation P (mm) falls on the catchment, some water is lost through evapotranspiration E (mm) while some water leaves the catchment as runoff Q (mm). The remaining water infiltrates into the soil causing an increase in soil moisture storage $\Delta S$ (mm).

The simple water balance equation for the process shown in **Figure 7.1** is:

$$P = E + Q + \Delta S \tag{7.1}$$

or in discrete time intervals, t

$$P_t = E_t + Q_t + S_t - S_{t-1} \tag{7.2}$$

where $S_{t-1}$ is the soil water store in the previous time step.

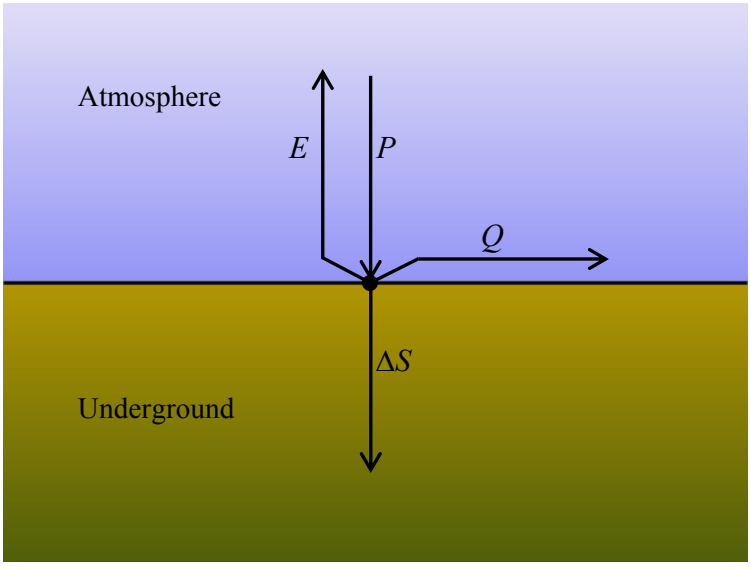


**Figure 7.1** The portioning of precipitation, P, at the ground surface into runoff,Q, evapotranspiration, E and change in the soil moisture store, $\Delta S$ (Jellett, 2005)

## 7.3 Methods

This section provides a description of the available data as well as the procedure used for data processing. In this study, meteorological data of rainfall and pan evaporation for Hunter, spatially interpolated data rainfall and pan evaporation data for Wybong Creek and Wollombi Brook were used. Streamflow data and bore water height data were also used. The streamflow data for the Wybong stream gauge (station #210040), Bulga (station #210028) and Warkworth (station #210004) stream gauge in the Wollombi Brook. Groundwater elevation data were sourced from the following bores: GW080944, GW080945, GW080946, GW080947, GW080948 and GW080434 in the Wybong catchment and bores GW079055, GW079056, GW079057, GW079058, GW079059 and GW079060 in Wollombi Brook (data source from NSW, DNR).

Missing streamflow and groundwater level data were set to -9.0 to avoid programming run-time error when the model was calibrated.

### 7.3.1 Groundwater Level

Continuous groundwater level data of bores in the Wybong catchment and Wollombi Brook were obtained from the DNR database (NSW DNR, 2008). The water level measured in monitoring bores is related to a common datum which the surveyed level of the top of the bore casing relative to Australian height datum. A groundwater rating is used to relate the measured water level in the bore back to this datum. The water level transducers record groundwater levels in the bores every 15 minutes using a pressure transducer connected to a data logger (**Figure 7.2**). The pressure transducer is positioned below the water level a known distance down the bore. The pressure of water above the pressure transducer is converted to a water level. The data logger stores the time of each change in groundwater level along with the groundwater level.

**Figure 7.2** shows the pressure transducer groundwater level gauge in a bore. Source: Department of Infrastructure, Planning and Natural Resources

One possible source of error in the groundwater level measurement is the deployment of the sensor on the very bottom of the bore which may cause blocking of the sensor by mud or silt. Another possible source of uncertainty includes air entrapment that may occur after an extreme rainfall event. Air may become trapped between the new recharge and the water table and cause higher pressure which pushes more water into the bore giving falsely high watertable level measurements (Freeze and Cherry 1979).

Information on the bores is listed in **Table 7.1. Table 7.2** shows the periods over which the bores were monitored, along with the bore depth, the mean groundwater

levels and the lithology. Bore drill logs revealed that bores #080944 and #080948 were in a consolidated, semi-confined aquifer, bore #080434 was in an unconsolidated unconfined aquifer, and #080945 and #080946 in the Wybong catchment were in a consolidated, unconfined aquifer.

**Figure 7.3a** and **Figure 7.3b** shows the location of the bores in the Wybong catchment and Wollombi Brook. The bores were subject to similar rainfall and evaporation rates, since their elevation ranges were from 153m to 165m above the Australian Height Datum (AHD) as shown in **Figure 7.3a**.

**Table 7.1a** Monitoring bore names, locations relative to the Global Positioning System (GPS) and elevations of the top of the bore relative to the Australian Height Datum (AHD) in Wybong catchment.

| BoreID | Name | Longitude (ºE) | Latitude (ºN) | Elevation (m)(AHD) |
|---|---|---|---|---|
| 080434 | Wybong Road | 150.6487 | 32.28159 | 165.3 |
| 080944 | Ridgelands Rd. | 150.6697 | 32.21729 | 163.0 |
| 080945 | Rockhall | 150.629 | 32.25581 | 153.0 |
| 080946 | Rockhall | 150.6331 | 32.26457 | 153.0 |
| 080947 | Rockhall | 150.6297 | 32.2511 | 159.0 |
| 080948 | Rockhall | 150.6224 | 32.24834 | 161.0 |

**Table 7.1b** Monitoring bore names, locations relative to the Global Positioning System (GPS) and elevations of the top of the bore relative to the Australian Height Datum (AHD) in Wollombi Brook.

| BoreID | Name | Longitude (ºE) | Latitude (ºN) | Elevation (m)(AHD) |
|---|---|---|---|---|
| 79055 | Wollombi #1 | 151.1458 | 32.9358 | 92 |
| 79056 | Wollombi #2 | 151.1458 | 32.9358 | 92 |
| 79057 | Fordwich #1 | 151.0514 | 32.9358 | 0 |
| 79058 | Fordwich #2 | 151.0514 | 32.9358 | 0 |
| 79059 | Warkworth #1 | 151.0211 | 32.8886 | 56 |
| 79060 | Warkworth | 151.025 | 32.7072 | 56 |

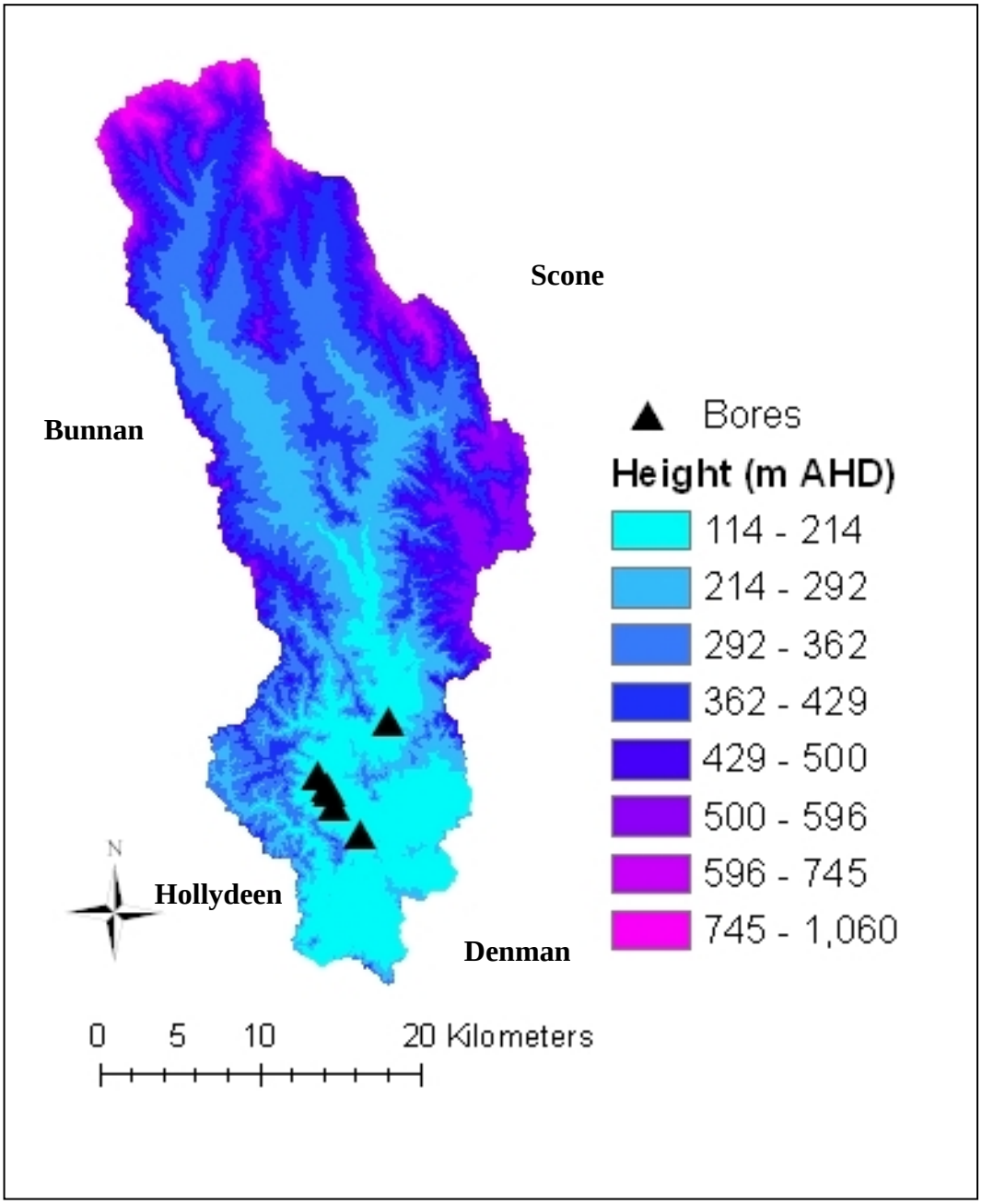


**Figure 7.3a** Elevation map of the Wybong catchment with bore locations marked

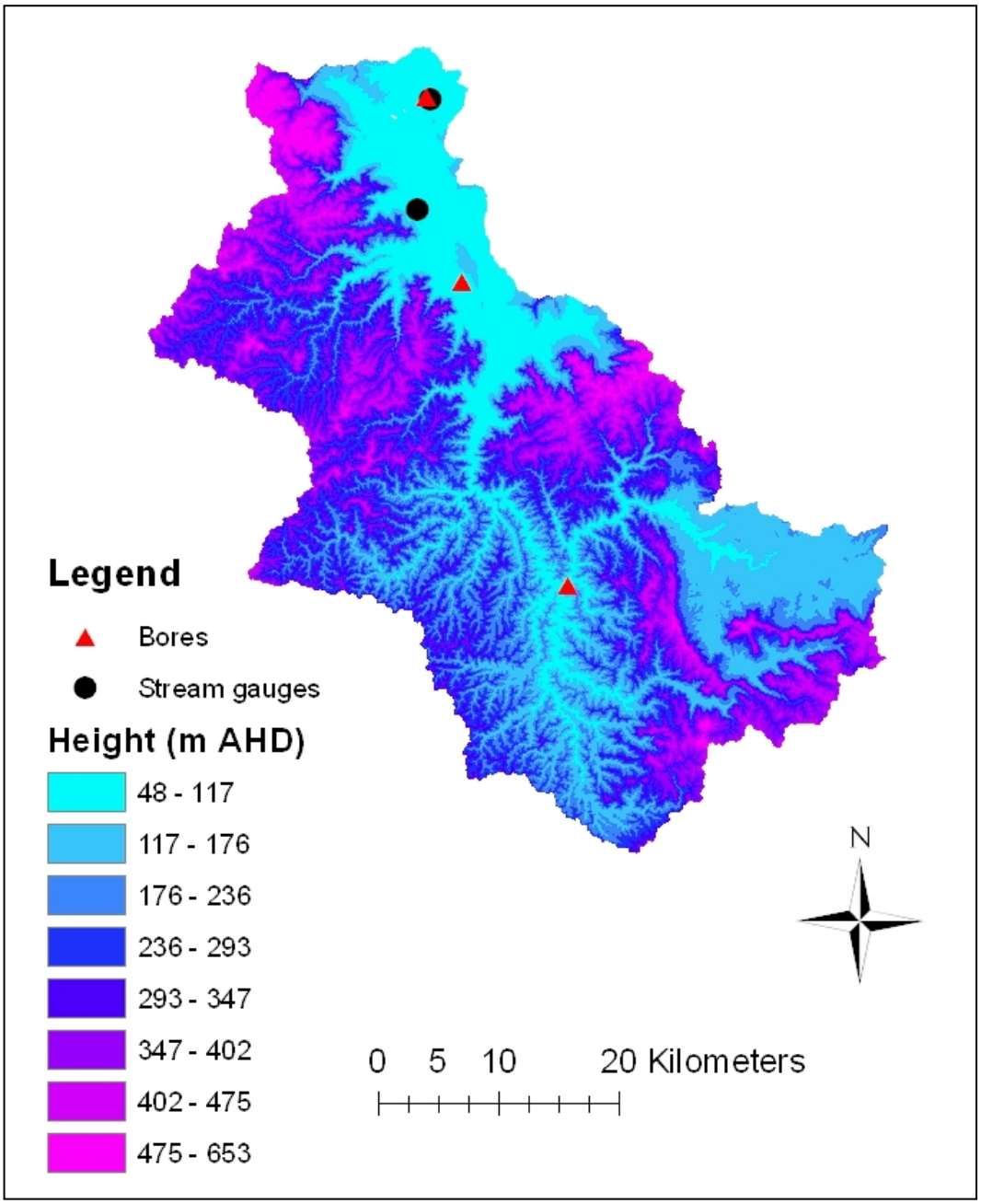


**Figure 7.3b** Elevation map of the Wollombi Brook with stream gauge and bore locations marked

**Table 7.2a** Bore monitoring periods and bore charecteristics in Wybong catchment

| BoreID | Start and End Date (day/m/y) | Aquifer type | Mean G.W. L (AHD m) | Field Water level (m)* | Depth of the bore (m)* | Water bearing zone (m)* | Lithology |
|---|---|---|---|---|---|---|---|
| 080434 | 1/7/2003-30/11/2008 | Unconsolidated unconfined | 137.74 | 15.20 | 17.4 | 14-17.4 | Clay, clay-sand, gravel |
| 080944 | 6/7/2006-31/12/2008 | Consolidated semi-confined | 162.95 | 10.0 | 30.0 | 24-26 | Clay, sandstone, pyroclastic, conglomerate |
| 080945 | 4/7/2006-31/12/2008 | Unconsolidated unconfined | 141.94 | 12.93 | 2.0 | 16-18 | Clay, Gravel, clay |
| 080946 | 4/7/2006-31/12/2008 | Unconsolidated unconfined | 137.61 | 12.05 | 19.5 | N/A | N/A |
| 080947 | 5/7/2006-31/12/2008 | Consolidated semi-confined | 142.27 | 12.57 | 60.0 | N/A | N/A |
| 080948 | 5/7/2006-31/12/2008 | Consolidated semi-confined | 144.26 | 9.2 | 41.0 | 27-29 | Clay, gravel, clay, sandstone |

***** Depth of groundwater level below top of bore measured during June 2007 and July 2008

### 7.3.1.1 Data Preparation

The groundwater level data for the Wybong and Wollombi were stored in the Hydstra database. The data were recorded as depth from the bore collar to water level and then inverted and adjusted to Australian Height Datum (AHD). Data were extracted as mean monthly data from Hydstra database. The quality codes accompanying the data were used to exclude poor quality data. Quality code 100 indicated good quality continuous measurement. Quality codes 2,5,6,8, 26, 51, 70, indicated good quality measurement and were used in this study.

**Figure 7.4** shows the groundwater level, rainfall and pan evaporation for the Bore 080434 which has the longest record of measurement. Groundwater level data for the bores were mean monthly groundwater level to represent mid-month groundwater level. Mean monthly groundwater level data were available and considered in this study, since the data were not much different from the end month groundwater level data.

**Table 7.2b** Bore monitoring periods and bore charecteristics in Wollombi Brook

| BoreID | Start and End Date (day/m/y) | Mean G.W. L (AHD m) | Field Water level (m)* | Depth Of the bore (m) | Water bearing Zone (m) | Lithology |
|---|---|---|---|---|---|---|
| 79055 | 14/1/2001-15/12/2008 | 81.92 | 37.49 | 50 | 4.4-15 | Topsoil Sand, gravel, sandstone |
| 79056 | 14/1/2001-15/12/2008 | 83.81 | 7 | 17 | 4.4-15 | Sand, gravel, gravel |
| 79057 | 14/1/2001-15/12/2008 | 64.34 | 7.04 | 50 | 12.6-14.7 | Topsoil, Clay & sand, fine gravel, shale-coal, coal, shale, coal, sandstone & shale, sandstone, shale & coal, |
| 79058 | 14/1/2001-15/12/2008 | 61.2 | 7.04 | 15.7 | 12.67-14.7 | Topsoil, clay & sand, shale, coal |
| 79059 | 14/1/2001-15/12/2008 | 44.94 | N/A | 50 | N/A | N/A |
| 79060 | 14/1/2001-15/12/2008 | 47.78 | 7.18 | 14.6 | 8.5-12.5 | Topsoil, sand gravel, sandstone |

***** Depth of groundwater level below top of bore measured during June 2007 and July 2008

### 7.3.2 Stream Flow

**Figure 7.5** shows Wybong stream gauge (station #210040) which provided continuous stream flow data. Details of the measurement procedures have already been discussed in Section 3.2.5 of Chapter 3. In this analysis, streamflow values of quality code 38, 40, 58, and 60 were used. Total monthly streamflow data were prepared from the daily data where the total monthly streamflow data represents the end-month streamflow.

As discussed earlier in Section 3.2.5, the location of the Wybong Creek stream gauge 210040 is shown in **Figure 3.6**. The gauge is in lower part of the catchment, at $32.269266^0$S and $150.63788^0$E and an elevation 145m AHD. The catchment area for discharging water through the gauge is 675 $km^2$. The mean monthly streamflow data are shown in **Figure 7.6**.

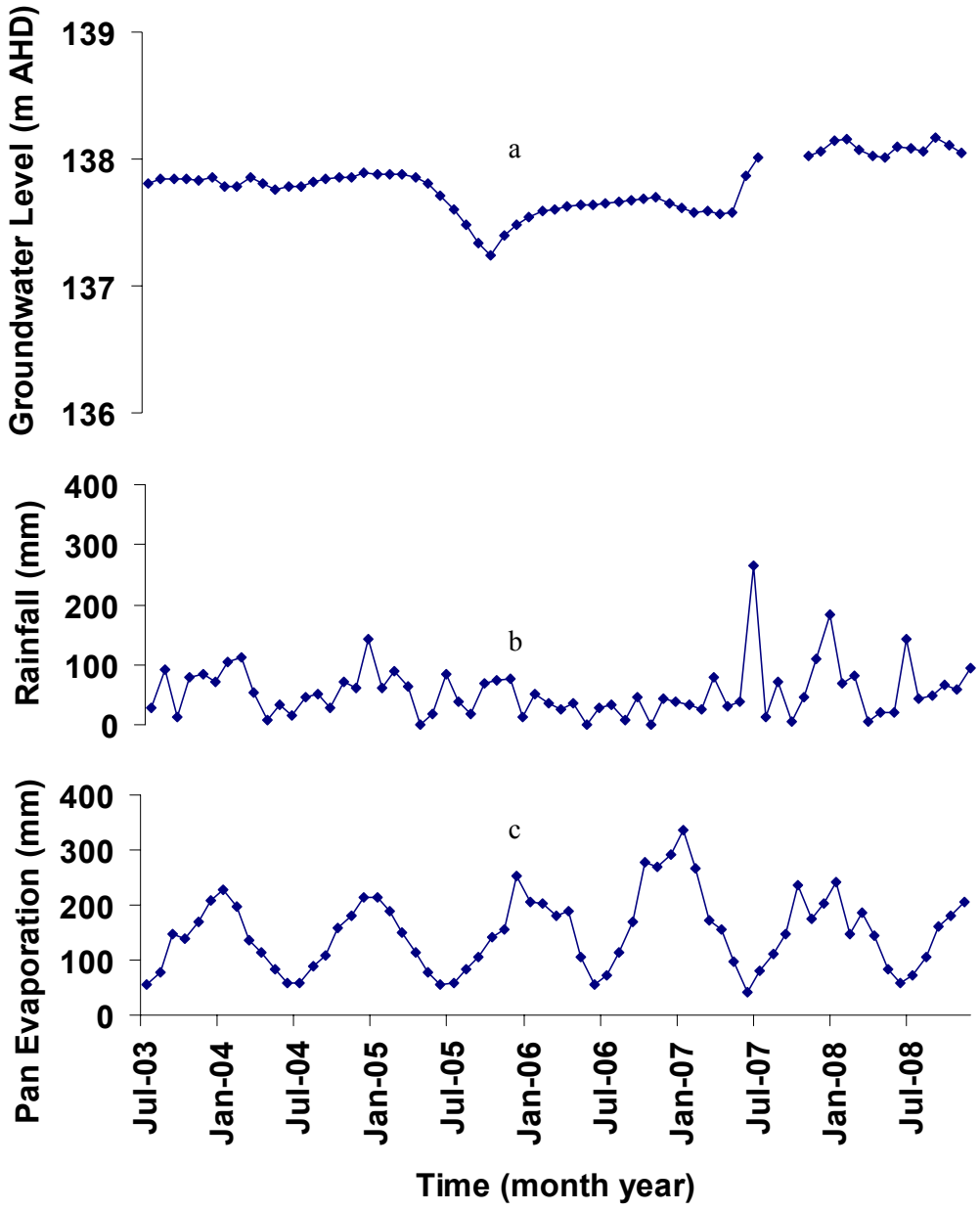


**Figure 7.4** Monthly values of **a.** Groundwater level for the Wybong Road bore (#080434), **b.** spatially averaged catchment monthly rainfall and **c.** spatially averaged catchment pan evaporation data

Bulga and Warkworth stream gauge and bores in the Wollombi Brook are shown in **Figure 7.3b.** The Bulga gauge is located in the mid-catchment within the Wollombi Coal Measures; the Warkworth gauge is located within the Whittingham Coal Measures (**Table 7.3**) which is about 2km upstream from the confluence with the Hunter River.

The catchment area for discharging water through the Bulga stream gauge is 1672 $km^2$ and Workworth stream gauge is 1848 $km^2$.

Streamflow data from 1973 to 2008 of Wybong and 1972 to 2008 for Wollombi were used for this modelling.

**Figure 7.5** Location of the Wybong stream gauge (station #210040) and Pressure sensors that measure stream height

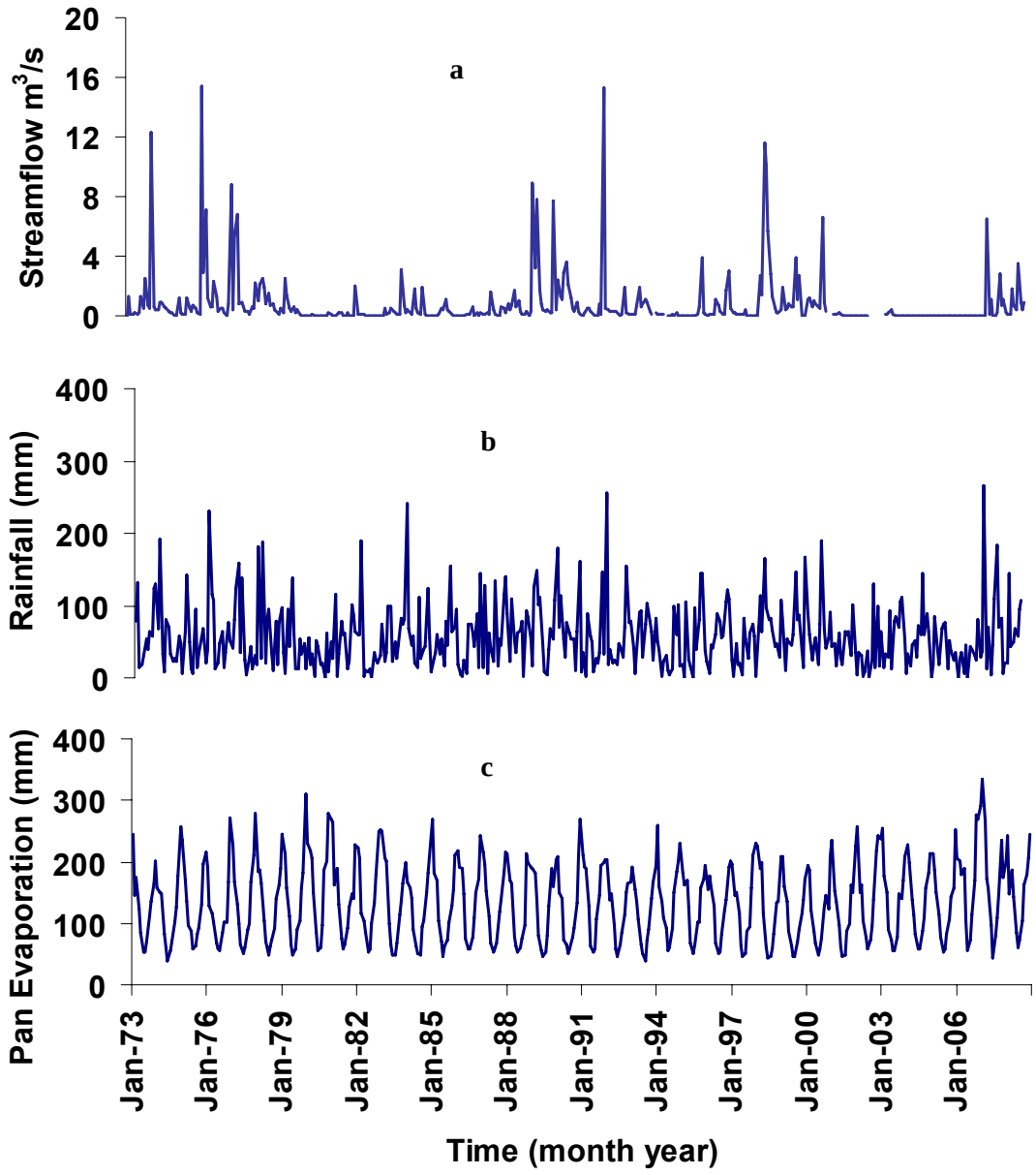


**Figure 7.6** Monthly values of **a.** Streamflow for Wybong stream gauge (#210040), **b.** spatially averaged catchment monthly rainfall and **c.** spatially averaged catchment monthly pan evaporation data

**Table 7.3** Stream gauge names, locations relative to the Global Positioning System (GPS), elevations relative to the Australian Height Datum (AHD)

| Stream gauge ID | Name | Longitude (ºE) | Latitude (ºN) | Elevation (m)(AHD) | Catchment |
|---|---|---|---|---|---|
| 210040 | Wybong gauge | 150.6487 | 32.2693 | 145 | Wybong |
| 210028 | Bulga | 151.0188 | 32.8192 | 56.49 | Wollombi |
| 210004 | Warkworth | 151.0319 | 32.57 | 47.75 | Wollombi |

### 7.3.3 Rainfall and Pan Evaporation

#### Rainfall

Monthly total rainfall data were obtained from the Bureau of Meteorology (BOM). Details of rainfall data preparation procedures were discussed in section 3.2.2. The monthly rainfall data were converted to a text file.

Possible sources of uncertainty in the rainfall data can give rise to errors in the order of 10% (Sharon, 1980). Monthly data are reasonably well determined from standard meteorological networks and are sufficient to resolve ecological and hydrological behaviour, particularly at spatial resolutions of a few kilometres (Hutchison, 1995a). The total monthly rainfall values were used to represent the end-of-month rainfall.

#### Pan Evaporation

Monthly totals for pan evaporation were obtained from the Bureau of Meteorology (BOM). Details of evaporation data preparation procedures were discussed in section 3.2.2. The monthly total pan evaporation data were converted into text file. The monthly total pan evaporation values were used to represent the end-of-month pan evaporation.

#### Rainfall and Pan Evaporation Correlation

The correlation between the rainfall and pan evaporation for the Wybong catchment was calculated to evaluate the possibility of model calibration problems that can arise if predictors (rainfall and pan evaporation) are correlated. **Figure 7.7** shows the correlation between monthly Rainfall and pan evaporation from 1972 to 2008.

The correlation coefficient between monthly rainfall and pan evaporation was small 0.073 and was not significantly different from zero. The coefficient of determination was $R^2$ = 0.0019 indicating that 0.19% of the variability in the pan evaporation was explained by variability in rainfall. Therefore, the correlation was small enough to be ignored in this research

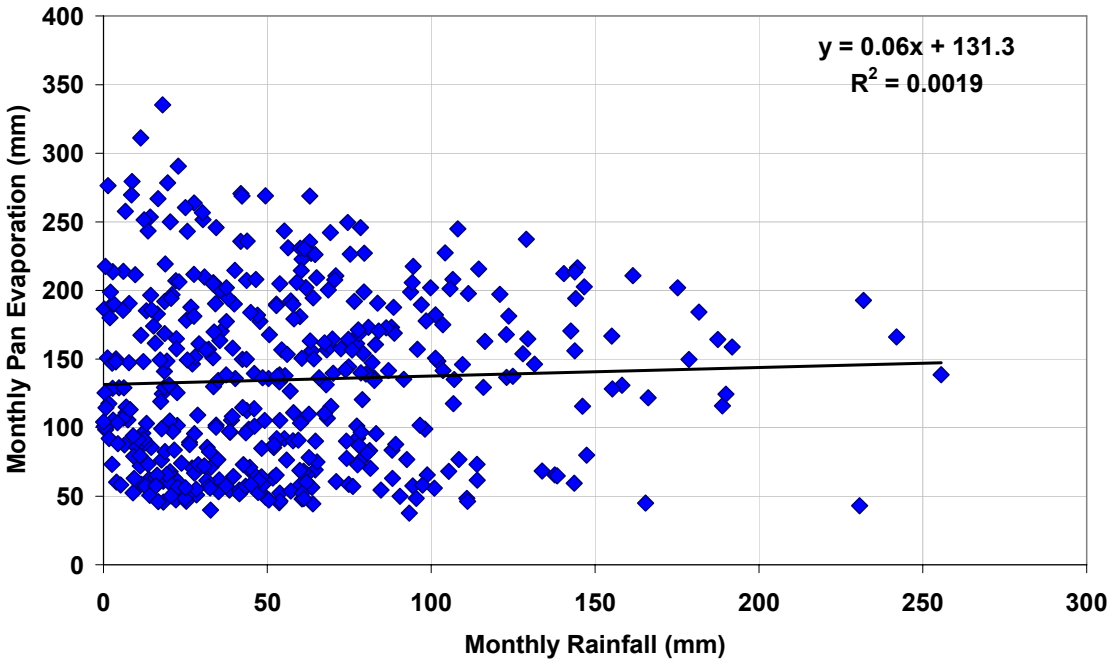


**Figure 7.7** The correlation between monthly spatially averaged rainfall from Bunnan gauge station #61007 and pan evaporation from Scone gauge station #61089 from 1972 to 2008

### 7.3.4 Spatial Thin-Plate Smoothing Spline Interpolation

As described in section 3.2.2.3 of chapter 3, each month of rainfall and pan evaporation data was spatially interpolated for estimating the rainfall and pan evaporation over the whole catchment. In order to include orographic effects, spline interpolated data were employed. If only the rainfall and pan evaporation data nearest to the streamflow gauge or groundwater piezometer are used to represent the whole catchment's rainfall and pan evaporation, underestimation of rainfall results due to orographic effects of higher elevation. Thin-plate smoothing splines are suitable for finding catchment rainfall and pan evaporation, particularly in ungauged catchments

(Jellett, 2005) so that groundwater levels can be simulated where there are no meteorological weather stations located at the groundwater bore sites.

## 7.4 The XG Model for Predicting Groundwater Level and Streamflow

The XG model has been shown to perform well (Xiong and Guo, 1999) in predicting monthly stream flow and groundwater level (Jellett, 2005) and is used here. The input data required by the model are monthly totals of rainfall and pan evaporation. The model output is monthly mean groundwater level and mean stream flow. **Figure 7.8** shows the various symbols used in the model for groundwater and streamflow.

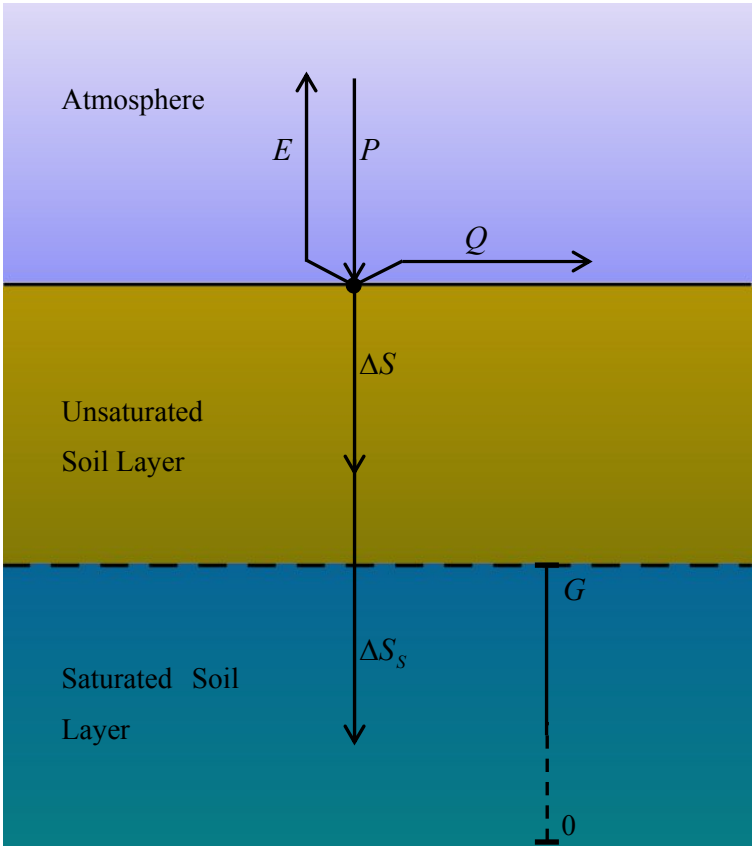


**Figure 7.8** Conceptual model used in the modify XG model, P=Precipitation, E=Evapotranspiration, Q = Runoff, $\Delta S$ = Unsaturated Soil layer, $\Delta S_s$ = Saturated Soil layer and G =Groundwater level (Jellett, 2005)

### 7.4.1 XG Model

The XG model (Xiong and Guo, 1999) assumes a single layer soil moisture store and requires monthly rainfall and pan evaporation data as inputs to estimate its two parameters, an evapotranspiration parameter and a runoff parameter. Guo *et al*. (2002) examined the performance of this model in predicting the impacts of climate change on streamflow in 70 large catchments in China. Xiong and Guo (1999) found that the two parameter model performed as well as a five-parameter model introduced by Guo (1992). In this thesis, a variation of the adapted by Jellett (2005) for groundwater XG model was tested for its ability to predict groundwater levels.

The assumptions of the XG model are that the soil and vegetation properties are stationary over time, rainfall and pan evaporation are the total over the entire month and the current month soil moisture content depends partly on the previous month's soil moisture content. Catchment properties are lumped spatially and temporally.

The XG model can be written as

$$E_t = \beta_E E_{pan_t} \tanh\left(\frac{P_t}{E_{pan_t}}\right) \tag{7.3}$$

$$Q_t = \left(S_{t-1} + P_t - E_t\right)\tanh\left(\frac{S_{t-1} + P_t - E_t}{\beta_Q}\right) \tag{7.4}$$

$$S_t = S_{t-1} + P_t - E_t - Q_t \tag{7.5}$$

where $E_t$ is the actual evapotranspiration (mm), $\beta_E$ is the dimensionless evapotranspiration parameter, $E_{pan_t}$ is the total pan evaporation (mm) in month t, $P_t$ is the total rainfall (mm) in month t, $Q_t$ is specific yield (runoff/catchement area, mm) in month t, $S_t$ is the unsaturated layer soil moisture content (mm) in month t and $\beta_Q$ is the runoff parameter (mm). $S_{t-1}$ is the soil water storage in the previous month; t-1. The two model parameters are $\beta_E$ and $\beta_Q$.

The evapotranspiration parameter $\beta_E$ is a positive number that converts pan evaporation to actual evapotranspiration. It has been found to have values from 0.7 to 1.3 in China (Xiong and Guo. 1999).

Equation 7.4 estimates the specific yield $Q_t$ given the previous month's soil moisture content, and the current month's rainfall, pan evaporation and the runoff parameter $\beta_Q$. The runoff parameter $\beta_Q$ can be thought of as the depth of soil in which moisture is stored. For large $\beta_Q$, runoff is small. Xiong and Guo (1999) found values of $\beta_Q$ ranging from 500mm to 2000mm for selected catchments in China.

Guo *et al*. (2002) demonstrated that the soil moisture content $S_t$ in the XG model cannot exceed $0.278\beta_Q$ hence the runoff parameter $\beta_Q$ does not represent the soil moisture capacity but is related to it and is proportional to the soil moisture capacity.

### 7.4.2 Extensions to the XG Model

The XG model was designed to predict streamflow. Jellett (2005) further developed the model to predict groundwater level *G* using a lagged model.

#### Recharge Model

The first recharge model assumes that the recharge to the saturated layer is a fraction of the infiltration to the unsaturated layer:

$$\Delta G_{t+L} = \frac{1}{\beta_G}\Delta S_t \tag{7.6}$$

where $\beta_G$ is the groundwater parameter (mm $m^{-1}$) that depends on both the soil porosity and the fraction of water that moves between the unsaturated and saturated soil layers. *L* is the time lag (months). Equation 7.6 linearly correlates the change in groundwater level with the change in soil moisture content $L$ time steps ago.

The saturated soil moisture content is not explicitly calculated here since the soil porosity relating the groundwater level and saturated soil moisture content is not known.

Changing the subject of Equation 7.5 gives:

$$\Delta S_t = P_t - E_t - Q_t \tag{7.7}$$

Substituting Equation 7.6 into Equation 7.7 gives Recharge Model:

$$G_{t+L} = G_{t+L-1} + \frac{1}{\beta_G}(P_t - E_t - Q_t) \tag{7.8}$$

Where $G_{t+L-1}$ is the groundwater level in the previous month.

### 7.4.3 Improvements of the XG Monthly Streamflow Model

This study processes some improvement of this model which can improve its physics and its agreement with measured streamflow without any additional parameters (White *et al*., 2007). The Wybong and Wollombi Brook catchments studied in this work have long dry periods with very low and even zero streamflow. The XG model was developed for predicting streamflow in regions with more reliablr streamflows. It is shown in the following that when rainfall is low, the XG model assumes that evaporation is sourced from rainfall so that in months with zero rainfall as can occur in Australia evaporation is also zero. This physically makes no sense since catchment evaporation is sourced from the soil. In the following a modification to the model is proposed to give more realistic estimates of the $\beta_e$ evaporation parameter for long dry periods.

For small values of $(S_{t-1} + P_t - E_t)/\beta_Q$ , equations 7.4 becomes

$$Q_t \approx \frac{(S_{t-1} + P_t - E_t)^2}{\beta_q} \tag{7.9}$$

While for large values

$$Q_t \approx (S_{t-1} + P_t - E_t) \tag{7.10}$$

The soil moisture storage at the end of the month, $S_t$ follows from mass balance in Equation 7.5. The relationship between streamflow and the current soil water storage follows from Equation 7.5, 7.9 and 7.10. For large $(S_{t-1} + P_t - E_t)/\beta_Q$

$$Q_t \approx \frac{S_t}{2} \tag{7.11}$$

and for small values

$$Q_t \approx \frac{\beta_q - 2S_t \pm \sqrt{\beta_q(\beta_q - 4S_t)}}{2} \tag{7.12}$$

It appears that the negative sign of the square root term is physically preferred

$$Q_t \approx \frac{\beta_q - 2S_t - \sqrt{\beta_q\left(\beta_q - 4S_t\right)}}{2} \tag{7.13}$$

As described in Section 7.4.1, $S_t$ cannot exceed $0.278\beta_q$. For large $\beta_q$, Equation 7.13 shows that $S_t$ cannot exceed $0.25\beta_q$. For many of the $\beta_q$ values found by Guo *et al.* (2002), the quadratic Equation 7.13 or Equation 7.9 fits the stream flow very well.

**Problems with the Evaporation Component of the XG Model**

For large rainfalls $P_t >> E_{pan}$ and Equation 7.3 becomes:

$$E_t = \beta_e E_{pan_t} \tag{7.14}$$

In Equation 7.14 the evaporation parameter $\beta_e$ should be the well-known pan factor which is typically less than 1 and usually around 0.7. However, in the XG model $\beta_e$ is often greater than 1. This occurs because the XG model has problems in fitting streamflow for low rainfalls.

For low rainfalls $P_t << E_{pan_t}$ the model assumes that actual evaporation is sourced from rainfall so that

$$E_t \approx \beta_e P_t \tag{7.15}$$

In the limit of zero rainfall for any month, Equation 7.15 predicts that $E_t$ is also zero. This physically makes no sense since evapotranspiration is sourced from soil water and $E_t$ is only zero when soilwater is zero, which is seldom the case. In order to accommodate the fact that evapotranspiration relies on soil water, the value of $\beta_e$ has to be greater than 1 in the XG model for small rainfalls.

**Improvements to the XG Model**

The physics of the two parameter XG model can be improved if evaporation from the soil is included in the evaporation term Equation 7.3:

$$E_t = \beta_e E_{pan_t} \tanh\left[(P_t + S_{t-1}) / E_{pan_t}\right] \tag{7.16}$$

with $S_{t-1}$ the previous months soil water store. This is physically a compromise since the actual evaporation must depend on the current soil water store. However it would

involve an iterative procedure since $S_t$ is found from the mass balance Equation 7.5. The inclusion of an extra parameter in the tanh function of the from $P_t + fS_{t-1}$ does not improve the fit of predicted groundwater flow but the inclusion of $S_{t-1}$ improves the fit of the model to streamflow.

It is noted that with the inclusion of the previous months soil water storage for large rainfalls $E_t = \beta_e E_{pan_t}$ as in Equation 7.15, $\beta_e$ has now physically more realistic values less than 1, and for low rainfalls:

$$E_t \approx \beta_e (P_t + S_{t-1}) \tag{7.17}$$

or in terms of the current month's soil water store:

$$E_t \approx \frac{\beta_e (S_t + Q_t)}{1 + \beta_e} \tag{7.18}$$

or if we use the low rainfall estimate for $Q_t$ in Equation 7.13

$$E_t \approx \frac{\beta_e \beta_Q \left(1 - \sqrt{\left(1 - 4S_t / \beta_Q\right)}\right)}{2(1 - \beta_e)} \tag{7.19}$$

**Fitting the $\beta_e$ parameter**

Here a way is suggested of fitting $\beta_e$ to attempt to ensure overall mass balance.

The long term mass balance of a catchment is given by:

$$\Sigma E_t + \Sigma G_t = \Sigma P_t - \Sigma Q_t \tag{7.20}$$

with $\Sigma G_t$ the deep seepage loss that does not appear as streamflow. To a first approximation, we can set $\Sigma G_t = 0$, so $\Sigma E_t = \Sigma P_t - \Sigma Q_t$. The value of $\beta_e$ is then chosen to ensure this overall mass balance.

The disadvantage with this method is that it involves an iterative process since the value of $S_{t-1}$ depends on estimates of $Q_t$ which in turn relies on the value of the parameter $\beta_q$ and the starting estimate of initial soil water storage, $S_0$. One way round this is to use the measured values of $Q_t$ to estimate $S_{t-1}$.

### 7.4.4 Stream Flow Prediction

The XG Recharge model predicts runoff as well as groundwater level (Jellett, 2005). From the runoff, streamflow can be estimated.

Streamflow $W_t$ ($m^3s^{-1}$) was calculated from runoff $Q_t$ (mm in month t) using Equation 7.21

$$W_t = \frac{\beta_A Q_t}{M_{j(t)}} \tag{7.21}$$

where *j(t)* is the Gregorian month (1 to 12) of time *t* of the data set, $M_{j(t)}$ (s) is the number of seconds in Gregorian month *j(t)* parameter and $\beta_A$ ($m^3$ $mm^{-1}$) is the streamflow parameter. The streamflow parameter is equal to the catchment area ($km^2$) multiplied by 1000 (to convert area from $km^2$ to $m^2$ and then runoff from mm to m) multiplied by the fraction of water leaving the catchment through the stream as opposed to that leaving the catchment as groundwater flow.

## 7.5 Summery of the Modified XG Model

The XG model is a two parameter monthly water balance model for predicting runoff in the catchment. The XG model assumes a single layer soil moisture store and requires monthly rainfall and pan evaporation data as inputs to estimate its two parameters, an evapotranspiration parameter and a runoff parameter. The assumptions of the XG model are that the soil and vegetation properties are stationary over time, rainfall and pan evaporation are the total over the entire month and the current month soil moisture content depends partly on the previous month's soil moisture content. Catchment properties are lumped spatially and temporally.

The advantage of the model includes its statistically sound testing procedures which are used to find the model parameters efficiently. Measurement of the hydraulic conductivity of the alluvial aquifer is not required in the modified XG model. The XG recharge model can predict stream flow accurately after being calibrated on a limited subset of groundwater level data. This is particularly useful because the model can be used to estimate recharge in areas where there are stream flow data but insufficient ground water level data. The next Chapter will discuss details of testing the XG model and discussion its suitability.

# CHAPTER 8: MODEL TESTING FOR STREAMFLOW AND GROUNDWATER LEVEL

This Chapter presents a discussion of parameter estimation for the XG and the modified XG model and the results of model testing and application of the model. *Hv-block* cross-validation has been used for model testing in this research (See Jellett, 2005).

## 8.1 Parameter Estimation

Model parameters for the modified XG model (Jellett, 2005) were estimated from the available groundwater level, streamflow data and the input data, rainfall and pan evaporation using a calibration procedure. The calibration procedure involved numerous executions of the model with different combinations of parameter values to arrive at the parameter set that offered the best agreement, as measured by goodness-of-fit between observed data and predicted values.

## 8.2 Goodness-of-fit

In order to objectively determine the level of agreement between observed data and the predicted values, a goodness-of-fit index was required. The coefficient of determination or $R^2$ value was used in this research as it has been widely used in statistical regression and in hydrological literature (e.g. Nash and Sutcliffe, 1970). The definition of $R^2$ (Neter *et al*., 1996) is

$$R^2 = 1 - \frac{SSE}{SST} \tag{8.1}$$

where *SSE* is the Residual Sum of Squares and *SST* is the Total Sum of Squares

$$SSE = \sum_{t=1}^{N} \left( Y_t - \hat{Y}_t \right)^2 \tag{8.2}$$

$$SST = \sum_{t=1}^{N} \left( Y_t - \overline{Y}_t \right)^2 \tag{8.3}$$

where $N$ is the length of the data record; $Y_t$ is the observed data at time $t$; $\hat{Y}_t$ is the predicted values data at time $t$; and $\overline{Y}$ is the mean of the observed response data.

The model can be written as:

$$Y_t = f_t(X_t;\beta) + \varepsilon_t \tag{8.4}$$

where $f_t$ is a prescribed function of the independent predictors $X_t$ and the model parameters $\beta$. The residuals $\varepsilon_t$ contain both model structural errors and data measurement errors. Once the model parameters have been estimated as $\hat{\beta}$, the predicted response is given by

$$\hat{Y}_t = f_t(X_t;\hat{\beta}) \tag{8.5}$$

For a linear model ($f_t$ is a f linear function in $\beta$), the range of $R^2$ is $0 < R^2 \leq 1$ and this is equal to the squared correlation between observed and predicted response data where the coefficient of correlation, r, is defined as (Neter *et al*., 1996)

$$r = \sqrt{\frac{\sum(\hat{Y}_t - \overline{Y})^2}{\sum(Y_t - \overline{Y})^2}} \tag{8.6}$$

$$r_{linear} = \sqrt{R^2} \tag{8.7}$$

The $R^2$ value of a linear model is equal to the squared correlation between observed and predicted response data. An $R^2$ of 1 indicates a perfect fit between the observed and predicted response data. A negative $R^2$ indicates that the fit is worse than predicting the observed response data with its mean value.

Maximising $R^2$ is equivalent to the ordinary least squares procedure of minimising the residual sum of squares *SSE* except that maximising $R^2$ can be used when the total sum of squares *SST* changes during calibration. This feature was required in this research as time lag was a parameter of the models. When the time lag is increased, the number of points available for calibration is decreased; hence the total sum of squares is decreased (Jellett, 2005).

The root mean square error *RMSE* was also used in this research (Hjorth, 1994)

$$RMSE = \sqrt{\frac{SSE}{N}} \tag{8.8}$$

where $N$ is the number of data points and *SSE* is the residual sum of squares. The range is $0 \le RMSE < \infty$ with a value of 0 indicating a perfect fit. The *RMSE* was used in this research in preference to the standard deviation because the *RMSE* is used for cross-validation scores in the statistical literature (Hjorth, 1994).

The bias was also calculated (Neter *et al*., 1996)

$$b = \frac{1}{N}\sum_{t=1}^{N}\left(Y_t - \hat{Y}_t\right) \tag{8.9}$$

The range is $-\infty < b < \infty$. The bias gives an indication of whether or not the model is consistently over-predicting or under-predicting with a value of 0 indicating neither.

## 8. 3 Automatic Calibration Procedure

The calibration procedure used to locate the parameter set with the maximum $R^2$ value was made automatic with the use of a search algorithm also developed by Jellett (2005). The search algorithm used in this research was the Downhill Simplex Method (Nelder and Mead, 1965; Press *et al*., 1992). The downhill simplex method was used because of the small number of parameters in the models being tested and because this method has frequently been used in hydrological research (Xiong and Guo, 1999). A simplex is defined as a figure of $k+1$ vertices in the $k$-dimensional search space ($k$ parameters). A starting simplex is specified and then the simplex is expanded, contracted and reflected according to simple rules until it is within a specified distance from the maximum or until a specified number of function evaluations have been exceeded.

Once the search algorithm located an optimum, it was started again with a simplex around that point to confirm that the point was an optimum. In addition, multiple starting parameter sets were used to increase the confidence and the optimal parameter set found was global rather than local. It was necessary in the calibration of some

models to place bounds on the parameter values to prevent overflow errors, where numbers become too large to be represented in the math processor of the computer.

## 8.4 Model Testing Methods

Split-sample validation has been used extensively in hydrological research (Guo *et al.*, 2002). The use of the word validation is not intended to imply that a model is a true representation of reality. The word 'verification' is often used in place of validation (Makhlouf and Michel, 1994; Xiong and Guo, 1999). In split-sample validation, the data are split into a calibration period and a validation period **(Figure 8.1)**. The model is calibrated over the calibration period, using then the parameter values thus obtained the goodness-of-fit is evaluated over the validation period. The best model is the one with the highest validation goodness-of-fit. This tests the persistence of model performance and gives an indication of the stationarity of model structure and the stationarity of the parameter values obtained during calibration. One problem with split-sample validation is that the choice of calibration and validation periods is left to the user who may introduce bias by choosing only the calibration and validation sets that give the highest goodness-of-fit values.

Cross-validation removed (Jellett, 2005) the bias of manual validation-period selection by calibrating and validating on many different subsets of the data. The simplest cross-validation method for independent data is leave-one-out cross-validation. In this, a point of data is left out of the calibration procedure and then the value at that point is predicted and compared with the observed value. This is performed for each point in turn in the data set. A cross-validation statistic is then calculated from these differences; usually the root mean square error (*RMSE*) is the calculated. Racine (2000) extended the cross-validation procedures to *hv*-block cross-validation which allows for consistent cross-validation using dependent data.

The *hv*-block cross-validation procedure (Racine, 2000) involves breaking the data into consecutive time blocks of data of size $B$ with the configuration shown in **Figure 8.2**. The model is calibrated on the data outside of the chosen block of size $B$ and validated on the validation data block of size $B$-2$h$ within the block of size $B$. Validating on blocks of data results in dependent error structures being preserved (Racine, 2000). Leaving a buffer of size $h$ each side of the validation data block removes dependence

between the calibration and validation period. The *hv*-block cross-validation procedure is asymptotically consistent for appropriately chosen block sizes, similarly to leave-k-out cross-validation (Racine, 2000).

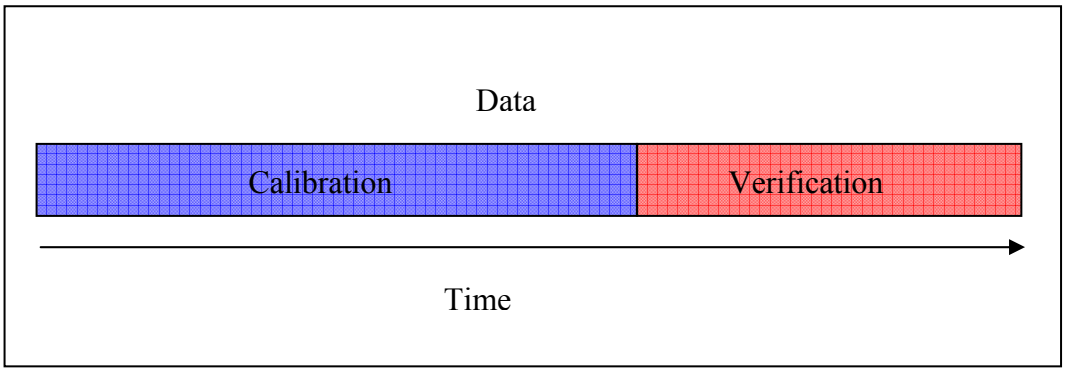


**Figure 8.1** Split-sample validation configurations of calibration and validation periods for dependent data

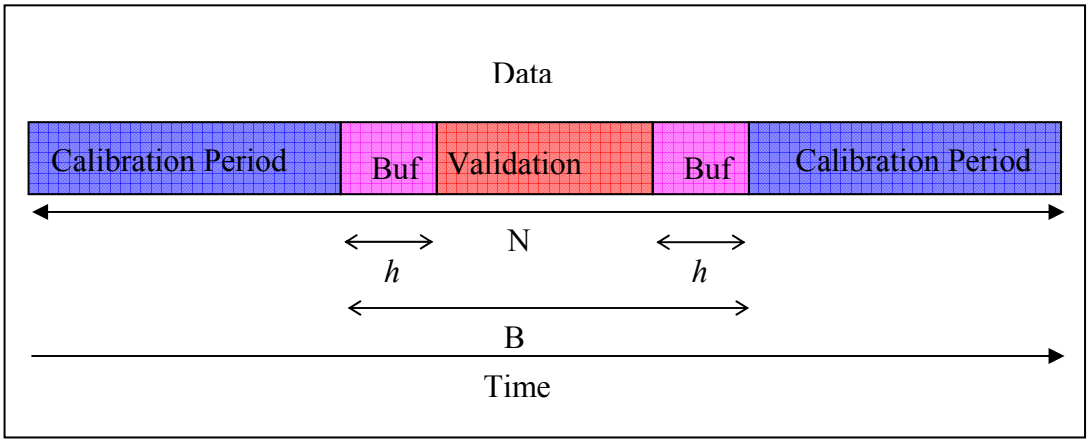


**Figure 8.2** *hv*-block cross-validation configurations of calibration, buffer and validation periods for dependent data

The blocks selected for analysis may overlap. For large data sets, the blocks may be chosen randomly with enough blocks chosen so as to generate useful statistics. For small data sets, every block of a particular size may be chosen. In this case the number of blocks is equal to the size of the data set *N* minus the block size *B* plus 1. The way cross-validation rewards simpler models is that an over-parameterised model will over fit in the calibration period, that is, random errors are modeled. When the model is

validated, the random errors will be different from the calibration random errors and hence a poor validation goodness-of-fit will result. In this way a balance is found between goodness-of-fit and model simplicity. Here *hv*-block cross-validation was employed due to its residual dependency and versatility.

## 8.5 Computer Program and Model Testing

The models, calibration and verification procedures and Monte Carlo (numerical simulation) procedures were all programmed (following Jellett, 2005) using an object-oriented approach. Source code and descriptions of the following modules and programs as follows:

**Modules**

| | |
|---|---|
| MthData | Contains an array of MthDataYr objects and routines to read and write the MthData format |
| StnData | Contains an array of monthly values and routines to read and write the StnData format |
| GWSystem | Contains StnData objects for rainfall, pan evaporation, groundwater level and streamflow, models |

**Main Program**

| | |
|---|---|
| Fitwbm | reads in data and runs the desired model on the data and saves the results |

Fitwbm has options allowing for monthly or weekly modes; different models; calibration on bore levels, streamflow and combinations of these; different starting values for optimal parameter search; different validation options including hypothesis testing, split-sample validation, cross-validation and bootstrapping. A sample Fitwbm log file is shown in appendix B.

### 8.6.1 Model Calibration

Mean monthly groundwater level, spatially interpolated rainfall and pan evaporation data and point rainfall and pan evaporation data, at monthly time scales, were examined in this section.

The XG model was calibrated and cross-validated on groundwater level data for each bore (see **Table 7.1**). The block sizes used for the cross-validation were calculated using

$$B = n - \frac{n}{\ln(n) - 1} \tag{8.10}$$

where $B$ is the total block size and $n$ is the number of monthly measurements of data. This satisfied the consistency criteria of *hv*-block cross-validation (Racine, 2000). The size of the buffer $h$ was

$$h=0.05B \tag{8.11}$$

which calculates $h$ as a fraction of the total block size (Racine, 2000). Since the data sets tested in this study were not particularly large, every block of the particular block size was included in the analysis, rather than randomly sampling the blocks.

### 8.6.2 Determination of Model Initial Values and Parameter Starting Values

The initial groundwater level $G_0$ and initial soil moisture content $S_0$ were calibrated as parameters in this study. The sample copy of Fitwbm log file is shown in Appendix C. Appropriate parameter starting values were estimated and used as the first vertex of the starting simplex in the parameter optimisation search algorithm. Starting distances to search around each parameter were also estimated and these determined the other vertices in the starting simplex. The number of times to start the model parameter optimisation search algorithm over again with a new starting simplex was also specified and a range for the time lag was selected. The values used for the parameter starting values for each bore appears in the model command files. Jellett (2005) found that the identified optimal parameter values were not sensitive to initial estimates. After calibration using the whole data set, the time lag was fixed at the optimal value and the optimal parameter values were used as starting values for the calibration periods in the cross-validation procedure.

### 8.6.3 Bounds on Parameter Estimates

Bounds were placed on some parameters when calibrating the XG model to force some parameters to be positive. This ensured the absence of 64- bit numerical overflows and also ensured that the models made physical sense. The bounds were programmed in the computer code by making the $R^2$ function return a value of –9999.0 when a parameter value to be tested was negative. Bounds were able to be placed on the parameters because the downhill simplex optimization method did not rely on function derivative (Jellett, 2005).

### 8.6.4 Values of the Cross-Validation Root mean Square Error

The cross-validation root mean square error *RMSE* (C.V.) for each groundwater bore was calculated from:

$$\mathrm{RMSE_i(C.V.)} = \sqrt{\frac{\sum_j SSE_{i,j}}{\sum_j n_{i,j}}} \tag{8.12}$$

where $i$ is the bore number, $j$ is the cross-validation block number; and $n_{i,j}$ is the is the number of non-missing data points in groundwater bore $i$, cross-validation block $j$ minus the time lag. The best performed model has the smallest *RMSE*(C.V.) value.

## 8.7 Model Testing Results

### 8.7.1 Groundwater Level Prediction

XGR model was calibrated using the available groundwater elevation data from July 2003 to 2008 (**Table 7.1**) using the adjusted $R^2$ value as the goodness of fit criterion. The model was fitted using spatially interpolated monthly rainfall and evaporation data for the catchment. **Table 8.1** shows the $R^2$ values and parameters of the model for predicted monthly groundwater level of government monitoring bores within the Wybong catchment.

The model was calibrated using groundwater level data from July 2006 to end of December 2008 for monitoring bores within the Wybong catchment and also for the unconfined bore in unconsolidated sediments (Wybong Road bore, #080434), which

had a longer time record (July 2003 to December 2008). The analysis here concentrates on bore #080434 where the split-sample cross-validation method gave $R^2 = 0.64$ for this bore and a validation $R^2 = 0.96$ for a time lag of 0 month. This zero month lag demonstrates that unconfined aquifer responds quickly to rain. The other much bores in **Table 8.1**, despite reasonable hv-block and split-sample cross-validation calibration $R^2$ values gave poor validation $R^2$ values. Comments on the values of the parameters in **Table 8.1** are given in Section 8.7.1.3 below.

**Table 8.1** Calibration and validation results for the XGR model for predicting groundwater level. Calibration $R^2$ values in black are for the hv-block cross-validation while those in blue are for the split-sample cross-validation method

L = Lag time, $G_o$ = initial ground water height, $S_0$ = initial soil moisture, $\beta_Q$ = run-off parameter, $\beta_E$ = evapo-transpiration parameter, $\beta_G$ = ground water parameter and C.V.=cross validation

| BoreID | Calibration | | | | | | | | C.V. | |
|---|---|---|---|---|---|---|---|---|---|---|
| | L (month) | $G_0$ (mAHD) | $S_0$ (mm) | $\beta_Q$ (mm) | $\beta_E$ | $\beta_G$ (mm/m) | Cal $R^2$ | RMSE (m) | RMSE (m) | Val $R^2$ |
| 080944 | 2 | 162.54 | 1.0 | 12032 | 0.73 | 577 | 0.96<br>0.85 | 0.06 | 2.4 | <br>0.12 |
| 080945 | 1 | 141.70 | 2150 | 206139 | 0.56 | 291 | 0.93<br>0.89 | 0.10 | 4.1 | <br>0.48 |
| 080946 | 0 | 137.31 | 1379 | 143728 | 0.76 | 326 | 0.95<br>0.88 | 0.026 | 3.2 | <br>0.21 |
| 080947 | 1 | 141.87 | 445.2 | 19755 | 0.69 | 301 | 0.93<br>0.83 | 0.075 | 3.7 | <br>0.23 |
| 080948 | 3 | 144.04 | 1.0 | 4779 | 0.89 | 674 | 0.97<br>0.81 | 0.033 | 0.535 | <br>0.27 |
| 080434 | 0 | 137.82 | 1693 | 385820 | 0.99 | 476 | 0.83<br>0.64 | 0.12 | 0.41 | <br>0.96 |

A significant drawdown in measured groundwater level occurred for bore #0809434 from August to December in 2005 **(Figure 7.4a).** The drawdown and recovery of the groundwater level was independent of rainfall or streamflow, suggesting that nearby groundwater abstraction during the drought caused the decline in water level. Unfortunately there are no records of how much groundwater was abstracted from

any bore in the catchment. Because of this perturbation, these 5 months of data were removed from the data set (**Figure 8.3**) and the model was recalibrated. The model for this filtered data set gave a calibration of $R^2$ value of 0.83 and Validation $R^2$ of 0.46 but still with a zero month time lag. **Figure 8.3** compares the fitted calibration model with hv-block cross-validation of the bore at Wybong Road (#0809434) with the measured, filtered data set.

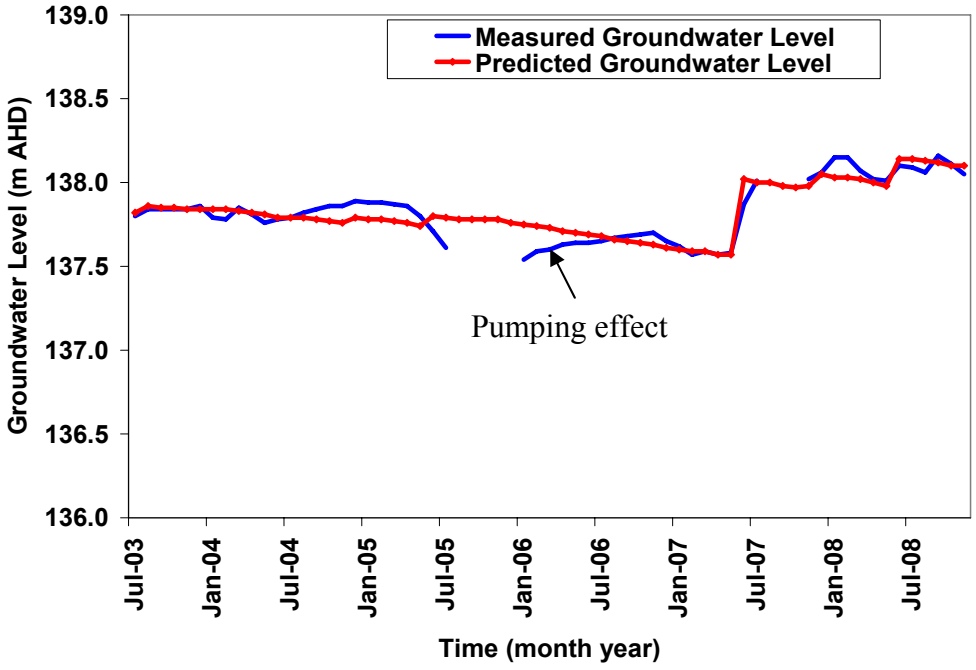


**Figure 8.3** Measured and predicted groundwater level data from 2003-2008 for bore Wybong Road bore (#0809434) with hv-blocks cross-validation, $R^2$ (Cal) =0.83

During the calibration phase, all the groundwater bores in **Table 8.3** gave high values of $R^2$ under hv-block cross-validation with time lags varying between 0 and 3 months. These time lags seem reasonable. For example for the semiconfined bore in consolidated material, Ridgeland Road bore (#080944), lies within the Narrabeen Group conglomerate with fractures from 24-26 m and a yield of about 5 L/s. A dense, 0-8 m thick and relatively impervious smectitic clay mantle overlies the Narrabeen Group rocks adjacent to Wybong Creek, and this layer confines the fractured conglomerate aquifer beneath. Using data from 2006 to 2008, when standing water level varied between 7 and 10 m the estimated recharge lag time was 2 months suggesting that

recharge may be from the escarpment nearby. This illustrates the longer time necessary for rainfall to recharge the semi-confined aquifer compared to the unconfined aquifer.

Some of the fitted parameter values in **Table 8.1** appear to be physically realistic, however, $\beta_Q$ values for all bores are much higher than the range of 500 to 2000 mm found for catchments in China by Xiong and Guo (1999). It is noted that despite the good calibration $R^2$ for all bores in **Table 8.1**, the validation $R^2$ for all bores except 08090344, were very poor. More detailed examination of the physical parameters is given in Section 8.7.2.1.

The relative bias calculated by Equation 8.13, given by the XG Recharge model for each bore was 0.0000. This indicates that there was no systematic over-prediction or under-prediction of groundwater levels by the XG Recharge model. **Figure 8.3** shows that the groundwater level for the #0809434 was under-predicted from 2004 (June) to 2005 (May), 2006 (August) to 2007 (January) and 2007 (October) to 2008 (April). Some over-prediction also occurred from the years of 2004 (January-February) and 2008 (June-September). This over prediction is almost certainly due to water extraction in these periods. Overall, the XG model gives reasonable predictions of both unconfined and confined aquifer bores; however, some adjustment of the model appears necessary for long dry periods.

#### 8.7.1.2 Statistical Test for Residuals

Statistical tests of normality, autocorrelation and constant variance of the XG Recharge model residuals for the Wybong Road bore (#080434) are presented here. These statistical tests are used to justify the use of hv-block cross-validation as the model selection procedure rather than hypothesis testing.

**Figure 8.4** and **8.5** shows the XG Recharge, Wybong Road bore (#080434) groundwater level residuals histogram and QQ-Plot respectively. In statistics, a Q-Q plot ("Q" stands for quantile) is a probability plot, which is a graphical method for comparing two probability distributions by plotting their quantiles against each other. The Shapiro-Wilk test for normality gave a P-value of 0.001 for the residuals. This indicated that residuals significantly deviated from normality at the 5% level of significance. At the 0.1% level of significance however, the residuals did not significantly deviate from normality.

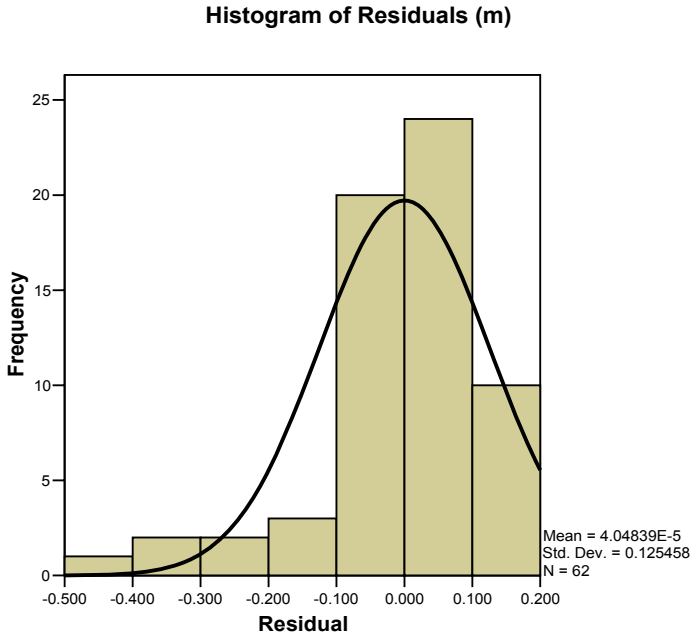


**Figure 8.4** Histogram of the residuals of the XGR model for the Wybong Road bore (#080434)

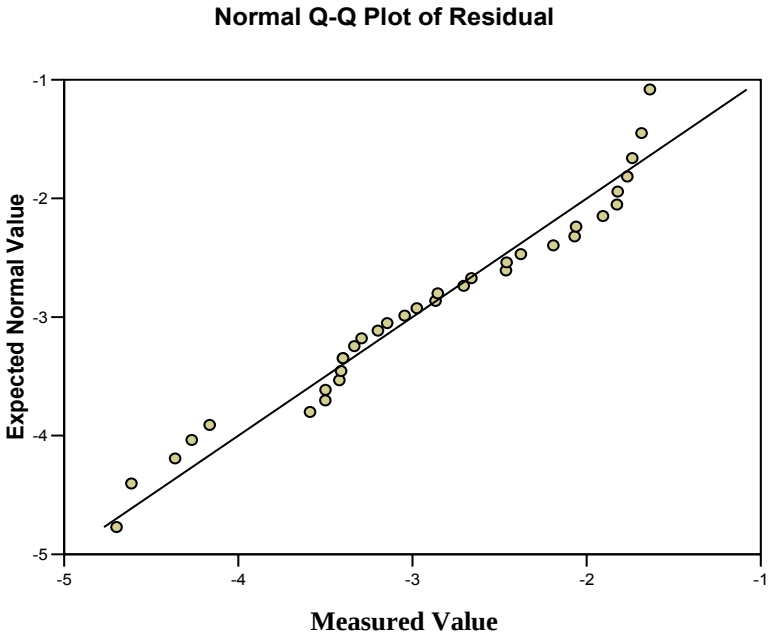


**Figure 8.5** Normal QQ-plot of the residuals of the XGR model for the Wybong Road bore (#080434)

**Figure 8.6** shows the autocorrelation of time lag 1 is 0.313 for the XGR model residuals for the Wybong Road bore #080434. This is inside of the Durbin-Watson confidence limits. This has a p-value of 0.00 and which indicates significant

autocorrelation at the 5% level of significance. This autocorrelation is due to the fact that groundwater level of the current month was dependent on the groundwater level of the previous month. The coefficient of determination $R^2$ = 0.361. Therefore 36.1% of the variability in the current residual was explained by variability in the previous residual.

**Figure 8.7** shows the residual as a function of predicted groundwater levels for the XGR model for the Wybong Road bore (#080434). The figure indicates that the variance of the residuals is constant. These tests indicated that the residuals are not normal, not independent and they are identically distributed.

The statistical test results were used to justify the use of hv-blocks cross-validation method as the model selection procedure rather than for hypothesis testing. The presence of autocorrelation in the residuals justified the use of hv-blocks cross-validation to test the significance of model performance.

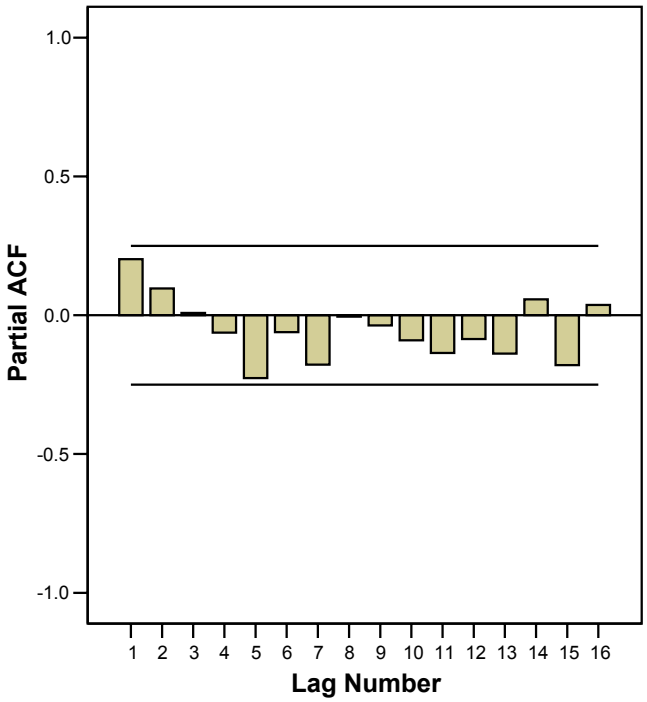


**Figure 8.6** Partial autocorrelation of the residual of the XGR model for the Wybong Road bore (#080434)

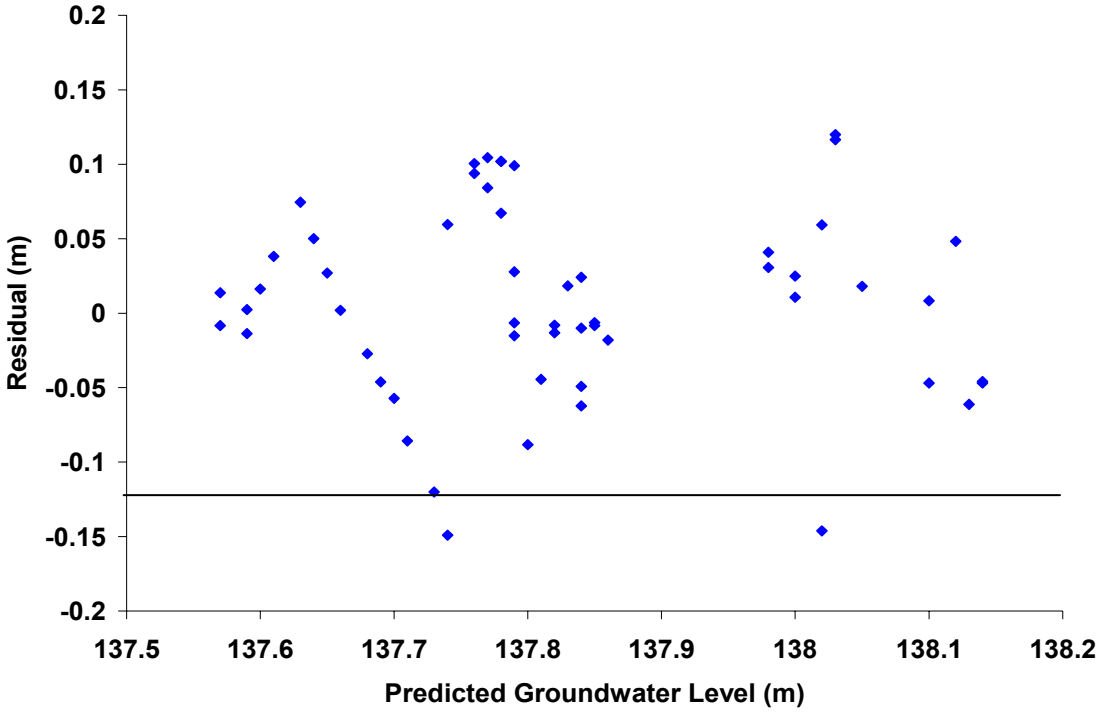


**Figure 8.7** Plot of the residual versus predicted groundwater levels using the XGR model for the Wybong Road bore (#080434)

### 8.7.1.3 Interpretation of Parameter Values

**Initial Soil Moisture**

It is noted that initial soil moisture content for the bore #080944 and #080948 is low. This appears due to the fact that the record started in the very dry year 2006.

**Time Lag**

The time lag that provided the best fit for Wybong Road bore (#080434) and Ridgeland Road bore (#080944) were 0 and 2 months respectively. The monthly groundwater level data was the mean monthly value as described in Section 7.31 of Chapter 7. This implies that the groundwater levels represent the mid-month groundwater levels. Both the rainfall and pan evaporation data used are monthly total values which imply the end-of-month values. Hence the model time lag of 2 months probably corresponded to a real time lag of 1 month. Therefore, on average it took between 0 and 2 months for the rainfall to affect the groundwater level for Ridgeland Road bore (#080944) and about 0.5 months for Wybong Road bore (#080434).

**Runoff Parameter**

Values of the runoff parameter, $\beta_{Q,}$ for all the bores in **Table 8.1** are greater than the range of values 500mm to 2000mm obtained by Xiong and Guo (1999) for catchments in China when the model was calibrated on streamflow alone. They are also greater than the values found by Jellett (2005) was calibrated on Orroral Valley bore in Australian Capital Territory (ACT). Some are much greater. For example, the value of the runoff parameter found for bore #080434 was 385820 mm. Such very large and physically implausible values indicate the problems the model was having in fitting the very low stream flows observed during the drought period when groundwater data was available.

**Evapotranspiration Parameter**

The range of evapotranspiration parameter, $\beta_{E,}$ for all the bores in **Table 8.1** ranged from 0.56 to 0.99 for the the Wybong Road bore (#080434). For China, Xiong and Guo (1999) found a range of 0.7 to 1.3 when the XG model was calibrated on streamflow. The range found here is physically more realistic since it means, under high rainfall periods that evapotranspiration can never exceed pan evaporation.

**Groundwater Recharge Parameter**

The range of values for the groundwater recharge parameter, $\beta_G$, in **Table 8.1** range from 291 to 577 mm $m^{-1}$, with $\beta_G$ = 476 mm $m^{-}1$ for the Wybong Road bore (#080434) was 476 mm m-1. This range is similar to the range of values of 21 to 579 mm $m^{-1}$ obtained by Jellett (2005) when the XG model was calibrated on groundwater level in bores in the ACT. The results here suggest that a change of between 291 to 577 mm in the soil moisture storage would change the groundwater level by 1m after a time lag of between 0 and 3 months. The groundwater parameter dere has been assumed proportional to the porosity and inversely proportional to the fraction of water that moves between the unsaturated and saturated soil layers. In some cases macroporosity, a very small fraction of the porosity can be more important. When macroporosity is important, small changes in soil water storage can give rise to large changes in groundwater level.

**Actual Evapotranspiration and Unsaturated Soil Moisture Content**

The XG model can be used to estimate the mean actual monthly evapotranspiration using measured pan evaporation equation 7.3. The change in soil moisture storage can then be estimated from equations 7.4 and 7.5. **Table 8.2** also shows the estimated actual mean monthly evapotranspiration and change in soil moisture storage predicted by the XGR model.

The estimate mean actual evapotranspiration values throughout the year in **Table 8.2** ranged from 21 mm/month to around 90 mm/month, or about 0.7 mm/day to 3 mm/day. Given the fact that these estimations covered a severe drought period, these are physically plausible. The period may through to September had low evapotranspiration while the period October to April had higher evapotranspiration. The mean change in soil moisture storage became progressively more negative through to May but was replenished in June when the change in soil moisture storage was a maximum. From there it progressively decreased again.

**Figure 8.8** show estimated actual evapotranspiration values from the XGR model versus time for bore# 80434. The measured rainfall and pan evaporation are also shown in this figure as these were used to calculate the actual evapotranspiration.

**Figure 8.9** shows calculated change in soil moisture storage content from the XGR model versus time for bore #80434. The measured groundwater level is also shown here for the comparison. The progressive decrease in the soil moisture storage to June 2007 is clearly evident in **Figure 8.9** as is the dramatic effect of the heavy rains in July 2007 and follow up rains in July 2008, showing the importance of winter rains for increasing recharge.

**Table 8.2** Estimated mean monthly actual evapotranspiration values and estimated mean change in soil moisture storage for bore #80434 calculated by the XGR1 model.

| Quantity | Month | | | | | | | | | | | |
|---|---|---|---|---|---|---|---|---|---|---|---|---|
| | 1 | 2 | 3 | 4 | 5 | 6 | 7 | 8 | 9 | 10 | 11 | 12 |
| Mean $E_t$ (mm) | 71 | 74 | 50 | 21.3 | 24.4 | 44.5 | 34.5 | 47.3 | 41.3 | 59.7 | 83.7 | 90.5 |
| Mean $\Delta S_t$ (mm) | 2.89 | -2.4 | -6.9 | -9.7 | -12 | 50.8 | 47.5 | 48.6 | 45.2 | 40.5 | 34.4 | 10.4 |

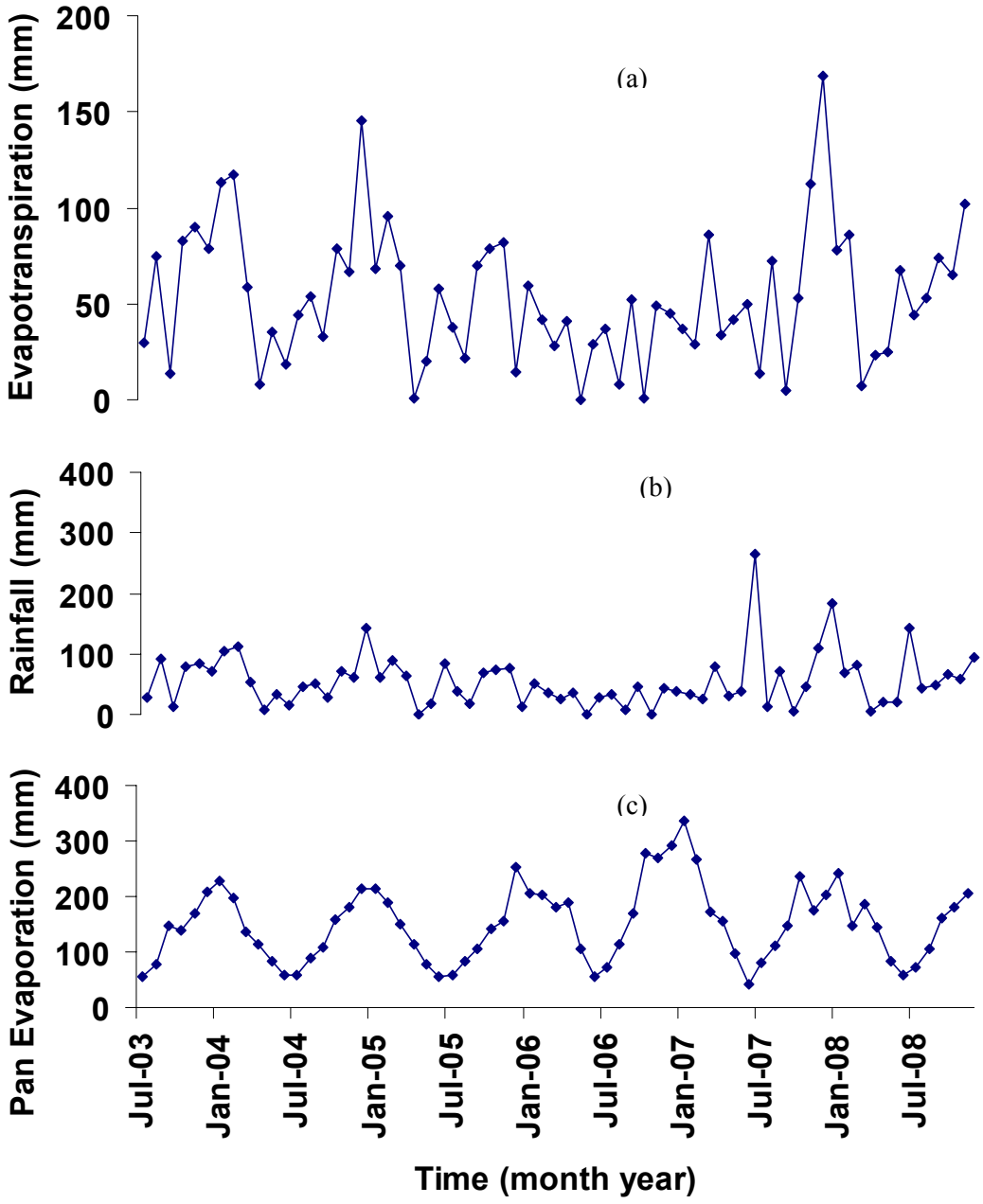


**Figure 8.8 a.** Modelled actual evapotranspiration using the XGR model for bore #80434, **b.** measured rainfall and **c.** measured pan evaporation

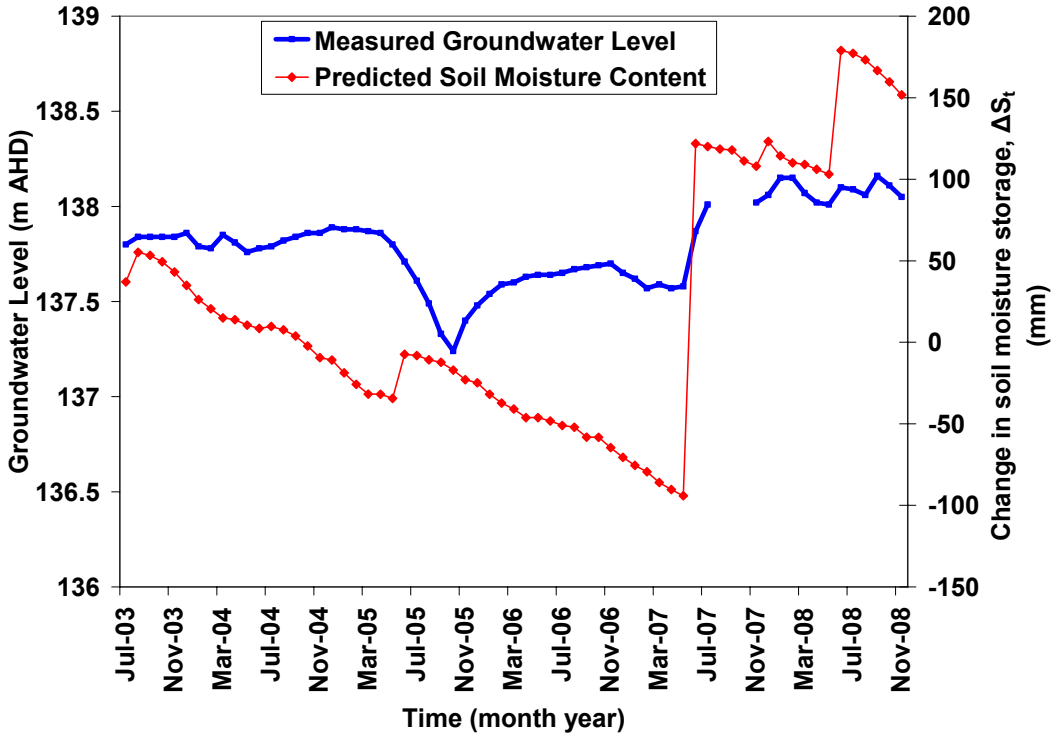


**Figure 8.9** Measured groundwater level and estimated change in soil moisture storage using the XGR model for bore # 80434

### 8.7.2 Model Application

This section presents practical applications of the XGR model. The XGR model has been claimed to be versatile, allowing for: use at different spatial scales; prediction of streamflow after calibration on groundwater level data; prediction of groundwater levels after calibration on streamflow data.

#### 8.7.2.1 Spatial Scale

The purpose of this section is to demonstrate that the XGR model may be used at different spatial scales. A comparison is given between model performance using monthly spatially interpolated rainfall and pan evaporation data, and uninterpolated point data of rainfall and pan evaporation compared for the Wybong Road bore (#080434). **Table 8.3** shows the parameter values and statistics for the XGR model at monthly time scales; uninterpolated (MU), spatially interpolated (MSI). The data used in this section were for the Wybong Road bore (#080434), and the uninterpolated data

came from Bunnan rainfall gauge (#61007) and Scone pan evaporation (#61089) from 2003 to 2008.

**Table 8.3** Parameter values and statistics for the XGR model for spatially interpolated and uninterpolated rainfall and pan evaporation data for 2003-2008

| ID | Calibration | | | | | | | | C.V. |
|---|---|---|---|---|---|---|---|---|---|
| | L | $G_0$ (m) | $S_0$ (mm) | $\beta_Q$ (mm) | $\beta_E$ | $\beta_G$ (mm $m^{-1}$) | $R^2$ | RMSE (m) | RMSE (m) |
| 080434 (MSI) | 0 | 137.82 | 1693 | 385820 | 0.99 | 475.55 | 0.83 | 0.12 | 0.41 |
| 080434 (MU) | 0 | 137.83 | 104.28 | 12968538 | 1.15 | 388.99 | 0.67 | 0.12 | 2.69 |

The best performing configuration with the smallest *RMSE*(C.V.) of 0.41m, is the monthly spatially interpolated data. The poor configuration with the largest *RMSE*(C.V.) of 2.69m, is the uninterpolated point data showing that the spatially interpolated data performed better than the uninterpolated point data. The possible reason for this is that the spatially interpolated data are more representative of the catchment region rainfall and pan evaporation across the whole catchment. An implication here is that interpolated rainfall and pan evaporation data can be used for estimating groundwater levels at monthly intervals where no local climate data are available. A large runoff parameter $\beta_Q$ indicates that runoff was modelled as unimportant in determining groundwater levels.

### 8.7.2.2 Prediction of Historic Groundwater Level

Groundwater levels in the past where no level data exists can be predicted by XGR model using the available rainfall and pan evaporation data**.** For predicting past historic groundwater levels, the model uses the calibrated parameters and initial values obtained for the measured data periods. **Figure 8.10** shows the results of predicting the groundwater level from 1973 to 2003 using the calibrated parameters and initial values of the data from July 2003 to December 2008 for the Wybong Road bore (#080434).

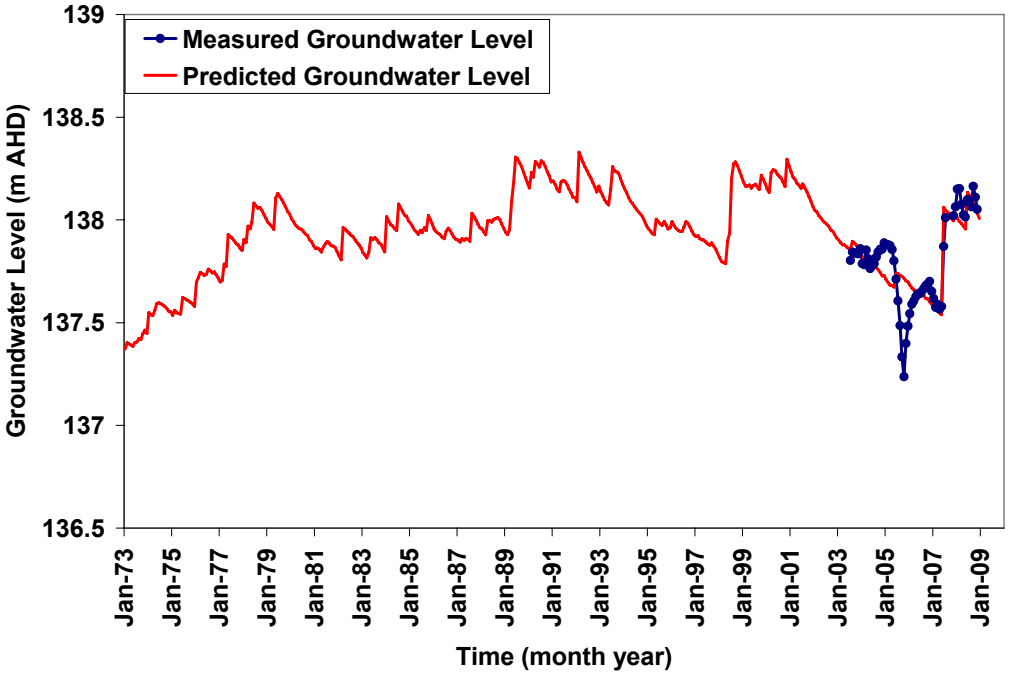


**Figure 8.10** Hisrtoric groundwater level predicted for Wybong Road bore (#080434) using the XGR model

### 8.7.2.3 Stream Flow Prediction

The model was also calibrated on streamflow data from Wybong Creek stream gauge at Yarraman from 1973 to 2008 using input data of the average rainfall of 3 stations surrounding the catchments and pan evaporation of the station Scone. The $R^2$ value found for predicted streamflow was 0.75. The model was also fitted on spatially interpolated monthly data of rainfall and evaporation as shown in **Table 8.4**. **Figure 8.11** shows the comparison between of the fitted model using the hv-blocks cross-validation for the 1990-2000 record of streamflow data and measured streamflow. The model was calibrated on streamflow data from 1990 to 1999 and verified using data from January to December 2000. The calibration $R^2$ value was 0.74 and the verification $R^2$ value was 0.86 giving a good model fit. However, a relatively poor $R^2$ (=0.69) value was obtained for the streamflow prediction during the full record 1973-2008. Despite this the model was able to predict streamflow reasonably well for the period 1990-9 but the fitted pan factor $\beta_E$ is greater than 1 in **Table 8.4**.

From equation 7.3 in chapter 7 it is expected that $\beta_E$ should typically be less than 1. This discrepancy arises due to fitting stream flow at low rainfall periods which are

typical for Australia. Essentially soil moisture deficiencies are large enough to significantly reduce run-off and, to compensate, the model adjusts the $\beta_E$ value. For Australian conditions it is clear that the evaporation component needs to be improved. Most under-prediction occurred most in summer (January 1996, February and December 1992) when storm cells delivered rainfall to the catchment, which were not captured measured in the point rain gauges. Over-prediction occurred in winter (June 1991, July 1993, 1998) possibly due to water extraction and/or groundwater losses. It is noted here that in the period 2000 to 2006 anomalous extraction may have occurred in the catchment. One of the advantages of the monthly spatial interpolation of rainfall used in this work is that it tends to smooth out local rainfall anomalies caused by small-scale thunderstorms.

Bias values were also calculated for evaluating whether the model is consistently over-predicting or under-predicting. The relative bias value found is 0.03 for the predicted streamflow during 1990-2000 as shown in **Table 8.4**. This means an average of 3% under prediction of the streamflow.

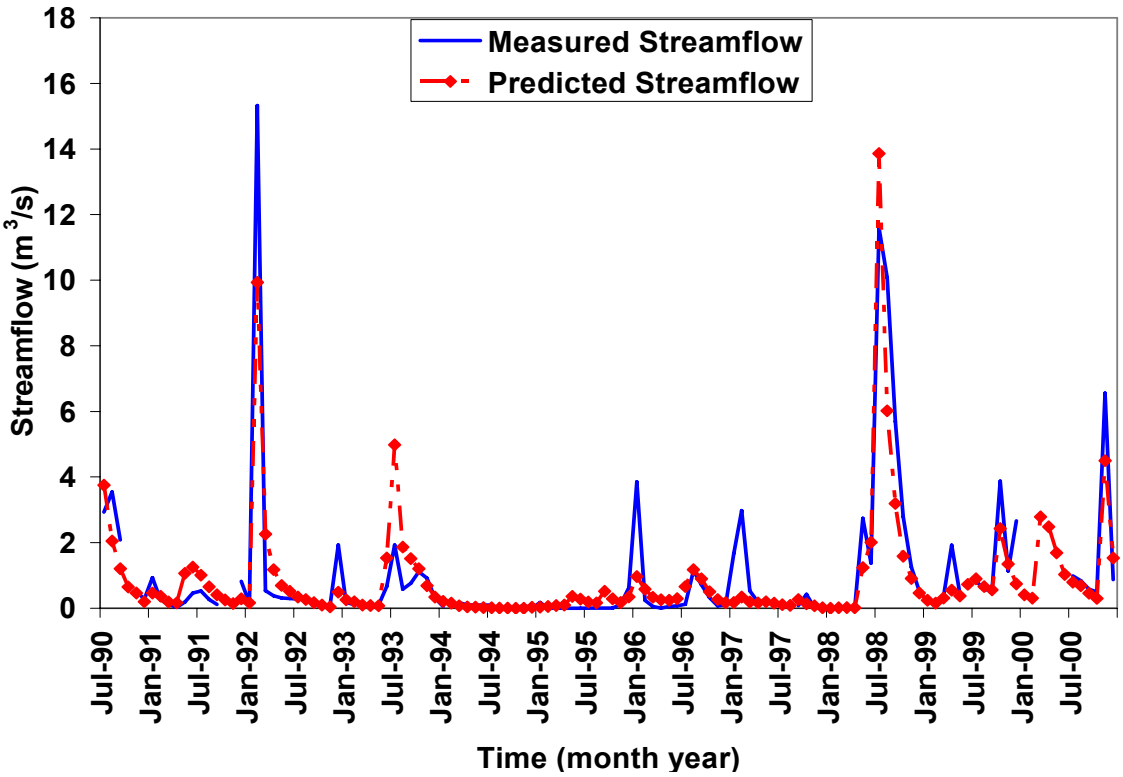


**Figure 8.11** Measured and predicted streamflow data for the period 1990-2000 using the hv-blocks cross-validation with $R^2$ (Cal) = 0.75 for the Wybong stream gauge (#210040)

**Table 8.4** Results of XGR model for predicting streamflow (SF) for Wybong (black and blue colour is for the Split-sample and hv-blocks cross-validation method respectively).

$S_0$ = initial soil moisture, $\beta_Q$ = run-off parameter, $\beta_E$ = evapo-transpiration parameter, MIP= monthly spatially interpolated data, MUIP =monthly un-interpolated data, Cv.=cross validation

| ID | Calibration | | | | | | | Verification |
|---|---|---|---|---|---|---|---|---|
| | $S_0$ (mm) | $\beta_Q$ (mm) | $\beta_E$ | (Cal) $R^2$ | Bias | Beta A | Stream fraction | (Val) $R^2$ |
| SF ( MIP 1990-2000) | 56.63 | 224.85 | 1.11 | 0.74 | 0.03 | 383408 | 0.57 | 0.86 |
| Hv-block cross-valid | | | | 0.75 | | | 0.58 | |
| SF(MUIP1990-2000) | 41.62 | 189.57 | 1.09 | 0.75 | | | | |
| SF (1973-2008) | 15.81 | 136.79 | 1.07 | 0.63 | 0.30 | | 0.40 | 0.68 |
| Hv-block cross-valid | | | | 0.69 | | | 0.43 | |
| SF(MUIP1973-2008) | 20.08 | 199.98 | 1.08 | 0.63 | | | | |
| SF (1973-1999) | 15.82 | 141.85 | 1.08 | 0.62 | 0.12 | 255792 | 0.39 | 0.77 |
| Hv-block cross-valid | | | | 0.66 | | | 0.48 | |
| SF (2000-2008) | 1.0 | 162.49 | 1.09 | 0.82 | 0.35 | 266107 | 0.41 | 0.27 |
| Hv-block cross-valid | | | | 0.67 | | | | |
| SF(1973-2008) Mean rainfall of 3 st. | 41.62 | 189.57 | 1.09 | 0.75 | | | | |

**Figure 8.12** shows the results of cumulative predicted streamflow volume versus the cumulative measured streamflow volume. The $R^2$ obtained is 0.98. Therefore, the long term performance of the model in terms of catchment yield is surprisingly good.

The Calculated stream fraction value (by Equation 7.21 in Chapter 7) is 0.58 for the periods of 1990-2000 as shown in **Table 8.4**. This indicates that 58% of the total water leaving the Wybong catchment each month is streamflow while the remainder (42%) is groundwater flow. **Figure 8.13** gives an indication of the cumulative groundwater flow out of the Wybong versus time.

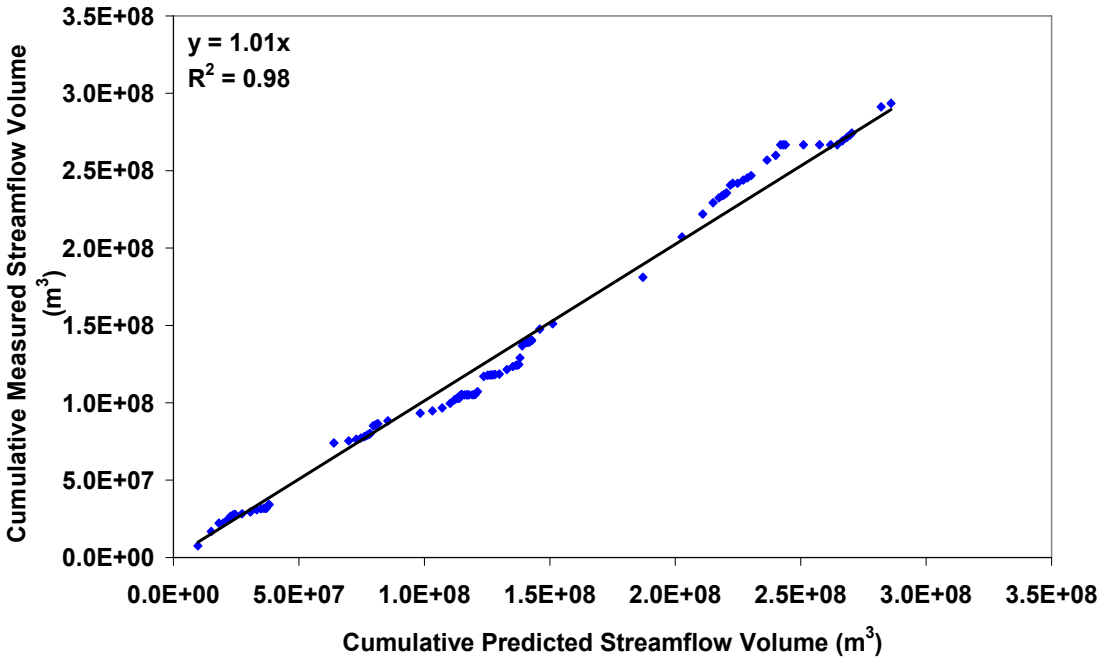


**Figure 8.12** Cumulative measured streamflow volume versus cumulative predicted streamflow volume of data from1990-2000

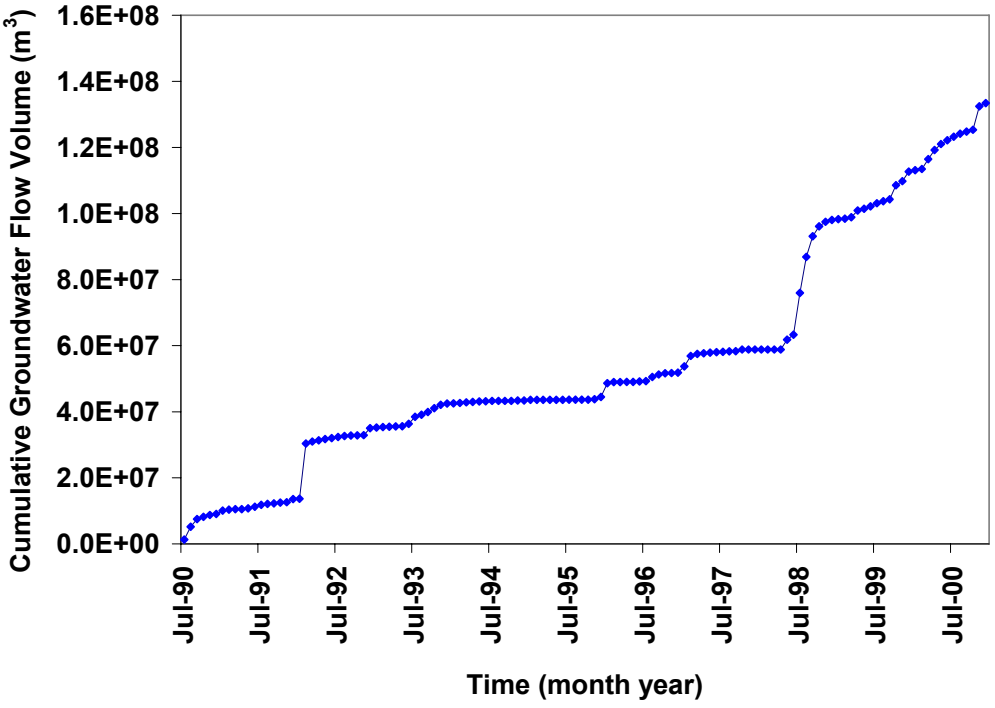


**Figure 8.13** Estimated cumulative groundwater flow out of the catchment for the period 1990-2000

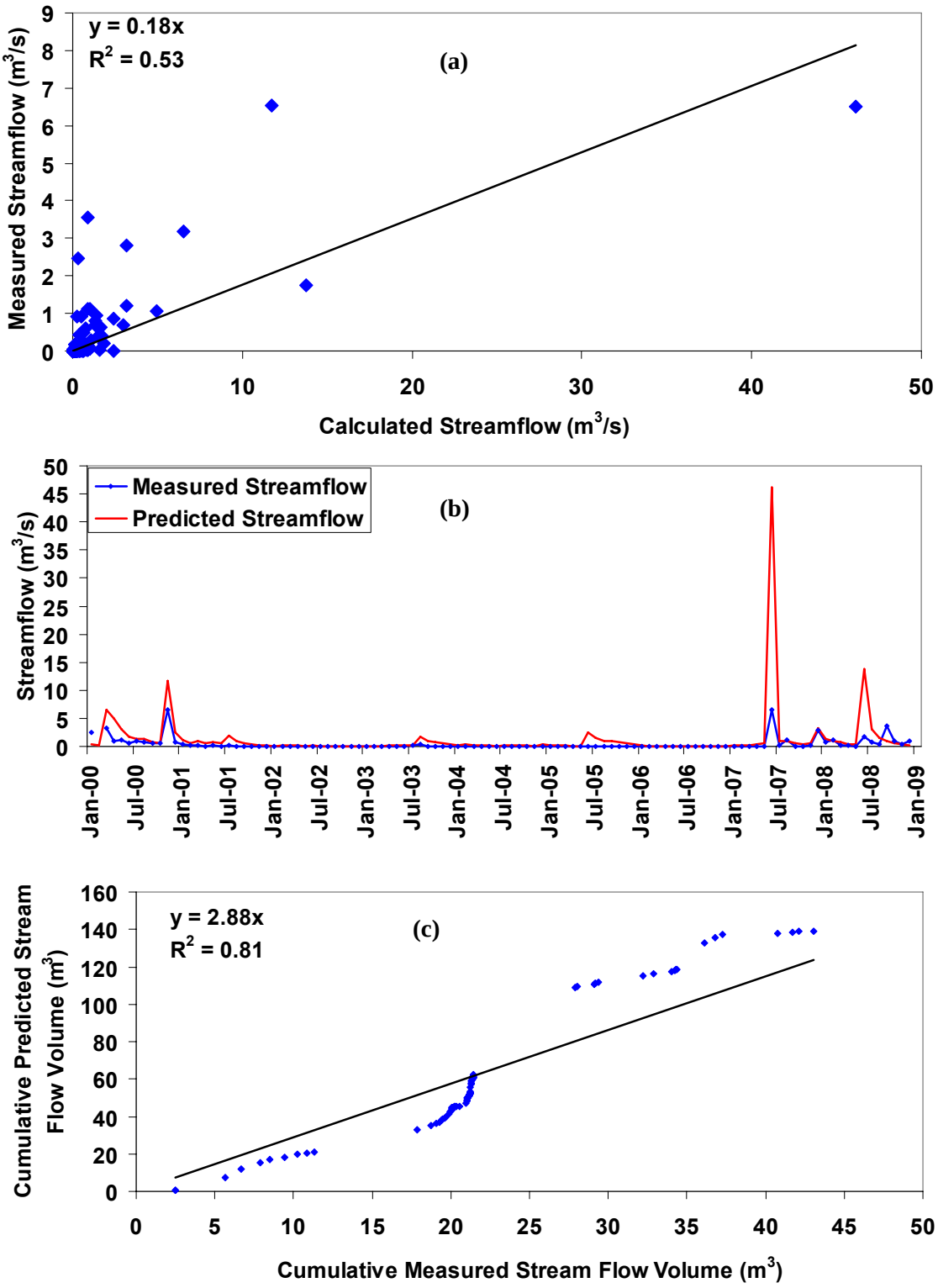


**Figure 8.14 (a)** Measured vs calculated streamflow data **(b)** Measured and calculated streamflow data with time **(c)** cumulative measured streamflow and cumulative predicted streamflow from 2000-2008

Calibrated parameters of stream flow from 1973-1999 shown in **Table 8.4** were used to estimate streamflow from 2000 to 2008. The calibration and validation $R^2$ were 0.62 and 0.77, respectively. **Figure 8.14a** shows the calculated and measured streamflow data during 2000-2008. The obtained $R^2$ of 0.53 reflects a poor linear relationship between the calculated and measured streamflow. The flow in the catchment has been reduced by 65% based on the long-term average calculated from the XG model (**Figure 8.14c)**. **Figure 8.14c** has also indicated the over prediction of stream flow particularly during winter time in 2007 as shown in **Figure 8.14b.** Since the XG model shows a much better fit prior to 2000, it is concluded that the catchment parameter values have changed in the past 2000 period. This may have been due to stream and groundwater abstraction during this period.

#### 8.7.2.3.1 Statistical Test of Streamflow Residual

Statistical tests of normality, autocorrelation and constant variance of the XG model residuals for the Wybong stremflow (#210040) are represented here. **Figure 8.15** and **8.16** shows the streamflow residuals histrogram and QQ-Plot respectively. The Shapiro-Wilk test for normality gave a P-value of 0.002 for the streamflow residuals. This indicated that residuals significantly deviated from normality at the 5% level of significance. At the 0.2% level of significance however, the residuals did not significantly deviate from normality.

**Figure 8.17** shows the autocorrelation of time lag 1 is -0.3 and this is outside of the Durbin-Watson confidence limits. This has a p-value of 0.00 and which indicates autocorrelation significantly differ from 0.0 at the 5% level of significance. The streamflow residuals are autocorrelated because the next month's streamflow depends on the current month's soil moisture content which also depends on the previous month's soil moisture content.

The coefficient of determination $R^2$ was $(0.546)^2 = 0.298$. Therefore 29.8% of the variability in the current residual was explained by variability in the previous residual.

**Figure 8.18** indicates that the variance of the residuals is constant with the predicted streamflow. These tests indicated that the residuals are not normal, not independent but they are identically distributed.

The statistical test results were used to justify the use of hv-blocks cross-validation method as of the model selection procedure rather than for hypothesis testing. The

presence of autocorrelation in the residuals justified the use of hv-blocks cross-validation to test the significance of model performance.

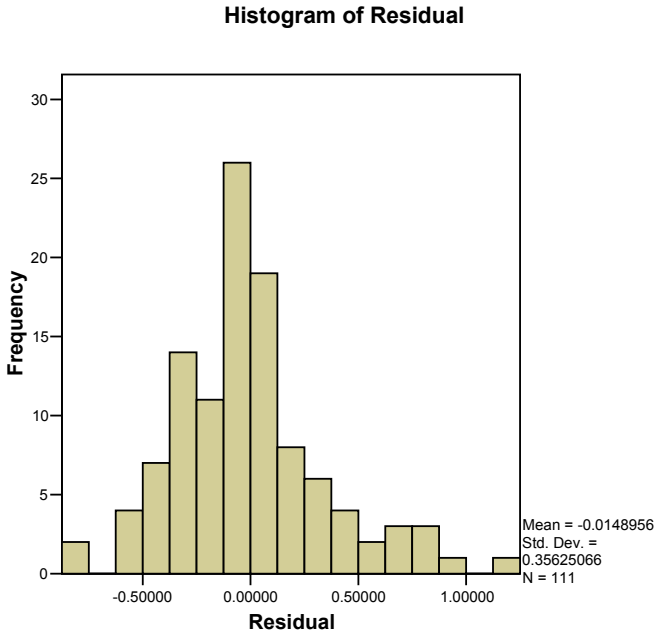


**Figure 8.15** Histrogram of the residuals of the XG model for the Wybong stremflow (#210040)

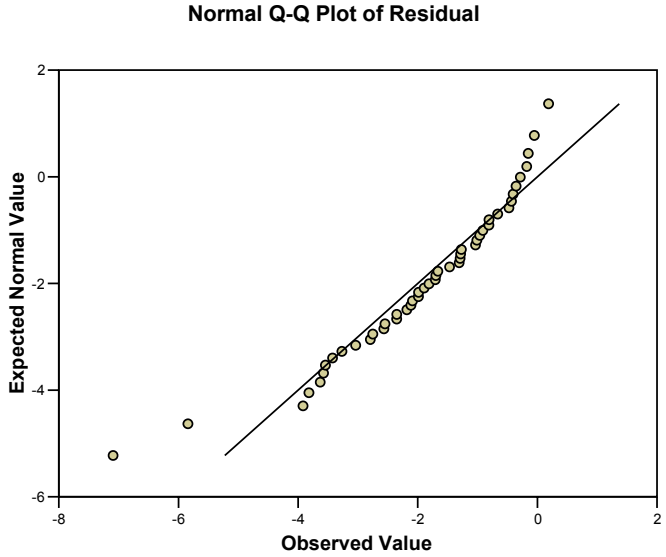


**Figure 8.16** Normal QQ-plot of the residuals of the XG model for the Wybong stremflow

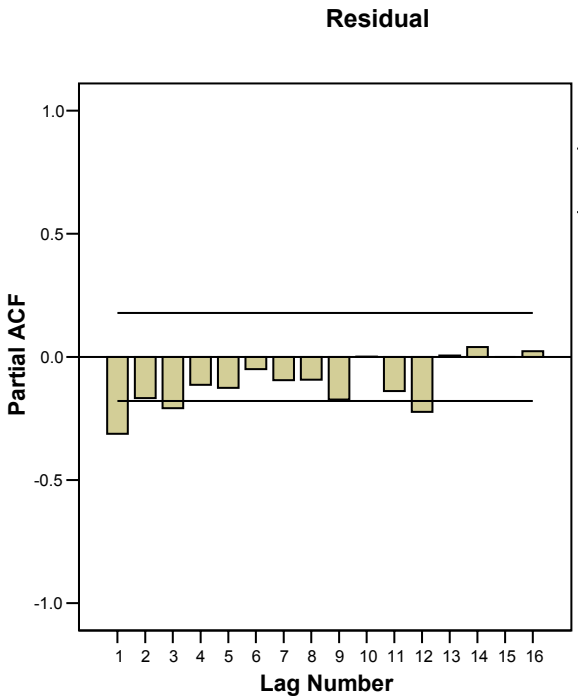


**Figure 8.17** Partial autocorrelation of the residual of the XG model for the Wybong stremflow (#210040)

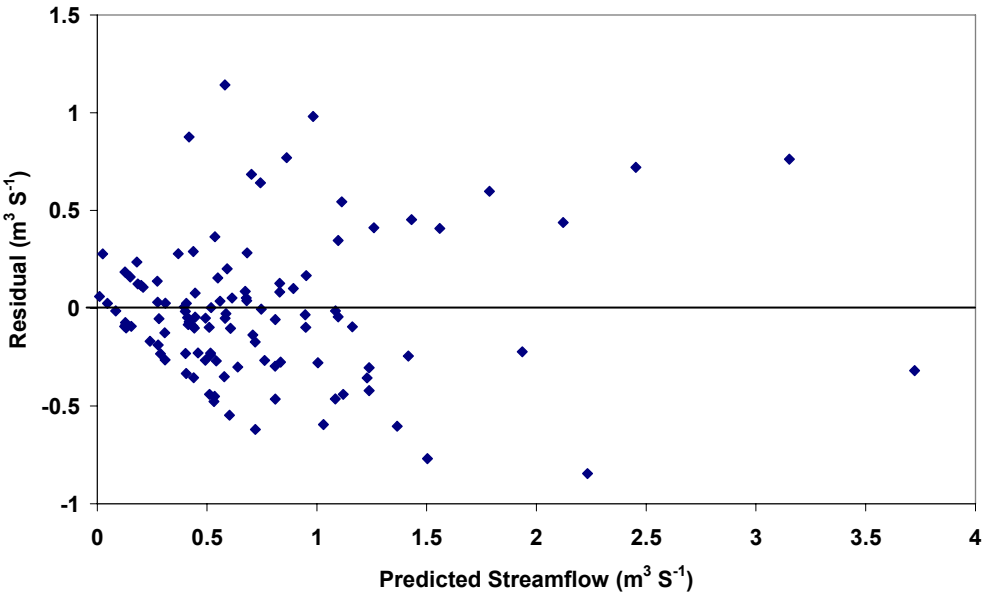


**Figure 8.18** Plot of the residual versus predicted streamflow using the XG model for the Wybong stremflow (#210040)

### 8.7.2.4 Stream Flow and Groundwater Level Prediction

**Table 8.5** shows the results of different configurations of calibration used for the XGR1 model. Calibration configuration **Str** denotes that all of the initial values and parameters were calibrated on streamflow data except the initial groundwater level.

The $G_0$ and the groundwater recharge parameter $\beta_G$ can only be calibrated on groundwater level data. Calibration configuration **GW** denotes that all of the initial values and parameters were calibrated on groundwater level data except the streamflow parameter $\beta_A$ which can only be calibrated on streamflow data.

Calibration configuration **GW+Str** denotes that all of the initial values and parameter values were calibrated on groundwater level and streamflow simultaneously with the total $R^2$ calculated as the mean of the groundwater level $R^2$ and the streamflow $R^2$:

$$R^2(total) = \frac{1}{2}(R^2(GW) + R^2(RtStr)) \tag{8.13}$$

which gives equal weight to the groundwater levels and streamflow data in determining the calibrated parameter estimates. Averaging the $R^2$ values allows for the groundwater level record and streamflow record to be different lengths with different variances.

The parameter estimation in **Table 8.5** and **Table 8.6** shows different values depending on the calibration configuration with unreasonably large estimates of $\hat{\beta}_Q$ for Gw and GW+Str. The $R^2$ values in **Table 8.5** and **8.6** indicate that the XGR model performed well only for the groundwater level prediction for the period under calibration configuration GW+Str and GW but the groundwater level and stream flow under calibration configurations of Str are poor. The ground and surface water data from Wybong catchments are from the drought period and water flow almost ceased during 2003 to 2007. During this time there were significant periods of little to no flow and predicting ground and streamflow was difficult.

In addition, short period data have been used for calibration and also surface and ground water abstraction have not been accounted in the model. Therefore, the calibrated parameters have not predicted bore and streamflow satisfactorily.

**Table 8.5** Parameters estimate and statistics of the XGR1 model calibrated using different calibration configurations for the Wybong Road bore (#080434) and stream gauge (#210040) from 2003 to 2008. (GW=groundwater, SF=streamflow)

| Calibration | $L$ | $\hat{G}_0$ | $\hat{S}_0$ | $\hat{\beta}_Q$ | $\hat{\beta}_E$ | $\hat{\beta}_G$ | $\hat{\beta}_A$ | GW $R^2$ | SF $R^2$ |
|---|---|---|---|---|---|---|---|---|---|
| Str | 1 | 137.78 | 1.0 | 162.49 | 1.09 | 284.77 | 266107.34 | 0.14 | -0.26 |
| GW | 1 | 137.83 | 38.93 | 101636065 | 1.15 | 455.18 | 7977598251 | 0.61 | 0.36 |
| GW+Str | 1 | 137.81 | 48.57 | 10456048 | 1.15 | 469.82 | 663917604 | 0.61 | 0.39 |

**Table 8.6** Parameters estimate and statistics of the XGR1 model calibrated using different calibration configurations for the Rockhall bore (#080947) and stream gauge (#210040) from 2006 to 2008

| Calibration | $L$ | $\hat{G}_0$ | $\hat{S}_0$ | $\hat{\beta}_Q$ | $\hat{\beta}_E$ | $\hat{\beta}_G$ | $\hat{\beta}_A$ | Stream fraction | GW $R^2$ | SF $R^2$ |
|---|---|---|---|---|---|---|---|---|---|---|
| Str | 1 | 141.89 | 2.68 | 162.49 | 1.02 | 50.18 | 96987 | 0.14 | 0.75 | -0.51 |
| GW | 1 | 141.87 | 705.48 | 45446.1 | 0.75 | 335.15 | 62564 | 0.09 | 0.93 | 0.09 |
| GW+Str | 1 | 141.76 | 86.60 | 25503.8 | 0.82 | 494.56 | 190571 | 0.28 | 0.91 | 0.18 |

### 8.7.2.5 Model Testing Results for Wollombi Brook

The model was calibrated using groundwater elevation data from 2001 to 2008 and streamflow data from 1972 to 2008 using the adjusted $R^2$ value as a goodness of fit criterion. The model was fitted using spatially interpolated monthly rainfall and evaporation data. **Table 8.7** shows the $R^2$ values and parameters of the model for predicted monthly groundwater level for bores (Wollombi township, Broke and Warkworth) and streamflow (Bulga and Warkworth) of Wollombi Brook.

The model was calibrated on Bulga streamflow data from 1972 to 2008 using the hv-blocks cross-validation method. The calibration $R^2$ value was 0.77 and the initial soil water content $S_0$ was 45.64mm, the evapotranspiration parameter $\beta_E$ was 1.1, the runoff parameter $\beta_Q$ was 162.99 mm. The model was also calibrated on groundwater level data from 2001 to 2008 for Wollombi bore (#79056) in Wollombi Brook. The calibration of

$R^2$ value was 0.79. The initial groundwater level $G_0$ was 83.80 m, the initial soil water content $S_0$ was 161.44 mm, the evapotranspiration parameter $\beta_E$ was 0.89, the runoff parameter $\beta_Q$ was 1892.75 mm, the groundwater parameter $\beta_G$ was 189.38 and the time lag was 0 month. These parameter values identified in the fit appear to be physically realistic. There was a 2-4 month lag in the aquifer response to rainfall at both Warkworth and Wollombi (**Table 8.7**). The results show that all of the other measured bores were responsive to rainfall (lag was 0 month) including deeper aquifer system at Broke (**Table 8.7**).

**Table 8.7** Results for Predicting Groundwater Level (2001 to 2008) and Streamflow (1972 to 2008) for Wollombi Brook (SF= streamflow, Wk=Warkworth, Bul=Bulga, spl= split-sample validation and hv=hv-block cross validation method).

L = Lag time, $G_o$ = initial ground water height, $S_0$ = initial soil moisture, $\beta_Q$ = run-off parameter, $\beta_E$ = evapo-transpiration parameter, $\beta_G$ = ground water parameter and C.V.=cross validation

| BoreID | Calibration | | | | | | | | C.V. | |
|---|---|---|---|---|---|---|---|---|---|---|
| | L (Month) | $G_0$ (m) | $S_0$ (mm) | $\beta_Q$ (mm) | $\beta_E$ | $\beta_G$ (mm/m) | $R^2$ | RMSE (m) | Va $R^2$l | RMSE (m) |
| 79055 | 4 | 86.20 | 1159 | 1901 | 0.0 | 454.19 | 0.77 | 0.10 | | 1.07 |
| 79056(spl) | 1 | 84.24 | 288.9 | 2006 | 0.74 | 186.29 | 0.81 | 0.10 | 0.59 | 3.09 |
| 79057(hv) | 0 | 65.33 | 1.0 | 2452 | 1.2 | 55.54 | 0.88 | 0.97 | 0.11 | 3.89 |
| 79058(spl) | 0 | 61.61 | 94.15 | 1721 | 1.19 | 176.26 | 0.82 | 0.21 | 0.81 | 20.3 |
| 79059 | 2 | 45.37 | 1936 | 18643 | 0.001 | 1541.36 | 0.83 | 0.07 | 0.46 | 1.36 |
| 79060(Hv) | 0 | 47.43 | 55.07 | 1249 | 1.03 | 141.64 | 0.80 | 0.18 | 0.21 | 8.67 |
| SF(Wk)spl | | | 27.0 | 139 | 1.14 | | 0.75 | | 0.46 | |
| SF(Bul)spl | | | 28.56 | 144 | 1.11 | | 0.81 | | 0.55 | |

The model predicts well the groundwater level for the measured bores and streamflow at Workworth and Bulga gauges in the Wollombi Brook, though prediction was difficult due to low and zero flows during drought between 2001-2008. A compounding problem in this sand bed stream system is that during drought periods, most of the flow is in the groundwater component. **Figure 8.19 and Figure 8.20** are the graphical representations of the fitted model for the bore at Wollombi (Shallow) and

the stream gauge at Bulga, respectively. **Figure 8.21** shows the results of cumulative predicted streamflow volume versus the cumulative measured streamflow volume. The obtained $R^2$ is 0.99. Therefore, the long term performance of the model in terms of catchment yield is good.

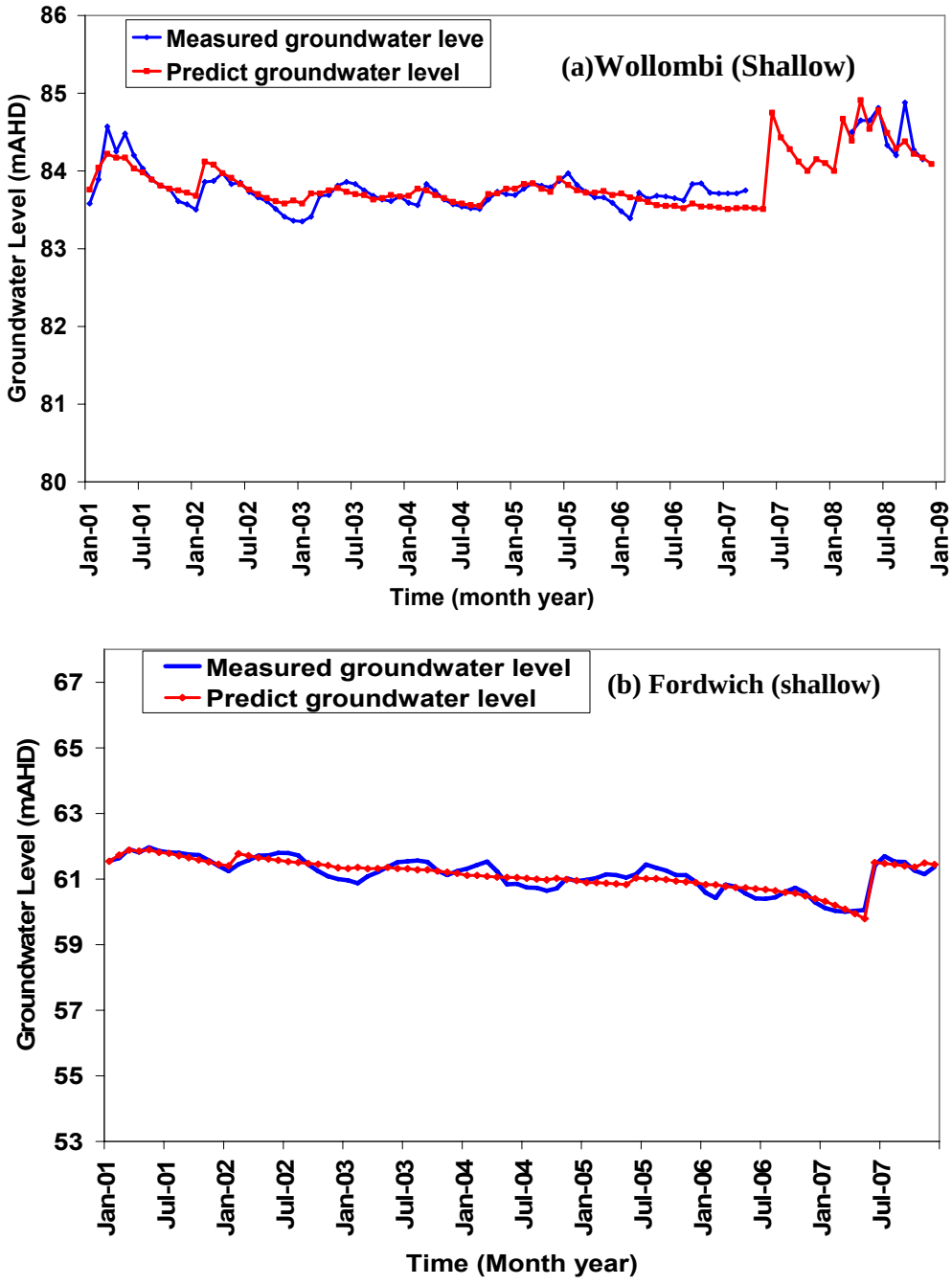


**Figure 8.19** Measured and predicted groundwater level for Bore **(a)** 79056 and **(b)** 79058 in Wollombi Brook, Calibration $R^2$ is 0.79 and 0.82 and validation $R^2$ are 0.59 and 0.81 using the hv-blocks cross-validation

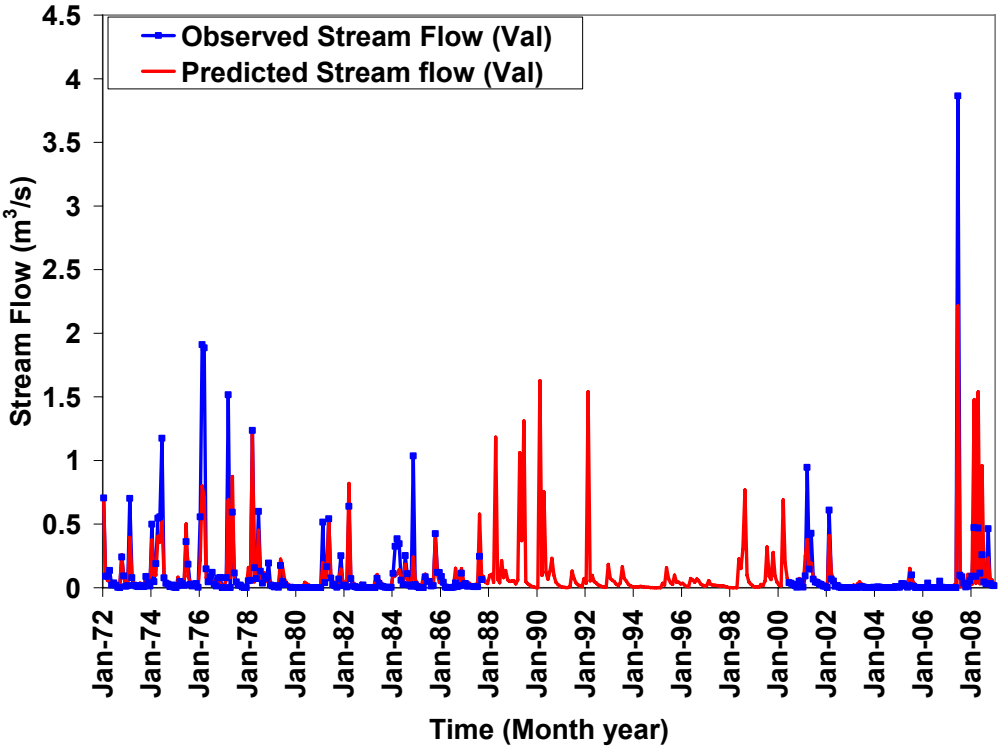


**Figure 8.20** Measured and predicted streamflow at Bulga gauge, calibration $R^2$ is 0.77 using the hv-blocks cross-validation for the period 1972-2008

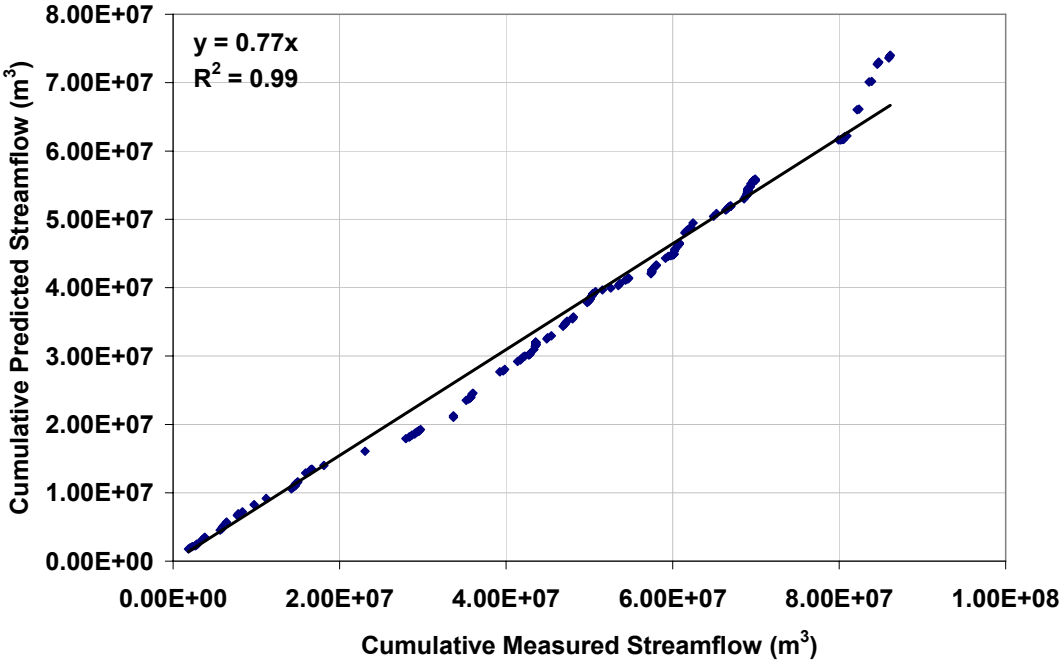


**Figure 8.21** Cumulative predicted streamflow volume versus measured streamflow volume at Bulga gauge from1972-2008 from1972-2008

The XGR model can be calibrated on groundwater level and streamflow simultaneously, or calibrated on groundwater and used to predict streamflow or calibrated on streamflow and used to predict groundwater level. **Table 8.8** shows the results of different configurations of calibration used for the XGR model.

The parameter estimates shown in **Table 8.8** have different values depending on the calibration configuration. The $R^2$ values in **Table 8.8** indicate that the XGR model performed reasonably better for groundwater level prediction under calibration configuration GW, GW+Str and Str but none performed well for streamflow prediction. For the calibration configuration **Str** the initial values and parameters were calibrated on streamflow data for the period of 2001 to 2003 with the calibration $R^2$ was 0.74.

**Table 8.8** Parameters estimates for the XGR1 model using different calibration configurations for the #79056 and Bulga stream gauge #210028 from 2001 to 2005

| Calibration | $L$ | $\hat{G}_0$ | $\hat{S}_0$ | $\hat{\beta}_Q$ | $\hat{\beta}_E$ | $\hat{\beta}_G$ | $\hat{\beta}_A$ | GW $R^2$ | SF $R^2$ |
|---|---|---|---|---|---|---|---|---|---|
| Str-(Bulga) | 1 | 83.60 | 1.0 | 135.90 | 1.13 | 66.16 | 277890 | 0.56 | 0.24 |
| GW(56) | 1 | 84.24 | 288.9 | 2005.82 | 0.74 | 186.29 | 2799.9 | 0.72 | 0.12 |
| GW+Str | 1 | 84.45 | 90.63 | 316.87 | 1.05 | 73.75 | 9304 | 0.77 | 0.39 |

The model had difficulties in any configuration in fitting streamflow. There appear to be at least four possible explanations for this discrepancy. The first is the extremely short period covered by the data. The second is that during this period there were many zero flows in the streamflow record. The third is that the bore is 33.6 km away from Bulga stream gauge. The fourth is that neither surface nor ground water abstraction has been allowed for in this estimation.

### 8.7.3 Outcomes of the Improved XG Model

XG model was modified in order to examine the fit for flow in the Wybong during low rainfalls periods (see Section 8.7.2.3). **Figure 8.22** shows the result of the fitted model for the 1973-2000 record of streamflow data. However, again the model did not fit well for small rainfall periods in case of 1981-83 droughts, as shown in **Figure 8.23a.** The

modified parameter was expected to perform best but the obtained correlation coefficient is 0.43 which is a poor value of the considered the calibration period of 1973-2005. Although this modified model did not perform well for the studied case, the model fit well for the streamflow of Cotter River at Gingera during the same time period as shown in **Figure 8.23b** (White *et al*., 2007). Therefore, poor performance of the modified model in our study appears due to the zero flows at most of the drought months. It is noted however that the values of the evaporation parameter, $\beta_E$ are now less than 1 and the values of the "soil depth" parameter $\beta_Q$ is less than two meter.

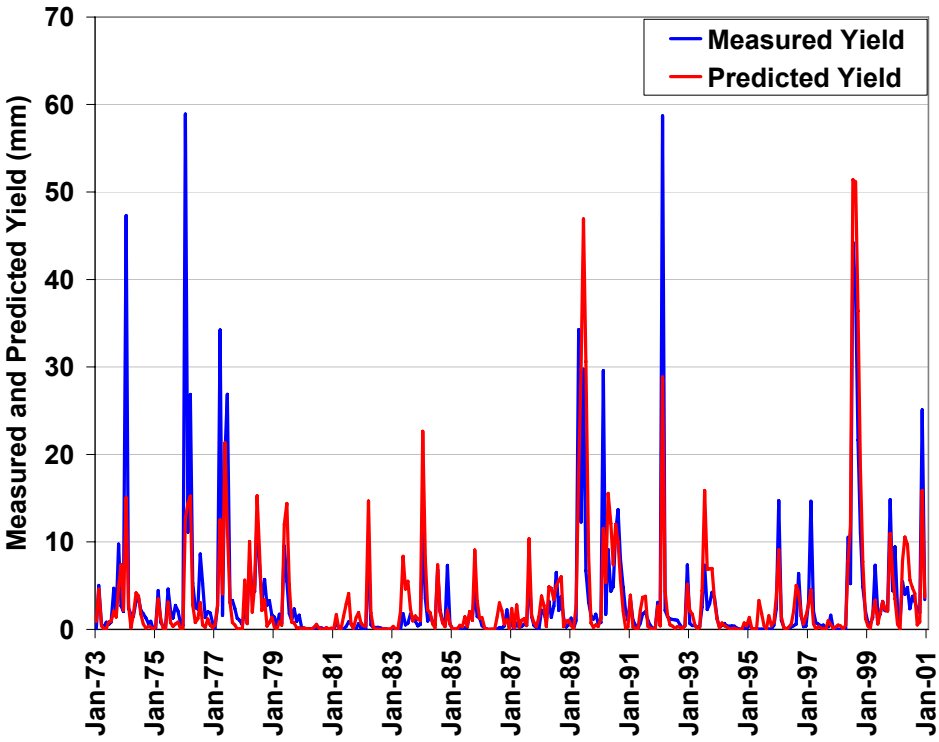


**Figure 8.22** Measured and predicted streamflow data for the period 1973-2000 of $R^2$ (Cal) = 0.55 for the Wybong stream gauge (#210040)

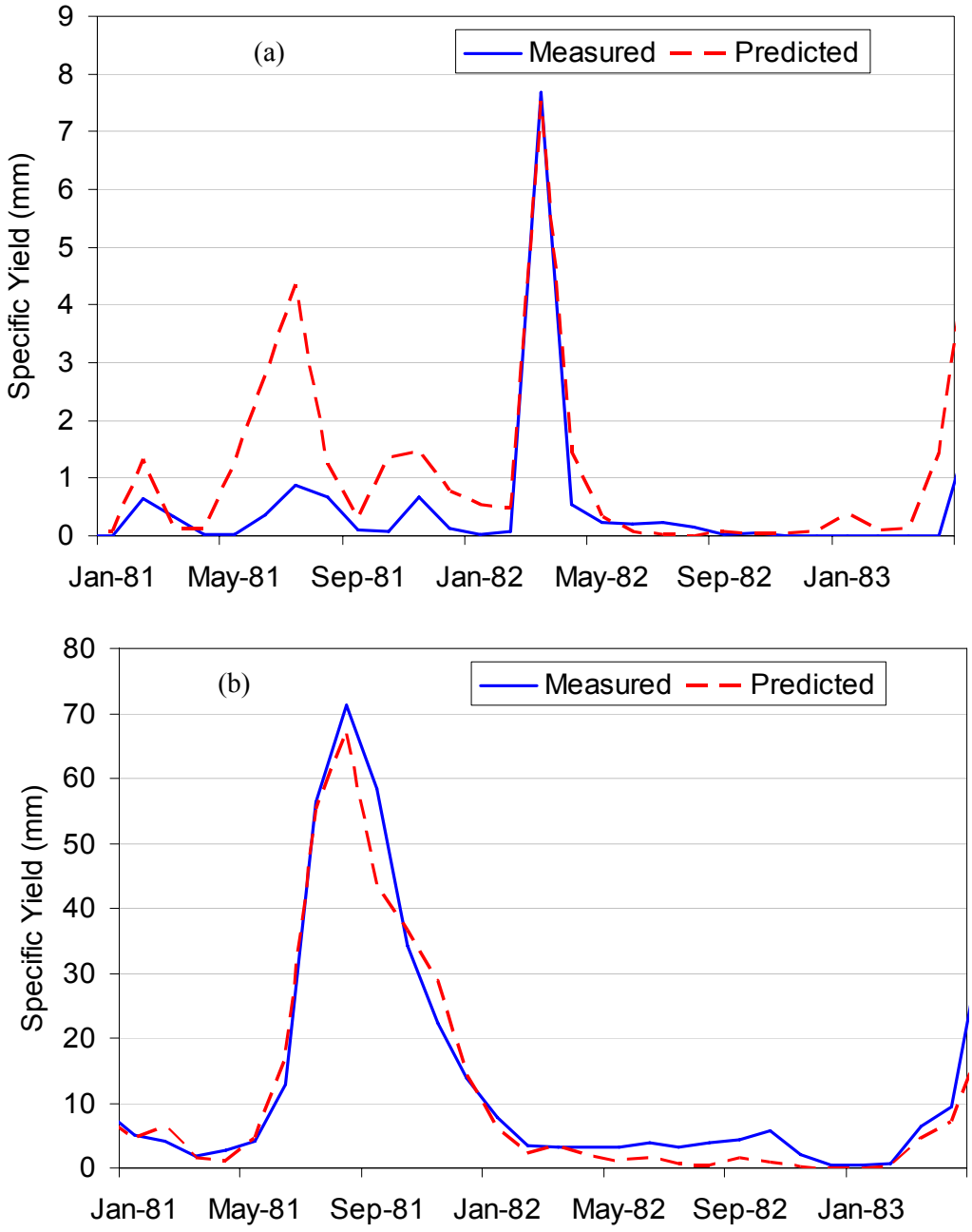


**Figure 8.23** Performance of the modified XG model in predicting specific yield of the **(a)** Wybong catchment following the 1981-1983 drought. Here $\beta_e = 0.72$, $\beta_Q = 1869$ and $S_{t=0} = 57$ with a correlation coefficient of 0.43 for the fit in the period 1973 to 2008 (calibration period of 1973-2005) and **(b)** Cotter River at Gingera following the 1981-1983 drought. Here $\beta_e = 0.7409$, $\beta_Q = 1847$ and $S_{t=0} = 213$ with a correlation coefficient of 0.894 for the fit in the period 1963 to 2005 (White *et al*., 2007).

## 8.8 Conclusion

The conceptual catchment yield model developed by Xiong and Guo (1999) and modified by Jellett (2005) to incorporate groundwater prediction was examined in this chapter for its ability to predict both monthly streamflow and groundwater level changes. The advantage of the modified model is the small number of physically related parameters, an evapotranspiration parameter, a runoff parameter and a groundwater exchange parameter. The model is capable of being calibrated on streamflow and then used to predict groundwater fluctuations, or calibrated on groundwater level to predict streamflow, or calibrated on both streamflow and groundwater data.

In this study the model has been applied to two sub catchments of the Hunter River, Wybong Creek and Wollombi Brook. In order to obtain catchment relevant climate parameters, rainfall and pan-evaporation were spatially interpolated using tri-variate thin-plate smoothing splines with longitude, latitude and elevation as predictors. This procedure enables realistic, catchment averaged values of rainfall and pan-evaporation to be obtained even in catchments without any climate measurements.

In testing the model, the model was first calibrated over part of the streamflow record then verified over the remaining record. The model performed well under a calibration with calibration $R^2$ values of more than 0.8 for spatially interpolated monthly rainfall and evaporation data indicating a good fit between observed and calibrated values. Under verification, however the model performed poorly. This appears to have been the result of testing the model under extreme drought conditions when stream flow ceased.

The XG Recharge model was tested using different configurations of monthly data that used spatially interpolated rainfall and pan evaporation data and uninterpolated point data. The spatially interpolated rainfall and pan evaporation data performed better than the uninterpolated point data except during summer, convective storms. It appears that the spatially interpolated data give more representative values of the rainfall and pan evaporation across the whole catchment.

The coupling of catchment ground and surface water processes were also investigated using the XG model. Results suggested that groundwater on average contributed 42% of the strean water flow each month. The poor linear relationship between the calculated and measured stream flow during the 2000-2008 drought was attributed to the impact of unmeasured groundwater abstraction from the catchment

during the drought. Evidence for such abstraction can be seen in the groundwater level changes (see Figure 7.4).

It has been claimed that the modified XG model could be useful of estimating recharge in the areas where there were streamflow data but little groundwater level data. Here, however, the model had difficulty in fitting streamflow for any of the configurations. This appears partly due to the fact that simultaneous measurements of groundwater levels and surface water discharge data in the Wybong catchment were only available for an extremely short period and that during a major drought. In addition, water flow in Wybong Creek ceased several times during the period 2003 to 2007. During this time abstraction data was not available for predicting groundwater level and stream flow. Unrealistically large runoff parameter values and very low initial soil moisture contents were evident in the very dry year 2006.

A modification to the model was also attempted which was designed to give more realistic estimates of the$\beta e$ evaporation parameter for long dry periods, so typical under Australian conditions. While this modified model gave much more physically realistic values for both the$\beta e$ and $\beta_Q$, it also fitted streamflow data poorly. Part of the reason for this seems to be the preponderance of zero river flows which occurred in the period 2000-2007.

It appears that the XG model, while useful for areas with high rainfalls and reliable streamflows has difficulty coping with prolonged droughts such as experienced in Australia.

# CHAPTER 9: CONCLUSIONS

## 9. 1 Introduction

This thesis has used to variety of techniques to study groundwater and surface water connectivity, solute source and salt export in the Wybong Creek subcatchment of the Hunter River. This final chapter summarises the main conclusions of this study. The aim of this work was to determine the water and salt balance and interactions between surface and groundwater in the upper Hunter and to attempt to incorporate these interactions in a parameter efficient model of both monthly stream flow and groundwater level. The Upper Hunter was chosen (Chapter 2) because of its economic importance to Australia, because of existing salinity problems in the region and because of the potential impacts of developments in the Upper Hunter on surface and groundwater interaction.

A variety of techniques have been used to study salinity the climate and stream flow, salinity and salinity sources and predicting stream flow and groundwater fluctuations (Chapter 3 to 8). The main conclusions from this work will now be discussed.

## 9.2 Climate Variability and Water Yield

In order to examine the climate variability within the Wybong subcatchment of the Upper Hunter a digital elevation model of the catchment was used together with tri-variate thin-plate smoothing splines (Section 3.2.2.3) to derive monthly rainfall and pan evaporation surfaces for the catchment. This enabled the monthly, spatial distribution of rainfall and pan evaporation as well as their spatially averaged values to be constructed for a catchment in which there was only one rainfall gauge (Section 3.2.2.4). Again this work has demonstrated the strength of this procedure for obtaining spatially realistic estimates of the key hydrologic drivers in catchments with limited data.

After filling-in missing data (Section 3.2.5.1), both rainfall and stream flow data were analysed to examine the variability of rainfall over both long and shorter time scales. The cumulative residual spatially interpolated rainfall showed a generally long drying period from 1903 to 1946 which was followed by a generally wetter period from

1947 to 2000. It is unclear whether the period following 2000 represents the start of another long-term drying period. These 40 to 50 year periods correspond to the droughtdominated and flood-dominated periods identified by Bell and Erskine (1981). These major swings in climate have significant implications for both stream and groundwater hydrology and catchment management.

While these periods were generally drier and wetter, the use of the non-parametric rainfall percentiles over 12 month periods (Section 3.2.4) enabled identification of significant droughts in both the FDR and DDR regimes. It was found over the period 1900 to 2008 that there were 23 droughts in which the rainfall over 12 months dropped below the $10^{th}$ percentile. There were 14 such droughts in the period 1900 to 1946 and 9 from 1947 to 2008. The most severe 12 month meteorological drought on record occurred in August 1902, followed in severity by March 1983 and August 1919. For these droughts the rainfall in the proceeding 12 months was only 270, 278 and 288 mm respectively. The highest 12 month rainfall on record occurred in 1950 when the rainfall in the preceding 12 months was 1264 mm. While this analysis is strictly for meteorological drought it is expected that the use of percentiles for 12 month rainfalls should also identify significant hydrological droughts (White *et al.,* 1999).

Analysis of the seasonality of monthly rainfall revealed some interesting trends (Section 3.3.5). While the cumulative residual summer rainfall showed the drying trend from 1903 to 1946 and a generally wetter period from 1947 to at least 1978, the winter rainfall showed quite different behaviour. Winter cumulative residual rainfall showed a wetter period from 1903 to about 1974 followed by a major drying out in winter rainfall between 1975 and 2006. This appears to indicate a switch in seasonality of rainfall. Spring rainfall seems to follow the summer trend while autumn rainfall appears to have no long-term trends. Since winter rainfall is hydrologically important for generating runoff, this switch in seasonality of rainfall has significant implications for runoff.

An examination of the relationship between rainfall in the Wybong catchment and the southern oscillation index found a relatively weak association (Section 3.34). This is consistent with previous findings that rainfall throughout most of eastern Australia is relatively weakly related to SOI (McBride and Nicholls 1983; Stone *et al.,* 1996).

An examination of catchment yield for the period where stream flow record exists, (1955-2008, Section 3.3.6) shows major variation in the runoff coefficient in line with

the extreme droughts and wet periods identified above. While the long term mean runoff coefficient is 0.07, annual runoff coefficients (Figure 3.20) varied between a high of 0.36 in 1957 to zero in 2006. Runoff in the period from 2000-2006 appears anomalously low and could be due to excessive water abstraction.

## 9.3 Salinity Dynamic and Salt Balances

In Chapter 4, the salinity dynamics, stream salt load and salt exports of the Wybong catchment were examined. Procedures were employed to fill in missing stream flow (Section 4.2.3) and stream salinity (Section 4.2.6) data to synthesise a complete record. The IHACRES model used to fill in missing flows (Section 4.3.1) had noticeable deficiencies under low flow conditions. However under these conditions, salt exports are small. Stream salt loads, sources of salinity and salt output/input ratios (O/I) were estimated using the in-filled stream flow, electrical conductivity and geochemical data. Stream EC and TDS analysis (Section 4.3.2) suggest that the stream chemistry in the lower catchment is different from that in the upper catchment. This suggested there are different sources of salinity in the upper and lower catchment. Stream discharge and EC analysis (Section 4.2.4) indicated that the relative magnitude of groundwater and salt discharge to the stream. Groundwater discharge is clearly the predominant source of salinity discharge in the Wybong.

The results of cumulative stream discharge and cumulative salt load (Section 4.3.5) show a consistent increase in stream salt load to accumulated salt discharge into the stream from the regolith, soil landscape draining and discharged of saline groundwater. The cumulative salt load rose above the long term trend during drought periods due to the reduction of the dilution of saline ground waters by the stream waters. This study determined the long term mean total dissolved salt concentration for the period studied (1993 to 2008) at the Wybong gauge is 650mg/L.

Estimation of O/I ratios (Section 4.3.7) show that, on average, the catchment exports more salt than is deposited on it. The most significant salt exports from the Wybong catchment occurred in the high flow periods generated by high rainfall and lowest salt export occurred in the drought years and salt was concentrated in the catchments during dry periods. The average annual salt O/I ratio was 5.5 and average annual specific salt load exported (1993 to 2008) from the catchment 17 tonnes $km^{-2}$ $year^{-1}$ respectively. The latter compares with salt loads of between 4 and 48 tonnes $km^{-2}$

year$^{-1}$ found for the mid-Murrumbidgee River above Wagga Wagga (Conyers *et al.,* 2008).

The salt O/I ratio, in most of the years, is greater than 1 (Section 4.3.7), which emphasises that the catchment is not equilibrium. Previous work on salt I/O ratios in the Murray-Darling Basin (Jolly *et al.,* 2001) has suggested that the principal reason for catchment salt imbalances in the Murray-Darling Basin is due to the replacement of deep rooted native vegetation by shallow rooted pastures and crops resulting in a rise of saline, evaporated cyclic salt, watertable and subsequent discharge to streams. Salinity due to marine-origin groundwater was discounted because of the geologic age of the Murray-Darling system. Other work (Conyers *et al.,* 2008; White *et al.,* 2009) has shown, however, that mineral weathering contributes significantly to salt loads, particularly in upland catchments of the Basin.

Salt-load and salt input/output analysis for catchments is useful in identifying areas of high salinity which can be targeted for further investigations and improved management. This identification is particularly important for determining the distribution, extraction rate and number of water abstraction licenses.

## 9.4 Sources and Trends in Salinity

Chapter 5 used hydro and geochemistry to examine salt sources and salinity trends in the Wybong catchment in both surface and groundwater. Potential sources of salts considered included evapotranspiration-concentrated cyclic salts, halite dissolution, marine-origin groundwaters within the Permian sediments and mineral weathering.

The transects of EC (Section 5.3.1), taken during dry periods (2000-2007), when groundwater discharge dominates, showed an increasing trend in stream salinity downstream. There is a marked increase in salinity between 46 to 60 km downstream, at a stream elevation between about 170 and 190 m AHD, between the Ridgeland and Dry Creek Road sites, which continues, increasingly downstream. This suggests intersection of the stream with groundwater from the Permian coal measures which is known to be saline (AGC, 1984; Crelman, 1994; Griffen, 1961; Kellet *et al*, 1989).

The difference between the upper and lower catchment, revealed by the pH and EC measurements were reflected in the major ion chemistry of surface and groundwaters (Section 5.3.2). These showed that the upper catchment is dominated by bicarbonate,

Na, Ca and Mg while the lower catchment is dominated by Cl and Na ions, suggesting again that the main solute sources in the upper catchment were from mineral weathering, possibly from basalt while those in the lower catchment are consistent with marine origin groundwaters from the Permian coal measures.

The major ion ratios in the upper catchment (Section 5.3.3) were significantly greater than those for cyclic salt rainwater, strongly suggesting that mineral weathering is a dominant source of salts in the upper catchment. The major ion ratios also suggest mineral weathering in the silicate-dominated Liverpool Range Volcanics and the sandstones and conglomerates of the Narrabeen Group in the upper catchment. Depletion of calcium and magnesium relative to bicarbonate indicate that Tertiary basalt contributes to sources of stream salinity in the upper catchment.

Further downstream in the catchment, the ion ratios approach that of seawater. Plots of the ion ratios as a function of 1/Cl indicate that seawater or possibly halite is an end member for most of the major ions in both stream and groundwater. These plots also generally show that rainwater is not an end member at low Cl concentrations, which is attributed to the impact of mineral weathering in the upper catchment. The downstream profiles of ion ratios show that there appears to be some mixing with marine origin water occurring down the catchment with a final transition to marine origin water, again at about 46 km downstream.

The relationship between $Ca^{2+}$ + $Mg^{2+}$ and $HCO_3^-$ (Section 5.3.4) showed that the sources of $Ca^{2+}$ and $Mg^{2+}$ in the upper catchment are not from carbonate dissolution and are possibly from basaltic and granitic weathering of the Liverpool Range Volcanics. In the lower catchment some sites may possibly be sourced either from carbonate dissolution or from deeper, marine origin groundwaters.

Analysis of the molar ratios of dissolved Na/Ca and $HCO_3/SiO_2$ (Section 5.3.5) were used to examine the relative dominance of silicate versus carbonate weathering and generally showed that the source of major ions in upper catchment surface and groundwater samples is from silicate weathering. The Ca/Sr ratios (Section 5.3.6) indicated that seawater was one end member for these ions in the lower catchment and that the end member in the upper catchment has a very high Ca/Sr ratio possibly suggesting a sandstone or conglomerate source.

The chemistry of the lowest salinity (<20 mmol $L^{-1}$) surface and ground waters with high Na/Cl ratios (Section 5.3.7) and variable Cl/Br ratios of ~600–1000 (Section

5.3.8) were attributed to rock weathering which is possible weathering of pyroxene and plagioclase, halite dissolution or marine origin, and mixing and evaporation. Stable isotope analysis (Section 5.3.9) indicated that that stream water isotopic line is due to the progressive mixing of evaporated groundwater with the evaporated rainwater.

Estimation of the weathering fraction of surface and groundwaters, based on either evaporated rainwater or evaporated seawater as the water source (Section 5.3.10) revealed significant weathering fractions in the upper catchment, up to 86% of stream salt load by weight, above 60 km downstream at Dry Creek Road. Two shallow groundwater samples in the upper catchment had weathering fractions relative to cyclic salt that were close to zero suggesting that the samples were essentially evaporated cyclic salt. From these samples it was estimated that the annual groundwater recharge was between 2 and 2.2 mm/yr. When it is assumed that marine origin water is the major source of water it appears that some mineral weathering still contributes to salinity to about 89 km downstream at the Railway Bridge site. Two groundwater bores in the lower catchments had weathering fractions relative to seawater suggesting that they close to zero were diluted seawater with fresh/seawater dilution ratios between 1/10 and about 1/14, close to the dilution factor in the stream at the Railway Bridge site. These analyses of weathering fractions assume that ion ratios of rainwater or seawater do not change on evaporation or dilution.

A conceptual model of the sources of salinity in the Wybong Creek catchment was developed from these results. In the upper catchment, the sources of stream and groundwater salinity are mineral weathering of basalts, Triassic Volcanics, sandstones and conglomerates. In general, evaporated cyclic salt is not an important source of salt in the upper catchment, it does occur in recently recharged shallow groundwater samples but its overall impact on the discharge of salinity is minor. In the lower catchment, below 60 km downstream, marine origin groundwater, most probably from the Permian coal measures is the source of salinity. The results here suggest that the shallow ground and surface water in dry periods have a salt to freshwater mixing ratio between 1/10 and 1/14.

The system is not one of simply two salt sources. Rather the profiles of salinity show that progressive mixing occurs in the upper catchment between weathering solutes and marine origin water since seawater is generally an end member of mixing curves. An issue raised by these results is the time period over which saline groundwater has

been discharging from the Permian and the time necessary for the depletion of the saline groundwater.

## 9.5 Surface and Groundwater Connectivity

Groundwater-surface water interactions were investigated in Chapter 6 in the three different Hunter River catchments, Wybong Creek, Wollombi Brook and Goulburn River. Stream height and groundwater elevation comparison, frequency analysis and baseflow separation technique were employed to investigate the dynamics of groundwater input into the stream during drought and non-drought periods in Wybong Creek. The results of Wybong stream height and ground water level comparison show that groundwater gradient is towards the stream and hence there is a significant potential groundwater discharge (Section 6.3.1).

Baseflow separation analysis indicated that about 53% of stream flow is baseflow (Section 6.3.2). Significant recessions occurred in the winter months of May and June, and very low recession occurred in December presumably due to influence of evapo-transpiration and groundwater higher. Low base flow indices during the dry years between 2002 and 2007 appear due to the high evapo-transpiration and possibly excessive water extraction during this period.

The Q-lag stream flow -rainfall percentile method (Brodie *et al.,* 2008) curves also provided insights into the nature of groundwater-surface water interactions in catchments (Section 6.3.3.1). Analysis of the Wybong, Wollombi and Coggan stream flow record demonstrated they are dominantly gaining streams interacting with relatively deep groundwater system.

In case of the Wybong's base flow systems much of the rainfall's recharge component returns to the stream as groundwater discharge over the year. The lag of 206 days found between stream flow percentiles and rainfall was attributed to catchment hydrogeology as well as climate. The impact of water extraction was also apparent in this analysis (Section 6.3.3.2). Differences in rainfall–stream flow correlation represent losses from the water budget with respect to the stream. The apparent deficit in stream flow relative to rainfall during the non-winter months appears to be due to and groundwater extraction.

The combination of Q-Lag analysis, baseflow separation and stream height and groundwater level analysis showed that Wybong stream was highly connected with groundwater aquifers with relative long time lags between rainfall and stream flow. Wybong differs in character to the behaviour of Wollombi Brook which had much shorter lag times. This difference was attributed to difference in aquifer properties in the two catchments.

## 9.6 Predicting Stream Flow and Groundwater Dynamics

The conceptual catchment yield model developed by Xiong and Guo (1999) and modified by Jellett (2005) to predict groundwater levels is attractive because it has a small number of physically related parameters. The model can be calibrated on stream flow and then used to predict groundwater level fluctuations, calibrated on groundwater to predict stream flow, or calibrated on both stream flow and groundwater data (Chapter 7).

In this study the model has been applied to two sub catchments of the Hunter River, Wybong Creek and Wollombi Brook. In order to obtain catchment relevant climate parameters, rainfall and pan-evaporation were spatially interpolated using tri-variate thin-plate smoothing splines with longitude, latitude and elevation as predictors (Section 3.2.2.3). This procedure enables realistic, catchment averaged values of rainfall and pan-evaporation to be obtained even in catchments without any additional climate measurements.

The XG model performed well under a calibration for predicting the stream flow and ground water level data with $R^2$ values of calibration more than 0.8 for spatially interpolated monthly rainfall and evaporation data for groundwater in Wybong Creek (Section 8.7.1) and Wollombi Brook (Section 8.7.2.5). The model was also found to predict successfully the groundwater level in a semi-confined bore in consolidated material. The recharge time lags were 0 to 2 months, showed that these bores were respond to rain. The calibration $R^2$ values were more than 0.75 for predicting Wybong (Section 8.7.2.3) and Wollombi stream flow. The XG model gave reasonable predictions of stream flow and groundwater levels in both unconfined and confined aquifer bores; however, some adjustment of the model appears necessary for long dry periods. None-the-less, it was noted that for groundwater predictions, values of the parameters used to obtain fit the model are physically unrealistic.

The XG Recharge model was tested using different configurations of monthly data that was spatially interpolated and un-interpolated point data. The spatially interpolated rainfall and pan evaporation data performed better than the un-interpolated point data (Section 8.7.2.1). This is probably because the spatially interpolated data are more representative of the catchment region rainfall and pan evaporation across the whole catchment.

Catchment scale ground and surface water processes were also investigated by the XG model. Results showed that 42% of the groundwater flowed from the catchment each month (Section 8.7.2.3). The poor linear relationship between the calculated and measured stream flow during the 2000-2008 drought was attributed to the impact of groundwater abstraction from the catchments.

It has been claimed that the modified XG model could be useful of estimating recharge in the areas where there were stream flow data but little groundwater level data. Here, however, the model had difficulty in fitting streamflow in any of the configurations studied here (Section 8.7.2.4). It is becouse the ground and surface water data in the Wybong catchment only covered an extremely short period. In addition, water flow in Wybong Creek almost ceased during the period 2003 to 2007. During this time there were significant periods of little to no flow and abstraction data was not available for predicting groundwater level and stream flow. Unrealistically large runoff parameter values and very low initial soil moisture contents were evident in the very dry year 2006 (section 8.7.1.3).

It has been noted that the evapotranspiration approximation in the XG model is physically unrealistic at low rainfalls. A modification to the model was attempted which was designed to give more realistic estimates of the $\beta_e$ evaporation parameter for long dry periods, so typical under Australian conditions. While this modified model gave much more physically realistic values for both the $\beta_e$ and soil thickness parameter, it again fitted stream flow data poorly. Part of the reason for this seems to be the preponderance of zero river flows which occurred in the period 2000-2007. It appears that the XG model, while useful for areas with high rainfalls and stream flows has difficulty coping with prolonged droughts such as experienced in Australia.

## 9.7 Conclusions

The main hypotheses considered in this thesis were that (1) salinity discharge in the Hunter is largely determined by mineral weathering and deep groundwater inflows and (2) a simple parameter-efficient coupled surface and groundwater model can accurately predict groundwater and stream flow behaviour over monthly time scales and is useful in determining surface–groundwater interaction.

As with most catchments, there are significant problems in attempting to test such hypotheses due to the limited and incomplete data on stream flow and stream salinity. In the case of stream salinity, despite the fact that salinity was recognised as a major issue in the Hunter more than 6 decades ago, there is an extremely short continuous salinity record. This limitation was compounded by the severe drought that extended for much of the salinity record. It has been shown here that catchments in eastern Australia are subject to approximately 50 year cycles of flood- and drought-dominated regimes. The relevance of a less than two decade salinity record to such long cycles is problematic.

Despite these difficulties it was possible here to reconstruct and fill in the stream flow and salinity record and to use these completed records to estimate stream and salt discharges from the catchment. The use of spatial interpolation of climate data made it possible to estimate catchment-averaged rainfall and pan evaporation in a catchment without a pan evaporimeter and is a powerful tool where site specific data is limited or absent data.

The specific salt yield estimated for the Wybong catchment falls within the mid-range of those estimated for the Murray-Darling Basin. The mean estimated salt output input ratio shows that, over the study period, the catchment salt storage is in disequilibrium with more salt being discharged from the catchment. In parts of the Murray-Darling Basin it has been suggested that this disequilibrium is due to the clearing of native vegetation and to the export of evapotranspiration-concentrated cyclic salt in groundwater. This suggestion was examined here.

A variety of physical and geochemical methods were used here to examine surface groundwater interaction and sources of stream and groundwater salinity. It was found that groundwater played a major role in both stream flow and salinity discharge. It was shown that while seawater was an end-member of surface and groundwater mixing curves, cyclic salt in rainwater is not the other end member. In the lower portion of the Wybong catchment, marine-origin water sourced from groundwater in the Permian coal

measures is the major source of salinity. In the upper catchment, the results here unequivocally show that weathering products make up the major portion of the stream salt load. So the results here have verified the first hypothesis.

The National Water Initiative of 2004 and the 2007 Commonwealth Water Act require catchment water sharing plans to be developed for catchments across Australia. This process is advanced in NSW and a water sharing plan for Wybong Creek was amended in 2004. The first step in the process described in the plan is to use historical river flow records to divide river flows into flow classes, as a basis for sharing water. The plan is silent about the use of historical information on water quality. This is perhaps partly because the record of water quality monitoring in the Hunter catchment is much shorter than the stream flow record. The work carried out in this thesis shows that there is a significant gradient in water quality downstream. It has been shown here that a relatively few number of major ion analyses, particularly under low flow conditions, can provide a significant amount of information on both sources and the distribution of salinity in catchments. It is recommended that water sharing plans as they evolve should also include information on water quality.

Another requirement of the National Water Initiative is that surface and groundwater be managed as a single resource. Traditionally these have been managed separately, and the detrimental impacts, noticeably reduced stream flows due to increased groundwater extraction, have been observed. In the Wybong water sharing plan, this separation of groundwater and surface water is still somewhat evident. In this thesis the geochemical "fingerprinting" of groundwater was used to examine its connectivity with stream water. It is recommended that, before licensing, all bores should be "fingerprinted" in an attempt to establish their connectivity with stream water.

There are few simple hydrologic models which connect both surface and groundwater. The modified XG model examined in this work offered the potential to be able to predict both stream flow and unconfined groundwater levels at monthly time scales from rainfall and pan evaporation data using simple and straightforward calibration procedures. Although the model could be fitted reasonably well to some of the data, the values required for the small number of physical parameters were physically unrealistic. It has been recognised that the evaporation component in the model is physically implausible, particularly for low rainfalls. Modification of the model to make actual evaporation dependent on soil water content rather than the

previous month's rainfall did not improve the model performance. One of the problems faced by the modeling was the extremely low stream flows for the period 2000 to 2006. It has been suggested here that these flows are the result of ungauged surface and groundwater extraction which are therefore almost impossible to incorporate in a model. While the model can incorporate coupled surface and groundwater interaction and fitted the groundwater data reasonably accurately, it cannot be claimed that the model was accurate in its prediction of stream flow and groundwater levels and therefore this work has rejected the second hypothesis above.

## 9.8 Recommendations for Future Research

In the Murray-Darling Basin, marine-origin groundwaters have been discounted as a source of salinity in the lower Basin. Besides the geochemical evidence, one of the reasons for rejecting this source is the great age of the lower Basin, ensuring that connate marine waters had sufficient time to discharge and be replaced from sediments. In this work it has been shown that marine origin water, presumably from Permian coal measures is still discharging from sections of the Hunter River. Further geochemical and hydro-geological research is required to estimate how long this saline water might be expected to discharge.

The modified XG model examined here remains attractive for the study of monthly stream flow and groundwater levels because of its conceptual simplicity. Xiong and Guo (1997) found that the model worked well, particularly in higher rainfall regions in China. Here it was found that the model performed relatively poorly in a significantly drier regime. This remained the case, even when a modification was made to the model to make it more physically realistic under low rainfall conditions. Here the impact of unmonitored water extractions from the catchment could have contributed to the lack of success of the model. Further research should be carried out to examine the performance of the model in drier regions.

# REFERENCES

Ackworth, R.I., and Jankowski, J. (2001). Salt source for dryland salinity-evidence from an upland catchment on the Southern Tablelands of New South Wales. *Australian Journal of Soil Research,* **39**, 39-59.

AGC, (1984). 'Effect of mining on groundwater resources in the Hunter valley'. (Commonwealth of Australia National Energy Research, Development and Demonstration Program: Prepared by the Australian Groundwater Consultants for the New South Wales Colliery Proprietor's Association).

AGO, (2002). Living with Climate Change: An Overview of Potential Climate Change Impacts on Australia. http://www.greenhouse.gov.au/impacts/overview/

Alley, W.M. (1984). 'On the treatment of evapotranspiration, soil moisture accounting and aquifer recharge in monthly water balance models,' *Water Resources Research*, **20** (8), 1137–1149.

Allison, G. B., and Schonfeldt, C. B. (1989). Sustainability of water resources of the Murray–Darling Basin. In '12th Invitation Symposium: Murray–Darling Basin – a resource to be managed'. Preprint **8**, 149–61. (Australian Academy of Technological Sciences and Engineering: Canberra.)

Allison, G. B., and Hughes, M. W. (1983). The use of natural tracers as indicators of soil-water movement in a temperate semi-arid region. *Journal of Hydrology,* **60**, 157–73.

ANZECC, (2000). *Australian water quality guidelines for fresh and marine waters*. Aust & NewZeland Env. Conservation Council.

ANZECC, (1992). *Australian Water Quality Guidelines for Fresh and Marine Waters,* Australian & New Zealand Environment & Conservation Council, Canberra, Australia.

Appelo, C. A. J., and Postma, D. (2005). '*Geochemistry, groundwater and pollution*.' (Balkema Publishers: Amsterdam A.A.)

Atkinson, W. (1966). A review of the land systems of the Hunter Valley, N. S.W., report, Hunter Valley Res. Found., Newcastle, N. S.W., Australia. Australian Bureau of Meteorology (1988), Climatic atlas of Australia, 67, Aust. Gov. Print. Serv., Canberra, A. C. T., Australia.

Australian Bureau of Meteorology (1988). Climatic atlas of Australia, 67 pp., Aust. Gov. Print. Serv., Canberra, A. C. T., Australia.

Bartarya, S. K. (1993). Hydrochemistry and rock weathering in a subtropical Lesser Himalayan river basin in Kumaun. *Journal of Hydrology,* **146,** 149–174.

Baskaran, S., Budd, K.L., Habermehl, R. and Carter, A. (2004). Groundwater-surface water interactions in upper Lachlan valley: preliminary investigation using hydrochemical and stable isotopes. In: Conference Proceedings 9th Murray Darling Basin Groundwater Workshop Bendigo, Victoria 1.

Baxter, C., Hauer, F. R., and Woessner, W. W. (2003). Measuring groundwater-stream water exchange: New techniques for installing minipiezometers and estimating hydraulic conductivity, Trans. Am. Fisher. Society, **132**(3), 493–502.

Beale, G., Gilmore, R., Simons, M., Realica, S. and Nanadakumar, N., (2000). *NSW coastal rivers salinity audit: Predictions for the Hunter Valley Issue 1*. Centre for Natural Resources, Wagga Wagga.

Beale, G.T.H., Beecham, R., Harris, K., O'Neill. D., Schroo. H., Tuteja, N.K., Williams R.M., (2000). Salinity predictions for NSW Rivers within the Murray-Darling Basin. Centre for Natural Resources, NSW, Department of Land and Water Conservation, Sydney, Report CNR 99.048.

Beavis S.G. (2000). Structural controls on the orientation of erosion gullies in mid-western New South Wales, Australia. *Geomorphology,* **33**, 59–72.

Bell, F.C., and Erskine, W.D. (1981). 'Effects of recent increases in rainfall on floods and runoff in the upper Hunter Valley', *Search* **12**: 82-3.

Beeton, R.J.S., Buckley, K.I., Jones, G.J., Morgan, D., Reichelt, R.E. & Trewin, D. (2006). Australia State of the Environment 2006: independent report to the Australian Government Minister for the Environment and Heritage, Australian State of the Environment Committee, Canberra.

Boughton, W.C. (1993). A hydrograph-based model for estimating water yield of ungauged catchments. Institute of Engineers Australia National Conference. Publ. 93/14, 317–324.

Boussinesq, J. (1904). Recherches theoretique sur l'ecoulement des nappes d'eau infiltrees dans le sol et sur le debit des sources. Journal de Mathematiques Pures et Appliquees, **10** (5), 5–78.

Branagan, D. F., and G. H. Packham (Eds.) (2000). Field Geology of New South Wales, 3rd ed., N. S. W. Dep. of Miner. Resour., Sydney, Australia.

Branagan, D., Herbert, C., and Langford-Smith, T. (1976). 'An Outline of the Geology and Geomorphology of the Sydney Basin.'(Science Press, Department of Geology and Geophysics: University of Sydney.)

Bridgman H. A. (1992) Evaluating rainwater contamination and sources in Southeast Australia using factor analysis. *Atmospheric Environment,* **26**A, No. 13, 2401- 2412.

Bridgman, H. A. (1984). Climatic Atlas of the Hunter Valley, Dep. Of Geogr., Univ. of Newcastle, Callaghan, N. S. W., Australia.

Brodie, R.S., Hostetler, S., Slatter, E (2008). Comparison of daily percentiles of streamflow and rainfall to investigate stream–aquifer connectivity. *Journal of Hydrology*, **349**, 56– 67.

Brodie, R.S., Hostetler, S., Slatter, E. (2007). Q-Lag: a new hydrographic approach to understanding stream–aquifer connectivity. Bureau of Rural Sciences, Canberra ACT.

Brodie, R. S. & Hostetler, S. (2006). A review of techniques for analysing baseflow from stream hydrographs. Bereau of Rural Sciences and Centre for Resources and Environmental Studies, ANU.

Brodie, R. S., Baskaran, S., Ransley, T. and Spring, J. (2005). The seepage meter: Progressing a simple method of directly measuring water flow between surface water and groundwater systerms. *Where Waters Meet* NZHS- IAH –NZSSS Conference Auckland, New Zealand.

Bureau of Meteorology (1989). Climate of Australia, Australian Government Publishing Service, Canberra.
CANA-Climatechange and water in Australia
http://www.cana.net.au/water/about/index.html

BOM, National Climate Centre of the Australian Bureau of Meteorology at *http://www.bom.gov.au/climate/*.

Cartwright, I., Weaver, T.R., and Fifield L. K. (2006). Cl/Br ratios and environmental isotopes as indicators of recharge variability and groundwater flow: An example from the southeast Murray Basin, Australia. *Chemical Geology,* **231**, 38-56.

Cartwright, I., Weaver, T. R., Fulton, S., Nichol, C., Reid, M. & Cheng, X. (2004). Hydrogeochemical and isotopic constraints on the origins of dryland salinity, Murray Darling Basin, Victoria, Australia. *Applied Geochemistry,* **19,** 1233-1254.

Chapman, T. G. and Malone, R. W. (2002). Comparison of models for estimation of groundwater recharge, using data from a deep weighing lysimeter. *Mathematics & Computers in Simulation,* **59**(1-3), 3-17.

Chapman, T. (1999). A comparison of algorithms for stream flow recession and baseflow separation, *Hydrology Processes*, ***13***, 701–714.

Chapman, T.G., Maxwell, A.I. (1996). Baseflow separation – comparison of numerical methods with tracer experiments. Institute Engineers Australia National Conference. Publ. 96/05, 539–545.

Chapman, T.G. (1991). Comment on evaluation of automated techniques for base flow and recession analyses, by R.J. Nathan and T.A. McMahon. *Water Resources Research,* **27** (7), 1783–1784.

Chapman, T. G. (1990). Construction of hydrological models for natural systems management. *Mathematics and Computers in Simulation,* **32**(1-2), 13-37.

Cherkauer, D.S., McBride, J.M. (1998). A remotely operated seepage meter for use in large lakes and rivers. *Ground Water* **26**:165-171.

Chiew, F. H.S. (2006). An Overview of Methods for Estimating Climate Change Impact on Runoff. *30th Hydrology and Water Resources Symposium 4-7 December 2006 Launceston, TAS*.

Chiew, F.H.S. and Mcmahon, T.A. (2002). Global ENSO-streamflow teleconnection, streamflow forecasting and interannual variability. *Hydrological Science journal,* ***47****, 505-522.*

Chiew, F.H.S., Piechota, T.C., Dracup, J.A., and McMahon, T.A. (1998). E1 Nino/Southern Oscillation and Australian rainfall, streamflow and drought: Links and potential for forecasting, *Journal of Hydrology,* **204** (1998), 138 -149.

Cocks, D. (1992). Use with care: managing Australia's natural resources in the twenty first century, University of New South Wales Press, Sydney.

Collins, D.A., Della-Marta, P.M. (2002). Atmospheric indicators for the state of the environment report 2001. Technical Report No. 74, Bureau of Meteorology: Australia, 25 pp.

Conyers, M.K., Hume, I., Summerell, G., Slinger, D., Mitchell, M. and Cawley, R. (2008). The ionic composition of the streams of the mid-Murrumbidgee River: Implications for the management of downstream salinity. *Agricultural water management*, **95**, 598 – 606.

Cook, N., (2002). Geomorphic Categorisation of Streams in the Wybong Creek Catchment, Australia, Department of Infrastructure, Planning and Natural Resources, Newcastle, 23 pp.

Cook, P.G., Herczeg A.L., McEwan, K.L. (2001). Groundwater recharge and stream baseflow: Atherton Tablelands, Queensland. CSIRO Land and Water, Tech Rep 08/01.

Cook, P.G., Telfer, A.L. and Walker, G.R. (1993). Potential for Salinisation of Groundwater Beneath Mallee Areas of the Murray Basin, Centre for Groundwater Studies Report No. 42/Engineering and Water Supply Department (S.A.) Report No. 93/6, Adelaide.

Cornish, P.M. (1977) Changes in seasonal and annual rainfall in New South Wales, *Search* **8**, 38-40.

Craig, H. (1961). Isotopic variations in meteoric waters. *Science,* **133**, 1702–1703.

Creelman, R.A. (1994). The Geological and Geochemical Framework for Assessing Salinity in the Hunter Valley. Draft report for the Department of Water Resources, River Management Branch Hydrological Modelling Unit.

Croke, B.F.W., Andrews, F., Spate, J., and Cuddy, S..M. (2005). IHACRES User Guide. ICAM. The Fenner School of Environment and Society, The Australian National University, Canberra, Australia. www.toolkit.net.au/ihacres.

Dahlhaus, P.G., MacEwan, R.J., Nathan, E.L., and Morand, V.J. (2000). Salinity on the southeastern Dundas Tableland, Victoria. *Australian Journal of Earth Sciences*, **47**, 3-11.

Davis, S.N., Cecil, L., Zreda, M., Moysey, S., (2001). Chlorine- 36, bromide, and the origin of spring water. *Chemical Geology*, **179**, 3–16.

Davis, S.N., Whittemore, D.O., and Fabryka-Martin, J. (1998). Uses of Chloride/Bromide ratios in studies of potable water. *Groundwater,* **36**(2), 338.

Davis, J.C. (1896). Statistics and data analysis in geology. 2nd Edition. Wiley, New York, 527-579.

Davie, T. (2002). Fundamentals of Hydrology, Routledge, New York.

DLWC, (2000). NSW Salinity Strategy-Salinity targets. NSW Department of Land and water Conservation.
http://www.dlwc.nsw.gov.au/salinity/government/pdf/salinity_targets.pdf

Dryland salinity prediction, National Land and Water Resources Audit, 2001. http://audit.ea.gov.au/ANRA/water/docs/national/water_contents.html

Eckhardt, K. (2005). How to construct recursive digital filters for baseflow separation. *Hydrological Processes,* **19**, 507-515.

Erskine, Wayne D. and Warner, R. F. (1998). 'Further assessment of flood- and drought-dominated regimes in southeastern Australia', *Australian Geographer*, **29**, 257-261.

Erskine, W. D. (1994). Flood-driven channel changes on Wollombi Brook, NSW since European settlement. In *The way of the river: Environmental perspectives on the Wollombi* (editors: Mahony D, Whitehead J). Newey and Beath Printers Pty. Ltd, Newcastle, Australia, 41-69.

Erskine, W.D., & Warner, R.F. (1988). Geomorphic effects of alternating flood- and drought dominated regimes on NSW coastal rivers, in Warner, R.F. (ed.) *Fluvial geomorphology of Australia,* Academic Press, Sydney, 223-44.

Erskine, W.D. (1986a). River metamorphosis and environmental change in the Macdonald Valley, New South Wales since 1949', *Australian Geographical Studies* **24**, 88-107.

Erskine, W.D. (1986b) River metamorphosis and environmental change in the Hunter Valley, New South Wales, unpublished PhD thesis, School of Geography, University of New South Wales, Sydney.

Erskine, W.D., & Bell, F.C. (1982). Rainfall, floods and river channel changes in the upper Hunter, *Australian Geographical Studies,* **20**, 183-96.

Evans, A. D., John, M. B. and Caecilia, M. E. (2008). South Australian rainfall variability and climate extremes. *Springer-Verlag*, Clim Dyn, **33**, 477–493.

Evans, RS. (2007). The Impact of Groundwater Use on Australia's Rivers. Technical Report in Land & Water Australia, Canberra.

Falkland, A. (1999b). Draft report. Impact of the 1998/1999 drought on Kiribati water supplies and recommended actions. Australian Agency for International Development. Canberra, 30 pp.

Finlayson, B.L., McMahon, T.A., (1991). Runoff variability in Australia: causes and environmental consequences. Proceedings of the International Hydrology and Water Resources Symposium, October, Perth, Institution of Engineers, Australia, National Conference Publication, 91/22, 504-511.

Freeze, R. A. and Cherry, J. A. (1979). *Groundwater.* Prentice Hall, New Jersey.

Furey, P.R., Gupta, V.K. (2001). A physically based filter for separating base flow from streamflow time series. *Water Resources Research* **37** (11), 2709–2722.

Gallant, A.J.E., Hennesy, K.J., Risbey, J. (2007). Trends in rainfall indices for six Australian regions: 1910 to 2005. *Australian Meteorological Magazine* **56**, 223–239.

Galy, A. and France-Lanord, C. (1999). Weathering processes in the Ganges-Brahmaputra basin and the riverine alkalinity budget. *Chemical Geoogy,* **159,** 31–60.

Garrels, R. M. (1967). Genesis of some ground waters from igneous rocks. In *Researches in Geochemistry*, (ed. P. H. Abelson), **2**, 405–420.

Gentilli, J. (1971). 'Climatic fluctuations', in Gentilli, J. (ed.) *Climate of Australia and New Zealand* (World Survey of Climatology, Volume **13**), Elsevier, Amsterdam, 189-211.

Ghassemi, F., Jakeman, A. J., and Nix, H.A. (1995). Salinisation of Land and water Resources; Human causes, Extent, Management and Case studies. (University of New South Wales Press: Sydney, Australia.), 526 pp.

Gibbs, W. (1975). Drought - its definition, delineation and effects. WMO Special Environment Report no. 5, World Meteorological Organisation, Geneva: 1-39.

Gibbs, W. and Mather, J.V. (1967). Rainfall deciles as drought indicators. Bulletin 48. Australian Bureau of Meteorology, Melbourne.

Gleick, P.H. (1987). 'The development and testing of a water balance model for climate impact assessment: modeling the Sacramento basin,' *Water Resources Research*, **23** (6), 1049–1061.

Grayson, R.B., Argent, R.M., Nathan, R.J., McMahon, T.A. (1996.) Hydrological recipes: estimation techniques in Australian hydrology. Cooperative Research Centre for Catchment Hydrology, Canberra.

Griffin, R.J. (1960). The groundwater resources of the Wollombi Brook catchment area in the Upper Hunter Valley, New South Wales. Department of mines, New South Technical Report no. 8.

Growns, J., Marsh, N., (2000). Characterisation of flow in regulated and unregulated streams in Eastern Australia. Technical Report 3/2000. CRC for Freshwater Ecology, Canberra ACT.

Gunn, R.H., (1985). Shallow groundwaters in weathered volcanic, granitic and sedimentary rocks in relation to drlyland salinity in southern New South Wales. *Australian Journal of Soil Research,* **23**, 355-71.

Guo, S.L., Wang, J.X., Xiong, L.H., Ying, A.W. and Li, D.F. (2002). A macroscale and semi-distributed monthly water balance models for predict climate change impacts in China. *Journal of Hydrology*, **268**(1-4), 1-15.

Guo, S., Yin, A. (1997). Uncertainty analysis of impact of climatic change on hydrology and water resource, *Sustainability of Water Resource Under Increasing Uncertaint.y* Proceedings of Morocco Symposium, July 1997, No 240, 331-338.

Guo, S. (1992). Monthly water balance models for climate change impact study. Proceedings of *First National Post doctoral Conference*, Beijing, 2034-2037.

Halford, K. J. and Mayer, G. C. (2000). Problems associated with estimating ground water discharge and recharge from stream-discharge records, *Groundwater*, **38**(3), 331–342.

Hall, L.D. (1927). The physiographic and climatic factors controlling the flooding of the Hawkesbury River at Windsor, *Proceedings, Linnean Society of NSW, 52*, 133-52.

Hancock, G.R.; Wright, A. and De Silva, H. (2005). Long-term final void salinity prediction for a post-mining landscape in the Hunter Valley, New South Wales, Australia. *Hydroogica. Procesess,* **19**, 387–401.

Hannula, S. R., Esposito, K. J., Chermak, J. A., Runnells, D. D., Keith, D. C., and Hall, L. E. (2003). Estimating ground water discharge by hydrograph separation, *Groundwater*, **41**(3), 368–375

Harris N., Bickle M., Chapman H., Fairchild I., and Bunbury J. (1998). The significance of Himalayan Rivers for silicate weathering rates: Evidence from the Bhote Kosi tributary. *Chemical Geolology,* **144,** 205–220.

Healthy Rivers Commission, (2002). *Hunter River: Independent inquiry into the Hunter river system.* Healthy Rivers Commission, Sydney.

Hem, J.D. (1992). *Study and Interpretation of the Chemical Characteristics of Natural Waters*. US Geological Survey Water Supply Paper 2254. (US Government Printing Office: Washington.), 263 pp.

Hem, J.D. (1982). Conductance: a measure of dissolved ions. In 'Water analysis, v.1, Inorganic species pt 1'. (Eds R.A. Minear and L.H. Keith.) (Academic Press: New York.), 137-61.

Herczeg, A., Lamontagne, S., Pritchard, J., Leaney, F., and Dighton, J. (2001). Groundwater-surface water interactions: testing conceptual models with environmental tracers. In '8th Murray Darling Basin Groundwater Workshop.' P. 6B.3 Victor Harbor, South Australia.

Herczeg, A.L., Simpson, H.J., and Mazor, E. (1993). Transport of soluble salts in a large semiarid basin: River Murray, Australia. *Journal of Hydrology,* **144**, 59-84.

Hjorth, J. S. U. (1994). *Computer Intensive Statistical Methods: Validation Model Selection and Bootstrap.* Chapman and Hall, London.

Hornberger, G. M., Raffensperger, J. P., Wiberg, P. L., and Eshleman, K. N. (1998). Elements of Physical Hydrology, The John Hopkins University Press, Baltimore, 297 pp.

Horton, R.E. (1933). The role of infiltration in the hydrological cycle. Transactions of the American Geophysical Union ***14,*** 446–460.

Hutchinson, M.F. (2002). ANUSPLINE User Guide. Centre for Resource and Environmental Studies Publications, Canberra, Australian National University. http://cres.anu.edu.au/outputs/anuspline.php

Hutchinson M.F. *and* Kesteven, J.L. (1998). Monthly Mean Climate Surfaces for Australia. Centre for Resource and Environmental Studies Publications, Canberra, Australian National University.

Hutchinson, M.F. (1998a). Interpolation of rainfall data with thin plate smoothing splines: I two dimensional smoothing of data with short range correlation. *Journal of Geographic Information and Decision Analysis,* **2**(2), 152-167. http://publish.uwo.ca/~jmalczew/gida_4.htm

Hutchinson, M.F. (1995). Interpolating mean rainfall using thin plate smoothing spline. *International Journal of GIS,* **9**, 305-403.

Hutchinson, M. F. (1995a). Stochastic space-time weather based models from groundbased data. *Agricultural and Forest Meteorology,* **73**: 237-264.

Hutchinson, M. F. (1995b). Interpolating mean rainfall using thin plate smoothing splines. *International Journal of Geographical Information Systems,* **9**(4), 385-403.

Hutchinson, M. F. and Bischof, R. J. (1983). A new method for estimating spatial distribution of mean seasonal and annual rainfall applied to the Hunter Valley, New South Wales. *Australian Meteorological Magazine,* **31**, 179-184.

IPCC, (2001). Climate Change 2001: The Scientific Basis – Summary for Policymakers and Technical Summary of the Working Group 1 Report. Intergovernmental Panel on Climate Change, Cambridge University Press.

Jacobson, A. D., Blum, J. D., Chamberlain, C. P., Poage, M. A. and Sloan, V. F. (2002). Ca/Sr and Sr isotope systematics of a Himalayan glacial chronosequence: carbonate versus silicate weathering rates as a function of landscape surface age. *Geochim. Cosmochim. Acta* **66**, 13-27.

Jakeman, A.J., Hornberger, G.M. (1993). How much complexity is warranted in a rainfall–runoff model? *Water Resources Research,* **29**, 2637–2649.

Jasonsmith, J.F. (2010). *Origins of salinity and salinisation processes in the Wybong Creek Catchment, New South Wales, Australia.* PhD Thesis, Australian National University, Canberra.

Jellett, (2005), 'Parameter efficient prediction of unconfined groundwater levels and streamflow', PhD Thesis, Centre for Resources and Environmental Study, Australian National University, 1-286.

Jolly, I., Williamson, D.R., Gilfedder, M., Walker, G.R., Morton, R., Robinson, G., Jones, H., Zhang, L., Dowling, T.I., Dyce, P., Nathan, R.J., Nandakumar, N., Clark,e R., and McNeill, V. (2001). Historical stream salinity trends and catchment salt balances in the Murray-Darling Basin, Australia. *Marine and Freshwater Research,* **52**, 53–63.

Jolly, I.D. (1998). The Effects of River Management on the Hydrology and Hydroecology of Arid and Semi-Arid Floodplains, in *Floodplain Processes,* Eds. M. G. Anderson, D. E. Walling and P. D. Bates, John Wiley & Sons Ltd, New York, 577-609.

Jolly, I.D., Morton, R., Walker, G.R., Robinson, G., Hones, H., Nandakumar, N., Nathan, R.,_Clarke, R. and McNeill, V. (1997). Stream salinity trends in catchments of the Murray–Darling Basin, Technical Report No. 14/97, CSIRO Land and Water, Canberra, 108 pp.

Jolly, I.D., Dowling, T., Zhang, L., Williamson, D.R., Walker, G.R. (1997a). Water and salt balances of the catchments of the Murray-Darling Basin._Technical Report 37/97, CSIRO Land and Water: Adelaide.

Jolly I.D., Morton R., Walker G.R., Robinson, G., Jones, H., Nandakumar H, Nathan RJ, Clarke R, McNeill V. (1997b). Stream salinity trends in catchments of the Murray-Darling Basin. Technical Report 14/97, CSIRO Land and Water: Adelaide.

Kalbus, E., Reinstorf, F. and Schirmer, M. (2006). Measuring methods for groundwater – surface water interactions: a review. *Hydrogeology Earth System Science*, **10**, 873–887.

Kellet, J.R., Williams, BJ, and Ward, J.K. (1989). Hydrogeochemistry of the upper Hunter Valley, New South Wales. Bureau of Mineral Resources, Geology and Geophysics, Bulletin no. 221. Australian Government Printing Service, Canberra, 74 pp.

Kovac, M., and Lawrie, J. W. (1991). *Soil Landscapes of the Singleton 1:250 000 Sheet*. (Soil Conservation Service of NSW: Sydney.)

Kraus, E.B. (1955). 'Secular changes of east coast rainfall regimes', *Quarterly Journal of the Royal Meteorological Society,* **81**, 430-439.

Landon, M. K., Rus, D. L., and Harvey, F. E. (2001). Comparison of instream methods for measuring hydraulic conductivity in sandy streambeds, *Groundwater*, **39**(6), 870–885.

Langmuir, D. (1997). Aqueous environmental geochemistry. Prentice Hall, Upper Saddle River, NJ.

Leaney, F.W.J. and Herczeg, A.L. (1999). The Origin of Fresh Groundwater in the SW Murray Basin and its Potential for Salinisation. CSIRO Land and Water Technical Report 7/99, Adelaide.

Locsey, K.L., Cox, ME. (2002). Hydrochemical variability as a tool for defining groundwater movement in a basalt aquifer: the Atherton Tablelands, North Queensland. Proceedings of the International Association of Hydrogeologists International Groundwater Conference: Balancing the Groundwater Budget, Darwin, 698-713.

Locsey, K.L., Cox, M.E. (2000). Chemical character of groundwater in a basalt aquifer, North Queensland, Australia. In: Sililo O, Appleyard S, Barrett M, Braune E, Burgess W, Cave´ L, Chiang W, Chilton J and others (eds) Groundwater: past achievements and

future challenges, Proceedings of the XXXth International Congress of the International Association of Hydrogeologists Cape Town, South Africa, Balkema, Rotterdam, 555–560.

Lyne, V., Hollick, M., (1979). Stochastic time-variable rainfall–runoff modelling. Institute of Engineers Australia National Conference. Publ. 79/10, 89–93.

Mackie Environmental Research, (2006). Surface water assessment. Appendix 7. Anvil Hill Project: Groundwater management studies. Centennial Hunter Pty limited. Australia.

Mackay, N., Hillman, T., and Rolls, J. (1988). Water quality of the River Murray. Review of Monitoring 1978 to1986. Murray-Darling Basin Commission Water Quality Report No. 1, (Murray-Darling Basin Commission, Canberra), 62 pp.

Macdonald, B.C.T., White, I.C., Somerville, P.D, and Bush, R.T. (2009). Surface and ground water connectivity and the impact on water quality in the Goulburn River, New SouthWales. *Groundwater in the Sydney Basin Symposium*, Sydney, NSW, Australia. IAH NSW, 160-167.

Mackay, N., Hillman, T., and Rolls, J. (1988). Water quality of the River Murray. Review of Monitoring 1978 to1986. Murray-Darling Basin Commission Water Quality Report No. 1, (Murray-Darling Basin Commission, Canberra), 62 pp.

Makhlouf, Z. and Michel, C. (1994). A two-parameter monthly water balance model for French watersheds. *Journal of Hydrology*, **162**(3-4), 299-3.

Maillet, E., (1905). Essais d'hydraulique souterraine et fluviale. Librairie Sci. Hermann Paris, 218 pp.

Mast M. A., Drever J. I., and Barron J. (1990) Chemical weathering in the Loch Vale watershed, Rocky Mountain National Park, Colorado. *Water Resources Research.* **26,** 2971–2978.

Mau, D.P. and Winter, T.C. (1997). Estimating ground-water recharge from streamflow hydrographs for a small mountain watershed in a temperate humid climate, New Hampshire, USA. *Ground Water,* **35**(2), 291-304.

McBridge, J.L. and Nicholls, N. (1983). Seasonal relationships between Australian rainfall and Southern Oscillation. *Monthly Weather Review*, **111**, 1998-2004.
*National Climate Centre of the Australian Bureau of Meteorology at http://www.bom.gov.au/climate/.*

Mckee, T.B., Doesken, N.J., and Kleist, J. (1993). 'The relationship between drought frequency and duration to time scales.' Preprints, 8th Conference on Applied Climatology, Annaheim, CA, 170-184.

McMahon, T.A., Finlayson, B.L., Haines, A.T., Srikanthan, R., (1992). Global Runoff--Continental Comparisons of Annual Flows and Peak Discharges. Catena Paperback, Cremlingen-Destedt, 166 pp.

McTainsh, G.H. and Craig, S. (2006). The role of aeolian dust in ecosystems. *Geomorphology*, **89,** 39–54.

McTainsh, G.H., Chan, Y.C., McGowan, H., Leys, J.F., Tews, E.K. (2004). The 23rd October, 2002 dust storm in eastern Australia: characteristics and meteorological conditions. *Atmospheric Environment,* **39**, 1227–1236.

Mimikou, M., Kouvopoulos, Y., Cavadias, G. and Vayianos, N. (1991). Regional hydrological effect of climate changes. *Journal of hydrology*, **123**, 119-146.

Monika, M. (2006). Assessment of risk to aquatic biota from elevated salinity-A case study from the Hunter River, Australia. *Journal of Environmental Management*, **79**, 266–278.

Moon, S.K., Woo, N.C., Lee, K.S. (2004). Statistical analysis of hydrographs and water-table fluctuation to estimate groundwater recharge. *Journal of Hydrology*, **292**, 198–209.

NAP (2005). National Action Plan for Salinity and Water Quality Natural Heritage Trust. Regional Programs Summary Report 2004–05.
http://www.napswq.gov.au/publications/annual-reports/index.html

Narayan, K.A., Jolly, I.D. & Walker, G.R. (1993). Predicting flood-driven water table fluctuations in a semi-arid floodplain of the River Murray using a simple analytical model, Division of *Water Resources* CSIRO, Report 93/2, Adelaide.

Nathan, R. J. & McMahon, T. A. (1990). Evaluation of Automated Techniques for Base Flow and Recession Analyses. *Water Resources Research,* **26,** 1465-1473.

Nash, J. E. and Sutcliffe, J. V. (1970). Rinver flow forecasting through conceptual models part I - A discussion of principles. *Journal of Hydrology,* **10**, 282-290.

Nelder, J. A. and Mead, R. (1965). A simple method for function minimisation. *Comput.* **7**(4), 308-313.

Neter, J., Kutner, M. H., Nachtsheim, C. J. and Wasserman, W. (1996). *Applied Linear Statistical Models.* McGraw Hill, USA.

Nicholls, N. & Lavery, B. (1992) 'Australian rainfall trends during the twentieth century', *International Journal of Climatology,* **12**, 153-63.

Nicholls, N. & Wong, K.K. (1990). 'Dependence of rainfall variability on mean rainfall, latitude, and the Southern Oscillation', *Journal of Climate,* **3**, 163-70.

Nicholls, N. (1988).El Niño-Southern Oscillation and rainfall variability *Journal of Climate*, **1**(4), 418-421.

Nigel Holmes and associates (1996). Air quality study: cumulative impacts due to atmospheric emission in the Hunter valley NSW. Report to the NSW Department of Urban Affairs and planning. Sydney.

NSW Department of Sustainable natural Resources (2003). A Guide to the Water Sharing Plan for the Wybong Creek Water Source.

NSW Department of Land and Water Conservation (2003). Integrated Catchment Management Plan for the Hunter Catchment. www.dlwc.nsw.gov.au

NSW Department of Planning (2005). Coal Mining Potential in the Upper Hunter Valley –Strategic Assessment. National Land and Water Resources Audit, 2001, *Australian Dryland Salinity.*

NSW Department of Infrastructure, Planning and Natural Resources (2002). Geomorphic Categorisation of Streams in the Wybong Creek Catchment. Australia.

NSW Department of Environment and Conservation (2003). Hunter River Salinity Trading Scheme Working together to protect river quality and sustain economic development. http://www.environment.nsw.gov.au/resources/licensing/hrsts/hrsts.pdf

NSW Geological Survey (2004). The Ridgelands Coal Drilling Programs, 2001 and 2003, Hunter Coalfield, New South Wales. Coal and Petroleum Resource Assessment Department of Mineral Resources, Geological Survey Report No. GS 2004/123.

NWI, (2004). Intergovernmental Agreement on a National Water Initiative. Council of Australian Governments.
http://www.coag..gov.au/meetings/250604/index.htm#water_initiative

Olley, J. M. and Robert J. Wasson. (2003). Changes in the flux of sediment in the Upper Murrumbidgee catchment, Southeastern Australia, since European settlement. *Hydrological Processes,* **17**, 3307–3320.

Olin, M.H.E. and Svensson, C. (1992). Evaluation of Geological and Recharge Parameters for an Aquifer in Southern Sweden. *Nordic Hydrology,* **23**(5), 305-314.

Palmer, W.C. (1965). 'Meteorologic drought'. Research Paper US Weather Buru, 45-58.

Pandey, S. K., Singh, A. K., and Hasnain, S. I. (1999). Weathering and geochemical processes controlling solute acquisition in Ganga Headwater-Bhagirathi River, Garhwal Himalaya, India. *Aquatic Geochemstry,* **5,** 357–379.

Peck, A.J., and Hatton, T. (2003). Salinity and the discharge of salts from catchments in Australia. *Journal of Hydrology*, **172**, 191-202.

Peck, A.J. (1978). Saliniation of non-irrigated soils and associated streams: A review. *Australian Journal of Soil Research*, **16**, 157-168.

Peck, A.J., and Hurle, D.H. (1973). Chloride balance of some farmed and forested catchments in south western Australia. *Water Resouces. Research*, **9**(3), 648-657.

Pickup, G. (1976). 'Geomorphic effects of changes in river runoff, Cumberland basin, NSW, *Australian Geographer,* **13**, 188-193.

Pittock, A. (1975). Climatic change and the patterns of variation in Australian rainfall, *Search*, **6**, 498–504.

Poulsen D. L., Simmons C. T., Le Galle La Salle C., and Cox J. W. (2006). Assessing catchment-scale spatial and temporal patterns of groundwater and stream salinity. *Hydrogeology Journal,* **14**, 1339-1359.

Press, W. H., Teukolsky, S. A., Vetterling, W. T. and Flannery, B. P. (1992). Numerical Recipes: The Art of Scientific Computing. In Second Edition. Cambridge University Press, Cambridge, 402-406.
http://www.ulib.org/webRoot/Books/Numerical_Recipes/bookfpdf.html

Pritchard, J. (2005). Dynamics of Stream and Groundwater Exchange using Environmental Tracers. Unpublished PhD Thesis, *School of Chemistry, Physics and Earth Sciences.* Flinders University of South, Australia.

Racine, J. (2000). Consistent cross-validatory model-selection for dependent data: hvblock cross-validation. *Journal of Econometrics,* **99**, 39-61.

Rancic, A. Salas, G. Kathuria, A. Acworth, I. Johnston, W. Smithson, A. Beale, G. (2009). Climatic influence on shallow fractured-rock groundwater systems in the Murray-Darling Basin, NSW. Department of Environment and Climate Change, Sydney.

Riley, S.J. (1981) 'The relative influence of dams and secular climatic change on downstream flooding, Australia', *Water Resources Bulletin,* **17**: 361-366.

Riley, S.J. (1980). 'Aspects of the flood record at Windsor', *Proceedings of the 16th Conference of the Institute of Australian Geographers, Newcastle,* 325-340.

Robinson, R.A., and Stokes, R.H. (1970). 'Electrolytes Solutions. 2nd revised edition'. (Butterworths: London) 571 pp.

Rothwell, R., Tio, P.H., Bridgman, H.A., and Pang way, C. (1987). State Pollution Control Commission (SPCC), National Energy Research, Development and Demonstration program. Acidity of precipitation in the Hunter region Volume D.

Sarazin, G. and Ciabrini, J. P. (1997). Water geochemistry of three mountain streams from carbonate watersheds in the Southern French Alps. *Aqutic Chemistry,* **3,** 233–265.

Sarin, M. M., Krishnaswami, S., Dilli K., Somayajulu, B. L. K., and Moore, W. S. (1989). Major ion chemistry of the Ganga-Brahmaputra River system: Weathering processes and fluxes to the Bay of Bengal.*Geochim. Cosmochim. Acta.* **53,** 997–1009.

Scanlon, B. R., Healy, R.W., and Cook, P. G. (2002). Choosing appropriate techniques for quantifying groundwater recharge, *Journal of Hydrology*, **10**(1), 18–39.

Schofield, N.J., and Ruprecht, .JK. (1989). Regional analysis of stream salinization in Southwest Western Australia. *Journal of Hydrology,* **112**, 19–39.

Schofield, N.J., Ruprecht, J.K. and Loh, I.C. (1988). The Impact of Agricultural Development on the Salinity of Surface Water Resources of South-West Western Australia. Leederville: Water Authority of Western Australia, Water Resource Directorate. (Report no. WS 27). 69 pp.

Sharon, D. (1980). The distribution of hydrologically effective rainfall incident on sloping ground. *Journal of Hydrology,* **46**, 165-188.

Sharples, J. J., Hutchinson, M. F. and Jellett, D. R. (2005). On the horizontal scale of elevation dependence of Australian monthly precipitation. *Journal of Applied Meteorology, submitted*.

Shih, D. C. F. and Lin, G. F. (2002). Spectral analysis of water level fluctuations in aquifers. *Stochastic Environmental Research and Risk Assessment,* **16**(5), 374-398.

Simpson, H.J. and Herczeg, A. L. (1994). Delivery of marine chloride in precipitation and removal by rivers in the Murray-Darling Basin, Australia, *Journal of Hydrology,* **154**, 323-350.

Simpson, H.J. and Herczeg, A.L. (1991). Salinity and evaporation in the River Murray Basin. *Journal of Hydrology* **124**, 1-27.

Singh, A. K. and Hasnain, S. I. (1998). Major ion chemistry and weathering control in a high altitude basin: Alaknanda River, Garhwal Himalaya, India. *Hydrology Science Journal,* **43,** 825–843.

Singh, A. K., Pandey, S. K., and Panda, S. (1998a). Dissolved and sediment load characteristics of Kafni Glacier meltwater, Pindar Valley, Kumaon Himalaya. *Journal of Geological Society. India,* **52,** 305–312.

Smakhtin, V.Y. (2001). Low flow hydrology: a review. *Journal of Hydrology*, **240**, 147–186.

Smith, D.I., Hutchinson, M.F., and Mcarthur, R.J. (1992). 'Climatic and agricultural drought: Payments and Policy.' RES7. Centre for Resource and Environmental Studies, ANU, Canberra, 103 pp.

SPCC, (1983.) Air Pollution from Coal Mining and Related Developments. State Polution Control Commission, Sydney.

Speer M.S. (2008) 'On the late twentieth century decrease in Australian east coast rainfall extrems', Atmospheric Science Letters, **9**, 160-170.

Stern, H., G. de Hoedt, and J. Ernst (2000). Objective classification of Australian climates, report, Bur. of Meteorol., Melbourne, Victoria, Australia. (Available at http://www.bom.gov.au).

Stone, R. C., Hammer, G. L., and Marcussen, T. (1996). Prediction of global rainfall probabilities using phases of the Southern Oscillation Index. *Nature,* **384**, 252-255.

Stone, R. C., and Auliciems, A. (1992). SOI phase relationships with rainfall in eastern Australia. *International Journal of Climatology,* **12**, 625-636.

Stonestrom, D. A. and Constantz, J. (2004). Using Temperature to Study Stream-Groundwater Exchanges, U. S. Geol. Surv. Fact Sheet, 2004–3010.

Story, R., R. W. Galloway, R. H. M. van de Graaff, and A. D. Tweedie (1963). General report on the lands of the Hunter Valley, Land Res. Ser. 8, Commonw. Sci. and Ind. Res. Organ., Melbourne, Victoria, Australia.

Tallaksen, L.M., (1995). A review of baseflow recession analysis. *Journal of Hydrology*, **165**, 349–370.

Tarboton, D. G. (1997). A new method for the determination of flow directions and upslope areas in grid digital elevation models. *Water Resources Research,* **33**, 309-319.

Thornthwaite, C.W., Mather, J.R. (1955). 'The water balance', Publication Climatoogy Laboratory, Climatol. Drexel Institute of Technology, vol. **8** (1), 1–104.

Timbal, B. (2009). The continuing decline in South-East Australian rainfall. Centre for Australian Weather and Climate Researc, Bureau of Meteorology, 4-46.

Timbal, B., Jones, D. A. (2008). Future projections of winter rainfall in southeast Australia using a statistical downscaling technique, Springer Science + Business Media B.V. 2007 Climatic Change, 86, 165–187.

Timbal B, Arblaster J (2006). Land cover changes as an additional forcing to explain the rainfall decline in the south west of Australia. Geophys Research Letter, 33(7) pp.

Timbal B, Arblaster J, Power S (2006) Attribution of the late 20th century rainfall decline in Southwest Australia. *Journal of Climatology,* **19**(10), 2046–2062.

Troup, A.J. (1965). The Southern Oscillation. Quarterly Journel of Royal Meteorological Society, **91**, 490-506.

Vandewiele, G.L., Elias, A. (1995). 'Monthly water balance of ungauged basins obtained by geographical regionalization', *Journal of Hydrology*, **170** (1-4), 277–291.

Wahba, G. (1990). Spline models for observational data. Proceedings of *Society for Industrial and Applied Mathematics*, Philadelphia.

Walker, G.R. and Zhang, L. (2002). Plot-Scale Models and Their Application to Recharge Studies. In Zhhang, L. and Walker, G.R. *The Basis of Recharge and Discharge*. CSIRO Publishing, Melbourne.

Wang, C. Y., Wang, C. H. and Kuo, C. H. (2004). Temporal change in groundwater level following the 1999 (M-W=7.5) Chi-Chi earthquake, Taiwan. *Geofluids,* **4**(3), 210-220.

Water Sharing Plan for the Wybong Creek Water Source, Department of Infrastructure Planning and Natural Resources.
naturalresources.nsw.gov.au/**water**/pdf/**wybong**-final%202.pdf

White, I., Macdonald, B.C.T., Somerville, P.D., Wasson, R. (2009). Evaluation of salt sources and loads in the upland areas of the Murray–Darling Basin, Australia. *Hydrolgical Processes,* **23**, 2485–2495.

White, I. (2007). Improvements of the XG Monthly Streamflow Model. The Fenner School of Environment and Society Publications, Canberra, Australian National University.

White, I., Wade, A. and Worthy, M. (2003). The vulnerability of water supply catchments to bushfires: Impacts of the January 2003 wildfires on the Australian Capital Territory. Technical paper.

White, I., Falkland, A., Etuati, B., Metai, E. and Metuera, T. (1999). Recharge of fresh groundwater lenses: Field Study, Tarawa Atoll, Kiribati. *In* Proceedings Second International Colloquium on Hydrology and Water Management in the Humid Tropics. Panama, 22-25 March, 1999. UNESCO-IHP and CATHALAC, Panama City (in press).

White, D.M., and O'Meagher, B. (1995). Coping with exceptional droughts in Australia.' Drought Network News, **7**, 13-17.

White A. F. and Blum A. E. (1995). Effects of climate on chemical weathering in watersheds. *Geochemica et Cosmica Acta,* **59**(9), 1729-1747.

Williamson, D.R., Stokes, R.A., and Ruprecht, J.K. (1987). Response of input and output of water and chloride to clearing for agriculture. *Journal of Hydrology,* **94**, 1–28.

Xiong, L., Guo, S. (1999). Two-parameter water balance model and its application. *Journal of Hydrology*, **216**, 111–123.

Xu, C.Y., Singh, V.P. (1998). A review on monthly water balance models for water resources investigations', *Water Resource Management*, **12**, 31–50.

Xiong, L., Guo, S. (1997). Water balance models and application in China. *Journal of Advance Water Science*, **7**, 74–78.

Zhang, L., Dawesand, W.R. and Walker, G.R. (1999). Predicting the effect of vegetation changes on catchment average water balance. Cooperative Research Centre for Catchment Hydrology, Technical Report 99/12, Canberra.

# APPENDIX A

Appendix A shows the procedure for generating the catchment boundary.

## Generating the Catchment Boundary

The steps for generating catchment boundary involve filling sinks, calculating $D_8$ flow direction, flow accumulation, snap pour point, generating watershed, and buffering watershed (Tarboton, 1997).

### Filling Sinks in the DEM

The presence of sinks may result in an erroneous flow-direction grid. An ArcGIS function is employed to fill all the sinks in the input DEM and create a depressionless DEM which is a desired input to the $D_8$ and $D_8 \infty$ (Tarboton, 1997) flow direction algorithms. It identifies all sinks in the DEM and raises their elevation to the level of the lowest pour point around their edge.

### Generating $D_8$ Flow Direction

The $D_8$ flow direction function calculates and assigns a flow direction to each grid cell in the catchment such that each grid cell flows to only one neighboring grid cell with the steepest descent / slope.

### Generating $D_8$ Flow Accumulation

In this sub-step, the numbers of grid cells contributing to each grid cell in the catchment are calculated and this value is assigned to this grid cell as $D_8$ flow accumulation.

### Snapping Outlet to Stream

Sometimes the gauging station / catchment outlet does not fall on the stream network because of positional errors. This function overcomes this problem by snapping the gauging station to the cell of highest flow accumulation within a specified neighborhood.

### Generating $D_8$ Watershed /Catchment Boundary

This function marks out all the grid cells contributing to the snapped catchment outlet and generates the catchment boundary and watershed.

The contributing area for each grid cell is taken as itself plus the upslope neighbors that drain in to it. This is evaluated recursively starting from the catchment outlet and moving back inside the catchment.

**Adding a Buffer to the Generated Watershed**

This function adds a buffer around the generated watershed. The purpose of this step is to avoid edge effects. The width of the buffer to be put around the catchment is a user configurable parameter and the user can enter the value through the interface.

# APPENDIX B

Appendix B shows the Baseflow separation of Wybong for wet and drought years using recursive filter

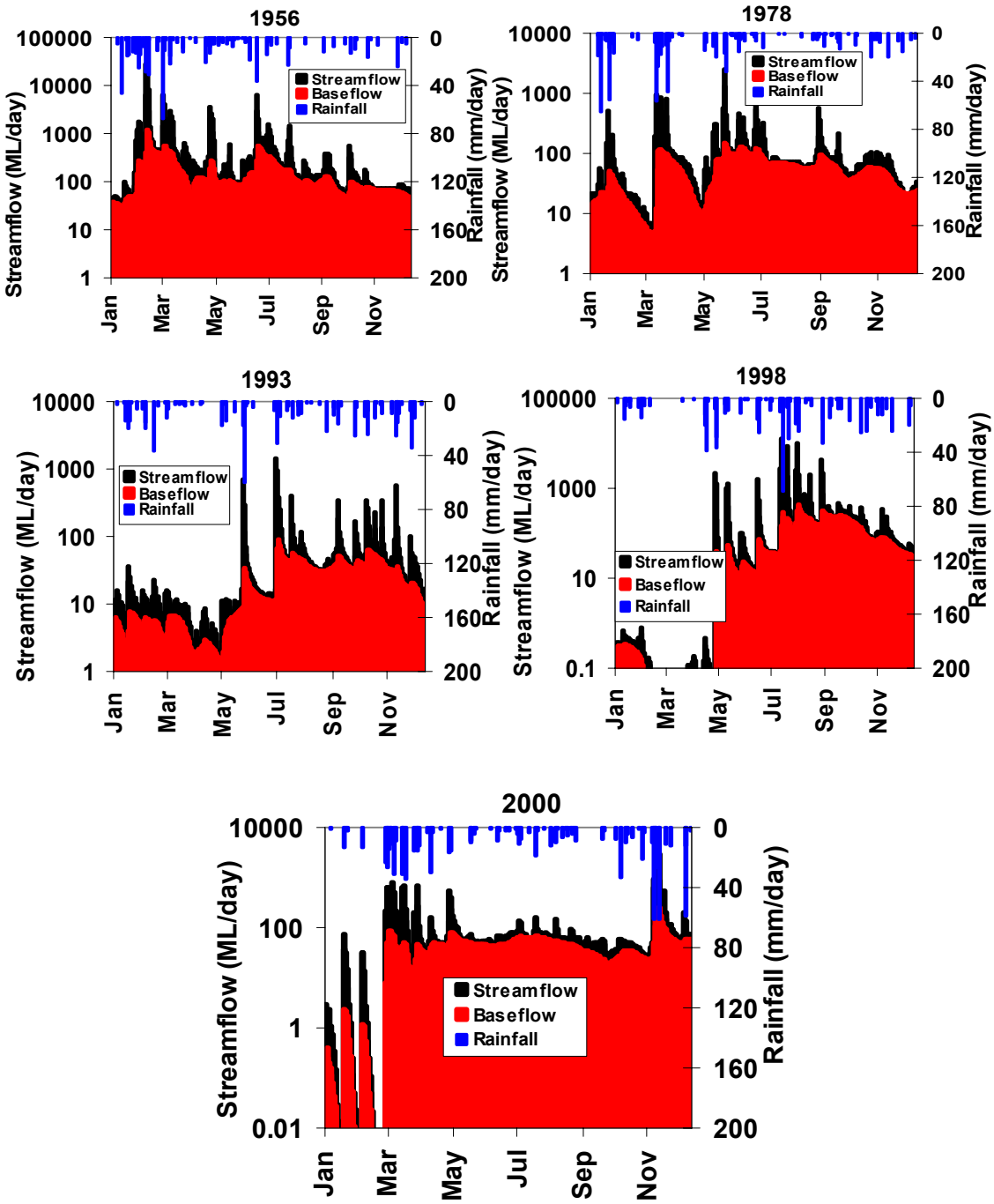


**Figure a** Baseflow separation of Wybong for wet years of 1956, 1978, 1993, 1998 and 2000 using recursive filter

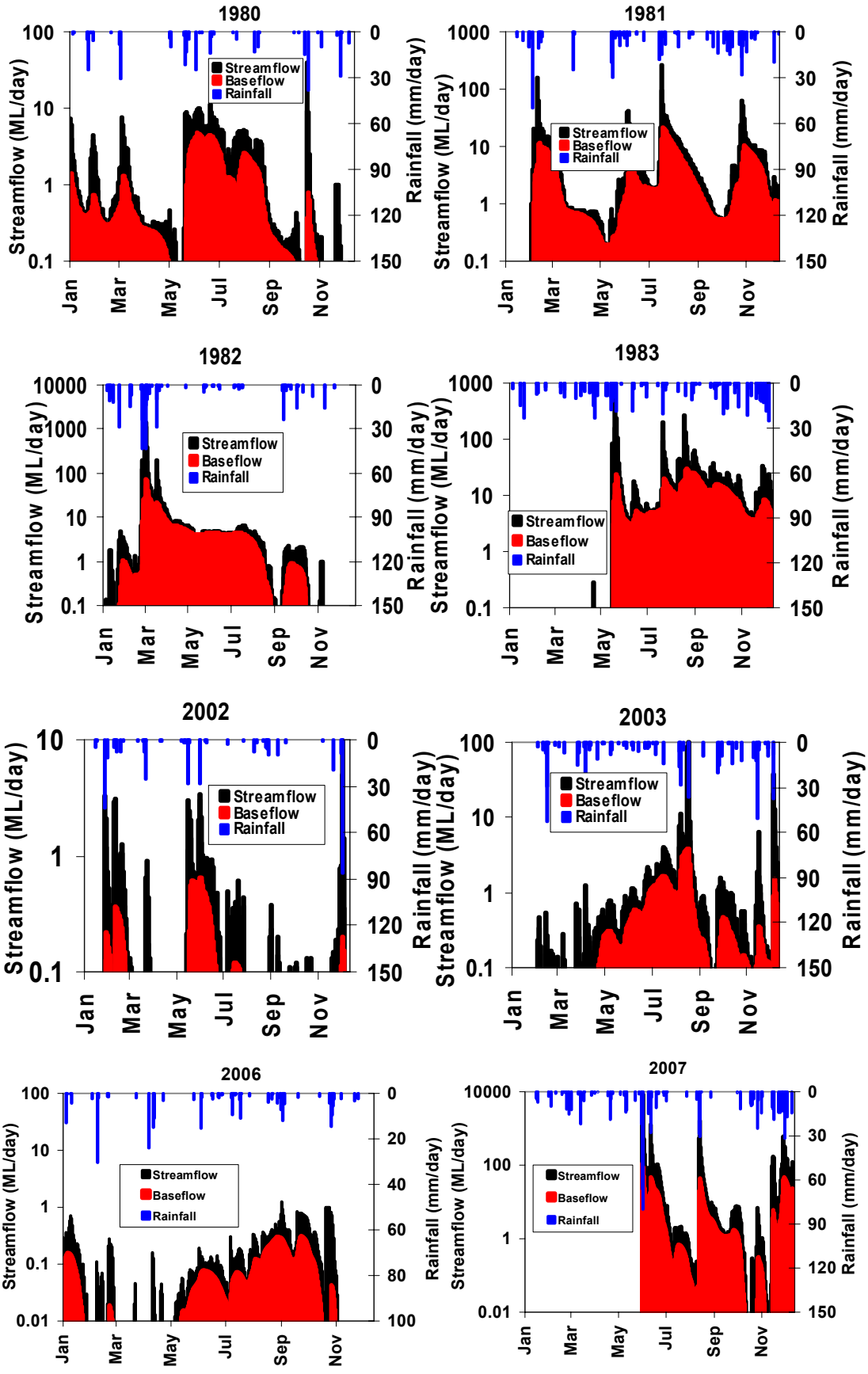


**Figure b** Baseflow separation of Wybong for drought years using recursive filter

# APPENDIX C

Appendix C shows the Fitwbm log file for the XGR model on the Wybong stream gauge 210040.

```
Fits a Water Balance Model to Water Balance Data

ID or -9 to Finish Data Entry:
210040
Data Time Scale (1=Monthly, 2=Weekly)

Model (1=XG, 2=Watbal, 3=HARTT, 4=HARTTPlusPanEvap, 5=HARTTPlusAct
    6=FreeModel, 7=XGR1, 8=XGR2, 9=GR2M, 10=XGR3
    11=HARTTA, 12=HARTTAPlusPanEvap, 13=HARTTAPlusAct
    14=WatbalR1,15=WatbalR2,16=WatbalR3)

Fit Mode (1=Bore, 2=DBore, 3=Streamflow, 4=Bore and DBore
      5=Bore and Streamflow, 6=DBore and Streamflow
      7=Bore, DBore and Streamflow
      8=No Fit)

Spin Up (Number of months at start of data not used in calibration)

Data Time Scale      Model      Fit Mode      Spin Up:
 1   7   3   0


Starting Point          (bore0 swat0 scParam etParam poParam frDown area):
 137.500   100.000   500.000     1.000    50.000     0.000 49600.000
```

Starting Point Perturbance (bore0 swat0 scParam etParam poParam frDown area):

(-9.0 for bore0/swat0 to estimate directly from Bore Data):

0.000 50.000 500.000 0.100 0.000 0.000 10000.000

Perturbance Divisions (bore0 swat0 scParam etParam poParam frDown area):

1 1 4 4 1 1 4

Bore, DBore and Streamflow

StartTimeLag FinishTimeLag:

1 1 1 1 0 4

Whole Period

StartYear StartMonth FinishYear FinishMonth:

1971 1 1999 12

Calibration and Validation Type

(1=split-sample validation, calibration period specified
as a fraction of the whole time period
2=split-sample validation, calibration period and validation period
specified explicity
3=hv-block cross-validation on whole period
4=moving-block bootstrap
5=iid bootstrap
6=no calibration or validation, load parameter-set file
7=uncertainty of parameters
8=calibrate on DBore then Bore, no validation)

Fraction of whole time period used for calibration

Validation Mode

(1=No Fit, 2=Fit bore0/swat0/swatS0)

Validation Type Fraction Validation Mode:

3 0.900 1

Calibration Period (May Be Blank If Validation Type is not 2)

StartYear StartMonth FinishYear FinishMonth:

1971 1 1988 12

Validation Period (May Be Blank If Validation Type is not 2)

StartYear StartMonth FinishYear FinishMonth:

1989 1 1999 12

Input Rain StnData Filename:

mthRain210040.txt

289 elements read

Input Evaporation StnData Filename:

mthEvap210040.txt

414 elements read

Input Bore StnData Filename (Blank If Not Required):

Input Streamflow StnData Filename (Blank If Not Required):

mthSflo210040.txt

414 elements read

Output Calibration GWSystem Filename (Blank If Not Required):

210040.X1SM.Cal.txt

Output Validation GWSystem Filename (Blank If Not Required):

210040.X1SM.Val.txt

414 elements

ID or -9 to Finish Data Entry:

.

.

.

.

-000009

# APPENDIX D

# SYMBOLS

## Variables

| | | |
|---|---|---|
| $E_t$ | is the actual evapotranspiration | (mm) |
| $E_{pan_t}$ | is the pan evaporation | (mm) |
| $\varepsilon_t$ | model residual | (m) |
| $G_t$ | is the groundwater level | (m) |
| $M_{J(t)}$ | Lenth of Gregorian month j(t) | (s) |
| $P_t$ | is the rainfall | (mm) |
| $Q_t$ | is the runoff | (mm) |
| $S_t$ | is the soil moisture content (mm) | |
| t | time | (mths) |
| $W_t$ | Streamflow | ($m^3$ $s^{-1}$) |

## Parameters

| | | |
|---|---|---|
| $\beta_A$ | streamflow parameter | ($m^3$ $mm^{-1}$) |
| $\beta_E$ | is the evapotranspiration parameter | |
| $\beta_G$ | is the groundwater parameter | (mm $m^{-1}$) |
| $\beta_Q$ | is the runoff parameter | (mm) |
| L | time lag | (mths) |

## Statistics

| | | |
|---|---|---|
| R2 | coefficient of determination | |
| MSE | mean square error | ($m^2$) |

| | | |
|---|---|---|
| RMSE | root mean square error | (m) |
| SSE | residual sum of squares | (m) |
| SST | total sum of square | (m) |